

Study of Motorcycle Dynamics for the Improvement of the Stability of Weave and Wobble Eigenmodes

Francesco Passigato

Vollständiger Abdruck der von der TUM School of Engineering and Design der Technischen Universität München zur Erlangung eines
Doktors der Ingenieurwissenschaften (Dr. -Ing.)
genehmigten Dissertation.

Vorsitz: Prof. Dr.-Ing. Wolfgang A. Wall

Prüfer*innen der Dissertation:

1. Prof. Dr. -Ing. Markus Lienkamp
2. Assoc. Prof. Dr. Silvio Sorrentino

Die Dissertation wurde am 05.05.2023 bei der Technischen Universität München eingereicht
und durch die/den TUM School of Engineering and Design am 09.08.2023 angenommen.

*"Se volete far impazzire un fisico,
chidetegli come funziona una bicicletta."
("If you want to drive mad a physicist,
ask how a bicycle works.")*

Stefano Oss, 2013, University of Trento, Physics Lecture

Acknowledgments

First of all I would like to thank Prof. Lienkamp for the the possibility to work on this interesting research project. These three years of research have been an immersive and challenging experience but I had the privilege to work in a familiar environment, where the colleagues always contributed to create a pleasant and stimulating working place. The team spirit that I have learned at the Institute of Automotive Technology is an enrichment that I will keep as fundamental part of my future career.

This research project would have not been possible without BMW Motorrad, who proposed the ideas and funded the whole research. Many thanks to my supervisor, Achim Gordner, for the support and exchange. Also, thanks to Martin Flossmann and Simon Ejechi Aramah for the interesting meetings and for the help in the modeling phase.

A special thanks to Dirk Wisselmann, who gave me valuable suggestions and a constant help during the whole Ph.D. The work and exchange with him has been fundamental for the progress of my research. I really enjoyed discussing about motorcycle dynamics during our motorcycle trips, which often resulted in new and ideas.

I would like to thank Prof. Martin Förg for the invaluable help in the modeling phase and for the suggestions for improving the models.

Several people helped me in the writing phase of this dissertation. Thanks to Prof. Silvio Sorrentino, Alexander Schramm and Alessandro De Felice from the University of Bologna, who are co-authors of my last paper and gave a significant contribution to the final part of my research. Also, thanks to Thomas Herrmann, Sebastian Huber and Frank Diermeyer for reviewing my thesis and providing valuable suggestions for its improvement.

Finally, I would like to thank my family for the constant support during my studies. You motivated me and always trusted in my potential. In particular, I want to thank my parents: knowing that you are at my side is the best gift I could ask for. Together we overcome even the biggest challenges and I am sure this will help us to face any other obstacle that life poses.

Garching, 22 April 2023

Francesco Passigato

Contents

List of Abbreviations.....	III
Formula Symbols.....	V
1 Introduction and Motivation.....	1
1.1 Ensuring the Stability of Weave and Wobble in Motorcycles	2
1.2 Thesis Goals	3
2 State of the Art and Fundamentals.....	5
2.1 Stability of Mechanical Systems	5
2.2 Eigenmodes in Motorcycles	7
2.2.1 In-Plane and Out-of-Plane Eigenmodes	7
2.2.2 Correlation between Motorcycle Design and Stability.....	10
2.2.3 Influence of Structural Flexibilities on Weave and Wobble	16
2.3 Motorcycle Modeling in Multibody Simulation.....	19
2.3.1 Modeling of Flexibility: Lumped Stiffness Approach.....	20
2.3.2 Modeling of Flexibility: Elastic Multibody Simulation (EMBS).....	21
2.4 Control Systems for Increasing the Stability of Weave and Wobble	29
3 Methodology	35
3.1 Research Gap	35
3.2 Research Questions	35
3.3 Proposed Approach.....	36
3.3.1 Methodology for Optimizing the Distribution of Structural Stiffness.....	36
3.3.2 Active Stabilization of Weave and Wobble	37
4 Steps Towards Optimized Distribution of Structural Stiffness	39
4.1 Analysis of the Phenomena causing Weave and Wobble [MDPI 2020]	39
4.2 Study of Weave and Wobble with Elastic Multibody Simulation (EMBS) [IDETC/CIE 2022]	69
4.3 Optimization of the Stiffness Distribution between Structural Components [IMSD 2023].....	83
4.3.1 Method for the Parameter Identification of Lumped Stiffness Models.....	83
4.3.2 Methodology for Optimizing the Stiffness Distribution	85
4.4 Application Example of the Optimization of Stiffness Distribution	110
5 A Control System for the Stabilization Weave and Wobble [ITSC 2021]	113
6 Conclusions.....	123
6.1 Summary	123
6.2 Outlook.....	124
List of Figures	i
List of Tables.....	iii
Bibliography.....	v
Prior Publications	xix
Supervised Students' Theses	xxi

List of Abbreviations

ANCF	Absolute Nodal Coordinate Formulation
CMS	Component Mode Synthesis
CRBF	Consistent Rotation-Based Formulation
DOF	Degree of Freedom
EIM	Effective Interface Mass
EMBS	Elastic Multibody Simulation
FEM	Finite Element Method
FFR	Floating Frame of Reference
FFRF	Floating Frame of Reference Formulation
MBS	Multibody Simulation
MOR	Model Order Reduction
RC	Reference Conditions
SVD	Singular Value Decomposition

Formula Symbols

Formula Symbols	Unit	Description
B_e	-	Input matrix in elastic equation
C_{q_e}	-	Output matrix in elastic equation (for nodal displacements)
$C_{\dot{q}_e}$	-	Output matrix in elastic equation (for nodal velocities)
d	Ns m^{-1}	Scalar damping (1 DOF oscillator)
D_e	Ns m^{-1}	Damping matrix in elastic equation
F	N	Force (scalar)
G	-	Transfer function
J	kg m^2	Scalar inertia (1 DOF oscillator)
k	Nm^{-1}	Scalar stiffness (1 DOF oscillator)
K_e	Nm^{-1}	Stiffness matrix in elastic equation
m	kg	Scalar mass (1 DOF oscillator)
M_e	kg	Mass matrix in elastic equation
q_{rbm}	m	Displacement due to rigid body motion
q_b	m	Elastic boundary DOFs
q_e	m	Elastic (nodal) displacement
q_i	m	Elastic internal DOFs
u	-	System inputs
V	-	Projection matrix
W_i	-	Weights used for loop shaping
y	-	System outputs
$\dot{\delta}$	rads^{-1}	Steering rate
ζ	-	Modal damping ratio
ξ	-	Modal coordinates
τ	Nm	Steering moment
Φ_m	-	Matrix containing m eigenvectors

$\dot{\psi}$	rad s^{-1}	Yaw rate
ω_d	rad s^{-1}	Damped natural frequency
ω_n	rad s^{-1}	Undamped natural frequency

1 Introduction and Motivation

Since 1817, when the first prototype of a bicycle was proposed [1], single-track vehicles—in particular those powered by motors—have become a common vehicle for private transportation. In the last 5–10 years and particularly in wealthy lands, the motorcycle has been increasingly used for leisure [2], therefore partly losing its original function as bare transportation system. The deciding aspects that contributed to the affirmation of motorcycles as a hobby are the driving experience and the sense of freedom [3, 4]. Therefore, to build successful products that satisfy the increasing expectation of the customers, the motorcycle manufacturers have to invest in improving the motorcycles performances. This trend can be recognized in the increase in engine power in every market segment: today's middle class motorcycles possess a power that some years ago would be reserved for sport motorcycles [5]. To manage this higher performance, an increasing effort has to be devoted to the optimization of driving dynamics, which is therefore fundamental in the development process.

More recently, electric mobility has massively gained importance and has affected the motorcycle market, which is demonstrated by the steadily increasing number of electric scooters and motorcycles [6]. Compared to conventional motorcycles, electric two-wheel vehicles are characterized by a different overall mass and mass distribution. Since changes in mass distribution strongly affect the motorcycle dynamics [7–9], the development of electric motorcycles is posing new challenges to motorcycle manufacturers, who have to ensure good driving dynamics while working with a substantially new platform.

From this brief introduction, it is evident that the improvement of the driving dynamics is determinant in the development of motorcycles. The concept of driving dynamics involves several aspects, which range from more subjective sensations to concrete engineering definitions. Considering the more technical aspects, driving dynamics involve acceleration and braking, maneuverability [10], controllability [11] and stability [12]. The stability is a key aspect of motorcycle dynamics, which also influences the previous ones. First of all, as opposed to cars, motorcycles are unstable systems at certain speeds and they become a self-stabilizing system only above this speed [12]. Moreover, motorcycles can be affected by oscillations, which impair the controllability [13, p. 432] and reduce the confidence of the rider [14, 15], thus negatively affecting the safety and the whole driving experience.

Therefore, it becomes clear that a big part in the development process of motorcycles is constituted by the study of their stability and its improvement. In particular, better stability improves the controllability because the rider is not disturbed by the presence of oscillation and can concentrate on the trajectory-following task [16]; moreover, the absence of oscillation phenomena when accelerating or braking ensures better road adherence and increases rider's confidence [17]. Finally, stability and maneuverability are sometimes considered as conflicting aspects [10], in the sense that a too stable motorcycle is often not well maneuverable. Therefore, considering the scope of a certain motorcycle, it is useful to study its stability in order to determine the ideal combination of stability and maneuverability.

In the present thesis, a set of methods is proposed to study and enhance the stability of motorcycles, with the further aim of improving the overall structural design. The stability is studied by leveraging the well-known concept of eigenmodes, which are intrinsic properties of each mechanical system (Section 2.1). In particular, motorcycles possess several eigenmodes, which are summarized in Section 2.2. The subject of this thesis is the study of two of these eigenmodes, which are called weave and wobble. The eigenfrequency of weave is in the range of 1-4 Hz [18, p. 272] and it involves the roll, yaw and rotation of the steering system, while the eigenfrequency of wobble is in the range 6-10 Hz and it is characterized by almost only rotation of the steering system [19]. These frequencies are all above the frequency range of the action of the rider and, therefore, it is almost impossible for a rider to actively stabilize the weave and wobble oscillations. For this reason, unstable weave and wobble eigenmodes can seriously compromise the driving dynamics of the motorcycle, even leading to loss of control and causing severe accidents [14, 20]. Under this point of view, improving the stability of these eigenmodes means increasing their damping or, equivalently, reducing the time needed for the oscillation to disappear.

1.1 Ensuring the Stability of Weave and Wobble in Motorcycles

Considering the previous introduction, it can be stated that the improvement of the stability of the weave and wobble eigenmodes is vital in the development of new motorcycles and in the optimization of the existing models. Several approaches can be used by motorcycle manufacturers to increase the stability of these oscillation phenomena:

- Adaptation of chassis geometry and mass distribution.
- Optimization of tires' characteristics.
- Optimization of the stiffness of chassis components.
- Development of active control systems.

Even if changing the chassis geometry [21, p. 533] and the mass distribution [7–9] has been proven to have the potential for increasing motorcycle stability, the space for optimization is quite limited. In fact, the chassis geometry has to also satisfy packaging and ergonomic requirement. Moreover, changes in mass distribution are often directly related to changes in the chassis geometry.

Tire characteristics certainly determine the stability of motorcycles [21, p. 532], [22, 23]. However, after a motorcycle is sold, the customer has the freedom to choose the tires from several tire manufacturer. In Europe, the mounted tires have to satisfy some requirements about dimensions, and maximal allowed load and speed [24]. Moreover, for motorcycles sold before September 2005, there is also an indication of the tire models that the customer can choose [25]. However, the situation varies worldwide and, therefore, from the perspective of motorcycle manufacturers, it is difficult to guarantee stability only by leveraging tire properties.

There is a strong correlation between the stiffness of chassis components and the stability of the weave and wobble eigenmodes of motorcycles, as several works in this field show (Section 2.2.3 provides a review on these works). The optimization of the stiffness of structural components is a well-known trade-off problem in the automotive industry [26, p. 152]. This trade-off usually

consists of maximizing the stiffness while minimizing the mass. While for cars the highest stiffness possible is desired, for motorcycles an additional challenge is present: it has been shown that introducing some flexibility on certain chassis components has positive effects on road holding and stability [27], so that the focus shifts to achieving the optimal stiffness distribution, rather than the highest stiffness possible. Besides these advantages on driving dynamics, an optimal stiffness distribution also implies optimal usage of material. This results in mass reduction, which has positive effects on fuel consumption, acceleration, and increases the maneuverability, particularly at low speed. Thus, finding the best stiffness distribution for motorcycles has always been a great challenge for manufacturers [28]. Historically, this optimization process has been tackled by “trial-and-error” [29]; however, this approach often leads to expensive development for the high number of prototypes required. The literature on motorcycle simulation examined in Section 2.3 demonstrates that this is why the importance of simulation in motorcycle development is steadily increasing. However, the main challenge for the simulation is the correct representation of reality, and, of particular importance for this thesis, the correct modeling of the effect of flexibilities on driving dynamics.

Thanks to the increasing availability of fast and precise control systems, the development of systems for active stabilization of motorcycles has become more feasible in the past few years. Prototypes of motorcycles able to self-stabilize when standing were proposed by Honda in 2013 with the name “Riding Assist” [30]. In 2022 Yamaha presented a prototype for a steering actuator that will be fitted in the next generations of motorcycles and should increase both agility and stability [31]. The use of an active system to prevent dangerous oscillation phenomena is therefore legitimate and could enhance the driving safety, thus increasing the acceptance of motorcycles.

1.2 Thesis Goals

This thesis will present a framework to assess and increase the stability of oscillating phenomena in motorcycles. As stated in the previous section, the two approaches that have a higher potential for achieving this aim are the determination of an optimal stiffness distribution of chassis components and the development of an active system for stabilization. The first one helps to improve the stability during the design phase of the motorcycle, while the second approach focuses on the online stabilization during operation.

Regarding the first aspect, this work contributes to a motorcycle model that presents the following functionalities:

- It reproduces the effect of the chassis stiffness on stability with high accuracy.
- It allows easy evaluation of the effect of changes in the stiffness of structural components on the stability, thus facilitating the achievement of an optimal distribution of stiffness and a reduction of the mass.

Regarding the aspect of active control, this work proposes a control system for a steering actuator with the following advantages:

- Prevention of unstable oscillating phenomena throughout the whole operating range of the motorcycle.
- It only needs signals from the motorcycle that can be easily obtained with common measurement equipment.

2 State of the Art and Fundamentals

This chapter reviews the relevant literature for the present thesis and introduces some basic concepts that are useful to understand and motivate the methods of the thesis. The chapter is divided into four main sections. Section 2.1 introduces the theme of stability in mechanical systems and the possibilities to evaluate it. Section 2.2 explains the concept of eigenmodes in motorcycles and highlights the correlation between some eigenmodes and structural flexibilities. Section 2.3 summarizes the approaches to model the flexibilities of structural components in the multibody simulation environment. Finally, Section 2.4 presents the relevant literature that developed active and passive systems for preventing unstable oscillations in motorcycles.

2.1 Stability of Mechanical Systems

In the present thesis, a methodology is needed to analyze the stability of mechanical systems. One possibility is to study motion in time. Defining x as the state vector, i.e., the vector containing every Degree of Freedom (DOF), the system is at an equilibrium point if the condition $\dot{x} = 0$ is satisfied [32]. The stability of a system can be studied by considering the amplitude of its motion around the equilibrium point, where $\|\cdot\|$ is the Euclidian norm. Lyapunov [33] distinguishes three cases of stability:

1. The system is Lyapunov stable if, given an initial condition x_0 satisfying the inequality $\|x_0\| < \delta$, the relation

$$\|x(t)\| < \epsilon \quad 0 \leq t < \infty \quad (2.1)$$

is true. δ and ϵ define two small numbers. This means that, given an initial condition close enough to the an equilibrium point, the system's reaction remains bounded by the limit ϵ .

2. The system is asymptotically stable if it is both Lyapunov stable and, in addition,

$$\lim_{t \rightarrow \infty} \|x(t)\| = 0. \quad (2.2)$$

3. The system is unstable if neither of the previous conditions are satisfied.

The study of stability can be carried out by also leveraging the eigenmodes. These are intrinsic properties of mechanical systems that directly correlate with the DOFs of the system itself [34, p. 137]. For linear systems, the time-domain answer to an external excitation is given by a linear combination of its eigenmodes [34, p. 142]. Eigenmodes are characterized by eigenvalues, which lead to the system's eigenfrequencies, and by eigenvectors (also called mode shapes), which describe the relative motion between the DOFs and are associated with a certain eigenfrequency [34, p. 135].

Eigenvalues, which are in general complex numbers, can be used to study a system's stability by looking at their real part. Recalling the definition of stability used above, a system's motion is asymptotically stable if all eigenvalues have a negative real part, stable if at least one of the eigenvalues is purely imaginary (the real part is equal to zero), and unstable if at least one eigenvalue has a positive real part [35, p. 64]. This statement can be demonstrated by looking at the free-response of a 1-DOF linear system with mass m , stiffness k , and viscous damping d , as in (2.3). This can be extended to the multiple DOFs case by using the transformation to modal coordinates, which decouples the equations of motion, and the solution can be found by solving n 1-DOF systems [36, p. 156].

$$m\ddot{x} + d\dot{x} + kx = 0. \quad (2.3)$$

Defining the undamped natural frequency as $\omega_n = \sqrt{\frac{k}{m}}$ and the modal damping ratio as $\zeta = \frac{d}{2m\omega_n}$, (2.3) can be rewritten as:

$$\ddot{x} + 2\omega_n\zeta\dot{x} + \omega_n^2x = 0. \quad (2.4)$$

The general solution of (2.4) is [35, p. 61]:

$$x(t) = C_1e^{\alpha_1 t} + C_2e^{\alpha_2 t}, \quad \alpha_{1,2} = -\zeta\omega_n \pm \omega_n\sqrt{\zeta^2 - 1}, \quad (2.5)$$

where α_1 and α_2 are the two roots of the characteristic equation $x^2 + 2\omega_n\zeta x + \omega_n^2 = 0$ and the eigenvalues of the 1-DOF system in (2.3). The two constants C_1, C_2 have to be calculated with the initial conditions. Depending on the value of ζ , the general solution in (2.5) shows different behaviors [35, p. 61]:

- $\zeta = 1$: critically damped case. The roots of the characteristic equation are coincident and real: $\alpha_1 = \alpha_2 = -\omega_n$. This leads to the solution:

$$x(t) = e^{-\omega_n t} [u_0 + (v_0 + \omega_n u_0)t], \quad (2.6)$$

where u_0, v_0 are the initial conditions on position and speed, respectively. (2.6) expresses that the system returns to its equilibrium position without vibrating.

- $\zeta > 1$: over-damped case. The roots $\alpha_{1,2}$ are distinct and real and the solution is:

$$x(t) = e^{-\zeta\omega_n t} (C_1 e^{\omega_n t \sqrt{\zeta^2 - 1}} + C_2 e^{-\omega_n t \sqrt{\zeta^2 - 1}}). \quad (2.7)$$

(2.7) represents again a non-oscillating solution but, in this case, the system takes longer than in (2.6) to reach the equilibrium position.

- $0 < \zeta < 1$: under-damped case. The roots $\alpha_{1,2}$ are complex conjugates and can be expressed as: $\alpha_{1,2} = -\zeta\omega_n \pm i\omega_n\sqrt{1 - \zeta^2}$. The solution becomes:

$$x(t) = e^{-\zeta\omega_n t} (C_1 e^{i\omega_n t \sqrt{1 - \zeta^2}} + C_2 e^{-i\omega_n t \sqrt{1 - \zeta^2}}). \quad (2.8)$$

This time, the solution represents an oscillating motion at the damped natural frequency $\omega_d = \omega_n\sqrt{1 - \zeta^2}$ with an exponentially decaying amplitude given by the envelope curves $\pm e^{-\zeta\omega_n t}$.

While critically damped systems are always stable, over-damped and under-damped systems may be unstable. At this point, the classification of stability based on the real part of the

eigenvalues becomes clear: if the real part of $\alpha_{1,2}$ is negative, the exponent of the solutions (2.7), (2.8) is negative, thus resulting in a motion with decaying amplitude, i.e., stable motion [37, p. 11]. In the under-damped case, this motion is oscillation with a decaying amplitude. If the real part of $\alpha_{1,2}$ is positive, the exponents in (2.7), (2.8) become positive, thus resulting in an unstable motion where the amplitude increases exponentially over time, either oscillating or not [35, p. 64], [37, p. 11].

The present thesis evaluates the stability of motorcycles by leveraging the eigenmodes, which are presented in the next section.

2.2 Eigenmodes in Motorcycles

This section presents the concept of eigenmodes in motorcycles. It is divided into three sub-sections: Section 2.2.1 introduces the in-plane and out-of-plane eigenmodes. Section 2.2.2 explains how the attempt of guaranteeing stable eigenmodes has influenced motorcycle design through the years. Finally, Section 2.2.3 presents several works that analyze the correlation between chassis flexibility and stability of eigenmodes through simulation.

2.2.1 In-Plane and Out-of-Plane Eigenmodes

Being mechanical systems, motorcycles possess typical eigenmodes as well. The principal eigenmodes of motorcycles can be studied with a motorcycle model containing at least the following 11 DOFs [18, p. 265], [38, 39]:

- 6 DOFs given by 3 translations and 3 rotations of the whole motorcycle about x , y , and z axes of the vehicle.
- Front and rear wheel spin.
- Front and rear suspension travel.
- Rotation of the steering system.

To study of eigenmodes of motorcycles with this model, it is useful to distinguish between in-plane (vertical) and out-of-plane (lateral) dynamics. When the motorcycle has zero lean angle, in-plane and out-of-plane dynamics are decoupled [19] and can therefore be analyzed separately. This allows for the definition of the in-plane and out-of-plane eigenmodes, which are presented in the remainder of this section for the straight running condition. Figure 2.1 shows the typical eigenvalues of a motorcycle with the so-called root-locus plot [19]. It presents the evolution of the eigenmodes with increasing speed by plotting the real part of the eigenvalues, which represents the damping, on the abscissa and the imaginary part of the eigenvalues, which represents the eigenfrequency, on the ordinate.

The in-plane eigenmodes involve the DOFs of the front and rear suspensions. To describe the in-plane eigenmodes, the concept of sprung and unsprung masses is useful, whereby sprung masses are condensed in a single body containing the main frame, the engine, and the rider, and unsprung masses represent the wheels and the moving components of the suspensions [18, p. 177] (Figure 2.2). This way, four in-plane eigenmodes can be identified for motorcycles: pitch, bounce, front hop, and rear hop [18, p. 181]. The pitch and bounce eigenmodes are characterized by the movement of the sprung mass involving a rotation about the lateral axis (pitch rotation) and vertical displacement, whereby in the pitch eigenmode, the front and rear

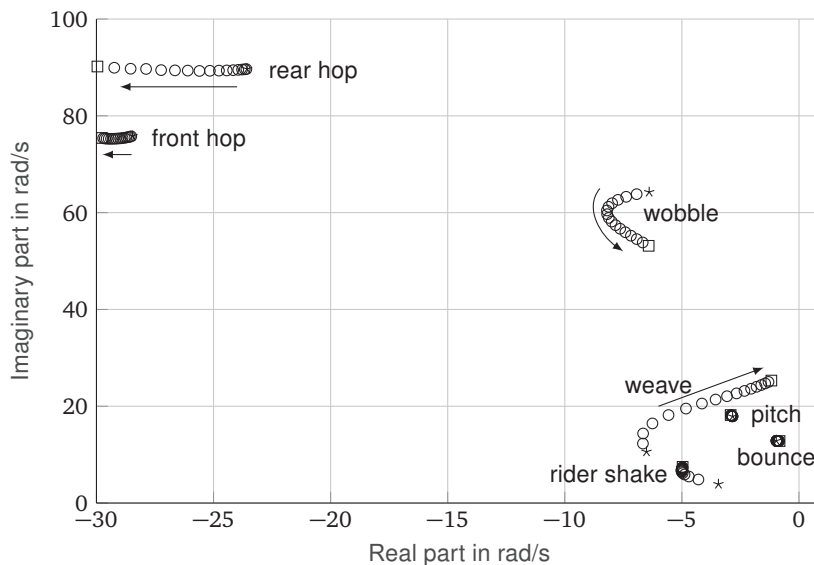


Figure 2.1: Root locus plot of the eigenvalues of a stable motorcycle calculated in straight running. The speed is varied from 40 km h^{-1} to 200 km h^{-1} in steps of 10 km h^{-1} ; the star represents the lowest speed and the square the highest speed. The arrows point in the direction of increasing speed. The rear wobble is not visualized because it has extremely high damping. Only the oscillating eigenmodes—i.e., those with non-zero imaginary part—are shown.

suspension move in counter-phase, while in the bounce eigenmode, they move in-phase [19]. The front hop involves only the DOF of the front suspension, while the rear hop includes only the DOF of the rear suspension [18, p. 181].

Damping of the in-plane eigenmodes is mainly related to damping of the suspensions and vertical damping of the tires, which should be non-zero. This is why, in straight running, the in-plane eigenmodes do not become unstable and remain well-damped, as the real part of the in-plane eigenmodes in Figure 2.1 confirms. Moreover, their change with increasing longitudinal speed is limited and it is entirely due to changes in the motorcycle trim due to aerodynamic forces [12, p. 68].

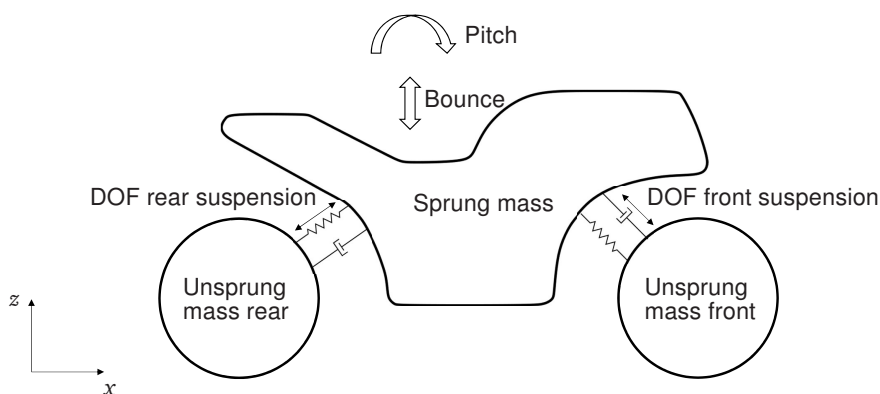


Figure 2.2: Schematic representation of the sprung and unsprung masses of a motorcycle. This scheme is useful for studying the in-plane eigenmodes.

The out-of-plane eigenmodes include capsizes, weave, wobble, and rear wobble [18, p. 267]. Capsize is a non-oscillating eigenmode, i.e., an eigenmode with zero eigenfrequency, and corresponds to the motorcycle tilting over [18, p. 268]. Capsize is generally unstable at low speeds and gets more stable with increasing speed. Its eigenvector also changes with speed, with the low speed capsizes mainly involving roll motion and the high speed capsizes mainly

characterized by lateral motion [12, p. 69].

Weave is an oscillating eigenmode with an eigenfrequency in the range of 1-4 Hz [18, p. 272] and its eigenvector is dominated by roll, yaw, and rotation of the steering system (Figure 2.3a), whereby yaw and rotation of the steering system are almost opposite in phase [40]. As Figure 2.1 shows, the weave eigenmode is strongly influenced by the longitudinal speed of the motorcycle. In particular, damping of the weave increases up to $70\text{-}90\text{ km h}^{-1}$, and after this point it decreases [18, p. 272], meaning that weave may become unstable at high speed, thus becoming a serious threat for safety [4, p. 457]. Moreover, the eigenvector itself is influenced by the longitudinal speed, with the roll component decreasing with increasing speed (Section 4.1). If the DOF of the rider lean is included, the so-called “rider shake” mode originates [12, p. 69], which can, with some combinations of parameters, merge with the weave eigenmode. However, the shake mode generally remains well-damped throughout the whole speed range [12, p. 69].

Wobble has a higher eigenfrequency than weave, in the range of 6-10 Hz, and its eigenvector includes almost only rotation of the steering system [19] (Figure 2.3b). Similarly to weave, the damping of wobble strongly changes with longitudinal speed. Moreover, the speed range where damping is minimal depends on the structural stiffness of the front assembly (in particular, its lateral bending stiffness): low stiffness causes the wobble to be lightly damped at low and medium speeds, while high stiffness shifts the low damping speed range towards higher speeds [23, 28, 41]. See also Section 4.1 for a detailed investigation of this correlation.

Rear wobble can be regarded as a pendant of wobble [12, p. 69] because it mainly includes yaw oscillation of the rear frame with a minor component of roll rotation, which is almost in-phase with the yaw rotation [18, p. 275]. This mode is generally heavily damped [12, p. 69] and, for this reason, it is not an object of study in the literature.

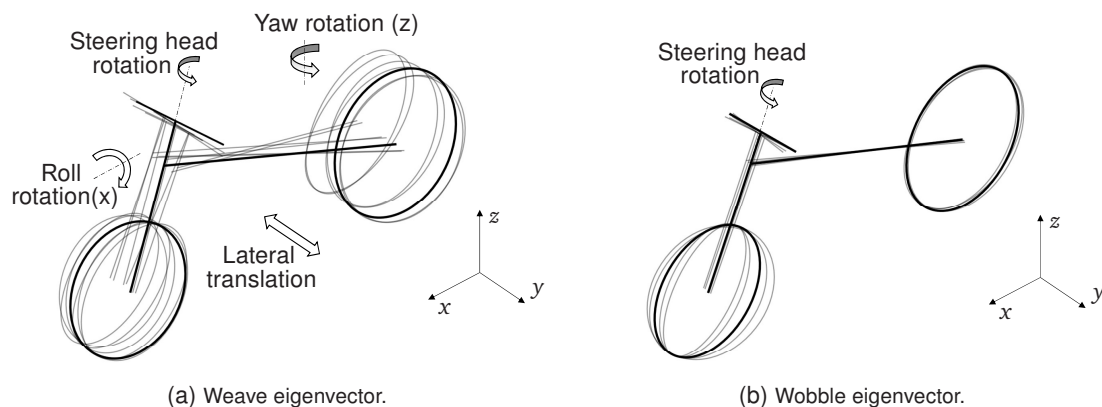


Figure 2.3: Schematic representation of the motorcycle motion during weave and wobble oscillations.

Acceleration and braking in straight running influence the stability of weave and wobble and may cause new modes to appear. In particular, wobble is destabilized by braking [17, 42, 43] due to the increase of the relaxation length with increasing load [44], while weave is unaffected [42, 43]. Evangelou et al. [17] identify a so-called burst oscillation that occurs under firm acceleration at high speed, which is caused by the interaction between weave and wobble.

As previously mentioned, decoupling between in-plane and out-of-plane dynamics is only valid in straight running. When cornering, the in-plane and out-of-plane dynamics become coupled, and therefore, in-plane and out-of-plane eigenmodes can interact [12, 45]. In fact, coupling of in-plane and out-of-plane dynamics provides a signal transmission path between road undulations and lateral dynamics, meaning that vertical excitation coming from the road also excites the lateral eigenmodes [14]. At high speeds, the weave eigenfrequency approaches the eigenfrequencies of

bounce and pitch [40, 46, 47] and, due to coupling between in-plane and out-of-plane dynamics, an interaction between these modes is possible, thus causing the so-called cornering weave [12]. The interaction can also be seen in the eigenvector of the cornering weave because the DOF of the rear suspension is present [40, 46]. Moreover, under cornering, there is the possibility that wobble interacts with the front hop, so that front suspension travel is present in the wobble eigenvector, thus creating the so-called front patter [12, 48].

While the previously described eigenmodes are self-induced, there are also oscillation phenomena that occur only under certain conditions and with a specific excitation, such as chattering and kick-back. Kick-back, also known as tank-slapper, is a violent form of wobble oscillation that is generally experienced at medium-high speed, depending on the motorcycle’s parameters [49, 50]. It is generally triggered by a series of road undulations that induce a periodic excitation with the eigenfrequency of wobble [50]. The excitation causes a periodic lifting of the front wheel that, when landing on the ground with a non-zero steering angle, produces periodic tire lateral forces, which quickly induce a limit-stop to limit-stop oscillation [4, p. 460].

Chatter is a phenomenon occurring under extreme braking conditions coupled with big lean angles [51–53] and has an eigenfrequency of 17-22 Hz [54]. Due to the severity of these conditions, chatter can only be seen in racing: it occurs mainly in the latter phase of corner entry, continues during the high-lean angle rolling phase, and disappears while accelerating [53]. The oscillation starts at the rear wheel, due to the interaction between tire longitudinal force and driveline mode, and propagates through the frame to the front wheel [53]. For an in-depth analysis of the physics behind chatter, the reader is referred to [54].

Table 2.1 summarizes the most relevant oscillation phenomena that can occur on motorcycles.

Table 2.1: Most relevant eigenmodes and external-induced oscillations of motorcycles. f is the abbreviation for eigenfrequency and d for damping.

		f	Relation with speed
In-plane	Bounce	1.5–2 Hz	-
	Pitch	2–3 Hz	-
	Front hop	10–12 Hz	Small change in d
	Rear hop	13–15 Hz	Change in d
Out-of-plane	Weave	1–4 Hz	Change in f, d
	Wobble	6–10 Hz	Change in f, d
Forced oscillations	Kick-back	ca. 10 Hz	Occurs at high speeds
	Chattering	17–22 Hz	-

2.2.2 Correlation between Motorcycle Design and Stability

The main structural components of motorcycles are frame, front fork, and swingarm. These components represent a “chain” of stiffnesses that connect the two wheels. The evolution of motorcycle structural design demonstrates that a great effort has been devoted to optimizing these stiffnesses in order to achieve the desired dynamic properties. Of course, this was not the only reason that motivated the evolution of structural design, which must satisfy requirements of strength and durability. The stiffness of structural components should be optimized considering different aspects such as:

- Good insulation from vibrations coming from the engine and road [4, p. 330].
- Road adhesion [55] when driving over road imperfections with a non-zero lean angle, whereby the excitation from the road has an out-of-plane component, which has to be absorbed by the stiffness of the structural components [27, p. 6-43].

- Precise steering [4, p. 330], [27, p. 1-3].
- Stability of the out-of-plane eigenmodes [56].

All these requirements must be satisfied, while at the same time minimizing mass [57]. In fact, achieving the desired stiffness distribution with a minimum mass is a major challenge in the development process of motorcycles [27, p. 10-1]. The history of motorcycle design motivates the effort in solving this trade-off, which can be seen in the numerous solutions developed for the design of structural components throughout the years.

Evolution of Frame Design over Time

The frame must provide a suitable connection for the swingarm and front fork and enough space for the powertrain [4, p. 330]. Due to these multiple functions, the history of motorcycle design shows several examples of design choices. The requirements mentioned above pose contrasting challenges to the designer of frames. In fact, for precise steering, relatively high torsional and bending stiffness is required—which ensures that the designed steering geometry is maintained in all conditions—while for good comfort, lower stiffness is advantageous [27, p. 1-3]. In the first motorcycles and up to the 1990s, cradle frames (Figure 2.4) were the dominant solution thanks to cheap production and the capability to fit with almost every type of engine [4, p. 344]. Tubular back-bone frames, which also belong to the category of cradle frames, are characterized by a beam on the upper side that ideally connects the front fork and swingarm-pivot [27, p. 10-5]. However, the achievable trade-off between stiffness and mass is disadvantageous [4, p. 345]. To avoid excessive mass, these frames therefore show relatively low stiffness, which could cause instabilities of the weave and wobble eigenmodes under certain loading conditions, as a study by Roe et al. [56] demonstrates. Nowadays, cradle frames can be found mainly on heritage motorcycles or on cheap models, which focus more on the homage to old-style design or on cost reduction rather than on achieving the best structural efficiency.

Cradle frames and tubular back-bone frames can be realized using triangulated tubes to increase structural efficiency, thus coupling low mass with high stiffness [27, p. 10-9]. The first examples of this frame construction can be found in the 1950s on several motorcycles from Moto Guzzi. Besides the beneficial stiffness-to-weight ratio, they offer the advantage that the tubes forming the triangulation can be adapted to different types of engines or motorcycles. The downside is the high production cost due to the numerous welded joints [27, p. 10-9].

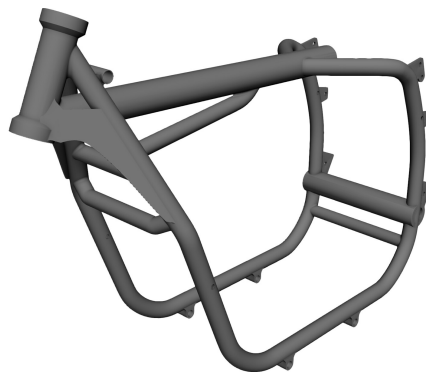


Figure 2.4: Example of a cradle frame from the BMW R80/R100 [58].

A decisive step towards stiffer frames was reached when the engine was used as a structural component. One of the first and most remarkable examples is the frame of the BMW K100 (1983) (Figure 2.5), where the frame was rigidly connected to the engine and provided support

only for the front fork, while the swingarm was directly connected to the engine itself [4, p. 342]. This construction was characterized by low total mass and high structural stiffness, as part of the stiffness was provided by the engine itself [27, p. 10-17]. However, because of this new configuration and increasing engine performance, some new high-speed instabilities appeared, such as kick-back (Section 2.2.1). It was understood that one of the reasons for this behavior was excessive stiffness, which reduces damping of the kick-back, thus favoring the occurrence of this dangerous phenomenon [49].

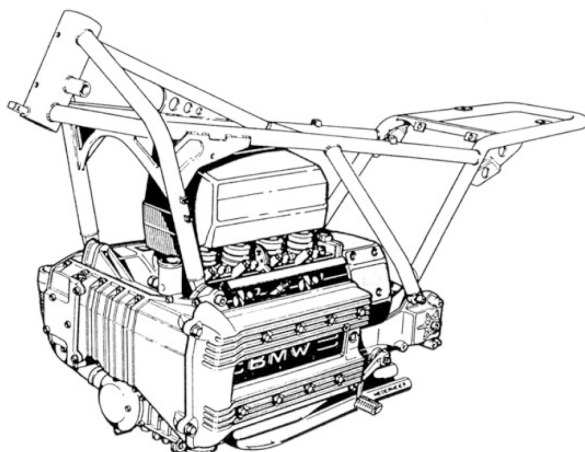
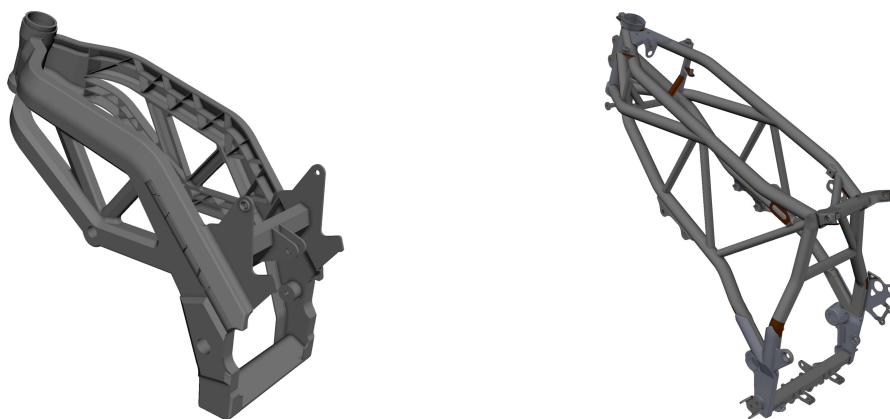


Figure 2.5: Frame of the BMW K100 [4].

Design solutions combining high stiffness and moderate mass were obtained when aluminum started to be adopted for the construction of motorcycle frames [27, p. 10-23], with the first examples presented in the 1980s, such as the Honda VFR from 1985. The general configuration, which has been then adapted to different motorcycle types, is characterized by two beams running on each side of the powertrain and joining the steering head joint to the swingarm pivot [27, p. 10-23]. This type of frame shows its advantages in terms of mass if the design is adapted to the intrinsic characteristics of aluminum [4, p. 333], [57], so that simply converting a frame made of steel to an identical version made of aluminum would not provide any mass advantages [27, p. 10-22]. The high stiffness reachable with aluminum frames is demonstrated by some reports about the Suzuki TL1000 (1997), which, similarly to the BMW K100, was affected by high-speed kick-back because of the excessive stiffness of its aluminum frame.



(a) Typical conformation of an aluminum frame.

(b) Triangulated steel frame from the KTM 950 Rally LC8.

Figure 2.6: Exemplary frames from modern motorcycles [58].

In modern motorcycles, aluminum frames are dominant thanks to the mass advantage and the capability to be adapted to different motorcycle types (Figure 2.6a). Moreover, triangulated steel frames employing the engine as a structural component are still used (Figure 2.6b), especially in some high-performance motorcycles, such as those from Ducati (e.g., the SuperSport) and KTM (e.g., the 1290 Super Duke). For the present thesis, it is particularly important to stress that motorcycle frames should include some compliance at determined points, which allows, for example, to ensure better road adherence when driving over road undulations [55], [27, p. 6-43] and to avoid dangerous high-speed kick-back phenomena. Knowing that, the designer should pursue an ideal distribution of the compliance, which would guarantee the desired dynamic properties with minimal mass.

Evolution of Front Fork Design over Time

The history of motorcycles shows several design solutions for the front fork. In this paragraph, only the solutions that are nowadays dominant on the market are considered; for an extensive review of all other types, the reader is referred to [4, 27]. The front fork must satisfy requirements on driving dynamics similar to the frame but, additionally, it must realize the desired suspension kinematics, which ensures good damping of road excitation and appropriate steering feedback under all driving conditions [4, p. 346]. This is why different design solutions for the front fork are mainly motivated by the attempt to achieve the required performances in terms of response to road excitation and during braking, accelerating, and steering [59, p. 32]. However, similar to the frame, achieving the desired stiffness was also one of the reasons for evolution: experimental tests in the 1960s demonstrated that a front suspension with insufficient stiffness would seriously impair the controllability when driving over road imperfections [59, p. 176].

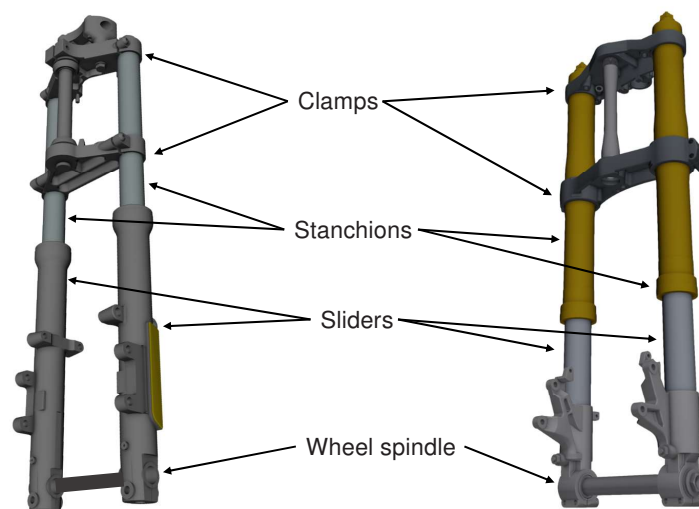


Figure 2.7: Types of telescopic forks: road-side-up (left) upside-down (right) [58].

The most common construction for the front fork is the telescopic fork. The traditional implementation, also called road-side-up (RSU), has a pair of stanchions fixed by two clamps and fitted over sliders with a bigger diameter that can slide on the two stanchions and are fixed together at the bottom by the wheel spindle [27, p. 7-2] (left side of Figure 2.7). Particularly in the first implementations, these forks were affected by low stiffness in the longitudinal and lateral directions, whereby low lateral stiffness may cause wobble instability phenomena at moderate speeds (Section 2.2.3). These problems have partially been solved in modern forks by increasing the diameter of the tubes. A relevant improvement was obtained with the introduction

of upside-down (USD) forks, where the smaller diameter tube is the slider and is connected to the wheel (right side of Figure 2.7). Due to the larger diameter of the stanchions and the longer sliders, upside-down forks have higher stiffness, thus partially solving the problems related to insufficient stiffness [4, p. 349]. Interestingly, one of the reasons for the dominance of telescopic forks in modern motorcycles is attributed to the aesthetic aspect rather than to engineering considerations [27, p. 7-2]. In fact, besides the potentially insufficient stiffness, telescopic forks are affected by a great amount of nose dive when braking [27, p. 7-3]; moreover, due to the rake angle, the vertical force applies a bending load to the tubes, thus causing stiction, which tends to clamp the fork [4, p. 349] and deteriorates the response over small bumps [27, p. 7-3].

To solve the problems of telescopic forks, motorcycle manufacturers have proposed several solutions, some of which found their way into the industry. An example is the Telelever presented by BMW in 1993 (Figure 2.8). It involves a structure similar to the telescopic fork. The main difference is the presence of a pivoted longitudinal arm that is connected to the sliders (lower fork) with a spherical joint; moreover, the stanchions (upper fork) are not rigidly connected to the fork bridge, but through spherical joints [4, p. 356]. This construction solves several problems of the telescopic fork: it realizes an anti-dive function when braking and the presence of the longitudinal arm strongly increases lateral stiffness [4, p. 356].

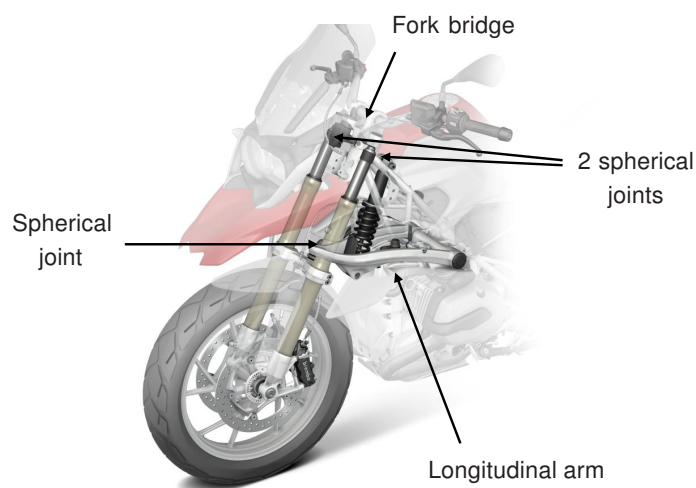


Figure 2.8: BMW Telelever system. Picture modified from [60].

Other constructive solutions named double-link suspensions have been implemented as alternative to the telescopic fork. The different examples can be found in [27, p. 7-18]; in this construction, the tubes that characterize the telescopic fork and the Telelever are missing and the front wheel is carried by a wheel carrier, which itself is connected to the main frame with two pivoted arms. Steering is realized with a link between the handlebar and wheel carrier, which can steer thanks to spherical joints on the pivoted arms [27, p. 7-19]. Modern examples of this front suspension are the Duolever system by BMW (2004) (Figure 2.9) and the front suspension of the Honda Gold Wing starting from the model year 2018. In the double-link suspension, the wheel carrier ensures high structural stiffness. Moreover, thanks to the support of two longitudinal arms and a small lever arm between the front tire contact point and the pivoted arms, the support structures on the main frame can be lighter [4, p. 358]. Finally, the presence of two pivoted arms allows for the precise implementation of the desired suspension kinematic. These advantages are contrasted by high implementation costs due to the high number of links; therefore, this front suspension is suitable only for upper-class motorcycles.

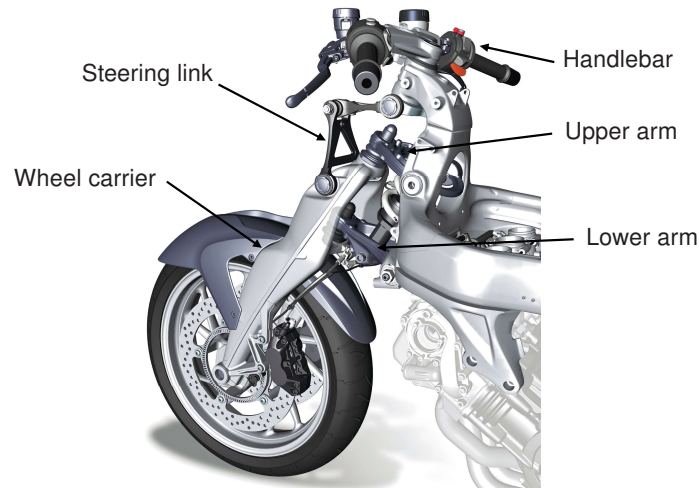


Figure 2.9: BMW Duolever system. Picture modified from [61].

Evolution of Swingarm Design over Time

The last important structural component of motorcycles is the swingarm, which must ensure precise guiding of the rear wheel and the desired suspension travel [4, p. 363]. In this case, the different constructive solutions do not differ much throughout the years; the two variations that can be found are the two-sided and the single-sided swingarm [27, p. 8-19]. In both cases, the evolution of design has led to increasing overall stiffness to avoid undesired steer and camber variations of the rear wheel that would be detrimental to handling [4, p. 366]. However, as explained above, in the last years, chassis stiffness has reached a level that may cause problems with bump absorption when cornering and this has brought some manufacturers to reintroduce some targeted compliance [27, p. 8-16].

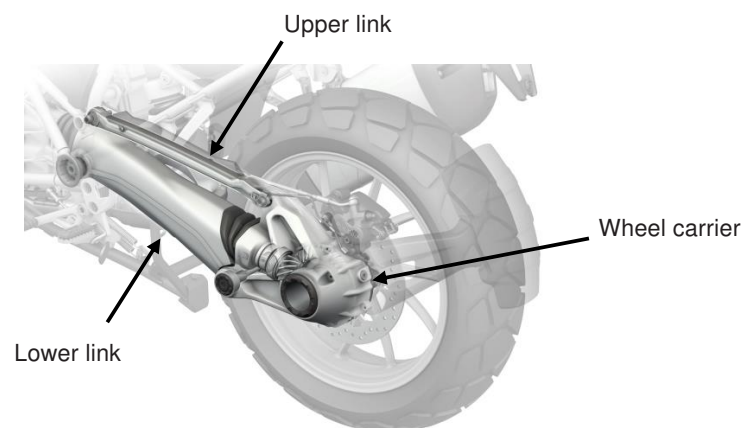


Figure 2.10: BMW Paralever system. Picture modified from [60].

In terms of achievable stiffness, two-sided and single-sided swingarms are equivalent, given that an appropriate design is chosen [27, p. 8-25]. The two swingarm types have been coupled with both chain and shaft drive. In modern motorcycles, however, the two-sided swingarm is coupled almost exclusively with the chain drive, while the single-sided can be found on motorcycles with either chain or shaft drive. The most significant variations for both swingarms were motivated by the attempt to achieve the anti-squat effect, i.e., to counteract the tendency of the motorcycle's back to lift when accelerating, or to realize a progressive spring rate. For the

anti-squat behavior, the single-sided swingarm has been extended with an additional link and the wheel carrier is connected to the two arms with revolute joints, whereby the swingarm becomes a four-bar linkage [4, p. 386]. An example is the Paralever from BMW (1988) (Figure 2.10). In motorcycles with chain drive, anti-squat can be realized by adjusting the relative position of the pinion center and the swingarm pivot [18, p. 210]. The progressive spring rate can be obtained with a rocker system, whereby the spring-damper element is connected to a rocker arm, which itself is connected to the swingarm and, thanks to appropriate dimensions of the rocker's arms, different leverage ratios between wheel travel and compression/extension of the spring-damper element can be obtained [27, p. 8-5].

Importance of Structural Design in the Development of Motorcycles

This overview shows that chassis stiffness strongly affects motorcycle dynamics and that it significantly motivated the evolution of chassis design. An important statement is made in [27, p. 8-25] and [56]: a good general rule is to balance the stiffness between the chassis components, meaning that it is pointless to have, for example, an extremely stiff swingarm mounted on a flexible frame. Moreover, as explained above, a common trend in chassis design is to include some targeted flexibilities, which avoids high-speed instability problems and allows for better traction when accelerating out of a curve on bumpy roads.

All these considerations demonstrate the need for a methodology to study the influence of chassis flexibilities on motorcycle dynamics. This would allow not only to easily include targeted flexibilities on chosen structural components but also to improve structural design, thus reducing mass. The development and application of this methodology are described in Chapter 4, where the focus is to study the effect of flexibility on the weave and wobble eigenmodes and to derive a structural design that optimizes their stability.

The following section reviews studies on the influence of the flexibilities of chassis components on the stability of the motorcycle with a particular focus on weave and wobble eigenmodes, which are the phenomena of interest in the present thesis.

2.2.3 Influence of Structural Flexibilities on Weave and Wobble

The previous section showed that the attempt to achieve the desired stiffness properties played a determining role in the evolution of structural design. Therefore, with the objective of understanding which level of stiffness should be aimed for, several works studied the influence of chassis stiffness on motorcycle stability. A common factor is the use of the so-called lumped stiffness approach to model elastic deformations. In this approximation, the stiffness is concentrated on a joint that connects two rigid bodies. In the following paragraphs, the works analyzing the influence of stiffness of the frame, front fork, and swingarm on weave and wobble are summarized.

Frame Flexibility

Since the frame represents the connecting element between the front and rear assembly, its flexibility turned out to highly influence motorcycle dynamics. Several works only consider the frame torsional flexibility at the steering head joint, which is modeled with a lumped stiffness characterized by a revolute joint on the steering head joint with its rotation axis perpendicular to the steering axis [17, 28, 38, 50, 51, 62, 63]. The effect of such a lumped stiffness is to let the

contact point of the front wheel move laterally, similar to the motion caused by the fork bending stiffness.

For example, Cossalter et al. [64] state that both frame twisting and lateral fork deformation should be included when studying wobble. Similarly, Pacejka et al. [21, p. 531] and Sharp et al. [65] underline how the inclusion of frame stiffness is necessary when simulating wobble. Sharp et al. [38] show with simulations that high-speed weave is compromised by a reduction in frame torsional stiffness. Moreover, the wobble problem is transferred from high speeds to medium speeds by this change. Roe et al. [9] carried out experiments to identify the effect of lateral and torsional stiffness of the frame: starting with a standard production frame from the 1980s, they state that increasing torsional stiffness is beneficial for wobble and does not greatly influence weave, which, instead, is positively affected by increasing lateral frame stiffness. Similarly, Kane [7] states, based on experiments, that increasing flexural stiffness of the frame was beneficial for attenuation of weave.

Besides the effect on weave and wobble, Bocciolone et al. [55] explain that frame torsional flexibility is important for driving dynamics because it absorbs the road excitation not directed towards the suspension system. This situation may occur, for instance, when driving on road undulations with a large roll angle. A somehow connected observation is given by Roe et al. [9]: they observe that too high frame torsional stiffness should be avoided because it makes the motorcycle “chop” sideways when cornering at high speeds over a bumpy road. Similarly, Lake et al. [29] underline that the frame should be as stiff as possible in torsion to guarantee high weave stability but potentially compliant in bending.

Doria et al. [66] leverage on the identification of the twist axis [67] for parameterizing a lumped stiffness model of the frame. The authors distinguish between static and dynamic deformation axis: they are in general different, so tuning the lumped stiffness model only while considering the static twist axis could introduce an error.

Front Fork Flexibility

Several works investigated the effect of bending flexibility of the front fork on weave and wobble [23, 41, 52, 64, 68–71]. They have in common the modeling of flexibility with a lumped stiffness using a joint along the fork and with its rotation axis perpendicular to the steering axis. These studies show that, while the weave mode is hardly affected, the wobble mode strongly correlates with fork stiffness. Spierings [41] notes that, while with low fork lateral bending stiffness, wobble damping shows a minimum in lower speed ranges (40 km h^{-1} to 80 km h^{-1}), when increasing this stiffness, wobble damping is lower in high-speed ranges. Similar results were obtained with simulations in [28] and experimentally in [56]. Spierings [41] recommends a value for the lumped stiffness used to model the fork bending stiffness between $100 \text{ kN m rad}^{-1}$ and $150 \text{ kN m rad}^{-1}$. He also states that motorcycles in those years (the 1980s) had a front fork with lateral bending stiffness of only about 35 kN m rad^{-1} . This could explain the trend of producing stiffer forks, as mentioned in Section 2.2.2.

Cossalter [23] and Spierings [41] motivate the particular influence of fork stiffness considering the gyroscopic moment caused by the additional motion that the front wheel has when modeling the lateral bending stiffness of the fork. In particular, this moment has a stabilizing action on the wobble; since the gyroscopic moment increases with speed, the presence of this moment motivates the higher stability of the wobble at high speeds when the lateral bending stiffness of the fork is lowered.

Cossalter et al. [64] provide another possible explanation for the correlation between wobble damping and lateral bending stiffness of the fork. By analyzing the structural modes of the whole motorcycle, it was noted that the first eigenmode, which is dominated by the lateral deformation of the front fork, has an eigenfrequency of only 12 Hz higher than the wobble eigenfrequency. For this reason, the fork lateral stiffness is likely to influence the wobble mode.

Few works analyzed the isolated influence of the torsional flexibility of the front fork. Only Sharp et al. [28] report a minor influence of this flexibility on weave and wobble.

As stated by Doria et al. [72], the position of the revolute joint used to model fork lateral bending stiffness with the lumped stiffness approach is a key factor. With the aim of better approximating the flexural behavior of the front fork while using the lumped stiffness approach, Doria et al. [68] start from an experimental modal analysis of the front assembly of a bicycle and use the collected data to tune a lumped stiffness model. The value obtained is verified using a static test, obtaining a good accordance. In the attempt to parameterize the lumped stiffness model of the front fork, Cossalter et al. [73] apply the concept of the twist axis [67] to the front fork. They discover that the twist axis changes when obtaining it with static or dynamic tests. For this reason, they propose three different models for the fork stiffness, which take into account the static, the dynamic, and a “mixed-approach” twist axis. The models using the static and “mixed-approach” twist axis show a similar influence on the stability of weave and wobble, while the the model using the dynamic twist axis is more similar to the rigid case.

Swingarm Flexibility

The swingarm connects the rear wheel to the main frame. Similarly to the front fork and frame, its stiffness has been observed to influence the stability characteristics of motorcycles [23, 52, 74].

Cossalter et al. [23, 52] simulate the swingarm torsion and bending with lumped stiffnesses. They discover that low values of these stiffnesses have a destabilizing effect on the weave, particularly at medium and high speeds. This effect is explained considering the gyroscopic couple caused by the additional motion of the wheel due to the flexibilities. Similarly, Limebeer et al. [75] report that the swingarm flexibility has little influence on wobble but destabilizes weave.

With the same procedure used in [66, 73], Taraborrelli et al. [74] use the twist axis method to identify the parameters for a lumped stiffness model of the swingarm. The study was applied to two motorcycles: a sports and an enduro motorcycle. The influence of the swingarm stiffness changed for the two motorcycles: it has almost no influence on the sports motorcycle, while in the enduro motorcycle, high torsional stiffness stabilizes the weave, and high bending stiffness destabilizes it.

While the previous works analyze swingarm stiffness with the lumped stiffness approach, Ferretti et al. [76] model the swingarm as a flexible body (Section 2.3.2). Simulation shows that, when driving over road imperfections, a flexible swingarm causes an unstable motorcycle oscillation that was not present in the rigid case.

2.3 Motorcycle Modeling in Multibody Simulation

The first works on motorcycle dynamics date back to the end of the 19th century, to the works of Whipple [77] and Carvallo [78], followed by the famous work of Sharp [79]. These are based on “handwritten” analytical motorcycle models. To limit complexity, some simplifying assumptions had to be made: the rider is rigidly attached to the main frame, the wheels are rigid discs, the DOFs related to the suspensions are not modeled, and only small perturbations from straight running are considered. While these models can capture the basics of motorcycle dynamics, the strong simplifications lead to a significant difference between model and reality.

With increasing availability of computational power, motorcycle models have been improved to better match reality. In this context, Multibody Simulation (MBS) has become a common tool for studying vehicle dynamics [80]. MBS gives the possibility to reproduce complex mechanical systems by specifying only the mass and inertia properties of the bodies involved, the joint types that constrain the relative motion, and the force elements, which may be external forces or interactions between bodies [81]. The equations of motion are generated internally by the MBS software and solved with numerical integration methods [82, chap. 7]. This way, the unknown internal joint forces are determined and the resulting time evolution of the system state variables is calculated.

In general, MBS software is either numerical or symbolic. Numerical software prepares equations in numeric form only, solves them, and post-processes them [83]. Symbolic software simply produces equations and it needs to be coupled with a numerical processing package to solve the equations [83]. Commercial software is available for both numerical and symbolic formalism: Adams [84], Simpack [85], Bikesim [86], and Simscape [87], which is the MBS library of Matlab-Simulink, are the most famous exponents of the numerical MBS software. Autolev [88], Autosim [89], Mesa-Verde [90], and Neweul [91] are some examples of symbolic MBS software. The present thesis uses a numerical open-source MBS software called MBSim (www.mbsim-env.de) [92].

The first works using the MBS formalism to study the dynamics of single-track vehicles were published in the 1990s [49, 93]. MBS allowed to significantly increase the accuracy of motorcycle models, as representative works in this field show [38, 52, 94]. The most relevant improvements were achieved in rider modeling [95–101], the tire model (next paragraph and Section 4.1), and modeling of structural stiffnesses (Section 2.2.3).

The most widespread tire model in the simulation of motorcycle dynamics is the Pacejka Magic Formula. It has been adapted in [44] to include the effect of the camber angle in the generation of tire forces, which is necessary when modeling motorcycles tires. The Magic Formula has been then continuously updated up to its most recent version [21]. This model, which neglects belt dynamics, is suitable to model tire phenomena with a frequency lower than about 15 Hz [39, 75]. Also, in these conditions, the tire lag phenomena can be described by first-order dynamics [75]. Lot [102] proposes a physical tire model as an alternative model to the Pacejka Magic Formula—which is an empirical tire model—where tire lag is implicitly accounted for, so no additional relaxation equations are needed.

For higher frequencies, other models have been implemented that account for belt dynamics. An example is “MF-SWIFT 6.2”, which can handle frequencies up to 60-80 Hz, and is, therefore, suitable for comfort studies or for modeling braking maneuvers with anti-lock systems [21, p. 587]. The advantage of this model is that the steady-state forces are still calculated with the Magic Formula while the belt dynamics are accounted for with the rigid ring model. In this model, a rigid ring, representing the belt, is connected to the rim and contact patch through a series of spring

damper elements, thus enabling the belt's relative motion [21, p. 588]. In [103], the rigid ring tire model is used for studying motorcycle dynamics and in [104] a test procedure is developed to find a parameterization of the rigid ring tire model.

Further literature reviewing the development of motorcycle modeling can be found in [19, 105] and, regarding the development of models suited for control purposes, in [11, 106, 107].

Thanks to the progress in modeling tools, it was possible to study the effect of structural stiffness on motorcycle dynamics. In particular, a remarkable effect has been noted on the weave and wobble eigenmodes. Two modeling approaches have been established for modeling structural flexibilities: the lumped stiffness approach and the flexible multibody approach, also called Elastic Multibody Simulation (EMBS). These two approaches are one of the central points of this thesis and are therefore presented in the next two sections.

2.3.1 Modeling of Flexibility: Lumped Stiffness Approach

The lumped stiffness approach is the most basic solution to include flexibility in MBS. It consists of approximating the flexural behavior of a structure with one lumped stiffness parameter [32]. This approach has been extensively adopted for studying the influence of structural flexibilities on the stability of motorcycles (Section 2.2.3). In the present section, the general concepts behind the lumped stiffness approach are presented.

Considering the simple example of a cantilever beam in Figure 2.11, a lumped stiffness model of its bending flexibility about the z-axis can be derived as follows. The original continuous beam is split into at least two bodies that are connected by a revolute joint with its rotation axis parallel to the z-axis and a rotational spring-damper element associated to it. This way, the continuous deformation shape is approximated with a piecewise linear deformation shape. In particular, the motion of the body with the free end can be described with the equation of a 1-DOF oscillator about the equilibrium [32, p. 12]:

$$J\ddot{\theta} + d\dot{\theta} + k\theta = Fl, \quad (2.9)$$

where, instead of the classical formulation with the translation DOF, the equivalent for the rotational DOF θ is used. J is the inertia of the moving body about the rotation axis of the revolute joint; d, k are the rotational damping and stiffness associated the revolute joint. (2.9) describes the linear elastic equation with the assumption of viscous damping; general nonlinear oscillators can be modeled by substituting the damping and stiffness terms with a generic nonlinear function $f(\dot{\theta}, \theta)$ [108, p. 35].

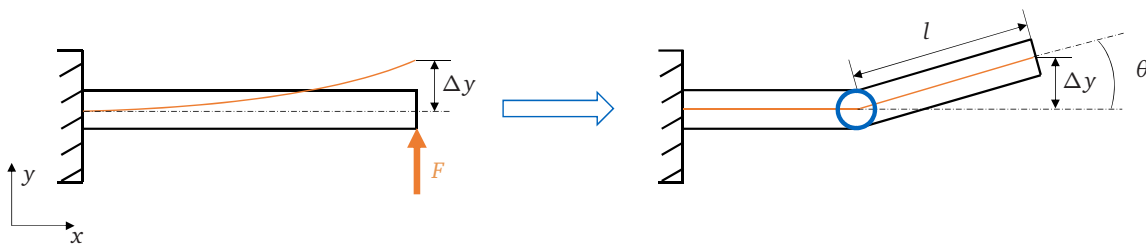


Figure 2.11: Lumped stiffness approach for modeling the bending of a beam.

Lumped stiffness models aim to approximate the displacement Δy of the free end caused by the load F [68]. The quality of the approximation depends on the parameters used to build the model itself. These involve the parameters in (2.9), whereby J and d influence the dynamic

response of the model, while k impacts both dynamic and static responses. Methods have been proposed for identifying the lumped stiffness parameters of structural components, e.g., in [66, 68, 72–74, 109] and in Section 4.3.

The example in Figure 2.11 can be extended to model the torsional flexibility of the beam [32, p. 6]; moreover, it is possible to split the continuous body into more bodies, thus better approximating the deformation shape of the continuous beam [32, p. 297] at the cost of increasing the number of DOFs.

Lumped stiffness models have the great advantage of limited modeling effort and complexity, which also lead to short computational time. However, as shown in Figure 2.11, the actual deformation shape of the original structure is strongly approximated, which limits the accuracy of this approach. Moreover the accuracy strongly depends on the method used for parameterizing the model itself. The requirements of higher accuracy and the desire to overcome this parameterization effort have led to the development of more complex approaches for modeling the stiffness in an MBS environment, which are explained in the next section.

2.3.2 Modeling of Flexibility: Elastic Multibody Simulation (EMBS)

EMBS is an extension of the classical theory of MBS, which only considers rigid bodies, for applications where the elastic deformations within bodies cannot be neglected [81]. EMBS gives the possibility to introduce flexible bodies in the standard MBS. Different formulations have been proposed to extend the theory of MBS: the Consistent Rotation-Based Formulation (CRBF), the Absolute Nodal Coordinate Formulation (ANCF), and the Floating Frame of Reference Formulation (FFRF). The first two formulations are developed to model flexible bodies undergoing large elastic deformations [110]. The FFRF, instead, is suitable for modeling flexible bodies whose motion is dominated by large nonlinear rigid body motions while they undergo only small elastic deformations [111, 112]. The present thesis investigates the influence of the flexibility of structural components on the weave and wobble eigenmodes of motorcycles. These components are likely to undergo small deformations while they have to “follow” the large nonlinear motions of the motorcycle itself. Therefore, the FFRF is well suited for the present study and is explained in more detail.

In the FFRF, a so-called Floating Frame of Reference (FFR) K_{FFR} is defined that is attached to the flexible body itself (Figure 2.12). Using this reference frame, the motion of each point of the flexible body is described through the superposition of two components [76, 111–115]: the nonlinear rigid body motion is described by the vector \mathbf{q}_{rbm} , which represents the displacement of the FFR with respect to the inertial frame K_I [115, 116]; the small elastic displacements of each point of the body—i.e., the nodal displacements—are instead expressed with respect to the FFR by the vector \mathbf{q}_e [112, 116]. Some constraints have to be specified for attaching the FFR to its flexible body to ensure that the description of the nodal elastic displacements is unique [115–117]. Different methods are available, briefly summarized thereafter.

- *Principal-axis frame*: this approach ensures that the kinetic energy resulting from the elastic deformations is minimal [118, p. 326], which is equivalent to saying that the elastic deformation is minimized [117, 119]. With this method, the FFRF has the origin in the center of mass and its axes are oriented so that the inertia matrix of the deformable body is diagonal [111].
- *Tisserand or mean-axis frame*: this approach is a simplification of the principal-axis frame where the internal momentum and angular momentum are zero for

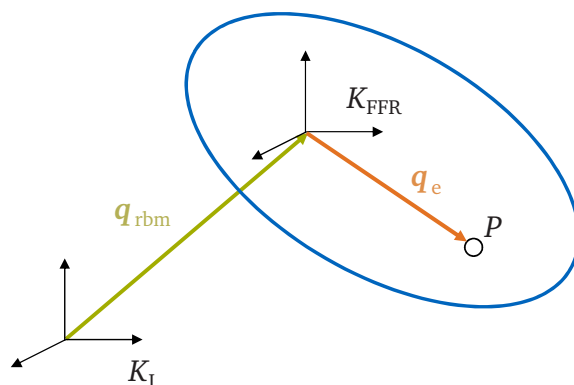


Figure 2.12: Representation of the motion of a flexible body with the FFRF.

every deformation of the body [118, p. 325]. The formulation of the Tisserand frame is valid in general. Its equivalent for small displacements is called Buckens frame [118, p. 326]. Both Tisserand and Buckens frames require the introduction of dynamic constraints on the nodal displacements [118, p. 325]. It has been shown—e.g., in [118, p. 326]—that these constraints are automatically fulfilled when the ansatz function for describing the nodal displacements are eigenmodes of the unconstrained structure where the rigid body modes have been eliminated.

- *Reference Conditions (RC) method*: in this case, the FFR is fixed to the flexible body by specifying kinematic constraints [81]; this way, the FFR is fixed to a node. A fundamental distinction should be made between boundary conditions and RC. Boundary conditions are used in the simulation (MBS or Finite Element Method (FEM)) to define the topology of the assembled mechanical system and are used to remove the relative DOFs between the bodies [120]. RC, instead, define the shape of deformation with respect to the FFR by eliminating the rigid body modes of the flexible body [121] and are used to attach the FFR to its flexible body. Therefore, they do not introduce any constraint that restricts the gross motion of the flexible body [120]. The main difficulty in using the RC is that there is not a general set valid for every application [120, 121]. However, some general guidelines are available. The use of labile RC, i.e., RC that do not eliminate all the rigid body modes, is discouraged [120], as it introduces some spurious modes in the system that compromise the quality of the numerical solution [121]. Isostatic RC generally provide good results. However, Cammarata et al. [120] showed that, for some applications, hyperstatic RC provide more accurate results. The decision whether to use isostatic or hyperstatic RC should be made according to the use-case, keeping in mind that the introduction of hyperstatic RC makes the flexible body stiffer. An application example is shown in Section 4.2.

In multibody simulations, the most common approaches are the Tisserand-Buckens frame [117, 122] and the RC [120, 121] method. The present thesis adopts both methods and compares them in Section 4.2

Model Order Reduction (MOR)

Before including a flexible body in MBS by using the theory of EMBS, the flexible body itself must be modeled. Generally, this is done with FEM [32, 118]. However, the resulting model has

a large order—up to 10^6 for some industrial applications [117]—and cannot be directly integrated into the MBS environment because the resulting computational time would make the MBS model unusable [114, 123]. For this reason, Model Order Reduction (MOR) techniques are used. Figure 2.13 visualizes the steps needed to include a flexible body in an MBS environment: after modeling the flexible body with FEM, the number of DOFs is reduced with MOR; at this point, the obtained reduced-order model can be introduced into the MBS environment by applying one of the formulations presented at the beginning of Section 2.3.2.

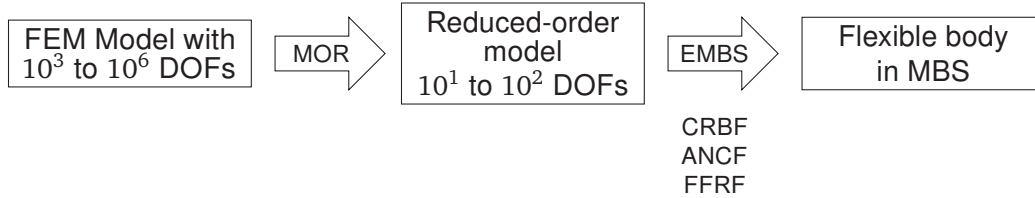


Figure 2.13: Steps for including a flexible body in an MBS environment.

The aim of MOR is to produce a reduced-order model that accurately approximates the behavior of the original system for the desired use-case [108, p.37]. In structural mechanics, the elastic deformations of a body are described by a second-order system. By assuming small displacements around the equilibrium and making the hypothesis of viscous damping, the equations of the elastic body can be written as (2.10) [108, p. 35]. These hypotheses will be valid for the structures considered in the present thesis because the structural components of motorcycles are only subjected to small deformation and their damping behavior can often be approximated with viscous damping.

$$\mathbf{M}_e \ddot{\mathbf{q}}_e(t) + \mathbf{D}_e \dot{\mathbf{q}}_e(t) + \mathbf{K}_e \mathbf{q}_e(t) = \mathbf{B}_e \mathbf{u}(t), \quad (2.10a)$$

$$\mathbf{y}(t) = \mathbf{C}_{q_e} \mathbf{q}_e(t) + \mathbf{C}_{\dot{q}_e} \dot{\mathbf{q}}_e(t). \quad (2.10b)$$

The behavior of the mechanical system (2.10) can be interpreted also considering its transfer function, which can be obtained by applying the Laplace transform on (2.10) [108, p. 36]:

$$\mathbf{G}(s) = (\mathbf{C}_{q_e} + s\mathbf{C}_{\dot{q}_e})(s^2\mathbf{M}_e + s\mathbf{D}_e + \mathbf{K}_e)^{-1}\mathbf{B}_e. \quad (2.11)$$

$\mathbf{q}_e(t) \in \mathbb{R}^N$ is the vector of the elastic displacements. $\mathbf{y}(t) \in \mathbb{R}^r$ is the output vector, $\mathbf{u}(t) \in \mathbb{R}^p$ is the input vector, and the matrix $\mathbf{B}_e \in \mathbb{R}^{N \times p}$ captures the distribution of the loads [113]. The matrices $\mathbf{C}_{q_e}, \mathbf{C}_{\dot{q}_e} \in \mathbb{R}^{r \times N}$ are the output matrices considering displacements and velocities, respectively [108, p. 36].

In structural mechanics, projective MOR is common, where a projection matrix $\mathbf{V} \in \mathbb{R}^{N \times n}$ is identified that projects the original system (2.10) with order N into a subspace with order $n \ll N$ [113]:

$$\mathbf{q}_e(t) \approx \mathbf{V} \hat{\mathbf{q}}_e(t), \quad (2.12)$$

where $\hat{\mathbf{q}}_e(t) \in \mathbb{R}^n$ is the reduced-order vector of elastic displacements.

By substituting (2.12) in (2.10) and left multiplying (2.10a) by \mathbf{W}^T to have a square system, the reduced-order equations are obtained:

$$\hat{\mathbf{M}}_e \hat{\ddot{\mathbf{q}}}_e(t) + \hat{\mathbf{D}}_e \hat{\dot{\mathbf{q}}}_e(t) + \hat{\mathbf{K}}_e \hat{\mathbf{q}}_e(t) = \hat{\mathbf{B}}_e \mathbf{u}(t), \quad (2.13a)$$

$$\mathbf{y}(t) = \hat{\mathbf{C}}_{q_e} \hat{\mathbf{q}}_e(t) + \hat{\mathbf{C}}_{\dot{q}_e} \hat{\dot{\mathbf{q}}}_e(t), \quad (2.13b)$$

with the reduced matrices:

$$\{\hat{M}_e, \hat{D}_e, \hat{K}_e\} = W^T \cdot \{M_e, D_e, K_e\} \cdot V, \quad \{\hat{M}_e, \hat{D}_e, \hat{K}_e\} \in \mathbb{R}^{n \times n}, \quad (2.14a)$$

$$\hat{B}_e = W^T B_e, \quad \hat{B}_e \in \mathbb{R}^{n \times p}, \quad \hat{C}_{\dot{q}_e} = C_{\dot{q}_e} V, \quad \hat{C}_{q_e} = C_{q_e} V, \quad \hat{C}_{\dot{q}_e}, \hat{C}_{q_e} \in \mathbb{R}^{r \times n}. \quad (2.14b)$$

(2.13) is valid if the Petrov-Galerking conditions $W^T r(t) = \mathbf{0}$ are satisfied, which means that the residual $r(t)$ vanishes [108, p. 37]. If $W = V$, the projection is called one-sided, as opposed to the two-sided projection where $W \neq V$ [124]. The one-sided projection preserves the passivity and structure of the original model [108, p. 38].

There are several methods for MOR, and one possible way to categorize them is according to the field in which they are commonly adopted. Depending on the application, different requirements to the MOR methods can be formulated:

- In structural mechanics, the models to be reduced have second-order form and, therefore, the MOR methods have to preserve the structure. This way, the sparsity pattern is kept and the original system preserves its physical meaning, thus facilitating the usage of the reduced-order model in further simulation programs, such as MBS [117]. Another important consideration is that in the study of mechanical systems, the global behavior of the system has to be considered, which also includes its frequency response [124]. For this reason, the most common MOR methods act in the frequency domain by projecting the original model into the subspace of its eigenmodes. Modal truncation [125] and Component Mode Synthesis (CMS) [126, 127] belong to this category.
- In control engineering and in the design of large electronic circuits, the system equations are generally described by a state space formulation, i.e., a first-order system [124]. Therefore, the MOR methods have to deal with a different structure with respect to mechanical systems. Moreover, the aim of MOR is to approximate the input-output behavior or, in other words, the transmission of energy between the input and the output, while the global behavior is not directly considered [108, p. 38], [124, 128]. Finally, in particular for control systems, the stability of the original system must be preserved after reduction [124]. The most common methods for MOR in these fields are balanced truncation (also called Singular Value Decomposition (SVD)-based methods) [129, 130] and moment matching (also called Krylov subspace methods) [131, 132].

This differentiation between structural mechanics and control engineering should not be understood as a strict division. Some works successfully applied SVD-based and Krylov subspace methods to MOR of second-order systems [113, 114, 119, 132, 133]. The idea behind this is that mechanical systems can also be regarded as input-output systems, whereby the inputs are external forces and the outputs are, for example, displacements. These methods present some advantages that make them interesting for application in structural mechanics.

Krylov subspace methods have high computational efficiency thanks to their recursive nature, which involves mainly basic linear algebra operations [114, 132]. The disadvantage of Krylov subspace methods is that the reduction quality strongly depends on the choice of the expansion points [117, 134], i.e., the frequencies at which the transfer function of the original model are exactly approximated in the reduced-order model [135]. Moreover, the Krylov reduction is challenging for systems with many inputs and outputs [113, 128].

Balanced truncation is attractive for the possibility of having an a-priori bound of the reduction error [113, 119, 130] but presents the disadvantage of high computational effort because it

requires the expensive computation of Gramian matrices and the solution of Lyapunov equations [114, 124].

Another challenge in using these methods for MOR of mechanical systems is that they were originally developed to be applied to first-order systems. The application of these methods on second-order systems would require reformulating the second-order equations in (2.10) into a first-order state space formulation [108, p. 36], [133, 136]. However, this would destroy the second-order structure, and coming back to the second-order formulation after MOR is not always possible [133, 137].

For this reason, solutions have been proposed to adapt balanced truncation and Krylov subspace methods to work directly on the second-order formulation: MOR of second-order systems with Krylov subspace methods is addressed in [133, 136, 138], which proposed the so-called SOAR algorithm (second-order Arnoldi), and in [117, 139], where the SOGA (second-order Global Arnoldi) algorithm is shown. MOR of second-order systems with balanced truncation is tackled in [140–142]. Moreover, in [128, 143], methods to calculate approximated second-order Gramians are proposed; this allows to apply balanced truncation on second-order systems with larger dimensions.

Both Krylov subspace and balanced truncation methods have been extended into their first-order formulation for automated MOR, whereby the order of the reduced-order model is determined by the reduction process itself and the user only has to specify the maximum allowed error; the paragraph below on reduction error describes the error measures. Balanced truncation naturally lends itself to automated MOR thanks to the presence of a global error bound [144]. As mentioned above, Krylov subspace methods offer higher computational efficiency but the reduction quality depends on the choice of expansion points. For carrying out automated MOR with Krylov subspace methods, Gugercin et al. [135] propose the algorithm IRKA (Iterative Rational Krylov Algorithm), where the expansion points are determined iteratively, leveraging on an idea first proposed by [132]. It has been demonstrated that, under certain conditions, the algorithm converges to an \mathcal{H}_2 -optimal solution, which means that the \mathcal{H}_2 norm of the error between the transfer functions of the original and reduced-order model is minimum.

Authors have also studied the application of automated MOR with Krylov subspace methods on second-order systems. In [145], the SO-IRKA is proposed, which extends the IRKA algorithm to the second-order formulation. Similarly, in [117], methods are developed for the automated selection of expansion points in second-order Multi-Input-Multi-Output (MIMO) systems, which allows to apply automated MOR with the Krylov subspace methods to second-order systems. Druskin et al. [146, 147] propose an alternative method to IRKA called adaptive tangential interpolation, where the Krylov subspace is built iteratively by positioning the next expansion point at the frequency where the reduction error is maximal.

In Section 4.2, MOR with CMS is carried out, and, for this reason, this method is explained in more detail in the next paragraph. In particular, the Craig-Bampton method and some of its extensions will be summarized.

Craig-Bampton Method

Mechanical structures are generally composed of several bodies or substructures. It could therefore be convenient to perform model reduction on the separated bodies and thereafter re-assemble the reduced-order bodies into the original structure. This procedure is called substructuring [115, 148, 149].

The Craig-Bampton method [127] is based on this concept and is widely used in the industry for MOR of models generated with FEM. An important step in the Craig-Bampton method is

the separation of the vector \mathbf{q}_e of the elastic DOFs in boundary \mathbf{q}_b and internal \mathbf{q}_i DOFs. The boundary DOFs represent the DOFs where the connections to the other subsystems are present or where the external forces are applied. To ensure inter-component compatibility and, this way, approximate the particular solution of the original system, constraint modes are used [113]. Constraint modes result from static condensation (also called Guyan condensation [126]), where the internal DOFs \mathbf{q}_i are projected onto the boundary DOFs \mathbf{q}_b . Constraint modes can be interpreted as the deformation that would occur in the body if one boundary DOF was subjected to a unit displacement, with all other boundary DOFs fixed and all interior DOFs left unconstrained. The concept can be mathematically expressed as follows.

The partition of the DOFs between interior and exterior leads to (2.15), where the time dependence has been omitted and an undamped system is shown. Moreover, it is assumed that no forces are applied on \mathbf{q}_i [150].

$$\begin{bmatrix} \mathbf{M}_{bb} & \mathbf{M}_{bi} \\ \mathbf{M}_{ib} & \mathbf{M}_{ii} \end{bmatrix} \cdot \begin{bmatrix} \ddot{\mathbf{q}}_b \\ \ddot{\mathbf{q}}_i \end{bmatrix} + \begin{bmatrix} \mathbf{K}_{bb} & \mathbf{K}_{bi} \\ \mathbf{K}_{ib} & \mathbf{K}_{ii} \end{bmatrix} \cdot \begin{bmatrix} \mathbf{q}_b \\ \mathbf{q}_i \end{bmatrix} = \begin{bmatrix} \mathbf{f}_b \\ \mathbf{0} \end{bmatrix}. \quad (2.15)$$

The internal DOFs \mathbf{q}_i can be split into two contributions:

$$\mathbf{q}_i = \mathbf{q}_{i,stat} + \mathbf{q}_{i,dyn}. \quad (2.16)$$

By neglecting the inertia forces in the second row of (2.15), one obtains:

$$\mathbf{q}_{i,stat} = -\mathbf{K}_{ii}^{-1} \mathbf{K}_{ib} \mathbf{q}_b. \quad (2.17)$$

At this point, the static condensation is obtained by neglecting $\mathbf{q}_{i,dyn}$:

$$\begin{bmatrix} \mathbf{q}_b \\ \mathbf{q}_i \end{bmatrix} = \mathbf{V} \mathbf{q}_b = \begin{bmatrix} \mathbf{I} \\ \mathbf{S} \end{bmatrix} \mathbf{q}_b, \quad \mathbf{S} = -\mathbf{K}_{ii}^{-1} \mathbf{K}_{ib}. \quad (2.18)$$

\mathbf{V} is the reduction matrix introduced in (2.12). At this point, the system (2.15) can be expressed in the reduced form as:

$$\hat{\mathbf{M}} \hat{\mathbf{q}}_b + \hat{\mathbf{K}} \hat{\mathbf{q}}_b = \hat{\mathbf{f}}_b. \quad (2.19)$$

As mentioned above, the system is reduced by projecting the internal DOFs \mathbf{q}_i onto the boundary DOFs \mathbf{q}_b .

This type of reduction is acceptable if applied to a static problem or if the highest eigenfrequency of interest is much smaller than the smallest eigenfrequency of the substructure [150]. In multibody simulations, however, this is often not the case. For this reason, Craig-Bampton methods also consider dynamic behavior in the reduction process. This is done by approximating the system eigendynamics with fixed boundary DOFs, thus obtaining the so-called fixed interface modes [127]. The projection matrix \mathbf{V} in (2.18) is extended as follows. First of all, the eigenvalue problem with fixed boundary DOFs must be solved:

$$\mathbf{K}_{ii} \mathbf{q}_i = \omega^2 \mathbf{M}_{ii} \mathbf{q}_i. \quad (2.20)$$

Only $m < N_i$ eigenvectors are kept in the reduced-order model (N_i is the number of internal DOFs), which typically correspond to the lowest eigenfrequencies [150], and are assembled in

the matrix Φ_m . The reduction matrix V results as:

$$V = \begin{bmatrix} I & \mathbf{0} \\ S & \Phi_m \end{bmatrix}. \quad (2.21)$$

The projection of the elastic DOFs on the reduced-order subspace then is:

$$\begin{bmatrix} \mathbf{q}_b \\ \mathbf{q}_i \end{bmatrix} = V \begin{bmatrix} \mathbf{q}_b \\ \xi \end{bmatrix}, \quad (2.22)$$

where ξ are the modal coordinates [127]. To summarize, the Craig-Bampton method combines static reduction on boundary DOFs with modal truncation on internal DOFs. Besides the Craig-Bampton method, other methods exist that maintain the same basic procedure but, instead of solving the eigenvalue problem for the internal DOFs with fixed boundary, they solve this eigenvalue problem with free boundary DOFs. They were first developed by MacNeal [151] and Rubin [152]. A more recent application of this technique can be found in [153].

Extensions of the Craig-Bampton Method

One challenge of the Craig-Bampton method is the selection of appropriate fixed interface modes. Generally, a solution is to keep the first m eigenvectors corresponding to the m lowest eigenfrequencies resulting from (2.20) because the first eigenmodes have the greatest contribution to the dynamic behavior. However, the mode shapes with smaller eigenvalues are not always those with the greatest contribution to the dynamic response of the substructure [154].

Kammer et al. [155] propose to solve this challenge with a measure of the modal dynamic importance called Effective Interface Mass (EIM). It was shown that EIM is an absolute measure of the contribution of each fixed interface mode to the loads at the boundary, so it is possible to choose the most important eigenmodes according to this measure. The method allows for a sort of automated MOR, where the designer only has to specify a threshold for the dynamic completeness of the reduced-order model and the fixed interface modes are automatically selected according to their EIM value so that the threshold is satisfied. Moreover, the authors demonstrate that ranking the modes based on the EIM measure is equivalent to ranking them based on the square of the approximate balanced singular value. For the definition of the approximate balanced singular value, this is equivalent to minimizing the peak of the transfer function of the error between the original and reduced-order model. This method was used in [156] to model the crank train of a motorcycle L-twin engine.

Another method for the selection of the fixed interface modes was proposed by Liao et al. [154], which itself is based on [157]. The method suggests reordering the fixed interface modes according to the norm of a coupling matrix, which is based on the moment-matching principle. Once reordered, only m modes are retained. This means that the order of the reduced-order model must still be specified by the designer but, for the same order, this method has higher accuracy than the Craig-Bampton method.

Kim et al. [158] propose to enhance the Craig-Bampton method by including the residual fixed-interface modes—i.e., the fixed-interface modes not included in Φ_m —in the projection matrix V . Since direct calculation of the residual modes is often not possible because it would involve the calculation of all eigenmodes in (2.20), the enhancement of V is achieved by leveraging a so-called residual flexibility matrix. The authors show that for the same order of the reduced system, the enhanced Craig-Bampton method shows higher accuracy than the standard Craig-Bampton in the whole considered frequency range.

Finally, Holzwarth et al. [113] developed the so-called CMS-Gram method, which, while still keeping the fundamental structure of Craig-Bampton with the distinction between boundary and internal DOFs, uses balanced truncation instead of modal truncation for the projection of the internal DOFs. The advantage of this method is that it allows considering the loading conditions and the inertia forces due to the acceleration of boundary DOFs, which should lead to faster convergence of the reduction method, i.e., faster decay of the error with increasing order of the reduced-order model. For the same reduction error, CMS-Gram should produce smaller reduced-order models compared to the Craig-Bampton method. The challenges resulting from the high computational time of balanced truncation are circumvented by applying the methods developed in [128, 143] for the approximation of second-order Gramians.

Reduction error

MOR aims at reducing the order of the original system while introducing the smallest error possible. The acceptable error depends on the application. Different error measures can be applied to calculate the reduction error. When considering the approximation of global dynamics, one possibility for calculating the error is to compare the eigenfrequencies of the original and reduced-order model [113, 158]. Another possibility is to use the modal assurance criterion [113, 159, 160], which looks at the eigenvectors [161]:

$$MAC = \frac{\|\psi^H \hat{\psi}\|^2}{\psi^H \psi \hat{\psi}^H \hat{\psi}}, \quad (2.23)$$

where ψ is an eigenvector of the non-reduced system, $\hat{\psi}$ is the corresponding eigenvector of the reduced system, and the superscript H indicates the complex conjugate transpose (Hermitian). The modal assurance criterion provides the degree of consistency (linearity) between two modal vectors and therefore indicates how well the reduced-order eigenvector correlates with the original one [161]: a value close to 1 indicates a good correlation, i.e., a small reduction error, while a value close to 0 indicates poor quality of the reduced-order model.

Besides the error measures considering the eigenmodes, other measures have been developed that analyze the input-output behavior of the reduced-order model. Two main categories can be distinguished [108, p. 37]:

1. Errors representing the approximation quality pointwise in time $\|y(t) - \hat{y}(t)\|_{(\cdot)}$ or pointwise in frequency $\|G(i\omega) - \hat{G}(i\omega)\|_{(\cdot)}$ using a certain matrix and vector norm $(\cdot) = \{1, 2, \infty, F, \dots\}$.
2. Normwise errors in the time domain as $\|y - \hat{y}\|_{(\star)}$ with $(\star) = \{\mathcal{L}_1, \mathcal{L}_2, \mathcal{L}_\infty, \dots\}$, or in the frequency domain as $\|G - \hat{G}\|_{(\star)}$ with $(\star) = \{\mathcal{H}_2, \mathcal{H}_\infty, \text{Hankel}, \dots\}$.

In the first category, the relative error ϵ_F^{rel} is commonly used [113, 114, 143]:

$$\epsilon_F^{\text{rel}}(\omega) = \frac{\|G(i\omega) - \hat{G}(i\omega)\|_F}{\|G(i\omega)\|_F}, \quad (2.24)$$

where $\|G(i\omega)\|_F = \sqrt{\text{trace}(G(i\omega) \cdot G^H(i\omega))}$ is the Frobenius norm and ω is the frequency range of interest.

In the second category, two norms are mainly used: the \mathcal{H}_∞ and the \mathcal{H}_2 norm. They are defined as follows [145, chap. 1]:

$$\|\mathbf{G}\|_{\mathcal{H}_\infty} = \sup_{\omega \in \mathbb{R}} \|\mathbf{G}(i\omega)\|_2, \quad (2.25a)$$

$$\|\mathbf{G}\|_{\mathcal{H}_2} = \left(\frac{1}{2\pi} \int_{-\infty}^{\infty} \|\mathbf{G}(i\omega)\|_F^2 d\omega \right)^{\frac{1}{2}}. \quad (2.25b)$$

For calculating the error, these norms are applied to the transfer function of the error system $\mathbf{G}_E = \mathbf{G} - \hat{\mathbf{G}}$.

The \mathcal{H}_∞ norm of the system error represents the worst-case error between the reduced and the original system for all inputs with a unit input gain [117]. A small \mathcal{H}_2 norm of \mathbf{G}_E implies, instead, that the \mathcal{L}_2 norm of the output error $y(t) - \hat{y}(t)$ is small [143], [145, chap. 1].

The relative error over all frequencies can be defined using the \mathcal{H}_∞ norm [141]:

$$\epsilon_{\mathcal{H}_\infty}^{\text{rel}} = \frac{\|\mathbf{G} - \hat{\mathbf{G}}\|_{\mathcal{H}_\infty}}{\|\mathbf{G}\|_{\mathcal{H}_\infty}}. \quad (2.26)$$

When carrying out MOR with balanced truncation, an a-priori error bound is available [162, p. 37], [114, 137]:

$$\|\mathbf{G}(i\omega) - \hat{\mathbf{G}}(i\omega)\|_{\mathcal{H}_\infty} \leq 2 \sum_{i=n+1}^N \sigma_i, \quad (2.27)$$

where n is the order of the reduced-order model, N is the order of the original model, and σ_i are the Hankel singular values. (2.27) shows that the a-priori error is limited by the double sum of the Hankel singular values that have been truncated by the balanced truncation [162, p. 37]. However, this has been demonstrated only for first-order systems. An extension to second-order systems is shown in [114].

2.4 Control Systems for Increasing the Stability of Weave and Wobble

As explained in Section 2.2, the design of motorcycles has been strongly driven by the attempt to improve their stability, in particular regarding the stability of the out-of-plane eigenmodes such as weave and wobble. Besides the improvement in structural design, this has led to the development of mechanical components having the aim of increasing the stability of potentially unstable eigenmodes. Passive, semi-active, and active systems have been proposed.

Evangelou [163] developed a control strategy for the rear shock absorber to address the cornering weave. As explained in Section 2.2.1, the rear suspension has a contribution to cornering weave and, therefore, a control strategy for the rear suspension has the potential to increase the stability of the cornering weave. The solution proposed in [163] is to shift the attachment point of the rear shock absorber to the swingarm through a linear actuator, thus changing the direction of the force applied by the shock absorber. A control strategy is then developed for this actuator using the Nyquist diagram. Results demonstrate how this control strategy can increase the stability of cornering weave for different speeds and roll angles while not affecting the stability of other modes. However, because it only acts on the rear suspension,

this method can not improve motorcycle stability in straight running, where the suspension system is almost not involved in the weave and wobble eigenvectors. Moreover, the feasibility of the actuator concerning the required forces and the package is questionable [163].

Watanabe et al. [164] propose a control system that employs the brakes as stabilizing system. The system compares the signal of the yaw rate with a calculated “intended yaw rate”; when these signals differ and the actual yaw rate show oscillations, the system applies the brakes. The control strategy was tested through simulations in cornering on a low-friction road surface, showing that the system is able to prevent a fall that would occur due to weave instability.

More common are stabilizing systems that apply a moment on the steering assembly to enhance stability. A well-known example is the steering damper, i.e., a damper connected between the main frame and the steering head that applies a counter torque proportional to the steering rate [165]. If its damping value is selected correctly, a steering damper can increase the stability of wobble and prevent the occurrence of kick-back [4, p. 460]. However, a steering damper with a high damping coefficient is detrimental to weave and cornering weave, so this coefficient is always a trade-off [14, 62]. For this reason, different solutions have been proposed to solve or at least improve this trade-off.

One possible solution is to use a semi-active steering damper, where the damping value can be adapted in real-time. The development of a magnetorheological semi-active steering damper has been tackled in [166]. Moreover, the idea of changing the damping coefficient of a steering damper employing an electrorheological or magnetorheological damper is reported in a patent by Schiffer et al. [167]. Wakabayashi et al. [168] propose to vary the damping coefficient according to static maps that are a function of longitudinal speed and acceleration. This system was implemented in series production by Honda and applied to the CBR1000RR [169]. In [170], a control strategy for the semi-active steering actuator is proposed, where the damping coefficient can assume a maximal or minimal value according to a selection strategy based on the sign of some state variables of the motorcycle, such as steering rate and yaw rate, and on the frequency content of these signals. Results show that the proposed strategy can merge the advantage of a passive steering damper with low damping value, which favors weave stability, with that of a passive steering damper with high damping value, which instead ensures high wobble stability. This partially solves the mentioned trade-off. In [165], this strategy was tested through simulation in challenging dynamic maneuvers such as emergency braking in steady cornering, μ -jump in steady cornering, and driving on road undulations that would excite the kick-back. One drawback of this solution is that performances cannot exceed those of an optimal passive steering damper, since even a semi-active damper only reacts to the steering rate and cannot bring active control inputs to the steering head.

Another solution based on passive components is proposed in [62], where the simple steering damper is substituted by a so-called steering compensator, which is composed of spring, damper, and inerter (a mechanical element reacting to acceleration [171]). This configuration allows to obtain a second-order mechanical impedance between steering rate and steering torque applied by the compensator to the steering head. The parameters composing the impedance are optimized with a sequential quadratic programming algorithm that ensures improved stability of weave and wobble over the whole operating range of the motorcycle. A similar system was used in [17] to counteract the burst phenomenon in racing motorcycles.

The systems described in the previous paragraph are reactive, meaning that the system applies steering torque only as a reaction to the movement of the steering system so that the torque is proportional to either steering angle, steering rate, or steering acceleration. Passive systems present some limitations [62]: because of their passivity, the coefficients must be real and

positive, to avoid excessive construction costs, the device must be low-order, and adaptive systems are not realizable. These disadvantages can be solved by an active system, such as a steering actuator. Considering this potential, [172] proposes a control strategy for a steering actuator based on the \mathcal{H}_∞ loop-shaping approach. This approach is adopted in the present thesis as well (Chapter 5). [172] is mainly focused on the stabilization of the wobble eigenmode. Moreover, the controller is built by leveraging a model linearized in a certain working condition.

H_∞ Controller

The \mathcal{H}_∞ controller belongs to the category of optimal controllers in the sense that it ensures robust stability and optimal disturbance rejection [173]. The robustness is achieved by directly taking into account model uncertainty so that the designed controller is able to handle a pre-specified range of model uncertainty [174, p. 309].

Figure 2.14 helps to understand how the controller works. The symbols have the following meaning:

1. p is the vector of inputs (disturbances, noise, references).
2. u is the vector of control inputs.
3. z is the vector of outputs.
4. y is the vector of signals provided to the controller.

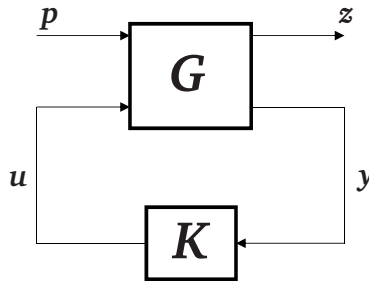


Figure 2.14: Block diagram of a typical \mathcal{H}_∞ controller structure.

The structure of the original plant G can be rewritten in the Laplace domain in the following form:

$$\begin{pmatrix} Z(s) \\ Y(s) \end{pmatrix} = \begin{pmatrix} G_{zp}(s) & G_{zu}(s) \\ G_{yp}(s) & G_{yu}(s) \end{pmatrix} \begin{pmatrix} P(s) \\ U(s) \end{pmatrix}. \quad (2.28)$$

The desired controller K has the form [175, p. 333]:

$$U(s) = -K(s)Y(s). \quad (2.29)$$

The equation for the closed-loop system can be expressed as [175, p. 333].

$$Z(s) = G_p(s)P(s), \quad (2.30a)$$

$$G_p(s) = G_{zp}(s) - G_{zu}(s)K(s)(I + G_{yu}(s)K(s))^{-1}G_{yp}(s). \quad (2.30b)$$

The controller synthesis consists in solving the \mathcal{H}_∞ optimization problem [175, p. 334], [176]:

$$\min_{K(s)} \|G_p(s)\|_\infty. \quad (2.31)$$

The result of the optimization process is a controller $K(s)$ that minimizes the \mathcal{H}_∞ norm of the transfer function $G_p(s)$ between the plant inputs, which are generally considered disturbances, and the plant outputs. This guarantees that the system's response remains bounded under a certain threshold. $\|\cdot\|_\infty$ is the infinity norm and denotes the largest singular value of the given matrix [175, p. 334]. Using this norm in the optimization problem (2.31) enforces the transfer function $G_p(s)$ to belong to the so-called Hardy-Space, which is the space of all stable linear time-invariant continuous-time systems [174, p. 310]. This way, the stability of the closed-loop system $G_p(s)$ is guaranteed.

The synthesis of an \mathcal{H}_∞ controller is often coupled with the loop-shaping approach [172, 173, 177, 178], whereby a designer specifies closed-loop objectives in terms of requirements on the open-loop singular values of the original system [173]. The next paragraph provides more details about this approach.

Loop Shaping Approach

In feedback design, many performance objectives can be written as a requirement on the singular values of the open-loop system. Considering that, generally, performance is required at low frequencies and robustness at high frequencies [179], the requirements are formulated by specifying weighting functions that shape the plant at different frequencies according to the requirements. Despite the advantage of being easily understandable and applicable, the loop-shaping approach does not ensure the stability of the closed-loop system [173]. For this reason, the combination of the loop-shaping approach with the \mathcal{H}_∞ control synthesis is particularly appealing, as it incorporates the performance/robustness trade-off given by the loop-shaping with the guarantee of robust stability of \mathcal{H}_∞ design procedures [179].

The loop-shaping \mathcal{H}_∞ design procedure can be divided into three steps [173]:

1. Loop-shaping: Using a precompensator W_1 and/or a postcompensator W_2 , the singular values of the nominal plant are shaped to obtain the desired open-loop behavior. The compensators are also referred to as weights and can be scalar or transfer functions (generally PI or PD filters). The open-loop system then becomes: $G_s = W_1 G W_2$. It is assumed that W_1 and W_2 are such that G_s contains no hidden poles.
2. Robust stabilization: a feedback controller K_∞ is determined that ensures the stability of the closed-loop system with a maximum stability margin ϵ_{\max} .

$$\epsilon_{\max}^{-1} = \inf_{K \text{ stabilising}} \left\| \begin{pmatrix} W_1^{-1} \\ W_2 G \end{pmatrix} (I - KG)^{-1} (W_1 - GW_2^{-1}) \right\|_\infty, \quad (2.32)$$

where the infimum is chosen over all stabilizing controllers K [180]. If $\epsilon_{\max} \ll 1$, step 1 is repeated and W_1 and W_2 are adjusted. A value $\epsilon_{\max} > 0.3$ is generally considered satisfactory [176]. Otherwise, $\epsilon \leq \epsilon_{\max}$ is selected and a controller K_∞ is synthesized which satisfies:

$$\left\| \begin{pmatrix} W_1^{-1} \\ W_2 G \end{pmatrix} (I - KG)^{-1} (W_1 - GW_2^{-1}) \right\|_\infty \leq \epsilon^{-1}. \quad (2.33)$$

3. The final feedback controller K is obtained by including the weights in the K_∞ controller: $K = W_1 K_\infty W_2$.

$\epsilon \leq \epsilon_{\max}$ is called stability margin and has multiple functions:

- It captures information on the compatibility of the desired closed-loop shape with the stability constraints and is therefore an indicator of the success of loop-shaping [179].
- It is a measure of robustness and, in particular, it provides a measure of the amplitude of the model uncertainties that can be handled by the controller [173]. This is further explained in the next paragraph, which describes the possibilities to include model uncertainties.
- It gives a bound on the norm of all closed-loop transfer functions [179].

Model Uncertainties

The uncertainties of the model G can be defined as ΔG . These can be either multiplicative, additive, or specified as a coprime factorization [174, p. 323]. In [173, 179, 180], the coprime factorization is used to show that the stability margin ϵ is a measure of robust stability. Using the left coprime factorization, the plant G can be expressed as:

$$G = \tilde{M}^{-1} \tilde{N}. \quad (2.34)$$

The perturbed plant can be obtained by perturbing the coprime factorizations [173]:

$$G_\Delta = (\tilde{M} + \Delta_M)^{-1} (\tilde{N} + \Delta_N). \quad (2.35)$$

Δ_M, Δ_N are stable, unknown transfer functions of the uncertainties and satisfy $\|\Delta_M, \Delta_N\| < \epsilon$. At this point, the concept of robust stability in the \mathcal{H}_∞ design procedure is equivalent to finding a controller K that stabilizes all G_Δ for a given stability margin ϵ [173], which is expressed in (2.33). Step 2 of the algorithm described in the previous paragraph is generally iterative. However, McFarlane et al. [173] show that, when the coprime factorization of G is normalized, a non-iterative method for finding ϵ_{\max} is available.

The possibility to introduce model uncertainties into the control synthesis is particularly useful to develop a stabilizing controller for a motorcycle. In fact, some motorcycle parameters, such as tire characteristics or rider's position and mass, are subjected to variations that are difficult to capture with a model. \mathcal{H}_∞ allows to include these effects indirectly by specifying the transfer functions Δ_M, Δ_N . The parameter ϵ can be interpreted as the entity of model uncertainty that the controller can handle.

3 Methodology

This thesis aims to enhance the stability of the weave and wobble eigenmodes in motorcycles by leveraging both design optimization and active control. In the previous chapter, several works have been summarized, which provide the basis for this thesis. In the present chapter, the research questions are presented and the methods used to answer them are summarized. The research questions are defined based on the gaps in the state-of-the-art, which are presented in the next section.

3.1 Research Gap

For a stability-optimized design of the structural components, it is important to understand how the chassis stiffnesses impact the stability of weave and wobble. Section 2.2.3 provides an insight on the literature dealing with this problem, however, all these works model the chassis stiffness with the lumped stiffness approach without providing any demonstration whether the accuracy of this approach is sufficient for the study of weave and wobble; in Section 4.2 of the present thesis, this aspect will be discussed. Moreover, none of these works tackle the challenge of optimizing the stiffness distribution of structural components for improving the stability of weave and wobble. Section 4.3 proposes a method to solve this challenge.

Among the works that developed mechanical systems for stabilizing weave and wobble, only Evangelou et al. [172] proposed a fully active control system. However, [172] is mainly focused on improving the stability of wobble, while the aim of the present thesis is to increase the stability of both weave and wobble. Moreover, the controller proposed in [172] is optimal only for a specific working point, thus limiting its applicability.

3.2 Research Questions

Based on the research gaps described in the previous section, the following research questions arise, which can be divided into two categories:

- Concerning the development of a methodology for optimizing the distribution of chassis stiffnesses considering the stability of weave and wobble:
 - Do simplified model layouts sufficiently reproduce the effect of chassis flexibilities on weave and wobble or is a more accurate model required? (Section 4.1 and 4.2)
 - How can the developed model be used to obtain indications for the design of structural components, which would lead to an optimized distribution of structural stiffness? (Section 4.3 and 4.4)

- Concerning the synthesis of an active controller for a steering actuator:
 - Which controller structure allows for the increase in the stability of weave and wobble while not impairing the rider's action? (Chapter 5)

3.3 Proposed Approach

The research questions will be answered in Chapter 4, where the steps towards the development of a methodology for optimizing the distribution of structural stiffness are explained, and Chapter 5, where two controllers are proposed that enhance the stability of weave and wobble. In the present section, the contents of these methods are summarized and it is highlighted how they build on each other.

3.3.1 Methodology for Optimizing the Distribution of Structural Stiffness

The first step for optimizing the distribution of structural stiffness with the aim of improving the stability of weave and wobble is to understand the basic phenomena behind these eigenmodes. For that, a motorcycle model is needed that enables such a study. In Section 4.1, a multibody motorcycle model is proposed, which serves as basis for the following works. MBS is chosen for the motorcycle model because it allows to include physical phenomena that are important for the modeling of weave and wobble. In particular, attention is devoted to the tire model, whereby the Pacejka Magic Formula for combined slip is used [38] and a first order lag for the tire lateral force is introduced, which is necessary for the modeling of wobble [68, 69, 79, 100]. Moreover, the MBS software used in the present thesis (MBSim [92]) provides a solver for carrying out an eigenvalues analysis, where the nonlinear equations of motion are linearized about a specified working point and the eigenvalues and eigenvectors are calculated. Finally, another reason for choosing MBS is that it offers the possibility to model the structural flexibilities either with the lumped stiffness or with the flexible multibody approach.

The second step towards a methodology for stiffness optimization is the development of a model where the structural flexibility is modeled with high accuracy. The aim of this model is to correctly represent the effect of structural flexibilities on weave and wobble. As stated above, previous works leveraged only the lumped stiffness approach. In Section 4.2, a flexible multibody motorcycle model is proposed, where the stiffness of the structural components is modeled with the flexible multibody approach. This way, the effect of structural flexibilities on weave and wobble can be represented with high accuracy and a comparison with the lumped stiffness approach can be made to understand whether the accuracy of lumped stiffness models is sufficient. This answers the first research question stated in Section 3.2.

In the third step, the methodology for optimizing the distribution of structural stiffness is developed, which is proposed in Section 4.3. Its objective is to generate guidelines that can be used to optimize the stiffness distribution between and within the structural components. For the development of this methodology, either the flexible multibody or the lumped stiffness approach can be used. The decision has to be taken considering pros and cons of these two approaches, which are summarized in Table 3.1. Even if it offers high accuracy, the flexible multibody motorcycle model has the disadvantage that it is difficult to carry out a parameter study where single stiffnesses within each structural component are treated separately. Moreover, its parameters

Table 3.1: Pros and cons of lumped stiffness and flexible multibody approach considering the requirements for the development of a methodology for stiffness-optimization.

	Lumped stiffness approach	Flexible multibody approach
<i>Pros</i>	<ul style="list-style-type: none"> • Each parameter has a physical meaning: stiffness value in a certain direction. • Easy to study parameters independently from each other. 	<ul style="list-style-type: none"> • Flexibility represented as a continuous property → high accuracy.
<i>Cons</i>	<ul style="list-style-type: none"> • Strong approximation of the flexural behavior. • Accuracy strongly dependent on the parameterization. 	<ul style="list-style-type: none"> • Separated study on single stiffnesses within each structural component is critical. • Difficult to give a physical interpretation to the underlying parameters.

do not always have a physical explanation, because part of their DOFs are expressed through modal coordinates (Section 2.3.2), so it is difficult to extract information which can be directly interpreted for design optimization. For this reason, the methodology is based on a lumped stiffness motorcycle model, where the flexibility of every component is represented through a bending and a torsional stiffness, which can be studied independently from each other. This way, it is possible to answer the second research question stated in Section 3.2. The potential disadvantage of lumped stiffness models lays in the accuracy, which is strongly dependent on the parameterization used. Therefore, a method for parameterization of lumped stiffness model is proposed, with which the lumped stiffness motorcycle model achieves similar accuracy as the flexible multibody model in reproducing the effect of structural stiffness on weave and wobble. The flexible multibody model presented in step two serves therefore as “ground truth”.

3.3.2 Active Stabilization of Weave and Wobble

In Chapter 5, two control strategies are proposed: proportional gain-scheduling and \mathcal{H}_∞ . The choice of the gain-scheduling controller is motivated by:

- The possibility to directly use the multibody motorcycle model to find the controller parameters.
- The simplicity of its structure, which allows the development of a look-up table where the controller parameters for different combinations of longitudinal speed and roll angle are contained.

The \mathcal{H}_∞ controller is chosen for the following reasons:

- It lends itself to the development of a disturbance rejecting controller, as is needed for a stabilizing control system. Moreover, it provides a background for implementing a robust controller, i.e., a controller able to tolerate a defined amount of model uncertainties.
- The loop-shaping approach makes it possible to shape the controller according to the frequency range where it should act. This is particularly useful for the controller proposed in this thesis, because it should act in the frequency range of weave and wobble but not in the low-frequency range, where driving maneuvers take place.

4 Steps Towards Optimized Distribution of Structural Stiffness

4.1 Analysis of the Phenomena causing Weave and Wobble [MDPI 2020]

The stability of the weave and wobble eigenmodes is central for the present thesis and it is therefore fundamental to understand the physics behind them.

In this publication, the basic phenomena characterizing the stability of weave and wobble are analyzed in detail. For that, a multibody motorcycle model is proposed, which is based on a state of the art model from Sharp et al. [38] for the motorcycle parameters and on Wisselmann [49] for the model structure and the calculation of kinematics of the contact point. This model serves as basis for the following works in this thesis, which are presented in Section 4.2, Section 4.3 and Chapter 5. The most important features of this model are:

- Use of the Pacejka Magic Formula (the version and tire parameters reported in [38] are used) for the calculation of the tire forces. A first-order lag is introduced in the generation of the lateral forces, which is necessary when modeling wobble. Given that the frequency of weave and wobble is lower than 15 Hz, it is not necessary to use the more complex rigid ring tire model [75].
- Model of the rider with two bodies to represent the upper and lower body. The rider's passive motion is modeled with 3 DOFs: lateral displacement of the rider, lean motion of the upper body (rotation about the longitudinal axis), and rotation of the upper body about the vertical axis. Moreover, the connection between upper body and handlebars provided by the arms is modeled.
- Lumped stiffness models of several structural components: bending and torsional stiffness of the front fork, and torsional stiffness at the steering head joint of the frame, torsional stiffness of the swingarm.

For more details on the motorcycle model the reader is referred to Section 3.1 of the publication.

The literature review shows that most works analyzing weave focus on the study of the motorcycle parameters that influence its stability, such as chassis stiffness, tire properties [21, p. 532], [23] and rider [15, 50, 95, 96, 181]. However, a physical explanation of the correlation between weave damping and longitudinal speed is still missing. As Figure 4.1 shows, the damping of weave has two opposing trends. In the lower speed range, the damping increases (decreasing real part) with increasing longitudinal speed, while after a characteristic speed (between 50 km h^{-1} and 90 km h^{-1} according to the motorcycle parameters) the damping decreases (increasing real part) with increasing speed. In this publication, this correlation is explained by analyzing how the weave eigenvector changes with increasing speed (Figure 4.2). From 30 km h^{-1} to 100 km h^{-1} , the eigenvector changes significantly, evolving from a lateral-displacement-dominated motion (y)

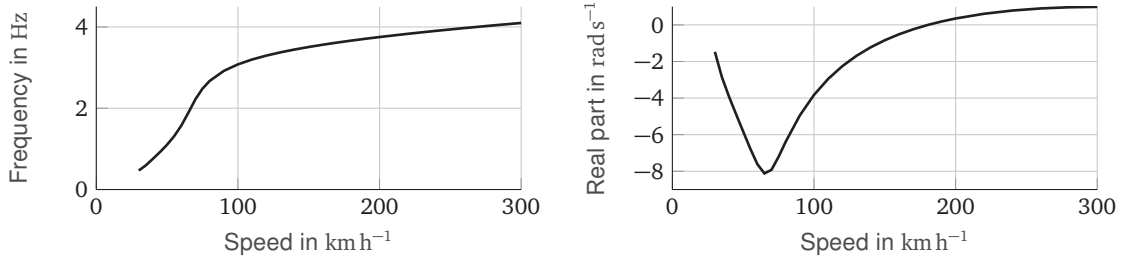


Figure 4.1: Weave eigenfrequency and real part as a function of speed [182].

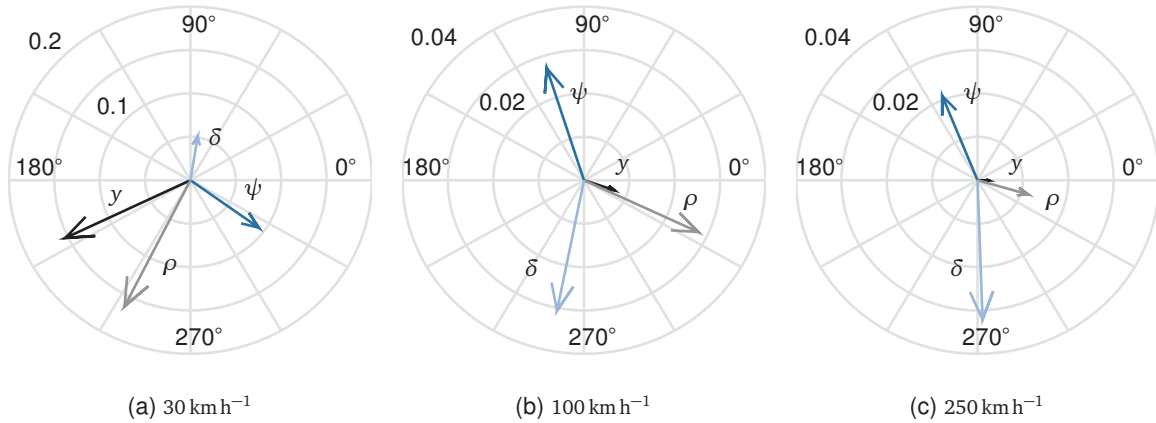


Figure 4.2: Compass plots of the weave eigenvector at different speeds [182]. δ is the steering angle, ψ is the yaw angle, ρ is the roll angle and y is the lateral displacement.

to a combination of roll ρ , yaw ψ and steering head δ motion, which represents the well-known weave eigenvector. This evolution explains the increase in damping with longitudinal speed in the lower speed range, because the weave eigenvector evolves from a low frequency self stabilizing motion to the classical weave. From 100 km h^{-1} to 250 km h^{-1} , the relative phase between the components of the weave eigenvector does not change but the roll component almost disappears (the length of the phasor decreases). The decreasing weave damping with increasing longitudinal speed can be explained considering that, when projecting about the steering axis the gyroscopic moments and the moments produced by the front tire, they act in phase opposition. This means that the gyroscopic moments tend to decrease the stabilizing action of the tire forces. As the gyroscopic moments increase with longitudinal speed, their destabilizing action also increases, thus explaining the reduction in weave damping with speed.

The literature review also summarizes the works that studied the influence of motorcycle parameters on the stability of wobble, whereby tire properties [68, 69, 79, 100] and chassis flexibilities [23, 41] are the most important. In particular, the modeling of the front fork bending flexibility is required for a correct description of the evolution of the wobble damping over speed. When adding the lateral flexibility of the front fork to a rigid body motorcycle model, the damping of the wobble eigenmode is decreased in the lower speed range while it increases at higher speeds, as Figure 4.3 shows. Cossalter et al. [23] and Spierings et al. [41] explain this behavior by using a lumped stiffness model of the front fork (Figure 4.4), and present the following hypothesis:

- The bending flexibility of the front fork has itself a destabilizing effect, which predominates at low speeds.
- The bending flexibility causes an additional rotation α_{ff} of the front wheel that creates a gyroscopic moment about the steering axis that stabilizes wobble. This

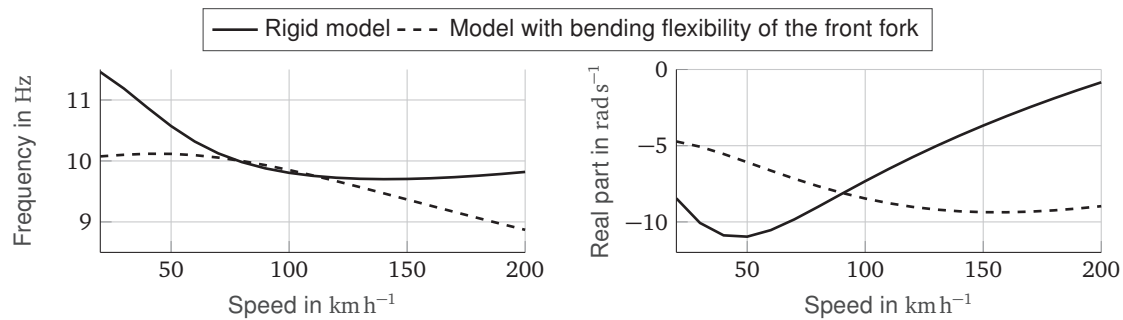


Figure 4.3: Wobble eigenfrequency and real part as a function of speed [182].

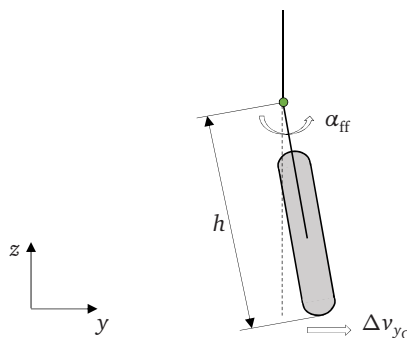


Figure 4.4: Lumped stiffness model of the front fork (front view) [182].

gyroscopic moment is proportional to the rotational speed of the front wheel and therefore prevails at higher speed.

While the second hypothesis about the stabilizing effect of the gyroscopic moment was verified, the first one—i.e., the destabilizing effect of the bending flexibility at low speeds—was presented as an assumption and not demonstrated. In the present publication, an explanation to the first hypothesis is provided. By modeling the fork bending flexibility with the lumped stiffness approach, it is shown that this flexibility causes a variation Δv_{y_c} of lateral speed of the front contact patch (Figure 4.4) and it reduces the lateral forces produced by the tire during the wobble oscillation. Since the tire lateral force contributes to stabilize the wobble, reducing it has a destabilizing effect on wobble. This explains why the front fork bending flexibility alone destabilizes the wobble at low speeds.

The last part of the publication shows the effect of the rider model on weave and wobble. In particular, the effects of the DOFs described above are studied. For weave, an important contribution derives from the lean DOF, while wobble is strongly stabilized by the arms of the rider, which act as a sort of steering damper.



The model used in the publication is published open-source: [183]

Contributions

F.P. is the leading author who wrote the whole paper. The project and problem formulation were conceptualized by F.P. and D.W.; these authors also built the motorcycle model and produced the results presented in this paper. D.W., A.E., F.D. and A.G. revised the paper critically for important intellectual content. Conceptualization, F.P. and D.W.; formal analysis, F.P. and D.W.; methodology, F.P. and D.W.; supervision, A.E., D.W., A.G. and F.D.; validation, F.P. and D.W.; visualization, F.P.; writing—original draft, F.P.; writing—review and editing, A.E., D.W., A.G. and F.D. All authors have read and agreed to the published version of the manuscript.

Article

Analysis of the Phenomena Causing Weave and Wobble in Two-Wheelers

Francesco Passigato ^{1,*}, Andreas Eisele ¹, Dirk Wisselmann ², Achim Gordner ²
and Frank Diermeyer ¹

¹ Chair of Automotive Technology, Technical University of Munich, 85748 Garching bei München, Germany; andreas.eisele@tum.de (A.E.); diermeyer@ftm.mw.tum.de (F.D.)

² BMW Group, 80937 Munich, Germany; dwisselmann@t-online.de (D.W.); Achim.Gordner@bmw.de (A.G.)

* Correspondence: francesco.passigato@tum.de

Received: 24 August 2020; Accepted: 24 September 2020; Published: 29 September 2020



Abstract: The present work follows in the tracks of previous studies investigating the stability of motorcycles. Two principal oscillation modes of motorcycles are the well-known wobble and weave modes. The research in this field started about fifty years ago and showed how different motorcycle parameters influence the stability of the mentioned modes. However, there is sometimes a minor lack in the physical analysis of why a certain parameter influences the stability. The derived knowledge can be complemented by some mechanical momentum correlations. This work aims to ascertain, in depth, the physical phenomena that stand behind the influence of fork bending compliance on the wobble mode and behind the velocity dependence of the weave damping behaviour. After a summary of the relevant work in this field, this paper presents different rigid body simulation models with increasing complexity and discusses the related eigenvalue analysis and time behaviour. With these models, the mentioned modes are explained and the physical phenomena only partly covered by the literature are shown. Finally, the influence of the rider model on weave and wobble is presented.

Keywords: two-wheeler; vehicle dynamic modelling; wobble; weave; fork bending compliance; rider influence

1. Introduction

Motorcycle dynamics have always been an extensive research topic due to the complexity and the influence on the riders' safety. The knowledge used to develop a stable motorcycle chassis comes, to a certain extent, from experience or sensitivity analysis which sometimes lack physical and theoretical understanding of the hidden phenomena. This paper wants to clarify these phenomena, in particular with regard the understanding of the effect of the front fork bending compliance and of the weave damping behaviour with changing speed.

Two of the principal eigenmodes of a motorcycle are known as wobble and weave. The first one includes almost solely the rotation of the front assembly about the steering axis whose frequency is in the range between 7 and 10 Hz depending on the motorcycle's parameters [1]; the second one is more complex, and when affected by this mode, the motorcycle shows roll, yaw, steering-head rotation and lateral displacement [2].

The starting point for this work is an observation resulting from the comparison of experience in reality and simulation results. Using the eigenvalue analysis, the earlier motorcycle models, such as the model of Sharp [3] which only includes a tyre model but no compliances, show a stable wobble mode in the lower speed range (up to 80 km h⁻¹), and this mode becomes unstable in the higher speed range. However, the experience with a real motorcycle shows an almost opposite behaviour: lower stability (or even instability) at low speed and increasing stability at higher speed. This was demonstrated

through measurements on a real motorcycle by Koch [4]. Previous research addressed this apparent incompatibility between simulation and reality, concluding that the front fork bending compliance is a key parameter when studying wobble [5–9], as discussed further in Section 2. Wisselmann [10] conducted an analysis where the motorcycle stiffnesses were progressively eliminated (i.e., set to infinity); in this case also, a remarkable variation in the motorcycle response was shown.

For weave mode, the situation is different: the well-known correlation between eigenmode-damping and speed is also reproduced by models without chassis compliances [2,5,6]. In this case, up to a certain speed, the weave mode becomes more stable with increasing speed. After a tipping point, the stability degenerates again when the speed increases. This behaviour is unexpected, as the increasing gyroscopic moments of the wheel should stabilise the motorcycle, as is the case, for example, with a gyroscope. This is a complex system to analyse because there are many possible gyroscopic moments and their combined influence is not trivial. This peculiar behaviour is further analysed in Section 4.2.

The different models that will be presented within this paper were produced using open source multibody simulation software named “MBSim” (www.mbsim-env.de) which was developed at the Institute of Applied Mechanics of the Technical University of Munich. An introduction [11] on the functionalities of this software is provided. Multibody simulation is common for vehicle dynamics, and was used, for example, by Cossalter in multiple publications [2,5,7,12]. It allows the building of the desired model through a CAD-like interface, by connecting the bodies with joints and assigning them stiffness and damping when needed. The present motorcycle model is described in Section 3.

To summarise, this work deeply investigates the influence of the front fork bending compliance on the wobble mode. Starting from the point reached by previous authors [1,5,6], Section 4.1 provides a different justification for the well-known effect of the fork bending compliance on wobble damping. Moreover, in Section 4.2 the weave mode is further analysed and a possible justification for its damping behaviour is provided. Finally Section 4.3 investigates the influence of the rider on wobbling and weaving.

2. Related Work

Vehicle dynamics is a very popular research topic which features in many books and publications. Most of the literature is focused on four-wheelers; nevertheless, there is also a huge collection of research on two-wheeled vehicles. The different relevant authors are mentioned below.

Back in 1971, Sharp [3] published a paper about the driving stability of two-wheeled vehicles. This research is considered the starting point of the modern motorcycle dynamics. In fact, thanks to a (linearised) tyre model it was possible to detect the wobble mode, which was not present in the even earlier and less complex motorcycle models by Whipple [13] (p. 195).

Cossalter [2] (p. 278) [5] and Spierings [6] presented a solution to overcome the previously mentioned incoherence between reality and rigid model simulations when analysing wobble. A fork bending compliance with a lumped stiffness was added: a revolute joint in the front fork, with its rotating axis (named twist axis [14]) perpendicular to the steering head axis. A certain stiffness and a damping are assigned to this joint. Lumped parameter models are described in [15]. This kind of modelling is also found in other sources, especially when a more complex non-rigid model is developed [16–21].

This additional fork bending results in a more realistic wobble-damping characteristic: wobble-instability at low speed and a clear stabilisation when increasing the speed. Cossalter [2] (p. 280) and Spierings [6] explain this change of characteristic with the combination of two opposed effects caused by the fork bending compliance:

1. The bending compliance itself reduces the stability.
2. The combination of wheel-spin and the rotation around the twist axis produces a gyroscopic moment about the steering axis, leading to stabilisation.

Since the gyroscopic moment is proportional to the speed, the first effect dominates at low speed, causing lower stability in this speed range. The second effect becomes dominant with increasing speed, which explains the restored stability at high speeds. Section 4.1 investigates the influence of the fork bending compliance considering another phenomenon caused by the bending compliance itself.

There are several parameters affecting a motorcycle's wobble stability; a complete list can be found in [2,3,17,21]. For this work, besides the fork bending compliance, two tyre parameters are of particular importance: the relaxation length and the cornering stiffness. Some research [3,16,17,20] has underlined that a tyre model with cornering stiffness is necessary in order to simulate the wobble mode. This also suggests an important consideration: the principal cause of the wobble is given by the tyre's response. When the wheel is subject to an outer disturbance steering the wheel itself, the tyre reacts with a side force which, thanks to the mechanical trail, produces an aligning moment around the steering axis. When returning to the equilibrium position, the wheel starts oscillating about the steering axis, thereby triggering the wobble mode [22]. Depending on the speed of the motorcycle, this oscillation will diverge (unstable behaviour) or converge to the equilibrium (stable behaviour).

The other important tyre parameter influencing wobble is the relaxation length [3,13,23]. Several works [3,16,17,20,24] investigated its effect on wobble damping, underlying how the relaxation length destabilises the wobble mode, since it generates a delay between the wheel steering and the tyre-lateral force generation. As a consequence, Sharp [3] (p. 323) clarifies that both tyre sideslip and tyre relaxation properties are fundamental for a proper representation of a motorcycle's dynamic properties. Like most of the tyre parameters, the relaxation length also depends on several factors. Pacejka et al. [25] and Sharp [1] report that the relaxation length increases with increasing speed. Moreover, a dependence on the vertical load is present. A more recent paper by Sharp [12] proposes a tyre model based on the Pacejka magic formula [26] where dependencies on both speed and vertical load are reproduced. This model and the related parameters are also used in the present work.

In summary, some minimal requisites for a correct analysis of the wobble mode can be defined. Pacejka [26] and Doria [16] suggest that the tyre properties have the greatest influence on motorcycle stability. The Pacejka magic formula [26] coupled with a first order dynamic response, as described in the previous paragraph, is necessary in order to produce reliable wobble stability analyses [13] (p. 324). This tyre model allows an accurate description of the tyre forces and moments if the frequency of the external forces is lower than 15 Hz [13]; these conditions are generally satisfied for common stability analysis, therefore the magic formula is used in almost all the latest researches based on multibody analysis [2,7,12,27–29]. In addition to the tyre modelling, the lateral compliance at the front of the machine is necessary when simulating wobble [13,30]. This can be obtained with a bending compliance of the front fork [5–9], or by adding a lumped torsional stiffness of the main frame at the steering head joint with its rotation axis perpendicular to the steering axis [12,26–28]; a combination of both stiffnesses can also be implemented, as in the present work.

Besides the wobble mode, many of the mentioned sources also analyse vehicle "weave" [2,3,5–7,17,19,21]. The weave mode can also be qualitatively represented with a motorcycle model having no flexibilities [13] (p. 195). However, the literature underlines that some additional degrees of freedom (DoF) notably influence the weave mode. In particular, Doria [17] (p. 17) and Splerings [6] (p. 28) underline that the fork bending compliance destabilises the weave mode. Taraborrelli [23] and Cossalter [7] analyse the effect of the swingarm torsional and bending compliance. Reference [23] simulated two motorcycle types with significantly different stiffness values: a super-sport motorcycle (higher stiffness), where the two swingarm compliances had almost no influence on weave, and an enduro-motorcycle, where the swingarm bending compliance slightly destabilised the weave mode, which was at the same time slightly stabilised by the torsional compliance of the swingarm. The results of [7], on the contrary, show the destabilising effect of both swingarm bending and torsional compliance; however, the influence was also small in this case.

Furthermore, the rider has proven to greatly affect the motorcycle's stability behaviour. In fact, Roe [31] points out that the stability analysis of a riderless motorcycle can be very

misleading. Significant changes in the weave stability due to the rider have also been reported by Pacejka [26] (p. 535). The modelling of the rider's passive response and its influence on stability is a broad topic which will be summarised in Sections 3.3 and 4.3.

An interesting argument strictly connected to weave is the so called "cornering weave". During cornering, the in-plane eigenmodes (bounce, pitch) become increasingly coupled with the out-of-plane eigenmodes (weave, wobble), whereby the former shows degrees of freedom typical of the latter and vice versa [9,13,32]. Concerning cornering weave, the eigenvector also shows front and rear suspension travels which are not present in the straight-running weave [32]. This mode-coupling is critical because it provides a signal transmission path from road undulations to lateral motions [33]. Moreover, under cornering conditions, bounce and weave have similar eigenfrequencies in the middle to high speed range ($70\text{--}120\text{ km h}^{-1}$) [9,24,32,34], thereby leading to mutual triggering [13,33,34]. From these considerations it should be clear that the suspension system must also be modelled when carrying out stability analysis of motorcycles under cornering conditions [13,34].

As mentioned in the introduction, the models for the present work were implemented with the "MBSim" multibody simulation software. Two interesting references in this field are the works of moreCossalter [29] and moreLot [35]. They did not use the same software, but developed two multibody-simulation tools that follow the same principle; they are both based on the symbolic calculation software "Maple" with the second one using a build-in library for multibody modelling called "MBSymba". These references underline the suitability of a multibody simulation tool for the dynamics and stability analysis of motorcycles. Another piece of software used in several works [12,27,36] is "Autosim"; in this case as well, the authors demonstrated the great advantages provided by multibody modelling when conducting both time and frequency analyses. Following this established research, this modelling and calculation method were chosen for the present work.

3. Modelling

Different models have been developed during the last 70–80 years. Their complexity is obviously related to the objectives they pursue. For example, the wobble has been simulated studying systems capable of shimmy behaviour [37] (p. 166). Limebeer [13] (p. 184) derived the equations of motion of such a system, which possesses two DoF:

1. Rotation about the steering axis (in this case perpendicular to the ground).
2. Lateral translation of the steering joint used to reproduce lateral flexibility.

The model does not take into account the gyroscopic influences. A linear model with relaxation effect is used for the tyre forces. Even with this strongly simplified configuration, some important effects are described, which also occur in motorcycle modelling. The destabilising effect of the cornering stiffness, as prescribed by Sharp [3], is reproduced. Moreover, the inversion of behaviour experienced in motorcycle simulation when using an infinite stiff front frame (Section 2) is also present. This is a remarkable result, as this model does not reproduce the gyroscopic moments, which are considered in [2,6] as responsible for the inversion of behaviour. This could suggest that also other phenomena influence the wobble stability. In Section 4.1 this hypothesis is further developed.

Limebeer [13] (p. 189) carries on his analysis by converting the shimmy model into a front fork model. In this case, the caster angle is considered for the steering axis and the gyroscopic effects are also considered. Another important feature is a revolute joint connecting the fork assembly to the ground. This simulates the motorcycle's frame torsional flexibility, which provides a lateral flexibility at wheel level, as described in Section 2. Thanks to this feature, the eigenvalue analysis of this system provides results similar to those generally obtained with motorcycle modelling. Cossalter [2] (p. 251) also produced a similar model with the aim of studying wobble; however, it lacks the mentioned lateral flexibility and transient tyre properties, thereby failing to capture the physics of the wobble mode.

The simplified front fork model is acceptable when the aim is to only reproduce wobble. When studying weave, however, a whole motorcycle model is needed. The "basic" motorcycle model

is generally updated with some additional degrees of freedom in order to reproduce, for example, the frame compliance or the rider motion.

In Section 3.1 the motorcycle model used in the present work is explained.

3.1. Motorcycle Model

The model used in this work is based on [10], where a model for BMW sport motorcycles from the 1990s was developed and validated with several experimental data, especially regarding the weave and wobble modes. The kinematic structure of the rear suspension and the dataset in the present paper are based on [12]. This reference uses a model with 13 DoF:

- Six DoF related to the main frame rigid body motion: translation about x, y, z axes, roll (ρ), pitch (ϕ) and yaw (ψ).
- Two wheel spins (θ_{fw}, θ_{rw}).
- Two suspension travels (z_f, z_r).
- Steer rotation (δ).
- Frame torsion (α_{fr}) at the steering head joint, simulated with a revolute joint with rotation axis perpendicular to the steering axis.
- Rider lean (α_{ri}) simulated with a revolute joint between the rider's lower and upper body with rotation axis parallel to the main frame x axis.

In the present work some additional DoF are added, which are shown in Figure 1.

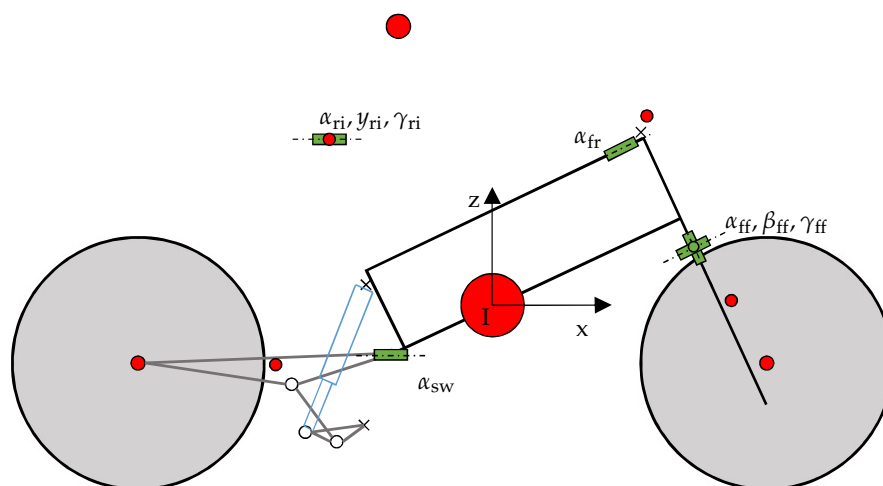


Figure 1. Motorcycle sketch with the DoF associated with the stiffnesses. The small rectangles indicate the related joints. The red points represent the bodies' centre of mass.

- Three compliances of the front fork, simulated with three revolute joints placed approximately at the half of fork length:
 - Bending about the x axis (α_{ff}); the rotation axis of the revolute joint is perpendicular to the steering axis. This compliance is particularly important for wobble, as explained in Section 2. It allows a lateral motion of the wheel along the y axis.
 - Bending about the y axis (β_{ff}); the rotation axis of the revolute joint is parallel to the front wheel axis. This flexibility allows a translation of the wheel along the x axis.
 - Torsion (γ_{ff}); the rotation axis of the revolute joint is parallel to the steering axis.
- Lateral motion of the rider's lower body with respect to the saddle (y_{ri}), simulated with a linear joint with axis parallel to the main frame y axis.
- Rider yaw rotation (γ_{ri}) simulated with a revolute joint between the rider's lower and upper body with rotation axis parallel to the main frame z axis.

- Swingarm torsion (α_{sw}), simulated with a revolute joint at the swingarm anchor point with rotation axis parallel to the main frame x axis.

The motorcycle parameters in [12] were obtained through experimental measurements or through estimates. However, some parameter variations have been used in the present work:

- The data for the rider's upper body mass and inertia tensor were taken from [12]. In [12] the mass and inertia tensor of the rider's lower body and of the motorcycle's main frame were fused together. In the present work, with the aim of allowing lateral translation of the rider's hip (considered as lower body in the present work), the mass and inertia tensor of the main frame in [12] were split between hip and main frame, while ascertaining that the combined inertia tensor and the overall centre of gravity remain unchanged. The data for hip's mass and inertia tensor were taken from [38]. According to these data, the mass and inertia tensor of the main frame were properly modified. In particular, the hip mass was subtracted from the main frame mass in [12]. Moreover, as explained above, the inertia tensor of the main frame was adapted so that the whole inertia tensor of the lower body and main frame together was equal to the main frame inertia in [12]. The rider's legs were considered fixed to the main frame, so their mass and inertia were included in it. As reported in [12] (p. 252), the rider's total mass was 72 kg.
- In the year of publication of [12] the experimental data of the front fork were not completely available. Some of them were judged by the authors of the present work as not realistic (for example, the mass of the lower fork and its lacking inertia tensor). For this reason, the front fork mass and inertia data were taken from [39], while retaining the overall geometry given in [12].

The motorcycle's parameters are reported in Appendix A.

The tyre forces and moments were reproduced with the Pacejka magic formula; further details on the tyre model are given in Section 3.4. The software for the motorcycle model is available on GitHub: https://github.com/TUMFTM/motorcycle_model.git.

3.2. Suspension

There are several types of motorcycle suspension. The simplest configuration is composed of a telescopic front suspension and a cantilever rear suspension. However, multi-link suspensions have been developed for both front and rear wheels. For the rear suspension, the multi-link solution allows a non-linear damping curve to be obtained even with a linear damper, as the kinematic function of the damper travel can be adjusted using a rocker. Multi-link at the front suspension generally increases the fork stiffness and favours the anti-dive property. For further details the reader is referred to [13] (p. 327). The motorcycle adopted in the present work uses a telescopic front suspension and a unitrack-like rear suspension (definition of [13]), where the spring-damper unit is connected to the chassis and to a rocker, while a pull rod connects the rocker to the swingarm. The kinematic functions of this rear suspension are presented in [12]. Figure 1 shows its geometry.

3.3. Rider Model

In contrast to cars, the rider's weight strongly influences the total motorcycle weight in riding conditions. Moreover, the rider has some relative motions with respect to the motorcycle. One can therefore expect the rider to have a great influence on motorcycle stability. This is indeed the case, as shown by both simulation [7,40] and experimental [41] results. In this work we only focus on the rider's passive motions. This is reasonable, as the eigenfrequencies of wobble and weave are too high for the rider to actively counteract them; therefore, it can be assumed that the rider behaves as a passive body when the motorcycle experiences wobble or weave. Under this assumption, different rider models can be developed. The most simple model has been adopted by several works [12,26–28] and includes only one DoF: the rider's upper body rotation about an axis parallel to the frame x axis. A different one-DoF model [42] reproduces the rider's rotation about the vertical axis (parallel to the frame z axis); moreover, the connection between the upper body and handlebar is included

with a parallel rotational spring-damper element. A 2-DoF model can then be obtained by combining the two previously described models [40]. Finally, the lateral displacement (frame y axis) of the rider’s hip can be added, thereby obtaining a 3-DoF rider model [7]. An interesting observation is made by Limebeer [13] (p. 326) about the influence of the rider’s parameters: he reports that the rider’s upper body parameters mainly influence the weave mode, while the lower body parameters have a greater effect on wobble. The literature also offers several examples of more complex rider models containing up to 28 DoF [43]. In this case, the rider model was used to faithfully evaluate the motorcycle race performances, so that the whole rider motion was needed, including his control action on the handlebars and his lean-in strategy. As introduced at the beginning of this paragraph, the current work pursues a very different objective, i.e., the analysis of the motorcycle eigenmodes, so that such a complex rider model is not necessary and would only complicate the interpretation of the results.

The rider model used in the present work is based on that presented in [7]. The rider is composed by two masses, representing the upper and lower body. The DoF are:

- α_{ri} : the rider’s upper body lean.
- γ_{ri} : the rider’s upper body yaw.
- y_{ri} : the rider’s hip (lower body) lateral motion.

As previously said, the connection with the handlebar is modelled by a rotational spring-damper element which reacts to the relative rotation between the upper body and handlebar, and applies equal and opposite moments for lower body and upper body, and frame and steering head, respectively.

3.4. Tyre Model

As introduced in Section 2, the present model uses the Pacejka magic formula to describe the tyre forces. The tyre model is analogous to that reported by Sharp [12] and is suited for motorcycles, as it accounts for the lateral force generation due to the wheel roll angle (camber angle). Moreover, it also describes the longitudinal forces, thereby allowing the motorcycle to be simulated in all possible conditions. Another peculiar factor is the description of the combined longitudinal and lateral force generation. This means that the maximal tyre-lateral force is reduced when the tyre simultaneously generates a longitudinal force (and vice versa). The model also takes into account the variation of the tyre potential with changing vertical load.

The present tyre model considers the tyre width. In this way, in contrast to thin disc models, the overturning moment must not be added separately, as the lateral migration of the contact point automatically generates this overturning moment [12,28].

The magic formula needs some inputs: longitudinal slip (κ), slip angle (α), camber angle (ρ_w), vertical load (F_z). κ can be calculated with Equation (1).

$$\kappa = -\frac{v_{x_C} - \omega_y (r_{rim} + r_c \cos \rho_w)}{v_{x_C}}, \tag{1}$$

where v_{x_C} is the longitudinal velocity of the tyre contact point, r_{rim} is the rim radius, r_c is the tyre crown radius and ω_y is the wheel rotation speed. α is calculated with a first order relaxation equation:

$$\frac{\sigma}{v_{x_C}} \dot{\alpha} + \alpha = \alpha_{ss}, \quad \alpha_{ss} = -\arctan \left(\frac{v_{y_C}}{v_{x_C}} \right), \tag{2}$$

where α_{ss} is the slip angle in steady-state conditions, while v_{y_C} is the lateral velocity of the tyre contact point. This means that the lateral force due to the slip angle is generated with some delay depending on the relaxation length σ . Its value is not constant and depends on both longitudinal speed and vertical load; these dependencies are taken into account in the present model. The longitudinal force and the lateral force due to the camber angle are assumed to build up instantaneously, so no relaxation equation is used.

At this point, a geometrical model of the tyre contact point and a related reference frame are needed in order to calculate the velocity components v_{y_C}, v_{x_C} at the contact point itself and the vertical load F_z . Firstly, the orientation of the reference frame at the contact point has to be obtained. It should satisfy the following requirements: z axis being perpendicular to the road; x axis being in the wheel plane and parallel to the road. Such a reference frame can be derived with two rotations starting from the reference frame of the wheel carrier, indicated in the following with the subscript W_c . The intermediate reference frame W is obtained as follows:

$$\begin{aligned} W e_x &= \frac{W_c e_y \times I e_z}{|W_c e_y \times I e_z|}, \\ W e_y &= W_c e_y, \\ W e_z &= W e_x \times W e_y, \end{aligned} \tag{3}$$

where ${}_{ref}e_i$ is the unit vector of the i th axis of the reference frame named "ref", and $I e_z = [0, 0, 1]^T$. The frame W has the x axis parallel to the ground. In order to get C , another transformation is needed, which allows the z axis to be perpendicular to the ground:

$$\begin{aligned} C e_x &= W e_x, \\ C e_z &= I e_z, \\ C e_y &= C e_z \times C e_x. \end{aligned} \tag{4}$$

The unit vectors in Equation (3) define the rotation matrix ${}_I S_W = [W e_x, W e_y, W e_z]$ from frame W to the inertial frame I . Similarly, the rotation matrix from frame C to I is defined as ${}_I S_C = [C e_x, C e_y, C e_z]$. Now the longitudinal and lateral velocities v_{x_C}, v_{y_C} can be calculated in the following steps:

$$\begin{aligned} {}_W v_{W_c} &= {}_I S_W^T {}_I v_{W_c}, \\ {}_W v_C &= {}_W v_{W_c} + {}_W \omega_{W_c} \times [0, -r_c \sin \rho_w, -r_{rim} - r_c \cos \rho_w]^T, \\ {}_I v_C &= {}_I S_W {}_W v_C, \\ {}_C v_C &= {}_I S_C^T {}_I v_C. \end{aligned} \tag{5}$$

${}_B v_A$ is the absolute velocity vector of the generic point A in the generic frame B . The vector ${}_C v_C$ represents the velocity of the contact point in frame C ; its first and second components provide v_{x_C}, v_{y_C} .

The last remaining input for the magic formula is the vertical load. This is composed by a constant $F_{z,stat}$ and a varying part $F_{z,dyn}$. The constant one is obtained in static equilibrium conditions. The second one depends on motorcycle trim and can be calculated using the tyre carcass compression Δz_{tyre} from the nominal state.

$$\Delta z_{tyre} = -r_{rim} \cos \rho_w - r_c + {}_I z_{0C} - {}_I z_{W_c}. \tag{6}$$

${}_I z_{0C} > 0$ is the vertical distance under static equilibrium conditions between the origin of the inertial frame I and the contact point. ${}_I z_{W_c} > 0$ is the instantaneous vertical distance between the origin of the inertial frame I and the wheel carrier W_c . Finally, the tyre vertical load F_z is calculated as follows:

$$F_z = F_{z,stat} + F_{z,dyn} = F_{z,stat} - c_z \Delta z_{tyre} - d_z v_{z_C}. \tag{7}$$

c_z, d_z are the tyre vertical stiffness and damping, respectively. It is worth pointing out that Δz_{tyre} is negative when the carcass is compressed; therefore, the carcass compression leads, through Equation (7), to an increased vertical load.

All the inputs for the magic formula are now available. The equations of the magic formula are taken from [12], so they are not repeated here. The outputs are: longitudinal force, lateral force and aligning moment. These outputs are applied in the wheel carrier and not at the contact point as in [12]. This choice was made because in MBSim the forces must be applied to a body, which would require the definition of a body in the contact point, which in the actual model structure is not an easy task. Shifting the tyre forces in the wheel carrier requires applying additional moments; this is, however, easily done, as all the lever arms are known or can be derived with geometric reasoning. The equivalence between this force system and the one with the forces applied at the contact point has been verified on a simplified model with a single wheel. The results are equivalent, thereby confirming the correctness of the choice made.

3.5. Validation

As explained in Section 3.1, the motorcycle model in the present work is based on the data of [12]. The obvious solution is then to validate the present model against this reference by Sharp. In order to do so, the front fork data were set to the values in [12]; moreover, the additional DoF were "switched off." This was possible thanks to a functionality developed for this purpose in MBSim, which allows the selection of the DoF to be considered. Reference [12] reports the simulation results of a steady-state cornering condition with fixed roll angle and at different speeds. Several variables are then shown under this condition; particularly important for steady-state cornering are: steering torque, front and rear tyre-lateral forces and aligning moments. The same condition has been tested in the present work and the variables compared. The accordance is very good, with deviations less than 5% for all values. This is shown Figure 2, where F_{y_f}, F_{y_r} are the front and rear tyre-lateral forces, while M_{z_f}, M_{z_r} are the front and rear tyre aligning moments and T_δ is the steer torque.

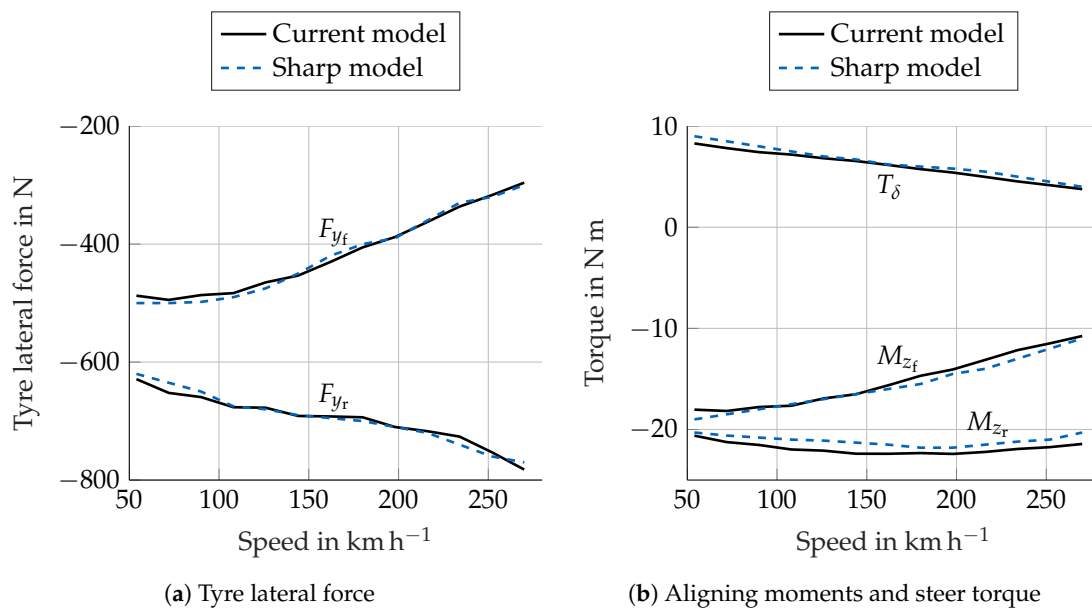


Figure 2. Model validation with steady-state analysis: comparison between the current model and the model of Sharp for a steady-state cornering maneuver. F_{y_f}, F_{y_r} are the front and rear tyre-lateral forces, while M_{z_f}, M_{z_r} are the front and rear tyre aligning moments and T_δ is the steer torque.

As further validation, the present model was also compared with that in [26] (p. 508) by Pacejka. This model renounces some DoF with respect to [12]: the suspensions are not modelled. Moreover, the frame torsional stiffness is not present, while the front fork has bending compliance. Using the same data of [26] and with the same DoF, a comparison of the eigenvalue analysis has been carried out. Additionally, in this case the agreement of the results is very good, with the curves of the wobble

and weave eigenfrequencies and damping as a function of the speed almost overlapping, as shown in Figure 3. In this figure, the frequency is expressed in rad s^{-1} in order to facilitate the comparison with the results of [26], where this unit of measurement is used. In the subsequent paragraphs, however, the frequency will be expressed in Hz. Additionally, the selection of the speed range in Figure 3 was made according to [26].

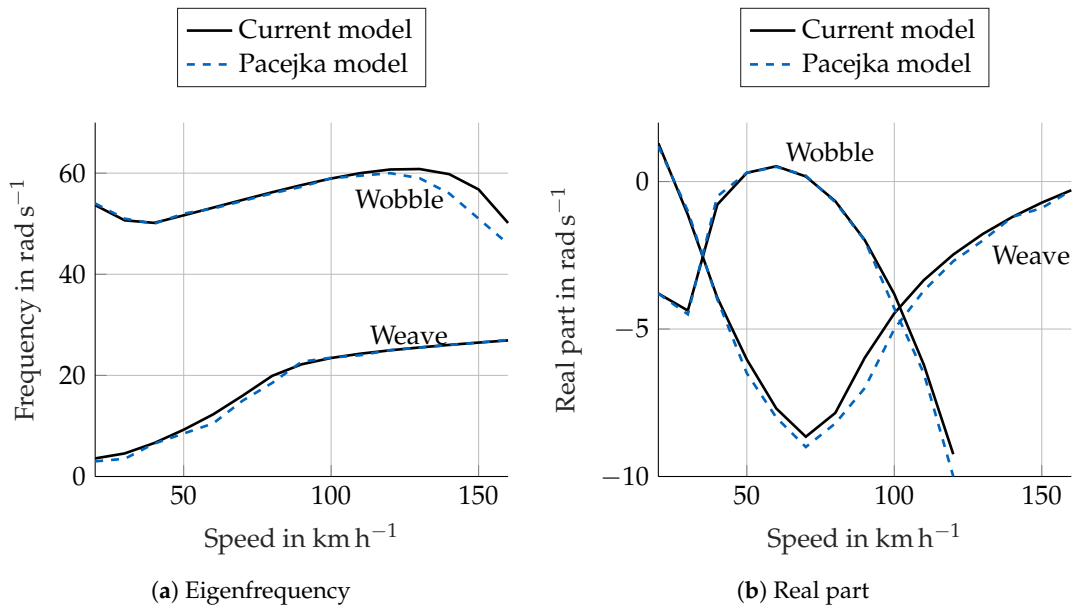


Figure 3. Model validation with eigenvalue analysis: comparison between the current model (parametrised with the same data of the Pacejka model) and the model of Pacejka.

4. Results

This section shows the eigenvalue analysis and the time response for the presented model. Starting from these plots, some physical relations will be derived and will help to understand the important phenomena influencing the behaviour of the wobble and weave eigenmodes as a function of vehicle speed.

4.1. Wobble

Section 2 describes how the front fork lateral flexibility (bending-compliance about the x axis) strongly influences the stability of wobble. This difference is shown in Figure 4. In order to isolate the influence of the fork compliance, the curve relative to the rigid fork was obtained with a 9-DoF model, wherein the DoF used to represent the motorcycle’s stiffnesses, as described in Section 3.1, have been eliminated. Moreover, the rider’s DoF are not present. In the curve relative to the flexible fork, only the DoF α_{ff} has been added, so that the DoF are 10 in total. With the parameter set used in the present work and in the speed range considered, the wobble mode remains well damped. This is due to the relatively high value of the steering damper. In the following part of this section, the reason for such a drastic behaviour change between rigid and flexible fork is addressed. In particular, a possible cause is presented which partially differs from the explanation provided by Cossalter [2] (p. 280) and Spierings [6].

A key concept described in Section 2 is the correlation between tyre properties and wobble. In particular, a tyre model with cornering stiffness is necessary to reproduce wobble [3,16,17,20]. Therefore, the tyre and specifically the lateral force due to the slip angle is a fundamental factor when considering wobble stability. However, what is the reason for the behaviour inversion in Figure 4 and how can it be attributed to the tyre response? Equation (2) shows how the slip angle depends on the

lateral velocity of the wheel contact point v_{yC} . The fork lateral flexibility allows some lateral motion of the wheel because of the rotation about the revolute joint axis (fork x axis), thereby influencing v_{yC} .

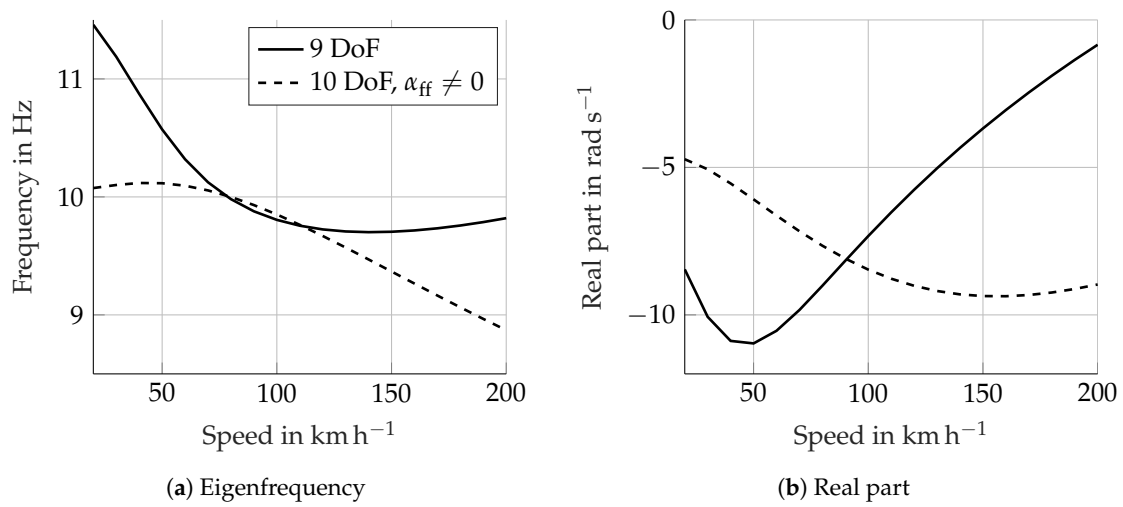


Figure 4. Influence of front fork flexibility on wobble.

This concept is shown schematically in Figure 5. The variation of v_{yC} due to the fork lateral flexibility can be expressed as:

$$\Delta v_{yC} = h \dot{\alpha}_{ff}. \tag{8}$$

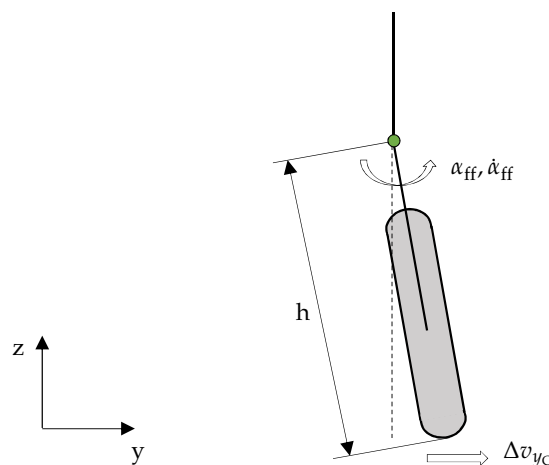


Figure 5. Variation of the lateral velocity at the contact point due to lateral fork flexibility.

To prove the effect of Δv_{yC} , it is compensated by subtracting its value from v_{yC} in Equation (2). Figure 6 shows the corresponding eigenvalue analysis with the dots-marked curve. The compensation of Δv_{yC} remarkably stabilises wobble. Moreover the curve shows the same behaviour for the 9-DoF model. At this point a conclusion can be drawn: the fork lateral flexibility influences the wobble stability through its effect on the lateral velocity v_{yC} of the contact point.

In a subsequent step, it is of particular interest to observe whether Δv_{yC} increases or reduces the value of v_{yC} . Figure 7 shows a time simulation at 50 km h⁻¹ with a steer torque impulse as excitation. The full line represents v_{yC} obtained from Equation (5); the dashed line was obtained with $v_{yC} - \Delta v_{yC}$, whereby Δv_{yC} was derived from Equation (8). The subtraction of Δv_{yC} increases the value of v_{yC} : Δv_{yC} , which is normally included in v_{yC} , thereby reduces the amplitude of v_{yC} . The tyre-lateral force is proportional to the slip angle, which is proportional to v_{yC} (Equation (2)). This force tends to

oppose the wheel motion due to the wobble oscillation. Therefore, the fork flexibility introduces a Δv_{yC} , which reduces the tyre-lateral force. This explains why the curve with $\Delta v_{yC} = 0$ in Figure 6 is significantly more stable than the 10-DoF case with $\Delta v_{yC} \neq 0$.

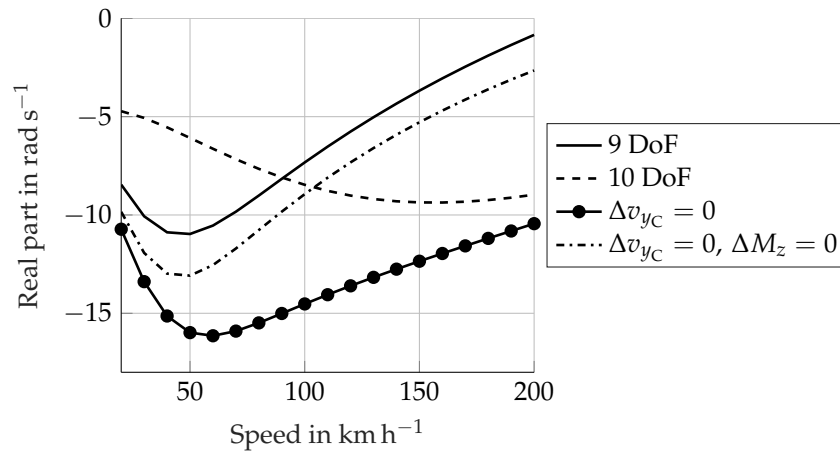


Figure 6. Effect of compensating Δv_{yC} on wobble damping. In the dotted curve only Δv_{yC} is compensated. In the dash-dotted curve both Δv_{yC} and ΔM_z (with Equation (9)) are compensated.

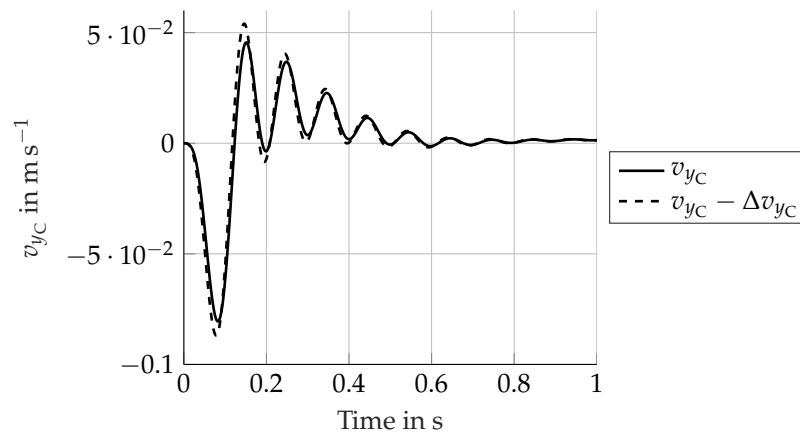


Figure 7. Variation of the lateral velocity of the contact point v_{yC} due to front fork flexibility. Time simulation at 50 km h⁻¹ and with a steer torque impulse as excitation.

Even if the curve with compensated Δv_{yC} in Figure 6 assumes the same qualitative behaviour as the 9-DoF model, the damping values are still significantly different. In order to get a curve similar to that of the 9-DoF model, the gyroscopic moment introduced by fork bending must be compensated. The moment acts about the steering axis and can be calculated with Equation (9) (this formula differs from the complete Euler equations (compare to Equation (10)), whose left-hand side defines the whole gyroscopic effects. Equation (9) is used here because its simple structure allows one to compensate the gyroscopic effects about the steering axis as external moments in the used multibody simulation software), as shown by Cossalter [5]. This formula is also well-known in the literature, as it is present in the book on vehicle dynamics by Mitschke [44]. The symbol Δ in Equation (9) indicates that the formula only refers to the gyroscopic moment due to the fork lateral flexibility.

$$\Delta M_z = \dot{\alpha}_{ff} \omega_{y_{fw}} I_{y_{y_{fw}}}, \tag{9}$$

where $\omega_{y_{fw}}$ is the front wheel rotation speed and $I_{y_{y_{fw}}}$ is its polar moment of inertia. The dash-dotted curve in Figure 6 shows the effect of compensating ΔM_z . As expected, the damping curve gets very

close to the 9-DoF model. The remaining offset can be attributed to other secondary phenomena, which have not yet been completely identified.

In summary, the influence of the fork bending compliance on wobble can be explained by considering two main phenomena:

1. Gyroscopic moment;
2. Variation of the lateral speed of the wheel contact point.

Both of them originate through the rotation α_{ff} and its time derivatives.

When observing the curve of the 10-DoF case in Figure 6, it is evident that it is less stable than the 9-DoF case only up to about 80 km h^{-1} . Above this speed, the higher stability of the 10-DoF model compared to the 9-DoF model can be justified with the same consideration made by Cossalter [5]: the gyroscopic moment ΔM_z about the steering axis stabilises the wobble with increasing speed.

At this point another question may be raised: Which phenomenon is responsible for the decreasing wobble damping shown by the 9-DoF model and the model with compensated Δv_{yC} compared to the 10-DoF one? To answer this question, a model containing only the front fork and front wheel has been used. With this model two cases are studied: two DoF characterised by the rigid fork and three DoF with a flexible fork; the first model correlates with the 9-DoF model, and the second with the 10-DoF model.

Figure 8a shows the damping curves for these two models. Different variations were made: the wheel inertia tensor I_{fw} was set to 1% of the original value (to eliminate the gyroscopic moments) and Δv_{yC} has been compensated as in Figure 6. Some important conclusions can be drawn:

- The 2-DoF model did not show a decrease in damping with increasing speed, as did the 9-DoF model.
- The damping of the 3-DoF model grew more rapidly than the one of the 10-DoF model.
- The case $I_{fw} = 1\%$, $\Delta v_{yC} = 0$ is very close to the curve of the 2-DoF model, as was expected by theoretical observations. In fact, the 2-DoF model had no gyroscopic moments about the steering axis, as no rotation about the fork x axis was present. In Figure 6 the curve with $\Delta v_{yC} = 0$ shows a remarkable offset compared to the 9-DoF curve because of the gyroscopic moments. With I_{fw} set to 1% they almost vanish, resulting in a smaller offset.

The difference in behaviour between the 2 and 9-DoF models can be justified by the additional roll motion of the 9-DoF case. This motion produces additional gyroscopic moments which apparently destabilise the wobble with increasing speed. These moments are also clearly present in the 10-DoF model. However, in this case they are compensated by the gyroscopic moment produced by the fork flexibility. The opposition of these two effects is underlined by the saturation shown in the 10-DoF model at about 150 km h^{-1} , which is not present in the 3-DoF model.

In summary, the wobble damping behaviour of a real motorcycle is determined by three principal mechanisms. The front fork flexibility produces a lateral movement of the front wheel, which can be represented with a rotation α_{ff} . This reduces the tyre-lateral force and thus decreases the wobble damping at low speed compared to a rigid fork. When the speed increases, the gyroscopic moment caused by the rotation α_{ff} increases in magnitude and stabilises the wobble, thereby making the 10 DoF model more stable than the 9-DoF model. The third mechanism is related to the gyroscopic moments caused by the motorcycle's roll motion. They destabilise the wobble with increasing speed, thereby explaining why the wobble damping in the 9-DoF model decreases with increasing speed. This does not happen in the 10-DoF model because the stabilising gyroscopic moment caused by α_{ff} outweighs the destabilising effect.

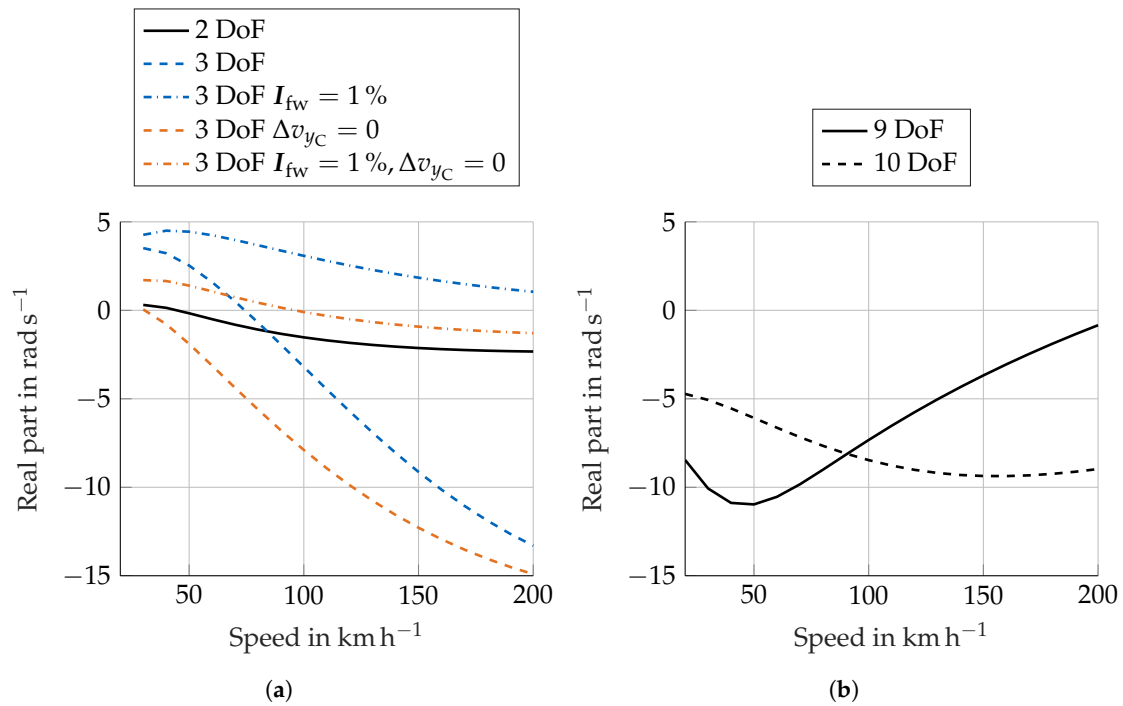


Figure 8. (a) Wobble damping for the 2 and 3-DoF models with variation of the tensor I_{fw} and compensation of Δv_{yC} . The curve with $I_{fw} = 1\%$ for the 2-DoF model is identical to that with $I_{fw} = 100\%$ so it was not plotted. (b) Figure 4b copied to facilitate the comparison.

4.2. Weave

The weave mode was already captured in its essence by the very first motorcycle model by Whipple [13] (p. 195). Moreover, there is no evidence of parameters which produce a behaviour inversion of the damping curve, as can be observed for the wobble mode. This already suggests that the weave mode reproduces in some way the "basic" motorcycle behaviour. This idea was also proposed by Schröter [45] (p. 28), who describes the weave mode as a degenerated dynamic stabilisation process involving steering, roll and yaw oscillations. This can be shown with a simple time simulation where the upright riding motorcycle is excited with a lateral force impulse applied to the frame. Assuming that the wobble is well damped, the motorcycle reacts to this excitation with a weave oscillation, which may diverge or stabilise depending on the motorcycle's speed and parameters.

Figure 9 shows the frequency and damping of the weave mode as a function of the speed. The effect of the rider is analysed in Section 4.3, so this figure refers to the case with a rigid rider; the other DoF are all present. In order to represent the saturation shown by the damping curve at high speed, the speed range differs from the one in Figure 4. The behaviour of the weave damping shows some interesting characteristics: below 70 km h^{-1} weave is stabilised with increasing speed; above it is destabilised. However, above 220 km h^{-1} the weave damping shows a plateau. This particular behaviour suggests that the weave mode changes with speed. Moreover, the speed dependency could be explained by a certain influence of the gyroscopic effects, which are also speed dependent. The gyroscopic effects are obtained with the whole left-hand side of the Euler equations, which is shown in Equation (10) for the front wheel.

$$I_{fw}\dot{\omega}_{fw} + \omega_{fw} \times (I_{fw}\omega_{fw}) = M_{ext}, \tag{10}$$

where ω_{fw} is the rotational velocity vector of the front wheel and I_{fw} is the front wheel inertia tensor.

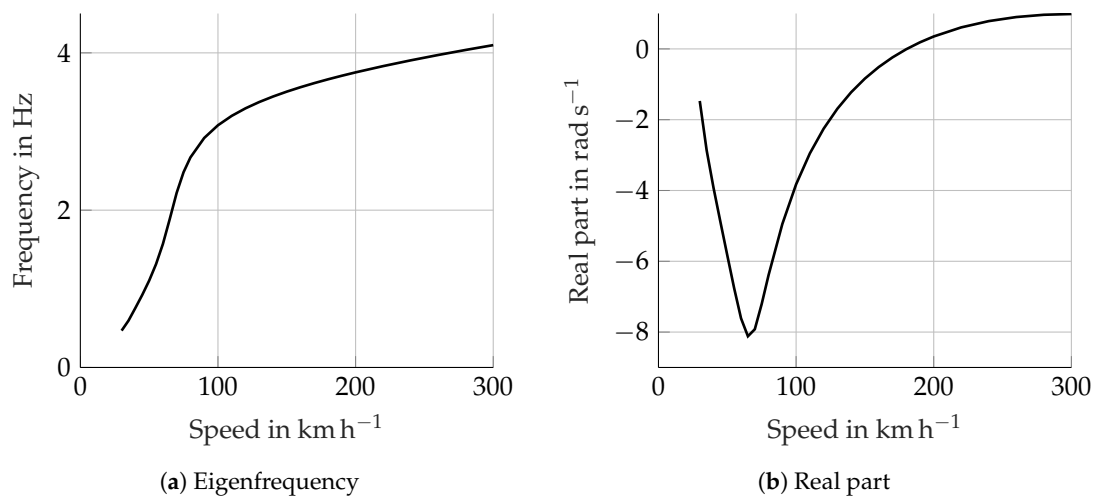


Figure 9. Weave eigenfrequency and damping as a speed function.

Figure 10 further illustrates this concept. In this figure, the weave eigenvector is shown with the so-called compass plot. The arrows are named phasors and represent how the motorcycle’s DoF are involved in the weave oscillation. An arrow’s length is the magnitude of the motion of the related DoF. In order to maintain the information about the absolute amplitude of the phasors, no normalisation is present. The phasor’s angle shows the phase. In the following paragraphs the relative angle between the phasors is called relative phase.

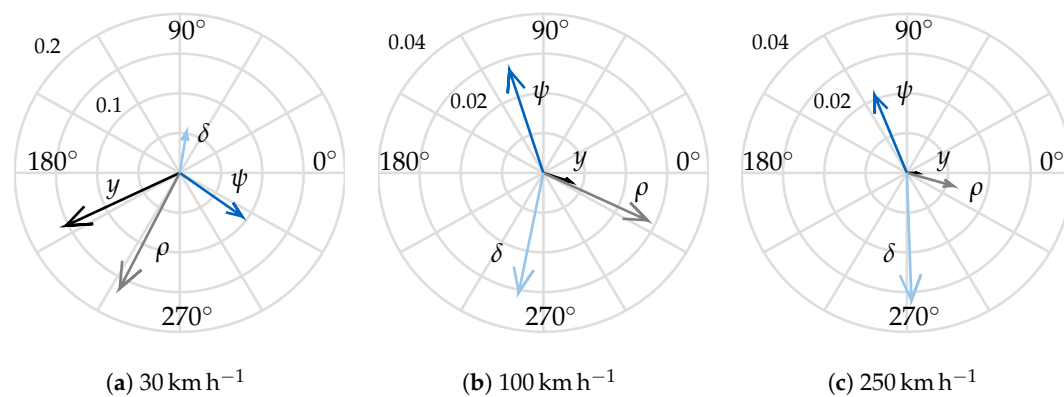


Figure 10. Compass plot of the weave eigenvector at different speeds. δ is the steering angle, ψ is the yaw angle, ρ is the roll angle and y is the lateral displacement.

At low speed, (Figure 10a) the roll (ρ) and lateral displacement (y) show big amplitudes. The latter is due to the small gyroscopic effects, so that if weave is excited (for example, with a lateral impulse), the motorcycle describes a “slalom” at low frequency (see Figure 9) involving a significant lateral displacement. This can be described as a low-frequency “self-stabilising” motion, which the literature already considers as weave.

As the speed increases (Figure 10b), the relative phase between the motions significantly changes, whereby the lateral displacement is no longer important. The other DoF show a similar amplitude. Finally, when the speed increases further (Figure 10c), the relative phase does not change remarkably. The most important observation, however, is the reduction of the roll (ρ) amplitude with increasing speed, which can be seen when comparing the related phasor in Figure 10b,c. This can also be observed in the time simulation. If the motorcycle is excited by a lateral impulse at high speed, the resulting weave oscillation does not show a significant roll motion, while the front wheel and the frame rotate

around the steering and vertical axis almost in opposition of phase, as shown by the vectors δ, ψ in Figure 10c. The reduction in roll motion with increasing speed is also shown by a free rolling wheel. This phenomenon can be explained considering the gyroscopic effects which increase with speed, thereby preventing the wheel (or the motorcycle) capsizing.

Which are the possible causes of the peculiar damping behaviour shown in Figure 9b? Some useful knowledge can be derived by an eigenvalue analysis with reduced wheel inertia. The correlation to Figure 10 is shown in Figure 11, for which the total wheel inertia tensors I_{fw}, I_{rw} was set to 10% of the original tensors. The first consideration resulting from the comparison is that in Figure 11 the relative phase between the phasors no longer changes with speed, as it happens in Figure 10. The plot at 30 km h^{-1} is not present, as the weave mode is no longer available at this speed. It is important to point out that, because of this massive inertia reduction, the gyroscopic effects almost disappear. Two main observations can be made:

1. The missing weave mode at low speed can be attributed to the (almost) missing gyroscopic effects. The time simulation at 30 km h^{-1} with a lateral force impulse shows that the motorcycle does not react to the excitation with a weave oscillation, but it capsizes. With the original inertia values the gyroscopic effects are present, despite the low speed. They prevent the motorcycle from capsizing immediately after the excitation and producing the low-frequency “self-stabilising” motion.
2. The gyroscopic effects are also the main cause for the change in the weave eigenvector shown in Figure 10. In fact, when they are very small, as in Figure 11, the relative phase between the eigenvector components is no longer speed dependent.

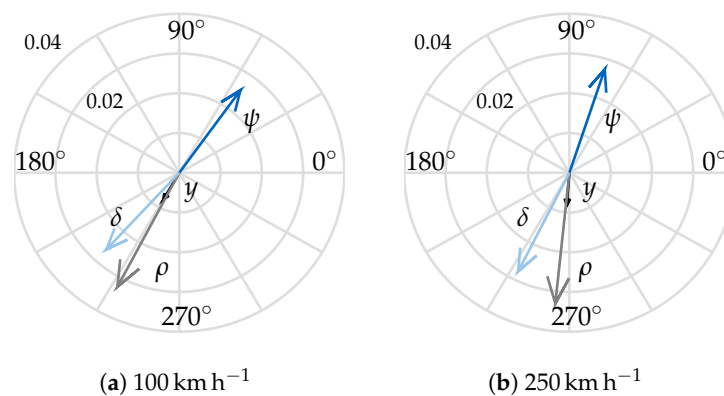


Figure 11. Compass plot of the weave eigenvector at different speeds with $I_{fw}, I_{rw} = 10\%$.

The correlation with Figure 9 is shown in Figure 12. The speed range starts now from 80 km h^{-1} , as for the following reasoning only this range is necessary. Moreover, the weave with reduced wheel inertia is not present up to about 50 km h^{-1} and in the range $50\text{--}80 \text{ km h}^{-1}$ it is extremely well damped (real part $> 25 \text{ rad s}^{-1}$). Similarly to the full inertia case, the damping continues to decrease with increasing speed in the small inertia case shown in Figure 12b. As the gyroscopic effects are almost missing, the reason for this behaviour can be determined by investigating in the tyre response. The tyre-lateral force is proportional to the slip angle which is in turn proportional to the ratio between v_{yC} and v_{xC} (Equation (2)). The authors verified that v_{yC} mainly depends on the kinematic steering angle (see [2] for its definition), which is proportional to the steering angle. Figure 11 shows that above a certain speed (100 km h^{-1}) the amplitude of steering motion in the weave eigenvector remains fairly constant. The numerator of α_{ss} in Equation (2) is therefore almost constant with speed. The denominator of α_{ss} is given by v_{xC} , which clearly increases with speed. As a result, α_{ss} decreases with increasing speed and so does the tyre-lateral force. The tyre-lateral forces tend to bring the motorcycle back to the equilibrium position, thereby stabilising the weave. The decreasing tyre force is therefore responsible for the decreasing weave damping and the hyperbolic behaviour of the dashed curve in Figure 12b.

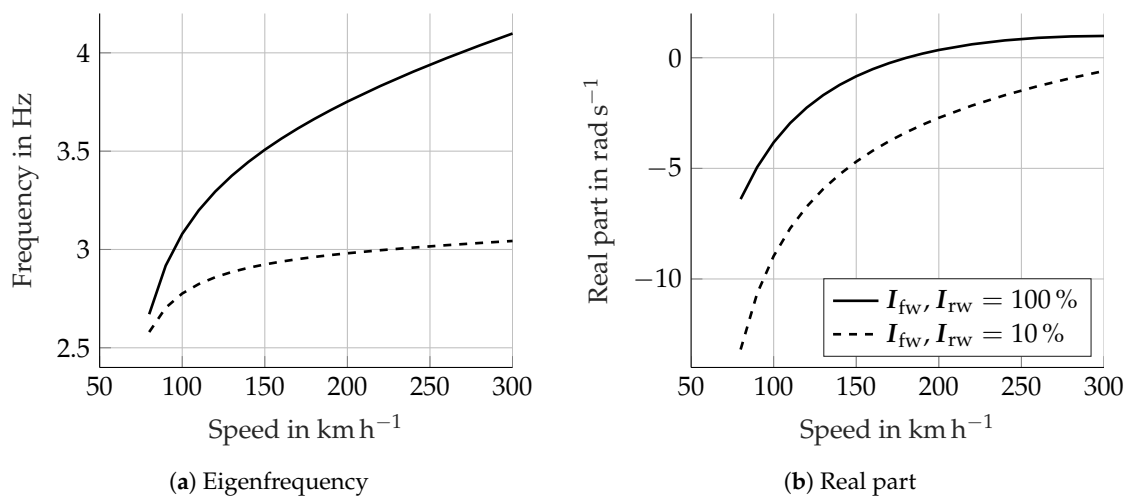


Figure 12. Comparison between the eigenvalue analysis with original wheel inertia tensors and reduced inertia tensors.

Considering again the curve with the original wheel inertia in Figure 12, the first observation is the smaller weave damping. This can be explained by taking into account the additional impact of the gyroscopic effects. The gyroscopic effects of the front wheel about the steering axis are in counterphase with respect to the tyre moments, as Figure 13 shows, therefore they work against them. For this reason, the weave damping is lower compared to the reduced inertia case. The gyroscopic effects also justify the slower damping decrease in the case with original wheel inertia (see Figure 12). In fact, due to the progressively changing eigenvector (Figure 10), i.e., the decreasing roll motion amplitude, the gyroscopic effects increase underproportionally with the speed. For example, in a time simulation with lateral force excitation, the first peak of the front wheel gyroscopic effects about the z axis increase from 100 to 150 km h⁻¹ by 37.5%, while they only increase by 14.5% from 250 to 300 km h⁻¹. As a consequence, they also underproportionally reduce the tyre forces with increasing speed. This, combined with the decreasing tyre forces, leads to the mentioned saturation above 220 km h⁻¹, which is not present in the reduced inertia case.

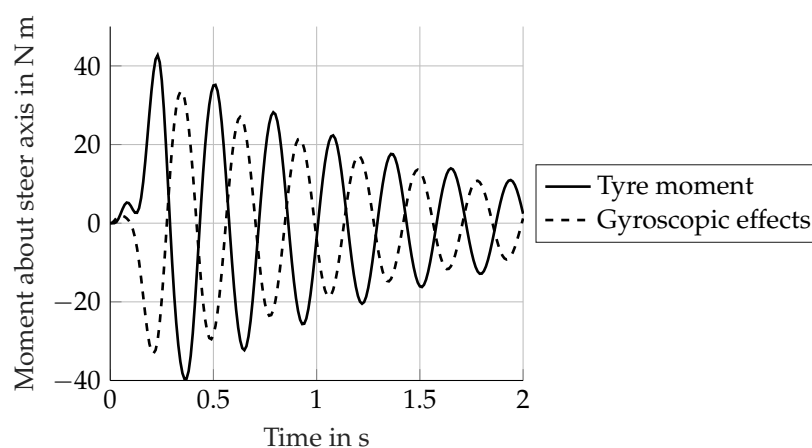


Figure 13. Front wheel gyroscopic effects and tyre moments about the steering axis. The time simulation was obtained with a lateral force excitation on the motorcycle frame at the speed of 150 km h⁻¹.

The last characteristic to be observed is the increase in damping shown below 80 km h⁻¹ in Figure 9b. The authors’ belief is that in this lower speed range the weave mode can still be seen as the already mentioned low-speed “self-stabilising” motion. When increasing the speed, this motion progressively changes to the “real” weave, thereby producing the observed increase in damping.

Figure 14 illustrates this fact. Following the three compass plots with increasing speed, one can see that the phase and amplitude of the phasors progressively change; i.e., the weave changes from the “self-stabilising” motion to the classical weave. In fact, above 100 km h^{-1} the relative angle between the phasors no longer changes significantly, as the comparison of Figure 10b,c shows.

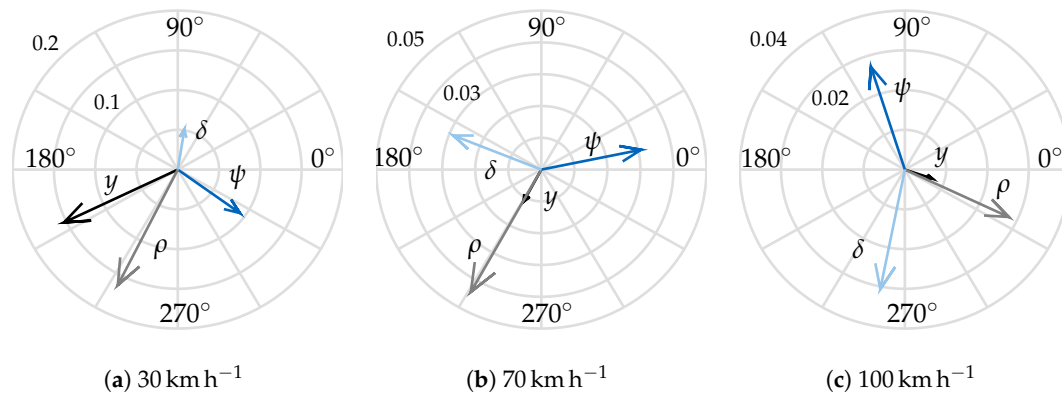


Figure 14. Compass plot of the weave eigenvector at different speeds.

4.3. Rider Influence

As explained in Section 3.3, the literature offers different examples of rider modelling. These references often analyse the influences of the rider on weave and wobble stability. For example, reference [42] investigates the effect of the rider yaw combined with the connection to the handlebar. Reference [7] proposes the eigenvalue analysis with the 3-DoF rider also used in the present work. In order to obtain a better overview of the single influences, this section aims to briefly summarise the essential differences between the three different DoF models used for rider modelling. This is shown in Figure 15. The effect of the single DoF can be summarised as follows:

- The rider lean α_{ri} stabilises the weave and destabilises the wobble at high speed. The increased stability of weave is a reasonable result because during the weave oscillation the rider lean is almost in counterphase to the motorcycle’s roll [41], thereby damping out this motion.
- The rider yaw γ_{ri} combined with the connection to the handlebar destabilises the weave, massively stabilises the wobble and also increases its eigenfrequency. This is in accordance with [42] and is a reasonable result, as the connection acts in a similar way to a steering damper, which also stabilises the wobble while destabilising the weave.
- The rider’s hip lateral motion y_{ri} hardly affects the eigenmodes, as also reported by [31]. The only remarkable influence is the increase in the wobble frequency at high speed.

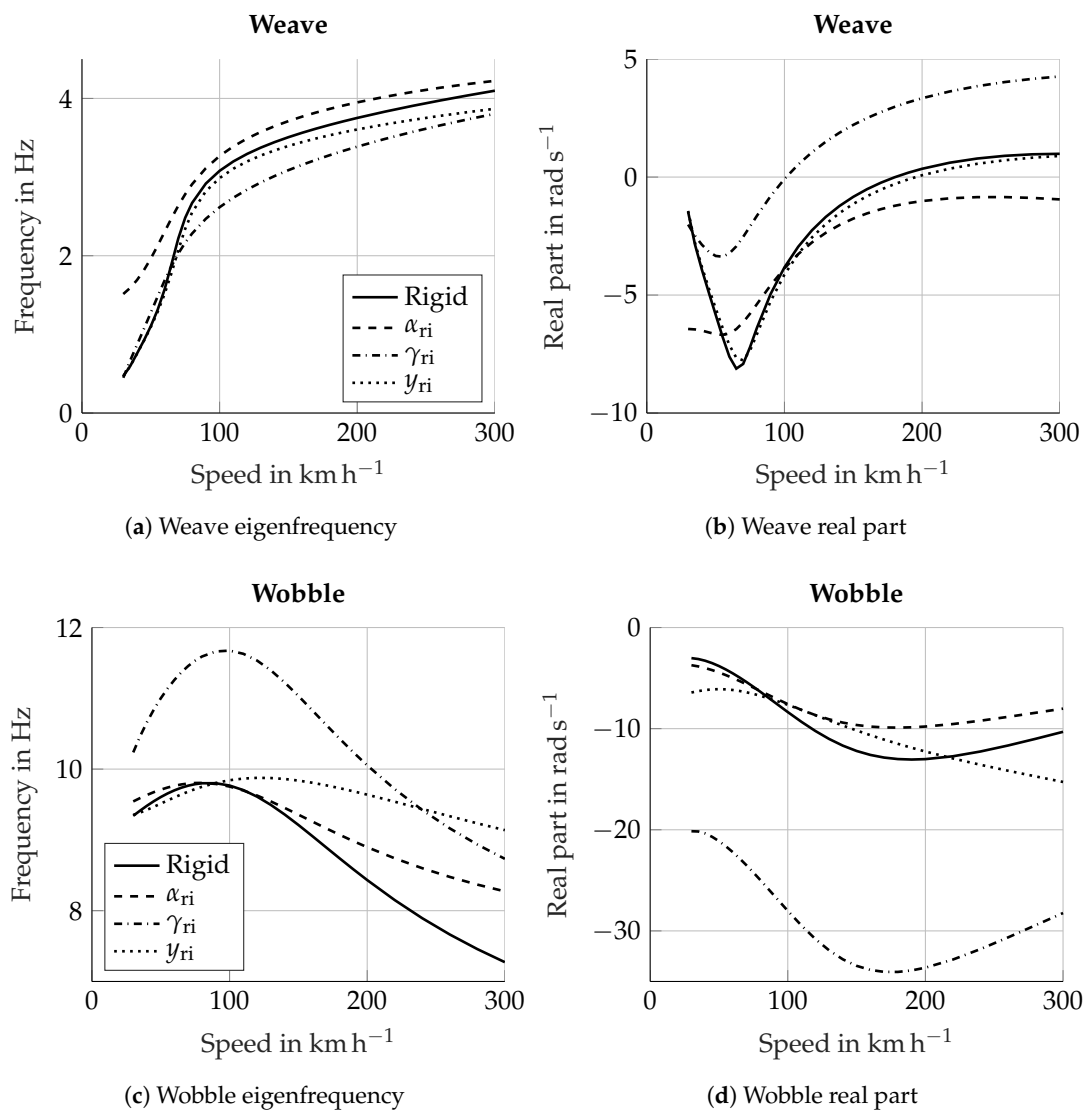


Figure 15. The effects of the single rider’s DoF on the weave and wobble modes.

Figure 16 shows the effect of the whole rider model, containing the three DoF α_{ri} , y_{ri} , γ_{ri} . In the weave the effect of α_{ri} overcomes the others, thereby causing the already mentioned stabilisation at high speed. When concerning wobble, the effect of γ_{ri} and the connection with the handlebar are dominant, leading to an increase in both frequency and damping.

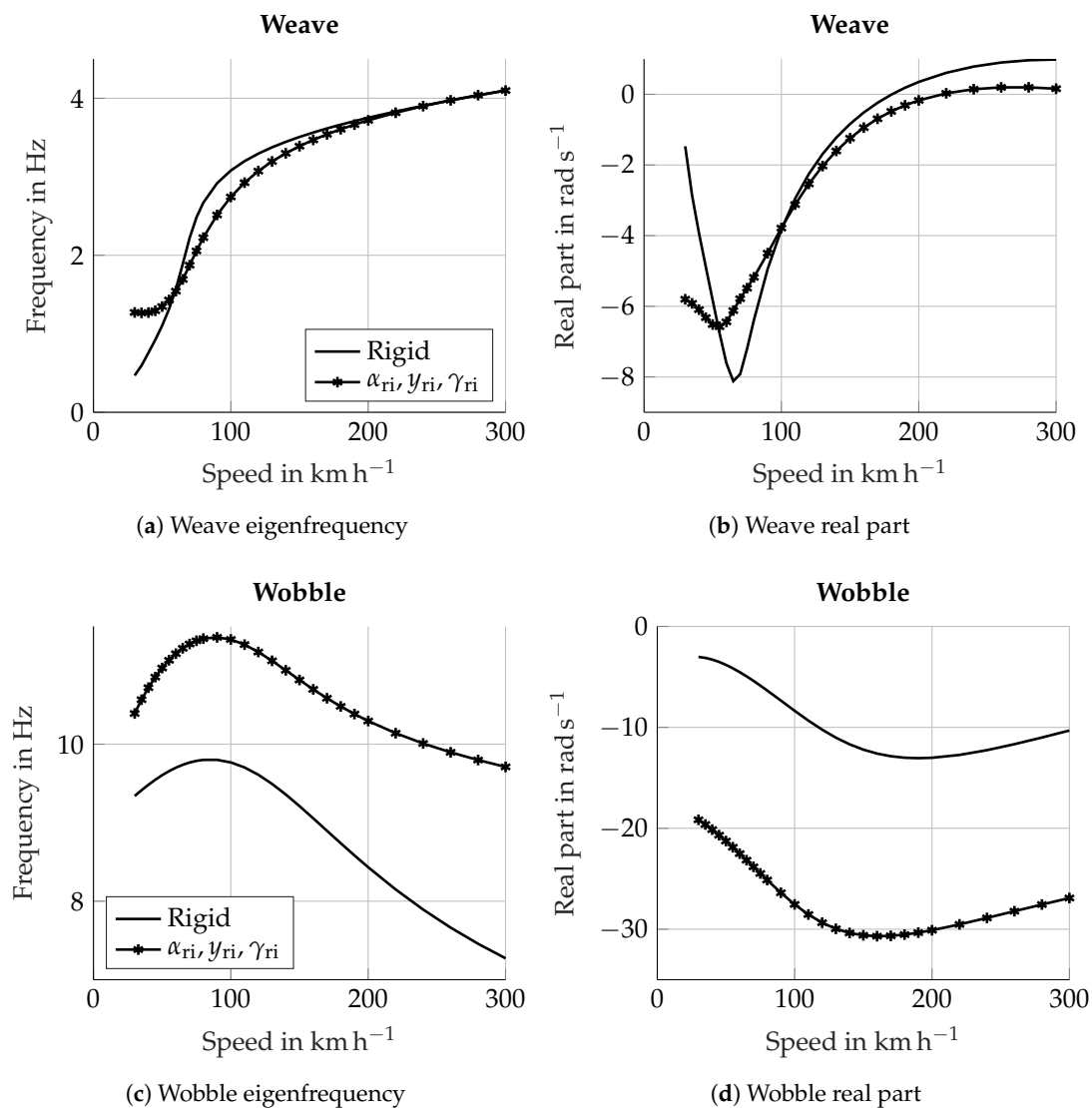


Figure 16. Effect of the whole rider model (3-DoF) on the weave and wobble modes.

5. Conclusions and Outlook

The present work further analysed the physical phenomena behind the wobble and weave eigenmodes. In particular, the effect of the front fork bending compliance has been discussed and a possible justification for the well-known weave damping behaviour with increasing speed is provided. Finally, the effect of the single rider’s DoF on the weave and wobble mode has been shown.

The first aspect has been addressed before by Cossalter [5] and Spierings [6]. They noticed that the modelling of the fork bending compliance allows very similar results to the real driving experience to be obtained: the wobble mode is unstable at low speed and stabilises with increasing speed. Without this parameter, the simulation results are not realistic. Cossalter [5] justifies this behaviour considering the superposition of two effects, both caused by the fork bending compliance: this compliance alone is destabilising but it also produces a gyroscopic moment about the steering axis that stabilises the wobble. The first effect dominates at low speeds, while the second prevails at high speed. The present work provides an additional perspective for explaining the effect of the fork bending compliance, though maintaining the validity of the previous results [5]. The additional insight is given by the tyre behaviour. It was demonstrated that the lateral motion of the wheel contact point caused by the fork bending compliance reduces the lateral component of the contact point velocity

v_{yC} . The tyre-lateral force is proportional to this velocity component through the slip angle. Reducing v_{yC} also reduces the tyre force. This causes a reduction in the wobble damping at below 80 km h^{-1} . At higher speeds, the effect of the gyroscopic moments introduced by the fork flexibility leads to increasing wobble damping with increasing speed, as explained by Cossalter [5].

The weave damping behaviour is well-known and involves a progressive stabilisation up to about 80 km h^{-1} (with the present parameters), then the damping decreases with increasing speed until it reaches a saturation above 220 km h^{-1} . This peculiar behaviour can now be explained. The weave eigenvector changes with speed. In the lower speed range this corresponds to a change from a low frequency self-stabilising motion involving a lot of frame lateral displacement to a weave oscillation where the lateral motion is no longer significant. The eigenvector change is supposed to be the main cause of the damping increase below 80 km h^{-1} . Above this lower speed range, the weave eigenvector does not change in the relative phase between phasors, but the roll component becomes progressively smaller. This influences the gyroscopic effects, which underproportionally increase with speed, thereby causing the plateau above 220 km h^{-1} .

The multibody model used in this work was provided with a functionality to select the different DoF. This gives the chance to investigate the separated influence of the single DoF used in the rider model. In particular, the rider lean stabilises the weave and slightly destabilises the wobble; the rider yaw plus the connection with the handlebar destabilises the weave and remarkably stabilises the wobble. The whole 3-DoF rider model produces the same effect of the rider lean as regards weave and the same effect of rider yaw as regards wobble.

The contributions of the present paper to general motorcycle dynamics knowledge can be summarised as follows. A review of the literature on motorcycle dynamics and stability behaviour; this knowledge has been interpreted in order to derive some minimal prerequisites to the motorcycle model, with the aim of conducting a stability analysis. After that, the effect of the tyre response on the wobble damping was analysed, thereby leading to considerations that fuse together with and partially complete the theory exposed by Cossalter [5] and Spierings [6]. Moreover, a possible justification for the well-known weave damping behaviour was given, which was not found in the literature. Finally, the influence of the rider model on stability, which was already studied in previous works, has been summarised, thereby facilitating the interpretation of the effect of the single rider's DoF.

Further development of the present paper could involve the inclusion of a "flexible body" to faithfully reproduce the different frame flexibilities without using lumped stiffnesses.

Author Contributions: F.P. is the leading author who wrote the whole paper. The project and problem formulation were conceptualised by F.P. and D.W.; these authors also built the motorcycle model and produced the results presented in this paper. D.W., A.E., F.D. and A.G. revised the paper critically for important intellectual content. Conceptualisation, F.P. and D.W.; formal analysis, F.P. and D.W.; methodology, F.P. and D.W.; supervision, A.E., D.W., A.G. and F.D.; validation, F.P. and D.W.; visualization, F.P.; writing—original draft, F.P.; writing—review and editing, A.E., D.W., A.G. and F.D. All authors have read and agreed to the published version of the manuscript.

Funding: This research received no external funding.

Acknowledgments: The motorcycle model is completely based on the multibody simulation software "MBSim". The author would like to thank Martin Förg (University of Landshut), who is one of the developers of "MBSim", for the support and suggestions during the building phase of the model. Several structural choices, such as the possibility to select the model DoF, were possible thanks to his contribution.

Conflicts of Interest: The authors declare no conflict of interest.

Nomenclature/Notation

Symbol	Unit	Description
α	rad	Tyre slip angle
α_{ff}	rad	Front fork bending about fork x axis
α_{fr}	rad	Frame torsion at steering head joint
α_{ri}	rad	Rider's upper body lean angle
α_{sw}	rad	Swingarm torsion
β_{ff}	rad	Front fork bending about fork y axis
γ_{ff}	rad	Front fork torsion
γ_{ri}	rad	Rider's upper body yaw rotation
δ	rad	Steer rotation
ΔM_z	N m	Gyroscopic moment due to fork flexibility
Δv_{yC}	m s ⁻¹	Variation of the lateral velocity of the wheel contact point
Δz_{tyre}	m	Tyre carcass compression
θ_{fw}	rad	Front wheel spin angle
θ_{rw}	rad	Rear wheel spin angle
κ	-	Longitudinal slip
ρ	rad	Main frame roll angle
ρ_w	rad	Wheel camber angle
σ	m	Relaxation length
ϕ	rad	Main frame pitch angle
ψ	rad	Main frame yaw angle
${}^B\omega_A$	rad s ⁻¹	Rotational velocity vector of the generic point A in the generic frame B
ω_{fw}	rad s ⁻¹	Front wheel rotational velocity vector
ω_y	rad s ⁻¹	Wheel rotational speed
c_z	N m ⁻¹	Tyre carcass vertical stiffness
d_z	N s m ⁻¹	Tyre carcass vertical damping
${}^{ref}e_i$	-	Unit vector of the <i>i</i> th axis of the "ref" reference frame
F_{yf}	N	Front tyre-lateral force
F_{yr}	N	Rear tyre-lateral force
F_z	N	Tyre vertical load
I_{fw}	kg m ²	Front wheel inertia tensor
I_{rw}	kg m ²	Rear wheel inertia tensor
M_δ	N m	Steer torque
M_{zf}	N m	Front tyre aligning moment
M_{zr}	N m	Rear tyre aligning moment
${}^B\mathbf{S}_A$	-	Transformation matrix from system A to system B
${}^B\mathbf{v}_A$	m s ⁻¹	Absolute velocity vector of the generic point A in the generic frame B
v_{xC}	m s ⁻¹	Longitudinal speed of the wheel contact point
v_{yC}	m s ⁻¹	Lateral speed of the wheel contact point
v_{zC}	m s ⁻¹	Vertical speed of the wheel contact point
y_{ri}	m	Rider's lower body lateral motion
z_f	m	Front suspension travel
z_r	m	Rear suspension travel

Appendix A

Appendix A.1. Geometric Parameters

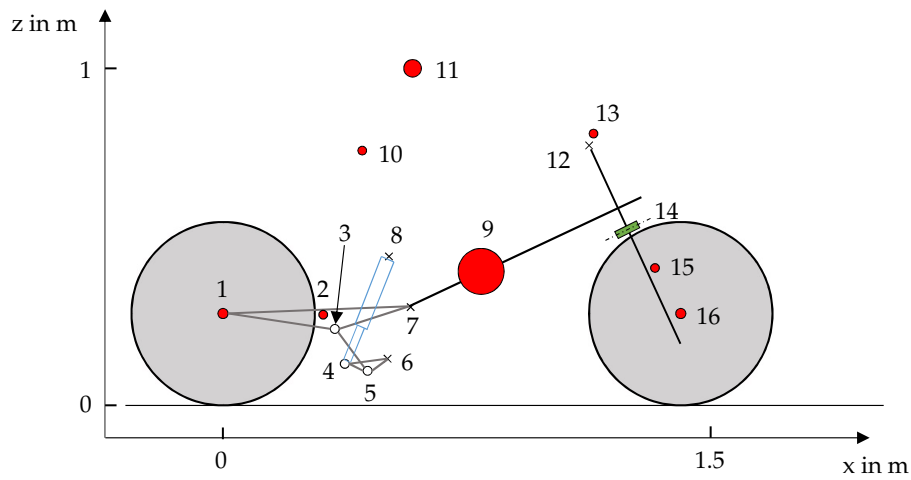


Figure A1. Scheme for the geometric parameters.

Table A1. Dimensions.

Point	x in m	z in m
1	0	0.297
2	0.196	0.3113
3	0.3722	0.2748
4	0.4443	0.1782
5	0.4946	0.1522
6	0.539	0.1878
7	0.549	0.3608
8	0.487	0.4888
9	0.6779	0.4724
10	0.364	0.8438
11	0.415	1.14
12	1.173	0.749
13	1.1803	0.7818
14	1.3036	0.5209
15	1.3125	0.4357
16	1.41	0.282

Table A2. Wheel geometry.

Parameter	Symbol	Value in m
Front wheel radius	r_{fw}	0.282
Front wheel crown radius	$r_{c\,fw}$	0.06
Front wheel rim radius	$r_{rim\,fw}$	0.222
Rear wheel radius	r_{rw}	0.297
Rear wheel crown radius	$r_{c\,rw}$	0.095
Rear wheel rim radius	$r_{rim\,rw}$	0.202

Appendix A.2. Tyre Coefficients

Table A3. Tyre vertical stiffness and damping.

Parameter	Symbol	Value
Front tyre vertical stiffness	$c_{z\text{ fw}}$	130,000 N m ⁻¹
Front tyre vertical damping	$d_{z\text{ fw}}$	800 N s m ⁻¹
Rear tyre vertical stiffness	$c_{z\text{ rw}}$	141,000 N m ⁻¹
Rear tyre vertical damping	$d_{z\text{ rw}}$	800 N s m ⁻¹

The other tyre coefficients used in the present work were taken from [12].

Appendix A.3. Stiffness and Damping

Table A4. Lumped stiffness and damping values. The DoF refer to Figure 1.

DoF	Stiffness	Damping
Frame torsion α_{fr}	163,000 N m rad ⁻¹	100 N m s rad ⁻¹
Front fork bending α_{ff}	55,300 N m rad ⁻¹	20 N m s rad ⁻¹
Front fork bending β_{ff}	55,300 N m rad ⁻¹	20 N m s rad ⁻¹
Front fork torsion γ_{ff}	16,000 N m rad ⁻¹	20 N m s rad ⁻¹
Swingarm torsion α_{sw}	63,700 N m rad ⁻¹	20 N m s rad ⁻¹
Rider rotation about x axis α_{ri}	380 N m rad ⁻¹	34 N m s rad ⁻¹
Rider rotation about z axis γ_{ri}	75.8 N m rad ⁻¹	4.79 N m s rad ⁻¹
Rider arms	1053.4 N m rad ⁻¹	19.28 N m s rad ⁻¹
Rider translation along y axis y_{ri}	38,416 N m rad ⁻¹	981 N s m ⁻¹

Appendix A.4. Suspensions

Table A5. Suspension's parameters.

Parameter	Value
Front spring stiffness	17,000 N m ⁻¹
Front spring unloaded length	0.35 m
Front spring preload	876.231 N
Front compression damping force at 2 m s ⁻¹	203 N
Front rebound damping force at 2 m s ⁻¹	865.8 N
Rear spring stiffness	58,570 N m ⁻¹
Rear spring unloaded length	0.3435 m
Rear spring preload	248.87 N
Rear compression damping force at 1 m s ⁻¹	9600 N
Rear rebound damping force at 1 m s ⁻¹	13,700 N

Appendix A.5. Mass and Inertia

Table A6. Mass parameters.

Parameter	Symbol	Value
Frame mass	m_{fr}	153.716 kg
Rider lower body mass	$m_{ri\ lo}$	11.414 kg
Rider upper body mass	$m_{ri\ ub}$	33.68 kg
Upper fork mass	$m_{ff\ up}$	9.3 kg
Lower fork mass	$m_{ff\ lo}$	6.5 kg
Front wheel mass	m_{fw}	11.9 kg
Swingarm mass	m_{sw}	8 kg
Rear wheel mass	m_{rw}	14.7 kg

Table A7. Inertia parameters.

Parameter	Symbol	Value
Frame inertia	I_{fr}	$\begin{bmatrix} 9.2774 & 0 & 2.267 \\ 0 & 19.0193 & 0 \\ 2.267 & 0 & 13.6702 \end{bmatrix}$ kg m ²
Rider lower body inertia	$I_{ri\ lo}$	$\begin{bmatrix} 0.1163 & 0 & -0.0055 \\ 0 & 0.0942 & 0 \\ -0.0055 & 0 & 0.1036 \end{bmatrix}$ kg m ²
Rider upper body inertia	$I_{ri\ ub}$	$\begin{bmatrix} 1.4280 & 0 & -0.443 \\ 0 & 1.347 & 0 \\ -0.443 & 0 & 0.916 \end{bmatrix}$ kg m ²
Upper fork inertia (z axis \equiv steer axis)	$I_{ff\ up}$	$\begin{bmatrix} 0.5 & 0 & 0 \\ 0 & 0.4 & 0 \\ 0 & 0 & 0.13 \end{bmatrix}$ kg m ²
Lower fork inertia (z axis \equiv steer axis)	$I_{ff\ lo}$	$\begin{bmatrix} 0.3 & 0 & 0 \\ 0 & 0.25 & 0 \\ 0 & 0 & 0.09 \end{bmatrix}$ kg m ²
Front wheel inertia	I_{fw}	$\begin{bmatrix} 0.27 & 0 & 0 \\ 0 & 0.484 & 0 \\ 0 & 0 & 0.27 \end{bmatrix}$ kg m ²
Swingarm inertia	I_{sw}	$\begin{bmatrix} 0.02 & 0 & 0 \\ 0 & 0.259 & 0 \\ 0 & 0 & 0.259 \end{bmatrix}$ kg m ²
Rear wheel inertia	I_{rw}	$\begin{bmatrix} 0.383 & 0 & 0 \\ 0 & 0.638 & 0 \\ 0 & 0 & 0.383 \end{bmatrix}$ kg m ²

References

1. Sharp, R.S. Stability, Control and Steering Responses of Motorcycles. *Veh. Syst. Dyn.* **2001**, *35*, 291–318. [CrossRef]
2. Cossalter, V. *Motorcycle Dynamics*, 2nd ed.; Lulu Press: Morrisville, NC, USA, 2006.
3. Sharp, R.S. The stability and control of motorcycles. *J. Mech. Eng. Sci.* **1971**, *13*, 316–329. [CrossRef]
4. Koch, H. *Zusammenhänge und Einflüsse von Lebensalter, Fahrerfahrung und Motorleistung auf die Unfallverwicklung von Motorradfahranfängern*; VDI-Berichte: Düsseldorf, Germany, 1987.
5. Cossalter, V.; Lot, R.; Massaro, M. The influence of frame compliance and rider mobility on the scooter stability. *Veh. Syst. Dyn.* **2007**, *45*, 313–326. [CrossRef]
6. Splerings, P.T.J. The Effects of Lateral Front Fork Flexibility on the Vibrational Modes of Straight-Running Single-Track Vehicles. *Veh. Syst. Dyn.* **1981**, *10*, 21–35. [CrossRef]
7. Cossalter, V.; Lot, R.; Massaro, M. An advanced multibody code for handling and stability analysis of motorcycles. *Meccanica* **2011**, *46*, 943–958. [CrossRef]

8. Koenen, C.; Pacejka, H.B. The Influence of Frame Elasticity and Simple Rider Body Dynamics on Free Vibrations of Motorcycles in Curves. *Veh. Syst. Dyn.* **1981**, *10*, 70–73. [[CrossRef](#)]
9. Cossalter, V.; Doria, A.; Mitolo, L. *Inertial and Modal Properties of Racing Motorcycles*; SAE Technical Papers; SAE International: Warrendale, PA, USA, 2002.
10. Wisselmann, D. *Motorrad-Fahrdynamik-Simulation. Modellbildung, Validierung und Anwendung*. Ph.D. Thesis, VDI-Berichte, Dachau, Germany, 1992.
11. Schindler, T.; Förg, M.; Friedrich, M.; Schneider, M.; Esefeld, B.; Huber, R.; Zandler, R.; Ulbrich, H. Analysing Dynamical Phenomenons: Introduction to MBSim. In Proceedings of the 1st Joint International Conference on Multibody System Dynamics, Lappeenranta, Finland, 25–27 May 2010.
12. Sharp, R.S.; Evangelou, S.A.; Limebeer, D.J.N. Advances in the Modelling of Motorcycle Dynamics. *Multibody Syst. Dyn.* **2004**, *12*, 251–283. [[CrossRef](#)]
13. Limebeer, D.J.N.; Massaro, M. *Dynamics and Optimal Control of Road Vehicles*; Oxford University Press: Oxford, UK, 2018.
14. Cossalter, V.; Doria, A.; Massaro, M.; Taraborrelli, L. Experimental and numerical investigation on the motorcycle front frame flexibility and its effect on stability. *Mech. Syst. Signal Process.* **2015**, *60–61*, 452–471. [[CrossRef](#)]
15. Meirovitch, L. *Elements of Vibration Analysis*; Mc Grow Hill: New York, NY, USA, 1975.
16. Doria, A.; Favaron, V.; Taraborrelli, L.; Roa, S. Parametric analysis of the stability of a bicycle taking into account geometrical, mass and compliance properties. *Int. J. Veh. Des.* **2017**, *75*, 91–123. [[CrossRef](#)]
17. Doria, A.; Roa, S. On the influence of tyre and structural properties on the stability of bicycles. *Veh. Syst. Dyn.* **2018**, *56*, 947–966. [[CrossRef](#)]
18. Klinger, F.; Nusime, J.; Edelmann, J.; Plöchl, M. Wobble of a racing bicycle with a rider hands on and hands off the handlebar. *Veh. Syst. Dyn.* **2014**, *52*, 51–68. [[CrossRef](#)]
19. Sharp, R.S.; Alstead, C.J. The Influence of Structural Flexibilities on the Straight-running Stability of Motorcycles. *Veh. Syst. Dyn.* **1980**, *9*, 327–357. [[CrossRef](#)]
20. Plöchl, M.; Edelmann, J.; Angrosch, B.; Ott, C. On the wobble mode of a bicycle. *Veh. Syst. Dyn.* **2012**, *50*, 415–429. [[CrossRef](#)]
21. Roa, S.; Doria, A.; Muñoz, L. Optimization of the Bicycle Weave and Wobble Modes. *Am. Soc. Mech. Eng.* **2018**, *3*. [[CrossRef](#)]
22. Diermeyer, F.; Eisele, A. Lecture notes of the course Motorradtechnik. 2018, Unpublished manuscript.
23. Taraborrelli, L.; Favaron, V.; Doria, A. The effect of swingarm stiffness on motorcycle stability: experimental measurements and numerical simulations. *Int. J. Veh. Syst. Model. Test.* **2017**, *12*, 240. [[CrossRef](#)]
24. Weir, D.H.; Zeller, J.W. Experimental investigation of the transient behaviour of motorcycles. *SAE Trans.* **1979**, *88*, 962–978.
25. De Vries, E.; Pacejka, H.B. Motorcycle Tyre Measurements and Models. *Veh. Syst. Dyn.* **1998**, *29*, 280–298. [[CrossRef](#)]
26. Pacejka, H.B.; Besselink, I. *Tire and Vehicle Dynamics*, 3rd ed.; Butterworth-Heinemann: Oxford, UK, 2012.
27. Evangelou, S.A.; Limebeer, D.J.N.; Sharp, R.S.; Smith, M.C. Mechanical steering compensators for high-performance motorcycles. *J. Appl. Mech. Trans.* **2007**, *74*, 332–346. [[CrossRef](#)]
28. Sharp, R.S.; Limebeer, D.J.N. A Motorcycle Model for Stability and Control Analysis. *Multibody Syst. Dyn.* **2001**, *6*, 123–142. [[CrossRef](#)]
29. Cossalter, V.; Lot, R.; Maggio, F. A Multibody Code for Motorcycle Handling and Stability Analysis with Validation and Examples of Application. In *SAE International400 Commonwealth Drive*; SAE Technical Paper Series; SAE International: Warrendale, PA, USA, 2003. [[CrossRef](#)]
30. Limebeer, D.J.N.; Sharma, A. Burst Oscillations in the Accelerating Bicycle. *J. Appl. Mech. Trans.* **2010**, *77*, 061012. [[CrossRef](#)]
31. Roe, G.E.; Thorpe, T.E. A solution of the low-speed wheel flutter instability in motorcycles. *J. Mech. Eng. Sci.* **1976**, *18*, 57–65. [[CrossRef](#)]
32. Cossalter, V.; Lot, R.; Maggio, F. The Modal Analysis of a Motorcycle in Straight Running and on a Curve. *Meccanica* **2004**, *39*, 1–16. [[CrossRef](#)]
33. Limebeer, D.J.N.; Sharp, R.S.; Evangelou, S.A. Motorcycle Steering Oscillations due to Road Profiling. *J. Appl. Mech. Trans.* **2002**, *69*, 724–739. [[CrossRef](#)]

34. Sharp, R.S. The Influence of the Suspension System on Motorcycle Weave-mode Oscillations. *Veh. Syst. Dyn.* **1976**, *5*, 147–154. [[CrossRef](#)]
35. Lot, R. A Motorcycle Tire Model for Dynamic Simulations: Theoretical and Experimental Aspects. *Meccanica* **2004**, *39*, 207–220. [[CrossRef](#)]
36. Evangelou, S.A.; Limebeer, D.J.N.; Tomas-Rodriguez, M. Suppression of Burst Oscillation in Racing Motorcycle. *J. Appl. Mech.* **2013**, *80*, 011003. [[CrossRef](#)]
37. Karnopp, D. *Vehicle Dynamics, Stability, and Control*, 2nd ed.; CRC Press Taylor and Francis: Boca Raton, FL, USA, 2013.
38. Robbins, D.H. *Anthropometry of Motor Vehicle Occupants: Final Report October 1980–December 1983*; University of Michigan Transportation Research Inst: Ann Arbor, MI, USA, 1983; Volume 83-53-2.
39. Wunram, K.; Eckstein, L.; Rettweiler, P. *Potenzial Aktiver Fahrwerke zur Erhöhung der Fahrsicherheit von Motorrädern: Bericht zum Forschungsprojekt FE 82.328/2007*; Berichte der Bundesanstalt für Strassenwesen, Fahrzeugtechnik; Wirtschaftsverl. NW Verl. für Neue Wiss: Bremerhaven, Germany, 2011; Volume 81.
40. Sharp, R.S.; Limebeer, D.J.N. On steering wobble oscillations of motorcycles. *Proc. Inst. Mech. Eng. Part C J. Mech. Eng. Sci.* **2004**, *218*, 1449–1456. [[CrossRef](#)]
41. Doria, A.; Formentini, M.; Tognazzo, M. Experimental and numerical analysis of rider motion in weave conditions. *Veh. Syst. Dyn.* **2012**, *50*, 1247–1260. [[CrossRef](#)]
42. Cossalter, V.; Doria, A.; Lot, R.; Massaro, M. The effect of rider's passive steering impedance on motorcycle stability: Identification and analysis. *Meccanica* **2011**, *46*, 279–292. [[CrossRef](#)]
43. Sequenzia, G.; Oliveri, S.M.; Fatuzzo, G.; Calì, M. An advanced multibody model for evaluating rider's influence on motorcycle dynamics. *Proc. Inst. Mech. Eng. Part K J. Multi-Body Dyn.* **2015**, *229*, 193–207. [[CrossRef](#)]
44. Mitschke, M. *Dynamik der Kraftfahrzeuge*; Springer: Berlin/Heidelberg, Germany, 1972.
45. Schröter, K.G. Brake Steer Torque Optimized Corner Braking of Motorcycles. Ph.D. Thesis, Technische Universität Darmstadt, Darmstadt, Germany, 2015.



© 2020 by the authors. Licensee MDPI, Basel, Switzerland. This article is an open access article distributed under the terms and conditions of the Creative Commons Attribution (CC BY) license (<http://creativecommons.org/licenses/by/4.0/>).

4.2 Study of Weave and Wobble with Elastic Multi-body Simulation (EMBS) [IDETC/CIE 2022]

In the previous section, it was shown how the flexibility of the front fork plays a deciding role in the stability of wobble. As reported in Section 2.2.3, the literature shows that the other chassis flexibilities also influence both weave and wobble. This suggests that, for an accurate modeling of these eigenmodes, a model of the whole chassis flexibility is required. Most of the works in this field use the lumped stiffness approach (Section 2.3.1). However, they have never demonstrated if the accuracy of the lumped stiffness models is sufficient for this type of simulation. In fact, lumped stiffness models strongly approximate the flexural behavior of the real component, so this approximation could lead to incorrect results when simulating weave and wobble.

In this publication, the effect of structural flexibilities on weave and wobble is analyzed with the flexible multibody approach, i.e., leveraging on EMBS. The aim is to construct a model where the flexibility of each structural component is modeled with high accuracy. For the implementation of the flexible multibody approach the FFRF formulation is used, which is suitable to model the deformation of components that undergo large nonlinear rigid body motions and small linear elastic displacements. For the MOR required in the EMBS, two common approaches are adopted: Craig-Bampton and modal truncation. Moreover, for the implementation of the FFRF itself, the Tisserand frame method and the Reference Conditions method are compared.

To verify the accuracy of the flexible multibody models of the structural components, stiffness tests on the real components are compared with the same tests carried out in the simulation. The deviation between real data and simulation is under 6.5% and, therefore, the flexible multibody models of the components are used to build the flexible multibody motorcycle model, which is needed to simulate weave and wobble.

For the simulations, the model presented in Section 4.1 is adapted to represent a touring motorcycle for which the FEM models of the structural components were available. These models are processed with MOR to reduce their dimension and then included in the MBS environment. The motorcycle considered in this publication has a Telelever front suspension and, therefore, in the following the term “front assembly” is used instead of front fork. Moreover, the swingarm is a four-bar linkage (Paralever, Section 2.2.2). The components modeled as flexible bodies are: the frame, front assembly, and swingarm; the front assembly and swingarm are composed of several sub-components, which are listed in the publication.

The main results are reported in Figure 4.5, where multiple cases are compared: the curves marked as “Rigid” are obtained with the motorcycle model without any flexibility; the curves marked as “Frame”, “Front assembly” and “Swingarm” are obtained with a motorcycle model where only the indicated component is modeled as flexible body while the other are rigid; the curves marked as “All flexible” are generated with a motorcycle model where all the structural components are modeled as flexible bodies. The front assembly is the structural component whose flexibility has the strongest effect on both weave and wobble: compared to the rigid case, its flexibility destabilizes wobble at low speeds and stabilizes it at high speeds, thus qualitatively confirming the correlation described in Section 4.1. Moreover, the flexibility of the front assembly destabilizes weave at high speed. The flexibility of the frame has a similar influence as the front assembly, however, it is less marked because the frame is significantly stiffer. Finally, the flexibility of the swingarm does not affect wobble and slightly stabilizes weave at high speeds.

In Figure 4.6, a state-of-the-art lumped stiffness model of the front assembly is compared with the model where the front assembly is modeled with the flexible multibody approach. The

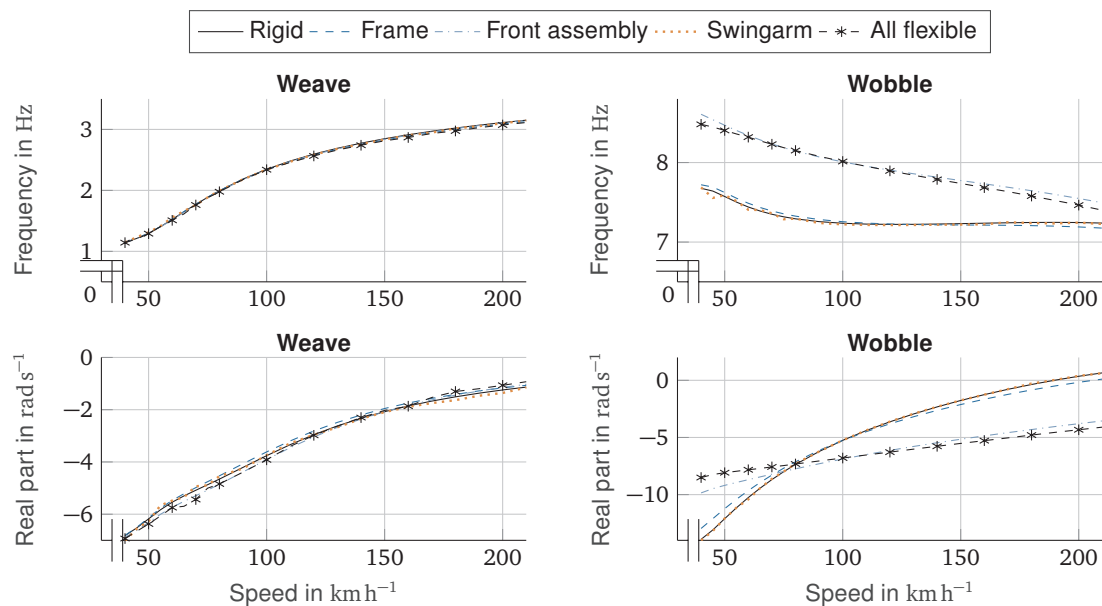


Figure 4.5: Effect of the flexibility of the structural components on weave and wobble [184].

state-of-the-art model is based on common assumptions on the position of the joints used to model the flexibility of the front assembly with the lumped stiffness approach. It presents a significant error with respect to the flexible multibody model. This confirms that lumped stiffness models can provide incorrect results if they are not parameterized appropriately. A method for solving this issue is proposed in Section 4.3.

Finally, some insights into MOR are provided and it is shown that, for modeling an assembly composed of several flexible bodies, the Craig-Bampton method provides better results than modal truncation. Moreover, it is shown that the Reference Conditions method, if applied correctly, can significantly reduce the computation cost of the model while preserving the accuracy.

Besides these results, the motorcycle model with flexible bodies serves as basis for the method presented in Section 4.3, where a lumped stiffness motorcycle model with high accuracy is proposed. In that context, the model presented in this publication is considered as “ground truth” to test the accuracy of the lumped stiffness motorcycle model.

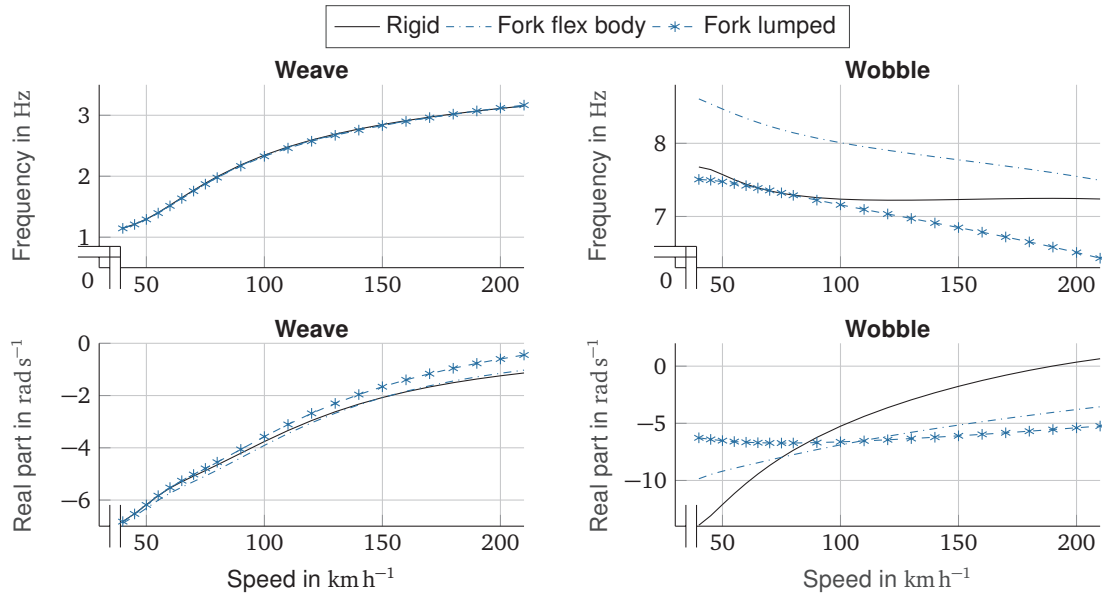


Figure 4.6: Comparison between the model with flexible front assembly and a state-of-the-art lumped stiffness model of the front assembly [184].

Contributions

F. P. as the first author initiated the idea of the paper and contributed significantly to the concept, modeling, and results. A. G. contributed to the review phase. F. D. contributed to the whole concept of the paper. F. D. gave final approval for publication of this version and is in agreement with all aspects of the work. As a guarantor, he accepts responsibility for the overall integrity of this paper.

Copyright notice

©ASME. Reprinted, with permission [184].

DETC2022-89945

MODELING OF THE WEAVE AND WOBBLE EIGENMODES OF MOTORCYCLES USING FLEXIBLE MULTIBODY SIMULATION

Francesco Passigato*

Chair of Automotive Technology
School of Engineering and Design
Technical University of Munich
Garching (Munich), Germany 85748

Achim Gordner

BMW Group
Munich, Germany

Frank Diermeyer

Chair of Automotive Technology
School of Engineering and Design
Technical University of Munich
Garching (Munich), Germany 85748

ABSTRACT

Weave and wobble are well known eigenmodes of motorcycles and have been studied by several authors because of their importance to the overall stability and safety of motorcycles. Studies have highlighted the importance of structural flexibility on these eigenmodes. A common approach in multibody simulation for modeling the flexibility is the lumped stiffness method. It is advantageous for its limited modeling effort and its small impact on computational time. However, it was never demonstrated if this approach leads to sufficient accuracy when simulating the weave and wobble eigenmodes. The present work answers this question by modeling the structural components of a motorcycle with the flexible multibody approach. The most relevant components for the stability of weave and wobble are identified. A comparison with the lumped stiffness approach is also proposed. Moreover, some implementation details concerning models with flexible bodies are discussed.

1 INTRODUCTION

Motorcycles are intrinsically unstable systems [1]. The rider's control inputs allow the stabilization of the capsized mode, thus avoiding the tilting of the motorcycle while at the same time following the desired trajectory. These control actions occur at a low frequency (about 0.5 Hz). However, motorcycles possess eigenmodes with higher frequencies that may also become un-

stable. If this happens the rider cannot actively stabilize the motorcycle. Two relevant eigenmodes in this context are weave and wobble [2–4]. Weave is characterized mainly by roll, yaw and steering-head rotation, where the last two are almost opposite in phase [5], and its eigenfrequency is in the range 1-4 Hz [4]. Wobble is dominated by steering-head rotation and has an eigenfrequency that varies in the range of 6-10 Hz [3] depending on motorcycle parameters. As the rider is not able to stabilize them, the free oscillation of these modes should remain well damped throughout the whole speed range of the motorcycle. Manufacturers use both simulation and experimental analysis in order to guarantee sufficient damping of these modes.

By conducting studies about the parameters influencing motorcycle stability, the stiffness of structural components was identified as an influential factor, see section 2 for more details. This somehow motivates the constant evolution that can be seen in the structural design of motorcycles, which always tries to solve the trade-off between weight reduction and achieving the desired structural stiffness. The research community proposes different methods with increasing complexity for modeling the flexibility of the structural components of a motorcycle. The most basic method is to use lumped stiffnesses, where the elastic behavior is approximated by introducing revolute joints with an associated stiffness and damping. This method allows for the unification of a primitive representation of the flexural behavior with moderate modeling overhead and advantageous computational time [6]. For this reason, it was the first one to be adopted. The most re-

*For correspondence: francesco.passigato@tum.de

cent studies on motorcycle stability make use of this modeling technique, and therefore the available information about the influence of the motorcycle flexibility on the weave and wobble eigenmodes is mainly provided by lumped stiffness models.

Thanks to the progress in computing power and software technology, new tools are available for accurately modeling flexibility. Finite-Element-Methods (FEM) are mainly adopted to conduct static simulations and evaluate the structural eigenmodes of a single body. When it comes to the dynamic simulation of an assembly, Multibody Simulation (MBS) is the most appropriate approach [7]. The standard version of MBS features rigid bodies, which are connected to each other with different type of joints in order to restrain the motion of the bodies and to define the assembly itself. The standard formulation can also be extended to include flexible bodies, thus obtaining the so-called Elastic Multibody Simulation (EMBS) [8]. This opens up new possibilities into the investigation of the effect of flexibility on the stability of motorcycles.

While EMBS has been already used to study the propagation of engine vibration [9] and road excitation to the rider [10], few studies have tackled the problem of analyzing the weave and wobble eigenmodes with a motorcycle model that includes flexible bodies. The present work will shed light on this topic by simulating the structural components of a motorcycle with flexible bodies. An example of the comparison between modeling with flexible bodies and lumped stiffnesses is also proposed. Moreover, the isolated influence of each substructure will be shown, in order to highlight which elements have the greatest influence on weave and wobble. Finally, this framework offers the possibility to investigate the role of the different methods involved in implementing flexible bodies in a MBS.

2 STATE OF THE ART

This section is divided into three subsections. The first summarizes the works that analyze the influence of the structural components of a motorcycle on the weave and wobble eigenmodes. The second presents the topic of EMBS. The third introduces the concept of Model Order Reduction (MOR).

2.1 Effect of Flexibility on Weave and Wobble

The investigation of the most influential parameters on the weave and wobble eigenmodes is a broad and active research topic. Beside the rider and tires, which have a major influence, importance has been attributed to the stiffness of the structural components of the motorcycle. The first evidence of this correlation was obtained experimentally in the 1980's [11, 12]. After these experimental results, models have been implemented that simulate the flexibility of the motorcycle components. As mentioned in the introduction, the lumped stiffness approach was the first method adopted for this aim. The first examples of its ap-

plication are found in [6, 13]. The authors noticed a remarkable influence of the front fork stiffness on the damping of the wobble mode. Most modern studies still rely on lumped stiffness for studying the correlation between stiffness and stability. However, while early works still relied on "hand-written" mathematical models, the most recent examples use modern MBS software. Thanks to the modeling advantages provided by MBS, the lumped stiffness approach has been adopted to model several structural components: the front fork bending stiffness [14–16], the frame torsional stiffness [17, 18], and the swingarm bending and torsional stiffness [14, 19].

The primary challenge when using the lumped approach is parameter estimation of the lumped stiffness and damping coefficients. Moreover, the initial rigid body for which the flexibility has to be modeled must be split into two or more rigid bodies, and therefore the related mass and inertia parameters must be estimated as well. For approximating the flexibility of the main frame with a lumped stiffness, Doria et al. [20] propose a method based on the twist axis approach, whereby the twist axis is defined as the intersection between the loaded and unloaded planes of the frame. Using a test rig for applying loads on the motorcycle frame, the authors identify a static twist axis, obtained with quasi-static application of the load, and two dynamic twist axes corresponding to the first and second frame eigenmodes, which are bending and torsional, respectively. The results show how it is impossible to define a single location of the lumped stiffness which correctly describes the frame deformation for every frame design. Therefore, the parametrization effort is quite high. The twist axis approach was employed also for the front fork in [21] and for the swingarm in [19]. Similarly to the previous case, it is not trivial to understand whether to use the parameters for the lumped stiffness resulting from the static or the dynamic test. [15] develops a method to tune the lumped stiffness on the first bending eigenmode to simulate the fork bending stiffness. The resulting stiffness was similar to that obtained with a static experiment. However, some assumptions on the deformation pattern have to be made, which may not be valid in general.

As highlighted in the previous paragraph, it is not a trivial task to find the correct parameters for a lumped stiffness model, therefore simulating weave and wobble with this approach could lead to errors. For this reason, some authors have studied motorcycle dynamics using flexible bodies. [22] models the swingarm as flexible body; compared to a rigid structure, the authors notice an increase in instability of the motorcycle when braking and driving over curbs. [10] models the main frame as flexible body and reports relevant differences in the vertical acceleration at chosen points compared to the rigid case when simulating a passage over road undulations. Finally, [23] analyzes the wobble phenomenon of a three-wheeled vehicle by modeling the frame and the steering column as flexible bodies. The steering column was the most influential element.

As this brief summary underlines, the weave and wobble eigen-

modes of motorcycles have not yet been investigated in detail using flexible multibody dynamics. The most common approach uses lumped stiffness. However, it has never been verified if this approximation provides reliable results for the simulation of the weave and wobble eigenmodes. In the present work, this topic will be tackled by modeling the structural components of the motorcycle using the flexible multibody approach and studying their effect on weave and wobble.

2.2 Elastic Multibody Simulation (EMBS)

EMBS extends the standard formulation of MBS to include the modeling of elastic bodies [24, 25]. For this purpose, different formulations have been proposed. The Consistent Rotation-Based Formulation (CRBF) and the Absolute Nodal Coordinate Formulation (ANCF) are suitable for modeling flexible bodies that undergo big elastic deformations [26]. Contrastingly, the Floating Frame of Reference Formulation (FFRF) is commonly used for the modeling of flexible bodies that are characterized by big nonlinear rigid body movements and small linear elastic deformations [22, 27, 28]. In the FFRF, a Floating Frame of Reference (FFR) is defined for each flexible body. The big nonlinear motions are expressed by the position vector of this frame with respect to an inertial frame. The elastic deformations are then expressed with respect to the FFR. The motorcycle structural components have to “follow” the big nonlinear displacements of the motorcycle and are likely to undergo small elastic displacements. For this reason, the FFRF is adopted in this work.

To attach the FFR to its flexible body, some constraints have to be defined: these are needed to uniquely define the motion of the body. Without these constraints, the matrices defining the flexible body would still contain rigid body modes, which as a result would be accounted for twice.

Different methods are available to express these constraints. The Tisserand frame method defines the FFR using dynamic constraints. In particular, the FFR is selected in such a way that the linear momentum and angular momentum due to body deformation are zero [8]. In this way, the FFR lays at every instant in the center of mass of the flexible body and is not necessarily attached to a material point [7]. Another method fixes the FFR to the flexible body with kinematic constraints [8]. This method consists in specifying so-called Reference Conditions (RC), which aim at eliminating the rigid body modes from the matrices of the flexible body [29]. The RC should be chosen according to the constraints that will be imposed on the flexible body during simulation. Otherwise, they would alter its deformation pattern [7, 29]. Further details on the implementation of these methods are presented in section 4.

The FFRF is the most used formulation for multibody simulations. In fact, it provides an interface between any multibody- and finite-element-code [25]. However, the models created with FEM contain many Degrees of Freedom (DOF), up to 10^6 for

some industrial applications. These models cannot be directly interfaced with a multibody code because the resulting computational time would render the model unusable [30]. For this reason Model Order Reduction (MOR) methods are required, which are further explained in section 2.3.

2.3 Model Order Reduction

MOR aims at reducing the number of DOF in a model of order N to make its computation more efficient. In the context of structural mechanics, and more specifically MBS, the common procedure is to start from an FEM of the component and then apply the MOR to reduce the high number of elastic coordinates and thus significantly reducing the computation time [31].

Assuming that the modeled component will undergo small displacements around an equilibrium position [32], as is the case with FFRF, a second-order linear equation can be used to express the elastic displacements:

$$\mathbf{M}_e \ddot{\mathbf{q}}_e(t) + \mathbf{D}_e \dot{\mathbf{q}}_e(t) + \mathbf{K}_e \mathbf{q}_e(t) = \mathbf{f}(t), \quad (1)$$

where $\mathbf{q}_e(t) \in \mathbb{R}^N$ are the elastic DOF of the body, $\{\mathbf{M}_e, \mathbf{D}_e, \mathbf{K}_e\} \in \mathbb{R}^{N \times N}$ are the mass, damping and stiffness matrices, respectively, and $\mathbf{f}(t) \in \mathbb{R}^N$ is the vector of the external forces. The reduction of the DOF is usually achieved by projective MOR [32]. The vector of the elastic DOF is approximated using the reduced displacements $\hat{\mathbf{q}}_e(t) \in \mathbb{R}^n$ by the relation:

$$\mathbf{q}_e(t) \approx \mathbf{V} \hat{\mathbf{q}}_e(t), \quad (2)$$

with $\mathbf{V} \in \mathbb{R}^{N \times n}$ being the projection matrix. The aim is to obtain a reduced model with less DOF than the original: $n \ll N$. The reduced form of Eqn. 1 is:

$$\hat{\mathbf{M}}_e \ddot{\hat{\mathbf{q}}}_e(t) + \hat{\mathbf{D}}_e \dot{\hat{\mathbf{q}}}_e(t) + \hat{\mathbf{K}}_e \hat{\mathbf{q}}_e(t) = \hat{\mathbf{f}}(t), \quad (3)$$

The reduced mass, damping and stiffness matrices and the reduced vector of external forces are obtained as follows:

$$\{\hat{\mathbf{M}}, \hat{\mathbf{D}}, \hat{\mathbf{K}}\} = \mathbf{V}^T \cdot \{\mathbf{M}, \mathbf{D}, \mathbf{K}\} \cdot \mathbf{V}, \quad \{\hat{\mathbf{M}}, \hat{\mathbf{D}}, \hat{\mathbf{K}}\} \in \mathbb{R}^{n \times n}, \quad (4)$$

$$\hat{\mathbf{f}} = \mathbf{V}^T \mathbf{f}, \quad \hat{\mathbf{f}} \in \mathbb{R}^n.$$

The projection shown in Eqn. 4 is called the one-sided projection, as opposed to the two-sided projection where, instead of left multiplying with \mathbf{V}^T , another projection matrix \mathbf{W}^T is used [33]. Different methods are available to obtain the projection matrix \mathbf{V} . In this work, two of the most common methods in structural mechanics are used. The reader is referred to [32, 34] for a survey on other methods proposed in the literature.

A simple method to carry out a MOR is the so-called modal truncation. It consists of approximating the original model with a linear combination of its undamped eigenmodes [34]. First of all, the unconstrained eigenvalue problem is solved:

$$(\mathbf{K}_e - \omega_j^2 \mathbf{M}_e) \boldsymbol{\phi}_j = \mathbf{0}, \quad (5)$$

where $\boldsymbol{\phi}_j$ is the eigenvector corresponding to the eigenfrequency ω_j . The matrix \mathbf{V} is then obtained by choosing $n \ll N$ eigenvectors, generally those corresponding to the lowest eigenfrequencies: $\mathbf{V} = \boldsymbol{\Phi}_n$. The main issue is choosing the proper number n that achieves the desired accuracy in the approximation.

Another very common MOR method in structural mechanics is the Craig-Bampton (CB) method [35]. It is based on the concept of substructuring and is particularly well-suited for MBS. It splits an assembly into substructures, which could be different flexible bodies of a multibody system. MOR is carried out separately on these substructures, which are assembled again after the reduction [36]. The DOF at the boundaries of the substructures are of particular importance because they are responsible for restoring the compatibility conditions between the substructures [36]. Therefore, the elastic DOF \mathbf{q}_e are split into boundary DOF \mathbf{q}_b and internal DOF \mathbf{q}_i . Equation 1 can be represented as:

$$\begin{bmatrix} \mathbf{M}_{bb} & \mathbf{M}_{bi} \\ \mathbf{M}_{ib} & \mathbf{M}_{ii} \end{bmatrix} \cdot \begin{bmatrix} \dot{\mathbf{q}}_b \\ \dot{\mathbf{q}}_i \end{bmatrix} + \begin{bmatrix} \mathbf{K}_{bb} & \mathbf{K}_{bi} \\ \mathbf{K}_{ib} & \mathbf{K}_{ii} \end{bmatrix} \cdot \begin{bmatrix} \mathbf{q}_b \\ \mathbf{q}_i \end{bmatrix} = \begin{bmatrix} \mathbf{f}_b \\ \mathbf{0} \end{bmatrix}. \quad (6)$$

Equation 6 describes an undamped system and the external forces are assumed to act only on the boundary DOF. The time dependency has been omitted for better readability.

The CB method expresses Eqn. 2 as:

$$\begin{bmatrix} \mathbf{q}_b \\ \mathbf{q}_i \end{bmatrix} = \begin{bmatrix} \mathbf{I} & \mathbf{0} \\ -\mathbf{K}_{ii}^{-1} \mathbf{K}_{ib} & \boldsymbol{\Phi}_m \end{bmatrix} \begin{bmatrix} \mathbf{q}_b \\ \boldsymbol{\zeta} \end{bmatrix} \quad (7)$$

The first column of this projection matrix \mathbf{V} represents the internal DOF as a function of the boundary DOF. It is obtained by imposing a unitary displacement to every boundary DOF while keeping the other boundary DOF fixed and calculating the resulting static displacements of the internal DOF. This part is therefore called static or Guyan condensation [37]. To approximate the dynamic behavior of the substructure, the eigenvectors $\boldsymbol{\Phi}_m$ are also used. These are obtained by solving an eigenvalue problem on the internal DOF with fixed boundary DOF for each substructure: $(\mathbf{K}_{ii} - \omega_j^2 \mathbf{M}_{ii}) \boldsymbol{\phi}_j = \mathbf{0}$. The matrix $\boldsymbol{\Phi}_m$ is then obtained by selecting $m \ll N_i$ eigenvectors, thus carrying out a modal truncation on the internal DOF. The terms of $\boldsymbol{\zeta}$ are the related modal coordinates and $\boldsymbol{\Phi}_m$ contains the so-called fixed-interface eigenmodes.

The fundamental characteristic of the CB method is that the boundary DOF are still present in the reduced model. As already mentioned, this is particularly important in substructuring because it allows the compatibility conditions to be satisfied when coupling the substructures in the final assembly.

3 OBJECTIVES OF THIS WORK

The present paper analyzes the effects of modeling the structural components of a motorcycle with flexible bodies on the weave and wobble eigenmodes. The components with the greatest influence are identified and the problems in approximating the real flexural behavior with lumped stiffnesses are highlighted. Moreover, the consequences of carrying out MOR with modal truncation or CB are analyzed. Some results about the implications on model efficiency when using the Tisserand frame or RC methods for the FFRF are shown. Finally, considerations about model validation are presented.

4 MODELING

This section gives a brief overview on the motorcycle model and provides some details about modeling using EMBS.

4.1 Motorcycle model

The motorcycle model used in this work is based on [38]. The FEM models of the structural components were available for a different motorcycle compared to that in [38], i.e. for a touring motorcycle currently available on the market. For this reason, the parameters of the model in [38] have been adapted to represent this motorcycle. Beside the changes in the mass and geometry, the main differences regard the suspensions: the front suspension is a multilink, while the rear suspension uses a four bar linkage. Without considering the DOF coming from the flexible bodies, the motorcycle has 11 DOF: 6 from rigid body translations and rotations, 2 wheel spins, steering head rotation and 2 suspension travels. Moreover, the rider is modeled with two rigid bodies, representing the upper and lower body, which are connected with a revolute joint and a spring/damper to simulate the roll motion of the rider with 1 DOF. The rider weight is 88 kg. The motorcycle is loaded with an additional total mass of 40 kg, which is distributed in three bags mounted on the rear frame. The model is fitted with a steering damper with a damping value of 7 N m s rad^{-1} . For the tire forces, the Pacejka Magic Formula adapted for motorcycles is used [39]. The aerodynamic forces are also modeled with a single force placed and directed in such a way that it produces a moment causing the same pitch rotation measured in real tests. Further motorcycle data cannot be provided because are property of BMW®.

The frame, front fork and swingarm are modeled as flexible bodies. The front fork is composed of five bodies: the fork bridge,

two stanchions, lower fork and wishbone. The swingarm is composed of three bodies: main arm, link and wheel carrier.

The simulations are performed with the multibody simulation software MBSim. The original matrices for the flexible bodies are exported from FEM models in Nastran® and the MOR is carried out with a Python code adapted from [40]. The original FEM models of the structural components have more than 10^6 DOF but their matrices are very sparse, therefore the code makes use of the `scipy` package, which uses the sparse nature of the matrices to save computational time and RAM when computing the eigenvalue problems during MOR. Still, the calculations for MOR require about 70 GB of RAM. Therefore, a high-performance computing machine with more than 360 GB of RAM and 20 CPUs has to be employed.

4.2 Implementation of FFRF

As explained in section 2.2, two methods are available to impose the constraint needed for an FFRF: the Tisserand frame and RC methods. In the Tisserand frame, these constraints, i.e. that the linear momentum and angular momentum due to the body deformations are zero, can be imposed by orthogonalizing the rows of the projection matrix \mathbf{V} with respect to the rigid body modes [8]. When using modal truncation for the MOR, it is sufficient to select only the eigenvectors with non-zero eigenfrequencies, since the eigenvectors with zero eigenfrequency are the rigid body modes. The orthogonality of the selected eigenvectors to the rigid body modes is then guaranteed by the mutual orthogonality of the system eigenmodes. When using CB for the MOR, the orthogonalization step must be carried out after calculating \mathbf{V} , since this method does not eliminate the rigid body modes [7]. In the present work, this step is done using a QR decomposition of the matrix \mathbf{V} .

For imposing the RC, the rigid body modes must be eliminated from the original matrices before applying MOR. This is done using a transformation matrix \mathbf{R}_c [29]. The matrix can be directly applied to Eqn. 1:

$$\mathbf{R}_c^T \mathbf{M}_e \mathbf{R}_c \ddot{\mathbf{q}}_e(t) + \mathbf{R}_c^T \mathbf{D}_e \mathbf{R}_c \dot{\mathbf{q}}_e(t) + \mathbf{R}_c^T \mathbf{K}_e \mathbf{R}_c \mathbf{q}_e(t) = \mathbf{R}_c^T \mathbf{f}(t). \quad (8)$$

When specifying the constraints for the RC method, some DOF must be eliminated from the original matrices. The matrix \mathbf{R}_c can be obtained by starting with an identity matrix with size $\mathbb{R}^{N \times N}$ and deleting the columns corresponding to the DOF that have to be eliminated. As stated by [7, 29], the RC must only eliminate the rigid body modes and define the shape of deformation with respect to its FFR. They do not introduce any constraint that restricts the gross motion of the body. Therefore, the RC are substantially different from the boundary conditions used in FEM simulations, which instead are introduced to constrain the kinematics of a body. However, the RC must be chosen according to the physical joints that the body will have once assembled. For

this reason, there is no unique set of RC that is suitable for all applications [7, 29]. When using the RC method, the designer has to carefully choose the DOF to be eliminated. Section 5.2 presents how to select the DOF for imposing the RC on the frame.

5 RESULTS

This section is divided into three subsections: the first analyzes in detail the influence of the flexibility of the structural components on weave and wobble, the second discusses some details about MOR and FFRF, and the third highlights some issues concerning model validation.

5.1 Influence of the flexibility of structural components

This section begins by presenting the effect of including the structural components of the motorcycle as flexible bodies on weave and wobble. Figure 1 shows how the eigenfrequency and real part (i.e. the damping) of the weave and wobble eigenmodes are affected when the components are added as flexible bodies one at a time while modeling the other components as rigid bodies. Also the curves corresponding to the case where all components are modeled as flexible bodies are shown.

The curves in Fig. 1 are obtained with eigenvalue analyses at different speeds using the multibody software MBSim: the equations of motion are internally linearized around a point that can be specified by passing a state vector. To generate this vector, a time simulation is carried out for each speed, where the motorcycle reaches the equilibrium in straight-running conditions. The state vector corresponding to this equilibrium is saved and used for the eigenvalues analysis.

For these results, the CB method has been used for MOR; moreover, the Tisserand frame method is adopted in the FFRF. The boundary DOF for each body are at the interfaces where the other bodies are connected; moreover, 20 fixed-interface eigenmodes are used for each body. 20 modes were chosen to represent a sufficiently big frequency range in the reduced model of every component. In the case of the frame, this includes frequencies up to 600 Hz, which is an order of magnitude more than the weave and wobble eigenfrequencies. The frame has the lowest frequency content, so selecting 20 modes also for the other components should lead to acceptable accuracy. Further optimization of the reduced order models could be an extension of the present topic. Table 1 shows the number of DOF of the structural components before and after MOR. The DOF after MOR are indicated as a sum to highlight how many boundary DOF and fixed-interface modes (20) are present.

The following considerations can be made for each structural component:

- The frame is very stiff so its flexibility marginally influences weave and has only a small effect on wobble. However,

TABLE 1: NUMBER OF DOF BEFORE AND AFTER MOR.

		original	after MOR
Frame		$3,8 \cdot 10^6$	20+54
Front fork	Fork bridge	$8,0 \cdot 10^5$	20+9
	Stanchions (each)	$2,1 \cdot 10^5$	20+9
	Lower fork	$1,7 \cdot 10^6$	20+18
	Wishbone	$4,7 \cdot 10^5$	20+12
Swingarm	Main arm	$2,7 \cdot 10^6$	20+15
	Link	$4,1 \cdot 10^5$	20+6
	Wheel carrier	$2,1 \cdot 10^6$	20+12

these effects already reflect the behavior known from practical experience: compared to a rigid frame, a flexible frame tends to destabilize high speed weave, while wobble is stabilized at high speed and destabilized at low speed.

- The flexibility of the front fork has a marginal effect on weave and has a similar effect on wobble as the frame. This effect is, however, more marked. This also overlaps with known behavior, i.e. that a more flexible fork reduces the wobble damping at low speed and increases it at high speed.
- The flexibility of the swingarm has no influence on wobble and a minor positive effect on the weave damping.

The model with all flexible components seems to combine the effects of the fork and frame on both weave and wobble.

To summarize, the flexibility at the front, due to either the frame or front fork, has a considerable effect on wobble. This correlation is similar to the results obtained in previous works, where the lumped parameter approach was used. For example, [13–15, 38] obtained similar qualitative results when representing the lateral flexibility of the front fork as a revolute joint with a rotation axis perpendicular to the steering axis and adding a torsional spring-damper element to it. [6, 17] model the frame torsional flexibility at the steering head joint with a similar approach. The effect of the frame and fork flexibility are qualitatively similar because they both allow a lateral movement of the front wheel. This influences the gyroscopic moments and the tire forces, as analyzed in [14, 38], thus causing the effect presented in Fig. 1. The swingarm flexibility slightly stabilizes the weave at high speed. [19] obtained a similar result modeling the torsion of the swingarm with a lumped stiffness. However, a destabilizing effect of the lateral bending on weave was also reported. As the present work uses flexible bodies, all possible flexibilities of the swingarm are considered. Their total effect is, as mentioned, to stabilize the weave at high speed. The wobble is not affected by the swingarm flexibility. This is plausible because the swingarm

has no structural function for the front wheel, which is the wheel that mainly influences wobble.

While general consideration can be made using lumped stiffness, it is difficult to approximate the real deformations of each body with this approach, as described in section 2. Moreover, it is not clear how the simplifications arising from the lumped stiffness approach impact the simulation of the weave and wobble eigenmodes. In the following, an example is proposed focusing on the front fork.

The differences between modeling the fork flexibility with lumped parameters or with flexible bodies is analyzed. Two lumped stiffnesses are used: one for the lateral (bending) stiffness and one for the torsional stiffness along a central axis parallel to the fork tubes, herein referred to as the fork axis, see Fig. 2. A simple way to estimate these parameters is to carry out static tests where the front fork is clamped at the steering head joint. In the present work, this test is done in a simulation where only the front fork is present and its components are modeled with flexible bodies. For measuring the bending stiffness, a lateral force is applied on the wheel axis and the resulting lateral displacement of the wheel center is measured [15, 21]. The linear stiffness k_l is obtained by dividing the applied force with the lateral movement; it is transformed then into a torsional stiffness k_t using the relation:

$$k_t = k_l b^2, \quad (9)$$

where b is the arm between the wheel center and the pivot of the revolute joint used for the lumped stiffness. In the present case, the revolute joint for modeling the bending stiffness is at the junction between the wishbone of the suspension and the lower fork, and has its axis perpendicular to the fork axis, see Fig. 2. This decision has been made due to the particular geometry of the fork in the present model. The wishbone is also subjected to lateral force and putting the lumped stiffness above this junction would lead to a higher stiffness at the wheel axis. For the identification of the torsional stiffness, a similar test is carried out by applying a moment directed along the fork axis at the wheel center. Dividing the moment with the resulting rotation directly gives the parameter for the lumped stiffness. The revolute joint is at the same point as the one used for the bending stiffness but has its axis parallel to the fork axis.

Because of the introduction of the revolute joints, the fork has to be split into two rigid bodies: the upper and lower fork. The mass and inertia data for these bodies were already available, so no additional identification for these data is required.

Figure 3 shows the comparison of the two models. Only the fork flexibility has been considered and modeled either with flexible bodies or with lumped stiffnesses. The model with lumped stiffnesses is able to approximate qualitatively the effect of the fork flexibility on the wobble eigenmode. However, some differ-

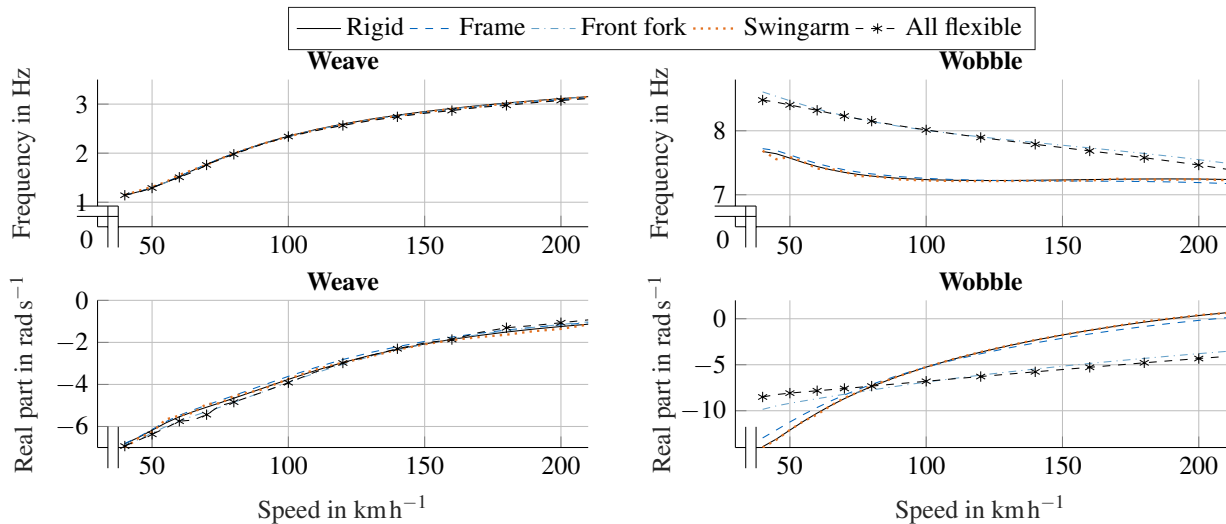


FIGURE 1: EFFECT OF THE FLEXIBILITY OF STRUCTURAL COMPONENTS ON WEAWE AND WOBBLE.

ences are present: compared to the results with flexible bodies, the wobble frequency is lower and its damping shows a slightly different trend. Moreover, the weave stability deteriorates more markedly at high speed. A possible reason can lay in the static test for the identification of the bending stiffness: when applying the lateral force at the wheel axis, a torsional deformation may also be present, as the wheel axis does not necessarily lay on the torsional axis of the fork. The resulting bending stiffness may be affected by this error. Moreover, the assumption on the position of the revolute joint, which affects the length b , is an approximation of the real deformation pattern.

Summarizing, the approximation of the front fork deformation with a lumped stiffness provides qualitatively comparable results when analyzing weave and wobble, but particular attention needs to be devoted to the test methods for the identification of parameters. Moreover, the positions of the lumped parameters were “chosen” considering the special geometry of the suspension, but it is in general a parameter needing identification. A similar approach for the frame is significantly more complex. In this case, it is not straightforward which test is required to identify the lumped stiffness parameters. Moreover, as explained in section 5.1, the frame must be split into two or more rigid bodies and their mass and inertia data identified. Therefore, a similar comparison as in Fig. 3 for the frame is an interesting research topic, but a suitable method for the approximation with lumped stiffness has to be developed.

5.2 Modeling details on MOR and FFRF

As presented in section 2, the designer has several possible paths when using flexible multibody dynamics. The first choice to be made is the method of MOR. In this work, two of the most

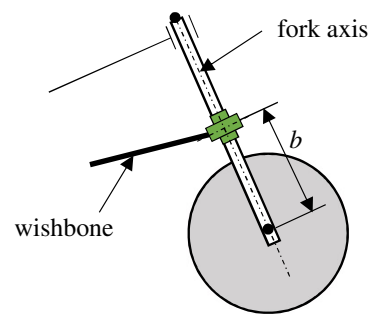


FIGURE 2: FRONT FORK GEOMETRY.

common methods are compared, i.e. CB and modal truncation. For the CB method 20 fixed-interface eigenmodes are used and in modal truncation the first 20 eigenmodes are kept, so that the frequency content of the reduced models is comparable. Moreover, the Tisserand frame is imposed in the FFRF. Figure 4 shows the curves of weave and wobble when modeling only the frame as flexible body and using these methods for MOR. Only the damping is shown because it is the main feature of interest when analyzing stability. Though, the following considerations are also valid for the eigenfrequencies. When using modal truncation, the curves are closer to those of the rigid case, in particular for wobble. This suggests that the modal truncation produces a reduced model with higher stiffness. This was also confirmed by static measurements on the lateral stiffness of the frame, whereby the reduction with CB provides results similar to the real measurements while the stiffness after modal truncation is too high. This difference can be due to the fact that CB maintains the boundary

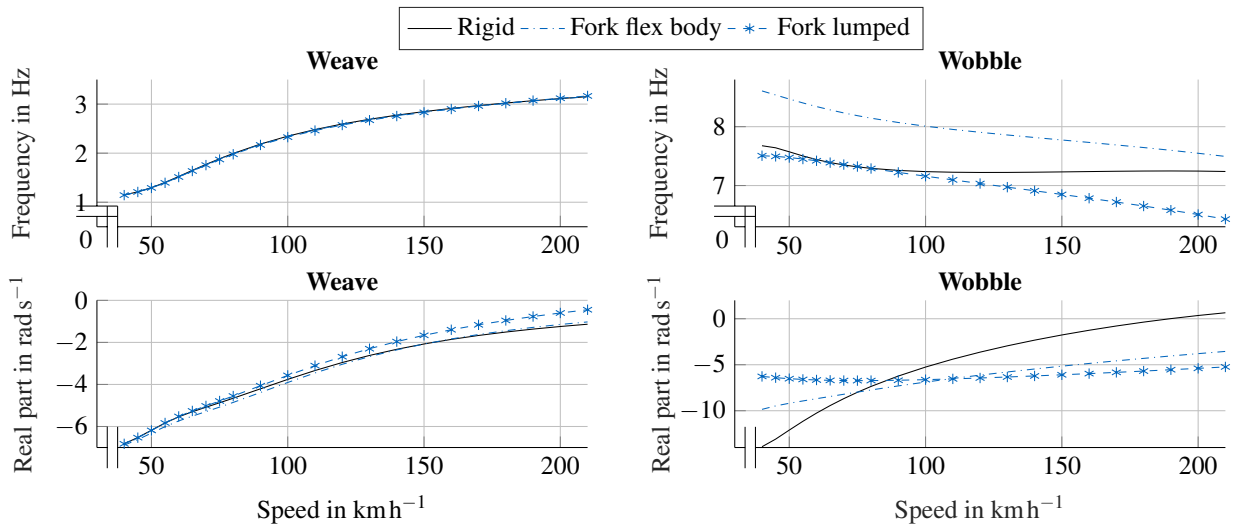


FIGURE 3: EFFECT OF FORK FLEXIBILITY WHEN MODELING WITH FLEXIBLE BODIES OR LUMPED STIFFNESSES.

DOF also in the reduced model. For this reason, the other bodies of the motorcycle are attached at “physical” DOF, which allows the correct transmission of constraint forces. With modal reduction all DOF are approximated by modal coordinates. The other bodies are not attached to “physical” DOF. The transmission of forces is not represented correctly, which erroneously increases the overall stiffness of the flexible body. This highlights the great importance of the boundary DOF within substructuring.

Another important aspect is the choice of method in implementing the FFRF. The Tisserand frame method is very common, as it provides good results in most of the cases. However, in some situations it does not allow a correct approximation of the real body deflection [7]. In the following, only the frame is modeled as a flexible body and the results using the Tisserand frame and the RC methods after model reduction with CB are compared. Again, in the CB method, 20 fixed-interface eigenmodes are kept. For imposing the RC, the DOF corresponding to the joints between frame and engine are eliminated. These joints are visualized with red marks in Fig. 6. Because of the joints, the frame is not able to deform at these DOF, so that they would never be “active” during simulation. Eliminating these DOF deletes the spurious rigid body modes, without changing the actual deformation pattern that the frame will experience in the final assembly. Figure 5 shows that, for the present case, there is no difference in the results choosing the one formulation over the other. Again, only the damping is shown, but the same is valid for the eigenfrequencies. Note that the reduced model with the RC method has less DOF: the reduced model after applying the Tisserand frame has 74 DOF while with the RC method it only contains 50 DOF because 8 nodes (each containing 3 DOF) corresponding to the engine mounts are eliminated. This leads to

a remarkable decrease in computation time of the whole motorcycle model: for a time simulation of 1.5 s, the model with the Tisserand frame needs about 1900 s, while the model with the RC method only takes 300 s. This advantage is not only due to the smaller model order, but also to the fact that the DOF eliminated for the RC method are boundary DOF. When applying MOR with CB, the boundary DOF are maintained in the reduced model with the so-called static modes, see section 2.3. These modes are associated with a very high frequency. For a time simulation high frequency contents are always critical, because when solving the differential equations the minimal time step has to be reduced. Deleting these DOF in the reduced model therefore brings the double advantage of reducing the model dimension and relaxing the required minimum step size. Of course, only the appropriate boundary DOF can be eliminated, otherwise one would alter the deformation pattern of the body.

5.3 Model validation and reduction error

As a conclusion to this section, some considerations on the validation of the results are presented. In particular, how to estimate if the real stiffness of the structural components is correctly represented by the reduced models. First of all, one has to estimate the reduction error as result of MOR, i.e. the error between the original FEM model and the reduced model. A common way to estimate this error is to compare the eigenvalues and eigenvectors of the original and reduced model [31, 41]. By applying the RC method, the original eigenmodes are certainly altered, therefore this measure of error would produce a large reduction error. However, as shown in section 5.2, this does not necessarily lead to poor simulation results when the assembled model is considered. This measure of error is therefore certainly

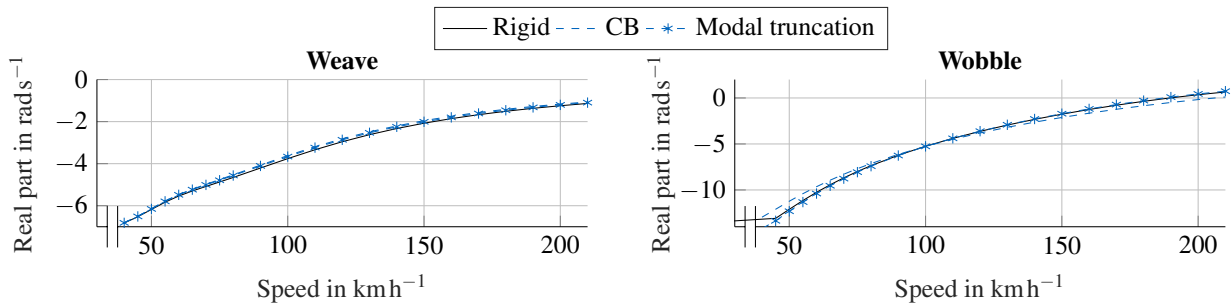


FIGURE 4: COMPARISON OF THE RESULTS USING MODAL TRUNCATION OR CB FOR MOR (FRAME).

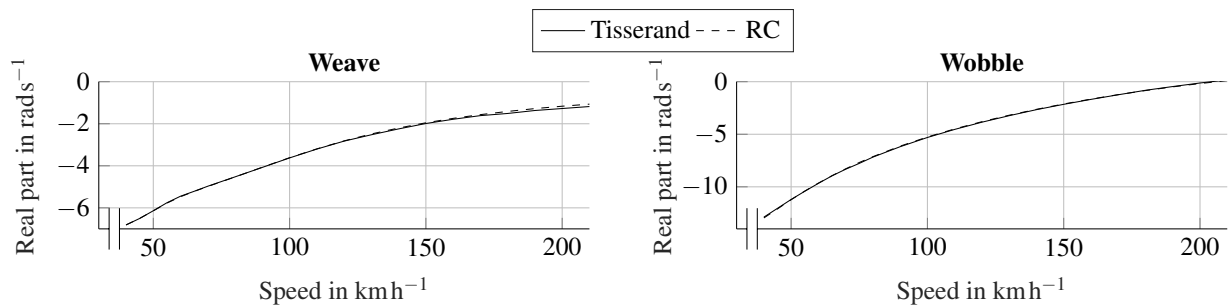


FIGURE 5: COMPARISON OF THE RESULTS USING TISSERAND FRAME OR RC METHODS FOR FFRF (FRAME).

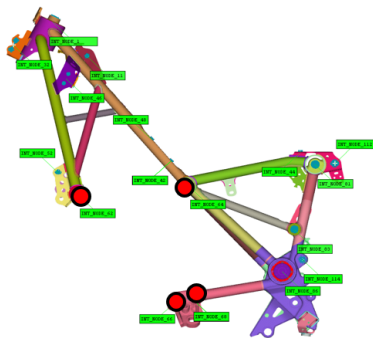


FIGURE 6: VISUALIZATION OF ENGINE MOUNTS.

well suited if one is interested in approximating a single body that has no connection to other bodies, however it does not fairly represent the reduction error of a whole assembly. In fact, error estimation for an assembly is a difficult task. In the present paper, one would have to model the whole motorcycle with the original non-reduced FEM bodies and compare the results with the model using reduced bodies. However, a simulation with the original bodies would imply more than 10^7 DOF, which leads to unacceptable computation time. A possibility is to carry out two MOR, one with the desired final dimension and one with a higher reduced order. The error is calculated considering the model with

higher order as “ground truth”. Another possibility is to compare the simulation with real measurements. This could involve static measurements, which allows for a quick comparison on the overall stiffness. In the present work, this methodology for validation was adopted. The bending stiffness of the frame was measured in the simulation by clamping it at the swingarm axis and applying a lateral force at the steering joint; the obtained stiffness deviates 6.4 % from experimental data. The lateral stiffness of the fork assembly was measured by clamping it at the steering head joint and applying a lateral force at the front wheel axis. The deviation between experimental and simulation data is only 0.5 %. This validation is not possible for the swingarm because static measurements are not available.

6 CONCLUSIONS

The present work analyzes the influence of the flexibility of structural components of a motorcycle on its stability, i.e. on the weave and wobble eigenmodes. The flexibility at the front of the motorcycle tends to degrade the weave stability, to increase the wobble stability at high speed and to decrease it at low speed. The swingarm flexibility slightly stabilizes the weave at high speed, while it does not affect wobble. The component with the highest influence on stability is the front fork. The components are modeled using EMBS, where each component is implemented as a flexible body. This approach allows

a more accurate modeling of the flexibility of components with respect to the lumped stiffness approach. The latter has major advantages when it comes to computation time, however it heavily approximates the deformation pattern. Moreover, the identification of the lumped parameters is a difficult task because a suitable method must be chosen. This choice is not trivial as the literature provides both static and dynamics methods that often identify different parameters. In the present work, it has been shown that for the front fork a lumped stiffness model with parameters identified by static tests leads to qualitative similar results to the simulation with flexible bodies when simulating weave and wobble. However, differences are still present and to get a perfectly consistent result would require additional experimental effort. A similar approach for the frame has not been shown, as a method for the correct identification of the lumped parameters is still an active area of research.

The framework of EMBS also makes it possible to analyze the methods that are available for modeling a flexible body. In the context of MOR, used to reduce the number of DOF in a flexible body, modal truncation and CB are compared. The result is that for an assembly consisting of several bodies, such as a motorcycle, CB better approximates the behavior of the original model because it maintains the boundary DOF, which are used to connect the other components to the flexible body.

The present work uses both the Tisserand frame and the RC methods for the FFRF. An example using the motorcycle frame shows that both methods provide the same results. However, the RC method can be more efficient in terms of computation time but at the cost of requiring more modeling effort from the designer, as suitable RC for the particular case must be chosen.

Further attention can be devoted to the optimization of the reduced order models. In particular the number of modes selected in MOR should be chosen depending on the frequency content of the component itself. This way, after fixing a frequency of interest, enough modes should be selected for every component to match that frequency. The comparison of alternative methods for MOR is another possible extension.

An interesting continuation of the present work could be the analysis of weave and wobble in a steady-state curve to analyze the effect of stiffness in this situation. Moreover, it could be interesting to investigate if the flexibility of the structural components affects the steering feedback perceived by the rider.

ACKNOWLEDGMENT

The authors would like to thank Prof. Martin Förg (University of Landshut) for help in the modeling phase. Thanks also to Andreas Zwölfer (Technical University of Munich) for the support in the application of model order reduction methods. They want also to thank Dr. Dirk Wisselmann for the valuable discussion of the results. Finally, thanks to Alexander Schramm (University of Bologna) for help during the writing phase.

REFERENCES

- [1] Hoagg, J. B., and Bernstein D.S., 2007. “Nonminimum-phase zeros - much to do about nothing - classical control - revisited part ii”. *IEEE Control Systems*, **27**(3), pp. 45–57.
- [2] Sharp, R. S., 1971. “The stability and control of motorcycles”. *Journal Mechanical Engineering Science*, **13**(5), pp. 316–329.
- [3] Sharp, R. S., 2001. “Stability, control and steering responses of motorcycles”. *Vehicle System Dynamics*, **35**(4-5), pp. 291–318.
- [4] Cossalter, V., 2006. *Motorcycle dynamics*, 2. english ed. ed. [Lulu press], S.l.
- [5] Cossalter, V., Lot, R., and Maggio, F., 2004. “The modal analysis of a motorcycle in straight running and on a curve”. *Meccanica*, **39**, pp. 1–16.
- [6] Sharp, R. S., and Alstead, C. J., 1980. “The influence of structural flexibilities on the straight-running stability of motorcycles”. *Vehicle System Dynamics*, **9**(6), pp. 327–357.
- [7] Shabana, A. A., and Wang, G., 2018. “Durability analysis and implementation of the floating frame of reference formulation”. *Proceedings of the Institution of Mechanical Engineers, Part K: Journal of Multi-body Dynamics*, **232**(3), pp. 295–313.
- [8] Schwertassek, R., Wallrapp, O., and Shabana, A. A., 1999. “Flexible multibody simulation and choice of shape functions”. *Nonlinear Dynamics*, **20**(4), pp. 361–380.
- [9] Bonisoli, E., Lisitano, D., Dimauuro, L., and Peroni, L., 2020. “A proposal of dynamic behaviour design based on mode shape tracing: Numerical application to a motorbike frame”. *Conference Proceedings of the Society for Experimental Mechanics Series*, pp. 149–158.
- [10] Oliveri, S. M., Cali, M., and Catalano, L., May 14-17, 2002. “Dynamics of motorcycle using flexible elements”. *International Design Conference*.
- [11] Roe, G. E., and Thorpe, T. E., 1989. “The influence of frame structure on the dynamics of motorcycles stability”. *SAE Technical Papers*.
- [12] Roe, G. E., and Thorpe, T. E., 1976. “A solution of the low-speed wheel flutter instability in motorcycles”. *Journal Mechanical Engineering Science*, **18**(2), pp. 57–65.
- [13] Spierings, P. T. J., 1981. “The effects of lateral front fork flexibility on the vibrational modes of straight-running single-track vehicles”. *Vehicle System Dynamics*, **10**(1), pp. 21–35.
- [14] Cossalter, V., Lot, R., and Massaro, M., 2007. “The influence of frame compliance and rider mobility on the scooter stability”. *Vehicle System Dynamics*, **45**(4), pp. 313–326.
- [15] Doria, A., Favaron, V., Taraborrelli, L., and Roa, S., 2017. “Parametric analysis of the stability of a bicycle taking into account geometrical, mass and compliance properties”. *International Journal of Vehicle Design*, **75**(1-4), pp. 91–

- 123.
- [16] Doria, A., and Roa, S., 2018. “On the influence of tyre and structural properties on the stability of bicycles”. *Vehicle System Dynamics*, **56**(6), pp. 947–966.
- [17] Sharp, R. S., Evangelou, S. A., and Limebeer, D. J. N., 2004. “Advances in the modelling of motorcycle dynamics”. *Multibody System Dynamics*, **12**(3), pp. 251–283.
- [18] Sharp, R. S., and Limebeer, D. J. N., 2004. “On steering wobble oscillations of motorcycles”. *Proceedings of the Institution of Mechanical Engineers, Part C: Journal of Mechanical Engineering Science*, **218**(12), pp. 1449–1456.
- [19] Taraborrelli, L., Favaron, V., and Doria, A., 2017. “The effect of swingarm stiffness on motorcycle stability: experimental measurements and numerical simulations”. *International Journal of Vehicle Systems Modelling and Testing*, **12**(3/4), p. 240.
- [20] Doria, A., and Taraborrelli, L., 2016. “The twist axis of frames with particular application to motorcycles”. *Proceedings of the Institution of Mechanical Engineers, Part C: Journal of Mechanical Engineering Science*, **230**(17), pp. 3026–3039.
- [21] Cossalter, V., Doria, A., Massaro, M., and Taraborrelli, L., 2015. “Experimental and numerical investigation on the motorcycle front frame flexibility and its effect on stability”. *Mechanical Systems and Signal Processing*, **60-61**, pp. 452–471.
- [22] Ferretti, G., Scaglioni, B., and Rossi, A., 2014. “Multibody model of a motorbike with a flexible swingarm”. In *Proceedings of the 10th International Modelica Conference*, March 10–12, 2014, Lund, Sweden, Linköping Electronic Conference Proceedings, Linköping University Electronic Press, pp. 273–282.
- [23] Karanam, V. M., and Ghosal, A., 2013. “Studies on the wobble mode stability of a three-wheeled vehicle”. *Proceedings of the Institution of Mechanical Engineers, Part D: Journal of Automobile Engineering*, **227**(8), pp. 1200–1209.
- [24] Schwertassek, R., and Wallrapp, O., 1999. *Dynamik flexibler Mehrkörpersysteme: Methoden der Mechanik zum rechnergestützten Entwurf und zur Analyse mechatronischer Systeme ; mit 25 Tabellen*. Grundlagen und Fortschritte der Ingenieurwissenschaften. Vieweg, Braunschweig and Wiesbaden.
- [25] Shabana, A. A., 1997. “Flexible multibody dynamics: Review of past and recent developments”. *Multibody System Dynamics*, **1**(2), pp. 189–222.
- [26] Kulkarni, S., and Shabana, A. A., 2019. “Spatial ancfc/crbf beam elements”. *Acta Mechanica*, **230**(3), pp. 929–952.
- [27] Canavin, J. R., and Likins, P. W., 1977. “Floating reference frames for flexible spacecraft”. *Journal of Spacecraft and Rockets*, **14**(12), pp. 724–732.
- [28] Nowakowski, C., Fehr, J., Fischer, M., and Eberhard, P., 2012. “Model order reduction in elastic multibody systems using the floating frame of reference formulation”. *IFAC Proceedings Volumes*, **45**(2), pp. 40–48.
- [29] Cammarata, A., and Pappalardo, C. M., 2020. “On the use of component mode synthesis methods for the model reduction of flexible multibody systems within the floating frame of reference formulation”. *Mechanical Systems and Signal Processing*, **142**.
- [30] Fehr, J., and Eberhard, P., 2010. “Error-controlled model reduction in flexible multibody dynamics”. *Journal of Computational and Nonlinear Dynamics*, **5**(3), pp. 1–8.
- [31] Holzwarth, P., and Eberhard, P., 2015. “Svd-based improvements for component mode synthesis in elastic multibody systems”. *European Journal of Mechanics - A/Solids*, **49**, pp. 408–418.
- [32] Lohmann, B., Bechtold, T., Eberhard, P., Fehr, J., Rixen, D. J., Varona, M. C., Christopher Lerch, Yuan, C. D., Rudnyi, E. B., Fröhlich, B., Holzwarth, P., Grunert, D., Meyer, C. H., and Rutzmoser, J. B. “Model order reduction in mechanical engineering”. In *Model Order Reduction, Volume 3: Applications*. pp. 33–74.
- [33] Salimbahrami, B., and Lohmann, B., 2006. “Order reduction of large scale second-order systems using krylov subspace methods”. *Linear Algebra and its Applications*, **415**(2-3), pp. 385–405.
- [34] Besselink, B., Tabak, U., Lutowska, A., van de Wouw, N., Nijmeijer, H., Rixen, D. J., Hochstenbach, M. E., and Schilders, W., 2013. “A comparison of model reduction techniques from structural dynamics, numerical mathematics and systems and control”. *Journal of Sound and Vibration*, **332**(19), pp. 4403–4422.
- [35] Craig, R., and Bampton, M., 1968. “Coupling of substructures for dynamic analyses”. *AIAA Journal*, **6**(7), pp. 1313–1319.
- [36] de Klerk, D., Rixen, D. J., and Voormeeren, S. N., 2008. “General framework for dynamic substructuring: History, review and classification of techniques”. *AIAA Journal*, **46**(5), pp. 1169–1181.
- [37] Guyan, R. J., 1965. “Reduction of stiffness and mass matrices”. *AIAA Journal*, **3**(2), p. 380.
- [38] Passigato, F., Eisele, A., Wisselmann, D., Gordner, A., and Diermeyer, F., 2020. “Analysis of the phenomena causing weave and wobble in two-wheelers”. *Applied Sciences*, **10**(19), p. 6826.
- [39] Pacejka, H. B., and Besselink, I., 2012. *Tire and vehicle dynamics*, 3. ed. ed. Butterworth - Heinemann, Oxford.
- [40] Meyer, C., Lerch, C., and Maierhofer, J. Amfe.
- [41] Kim, J.-G., and Lee, P.-S., 2015. “An enhanced craig-bampton method”. *International Journal for Numerical Methods in Engineering*, **103**(2), pp. 79–93.

4.3 Optimization of the Stiffness Distribution between Structural Components [IMSD 2023]

The model presented in Section 4.2 leverages the flexible multibody approach to simulate with high accuracy the effect of the flexibility of structural components on weave and wobble. However, as introduced in Section 3.3.1, it is difficult to carry out parameter studies on the stiffness with the flexible multibody motorcycle model. In fact, each flexible body contains the flexibility in all directions, so that, when trying to change the stiffness in one direction, all the stiffness properties of the body are affected. For such a parameter study, the lumped stiffness approach has the advantage that every stiffness parameter possesses a physical interpretation because it represents the stiffness of the component in a certain direction. A study leveraging a lumped stiffness model would therefore provide useful information for design optimization. However, the disadvantage of lumped stiffness models is the lower accuracy compared to flexible multibody models.

For this reason, the present publication proposes a preliminary procedure for parameterizing lumped stiffness models, which increases the accuracy of lumped stiffness models. This procedure and its advantages are presented in Section 4.3.1.

The obtained lumped stiffness motorcycle model is then used to develop the actual methodology for optimizing the stiffness distribution between the structural components. The development of this methodology is presented in Section 4.3.2.

The sequence for optimizing the stiffness distribution is shown in the schematic of Figure 4.7. The indications provided by the methodology for stiffness optimization can be used to design new components, which can be subjected to a further optimization-loop (dashed arrow).

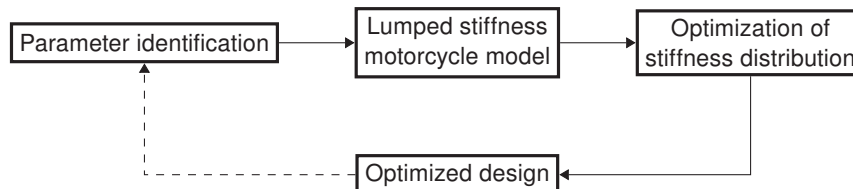


Figure 4.7: Pipeline for building a high accuracy lumped stiffness motorcycle model and carrying out a sensitivity analysis with it.

4.3.1 Method for the Parameter Identification of Lumped Stiffness Models

In this publication, a method is proposed to increase the accuracy of lumped stiffness models. The aim is to model the influence of structural flexibilities on weave and wobble with an accuracy similar to that of flexible multibody models.

The method leverages previous works where a procedure for the identification of the deformation axis of elastic components is proposed [66, 68, 73, 74]. In this publication, the procedure is generalized and applied to every main structural component of the motorcycle, i.e., frame, front assembly and swingarm. The deformation axis is determined by clamping the component on one end and by applying a quasi-static or dynamic load perpendicular to the symmetry plane of each component and measuring the displacement and rotation of the free end. These tests are carried out in simulations where the structural components are modeled as flexible bodies. The identified parameters are then used to parameterize a lumped stiffness model for every structural component. According to the type of load applied, different deformation axes results. From the

previous works, it is not clear which deformation axis should be used for the parameterization of a lumped stiffness motorcycle model having the aim of modeling weave and wobble.

In the present publication, the accuracy of the lumped stiffness motorcycle model compared to the flexible multibody motorcycle model described in Section 4.2 is determined. In particular, the frequency (f) and the real part (Re) of the weave and wobble modes are calculated in the relevant speed range ($40 - 210 \text{ km h}^{-1}$) with both models to determine the error of the lumped stiffness model.

The error is calculated separately for each structural component and is shown in Figure 4.8. For each component, four lumped stiffness models are presented: “State of the art” is based on the common assumptions for building lumped stiffness models; “Static”, “Torsion” and “Bending” are the lumped stiffness models based on the proposed identification process and parameterized with the quasi-static test or the harmonic test with the frequency of the first torsional and bending modes, respectively. The lumped stiffness models parameterized with the quasi-static test provide the best accuracy. This way, the error of lumped stiffness models is less than 15 %, thus providing a significant improvement compared to state-of-the-art lumped stiffness models, where the maximum error is more than 35 %. In fact, the state-of-the-art lumped stiffness models rely on assumptions on the deformation pattern of the structural components, which often prove to be wrong.

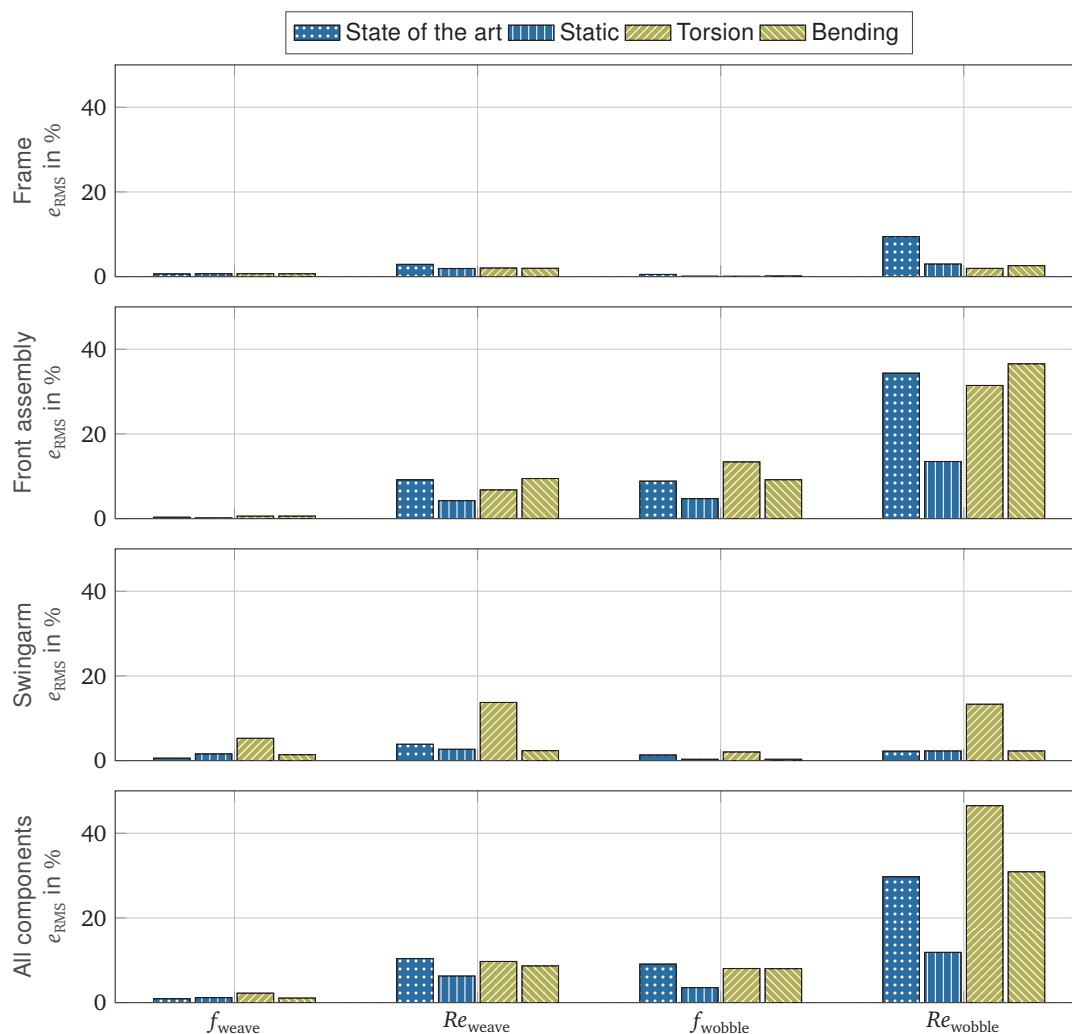


Figure 4.8: Error of lumped stiffness models with respect to the flexible multibody model [185].

4.3.2 Methodology for Optimizing the Stiffness Distribution

Since the accuracy of lumped stiffness models is significantly increased and can be considered sufficient thanks to the proposed method, the lumped stiffness motorcycle model can now be used to carry out a parameter study on the structural stiffnesses. In the present publication, this is done with a sensitivity analysis where, for every structural component, the influence of bending and torsional stiffness on the stability of weave and wobble is studied. The information of this sensitivity analysis can be used to optimize the stiffness distribution between the structural components.

After defining an index (stability index) that indicates the stability of weave and wobble, the linear Pearson correlation coefficient ρ is used to determine the sensitivity of each stiffness on the stability of weave and wobble. The lumped stiffness motorcycle model contains six stiffnesses: bending and torsional stiffness for the frame, front assembly and swingarm. Each of them is varied by $\pm 10\%$; bigger variations are avoided in order to study stiffness configurations consistent with the values of the motorcycle model considered. The results of the sensitivity analysis are shown in Figure 4.9. A positive coefficient indicates that increasing the stiffness enhances the stability. By analyzing separately the low and high speed range, it is evident that there are some stiffness parameters, such as the bending stiffness of the front assembly, which impact in an opposite way according to the speed.

The results in Figure 4.9 confirm some observations made in Section 4.2: the front assembly is the component with highest impact on the stability of weave and wobble; due to its high stiffness, the frame has lower sensitivity; the swingarm influences only the weave eigenmode. However, the sensitivity analysis provides some additional information. Particularly interesting is to note that the torsional stiffness of the front assembly $k_{t,a}$ has a negative correlation coefficient for wobble (i.e., destabilizing effect) over the whole speed range, thus suggesting that, under the perspective of stability, excessive values of this stiffness should be avoided. Moreover, the swingarm bending stiffness $k_{b,s}$ has a negative correlation coefficient for high-speed weave, thus suggesting that an optimized design of the swingarm would imply relatively low bending stiffness but high torsional stiffness. These considerations are employed in Section 4.4, where an example is shown on how to apply the proposed methodology for achieving the objective of enhancing the overall stability while reducing the total mass.

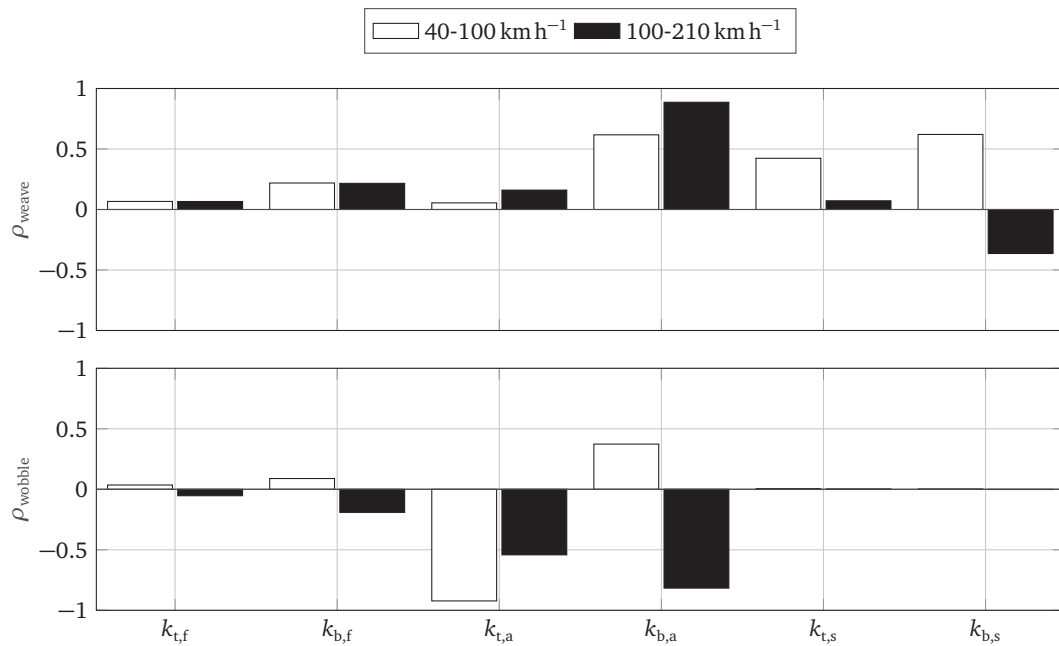


Figure 4.9: Person correlation coefficients of weave and wobble for every structural stiffness. Nomenclature of $k_{x,y}$: The first letter indicates the bending (b) or torsional stiffness (t). The second letter is the structural component (f: frame, a: front assembly, s: swingarm) [185].

Contributions

F. P. as the first author initiated the idea of the paper and contributed significantly to the concept, modeling, and results. A. S. made significant contributions in the development of methods and in the review phase. S. S. and A. D. F. contributed to the review phase. A. G. contributed to significant discussion of the results. F. D. contributed to the whole concept of the paper. F. D. gave final approval for publication of this version and is in agreement with all aspects of the work. As a guarantor, he accepts responsibility for the overall integrity of this paper.

Copyright notice



Identification of lumped stiffness parameters for a motorcycle model in investigating weave and wobble

Francesco Passigato¹ · Alexander Schramm² · Frank Diermeyer¹ · Silvio Sorrentino² · Achim Gordner³ · Alessandro De Felice²

Received: 30 August 2022 / Accepted: 15 March 2023
© The Author(s) 2023

Abstract

In motorcycle dynamics, great importance is attributed to the study of the weave and wobble vibration modes and, in particular, to the effects of the flexibility of structural components on their stability. Therefore, appropriate motorcycle models for studying weave and wobble should include flexible elements for describing the flexural behavior of components such as the main frame, front assembly, and rear swingarm. Different approaches are possible for modeling flexibilities: the most common among them are the lumped stiffness and the flexible multibody approaches. While the latter certainly provides higher accuracy, the former has advantages in terms of computational load, but, above all, it makes it easier to understand in the design phase how technical parameters, such as torsional and bending stiffness of a given structural component, can influence the stability of weave and wobble. The accuracy of lumped stiffness models strongly depends on parameter identification. In this study, a general method is proposed to determine appropriate lumped stiffness parameters for any given motorcycle component. The proposed method is tested and validated by comparing the weave and wobble modal behavior with the results of flexible multibody analysis. The lumped stiffness model is then adopted to carry out a sensitivity analysis aimed at identifying the effects on the weave and wobble stability of the torsional and bending stiffness of specific structural components of the motorcycle to optimize their design.

Keywords Parameter identification · Lumped stiffness · Weave · Wobble · Motorcycle dynamics · Stability analysis

1 Introduction

Weave and wobble are well-known eigenmodes of motorcycles, both involving lateral dynamics. The weave eigenvector is dominated by roll, yaw, and steering head rotation [1]

✉ F. Passigato
francesco.passigato@tum.de

¹ Institute of Automotive Technology, TUM School of Engineering and Design, Technical University of Munich, Boltzmannstrasse 15, Garching, 85748, Germany

² Department of Engineering Enzo Ferrari, University of Modena and Reggio Emilia, Via Pietro Vivarelli 10, Modena, 41125, Italy

³ BMW Group, Munich, Germany

with an eigenfrequency in the range 1–4 Hz [2]. Wobble is characterized mainly by steering head rotation, and its eigenfrequency varies from 6 to 10 Hz [3]. The stability of these eigenmodes is a safety critical problem because the motion caused by an unstable weave or wobble is not controllable by the rider and would likely lead to an accident. For this reason, weave and wobble have been extensively studied in the literature, with the first works dating back to the 1970s [4]. A deciding step in modeling weave and wobble was made when the flexibility of the structural components was included in the models. In fact, particularly for wobble, this step allowed the correct prediction of the change of mode damping with speed [5–8].

For modeling the stiffness of structural components, different approaches are possible: the most used and simple is the lumped stiffness approach. It consists of representing the flexibility of a component with a single parameter, i.e., a concentrated stiffness, see Sect. 2. The second approach is the Elastic Multibody Simulation (EMBS) [9], where the classical formulation of multibody simulation is extended to include flexible bodies. In this case, the flexibility is represented as a distributed property so that the real deformation is better approximated. The lumped stiffness approach is attractive for its limited modeling effort, short computational time, and, above all, because it makes it easier to understand in the design phase how technical parameters, such as the torsional and bending stiffness of a given structural component, can influence stability. However, the strong approximation of the actual flexural behavior, which is intrinsic in this method, may negatively affect the accuracy when modeling weave and wobble.

The crucial part of the lumped stiffness approach is the identification of the parameters [10]. In the literature, most models using the lumped stiffness approach make assumptions about the position of the joints for modeling flexibility. However, as shown in [11], these assumptions may lead to inaccurate results when studying weave and wobble.

This paper presents a method for parameterizing a lumped stiffness model of any structural component. It is based on the identification of the deformation axis of each component and can be applied to real components or using a simulation environment, as in the present paper. The method is applied to each structural component of a motorcycle, and the obtained lumped stiffness model is compared to a flexible multibody model in the simulation of weave and wobble. The decision to use the lumped stiffness approach for studying the effect of structural flexibilities on weave and wobble is justified by the necessity of obtaining stiffness values with a physical meaning that can be easily interpreted and adapted. In fact, the developed lumped stiffness model lends itself to carrying out a sensitivity analysis to understand, for every component, if its torsional or bending stiffness is more important for the stability of weave and wobble. The results of the sensitivity analysis can help to optimize the stiffness in the early design phase of structural components so that the overall weight can be minimized while ensuring the stability of weave and wobble.

2 State of the art

As mentioned in the introduction, structural flexibility is important to the stability of weave and wobble. The first works modeling the flexibility of structural components for the study of weave and wobble are [5, 6]. They use two different approaches to model the flexibility at the front of the motorcycle. The authors of [5] model the frame torsional flexibility with a revolute joint and a coaxial rotational spring/damper at the steering head joint with its rotation axis perpendicular to the fork axis. In [6], the bending flexibility of the front fork is modeled with a revolute joint and a coaxial rotational spring/damper along the fork with

its rotation axis perpendicular to the fork axis. The aim is mainly to investigate the effect of this stiffness on weave and wobble and not to exactly reproduce the fork deformation. For this reason, the position of the revolute joint and the stiffness value are not based on real measurement but are varied to draw information about a possible optimized design. Based on this first experience, other works followed in its stead, by adopting the lumped stiffness approach for modeling the flexibility of structural components. In [12], the approaches in [5, 6] are combined, and the stiffness values are derived from real measurements, still maintaining the assumptions on the position and orientation of the revolute joints. The author of [13] proposes an analysis where the position of the deformation axis of the frame is varied and the effect on weave and wobble investigated. These modeling approaches, where the position of the joint and the value of the lumped stiffnesses is assumed or estimated, can be found in several other works, e.g., the works based on the model developed in [5], see, e.g., [14–19], or in independent works from other authors [7, 20].

The first attempt to parameterize a lumped stiffness model with a consistent procedure is found in [21, 22] for the front fork and in [23] for the swingarm. In [21], a procedure is developed where, using the mass properties and the bending eigenfrequency measured with experimental test, a lumped stiffness model is developed for the front fork bending flexibility. However, the orientation of the revolute joint axis is assumed to be perpendicular to the fork axis. The authors of [22, 23] identify the deformation axis of the structural component with either static or dynamic excitation. Dynamic excitation with a frequency equal to the first bending and torsional eigenfrequencies allows the identification of the bending and torsion axis, while the static test identifies the so-called twist axis, and the resulting deformation is generally a combination of bending and torsion. The authors provide different lumped stiffness models for the fork and swingarm, using the parameters identified through static or dynamic tests or a combination of the two. The weave and wobble eigenmodes are simulated with these models and compared to the rigid body case. However, the question remains about which combination provides the most realistic results. A similar approach was proposed in [24] for identifying the twist, bending, and torsion axes of a frame. However, no lumped stiffness model was parameterized with the resulting data.

The present paper answers the remaining open questions. In particular, the most suitable test for parameterizing a lumped stiffness model to study the influence of flexibilities on weave and wobble is identified. For that, a comparison with flexible multibody models is presented, which are considered the “ground truth”. This way, it is demonstrated that the common assumptions on the location of the revolute joints to model the different flexibilities do not always lead to correct results.

Moreover, a sensitivity analysis will be carried out to separate the effect of bending and torsional flexibility of each component in the study of weave and wobble. Other works have already used this method to identify the most relevant parameters for motorcycle stability [25–27]. The common procedure is to calculate the analysis of variance (ANOVA) with a full factorial design of experiments. The results provide information on whether the varied factors interact with each other or only the main effects may be considered. In the latter case, a statistical model without interactions can be adopted [25]; in particular, a linear correlation technique (Pearson correlation coefficients) is used. More information about the sensitivity analysis is provided in Sect. 4.3.

3 Aim of the paper

The present paper is focused on two contributions. The first is the development of a unified procedure for parameterizing lumped stiffness models of the main structural components of

motorcycles. Attention is devoted to correctly reproducing the effect of structural flexibilities on weave and wobble with the lumped stiffness model. In particular, a test procedure is identified that allows the best approximation of a flexible multibody model with the lumped stiffness approach. The decision to use the lumped stiffness approach instead of leveraging on more advanced techniques for model condensation (e.g., dynamic condensation) is motivated by the necessity of identifying technical parameters that define the stiffness of each structural component. Then, in contrast to lumped stiffness models, condensation methods do not provide any physical parameters, which the engineer can directly interpret to derive an optimized design. Moreover, when applying condensation methods to the mechanisms of the front assembly and swingarm, it has to be determined at which level to apply the condensation. If it is applied to the whole assembly, composed of different bodies, the problem is preserving the kinematics of the mechanism itself. If condensation is applied to the single bodies of each assembly, further analysis will provide indications about the effects of the stiffness of single bodies, thus failing to analyze the effect of the stiffness of the whole assembly, which makes it difficult to derive information for an optimized design. The obtained lumped stiffness models are particularly useful for the second main contribution of this paper, i.e., a sensitivity analysis with the lumped stiffness model to study the separated effect on weave and wobble of bending and torsional flexibility for each structural component.

4 Methods

In this section, the methods used in this paper are presented. Section 4.1 briefly describes the motorcycle model used to generate the results. Section 4.2 provides details on the methods for the parameterization of lumped stiffness models. Section 4.3 summarizes the steps needed to conduct a sensitivity analysis with the motorcycle model and to calculate the stability index and correlation coefficients.

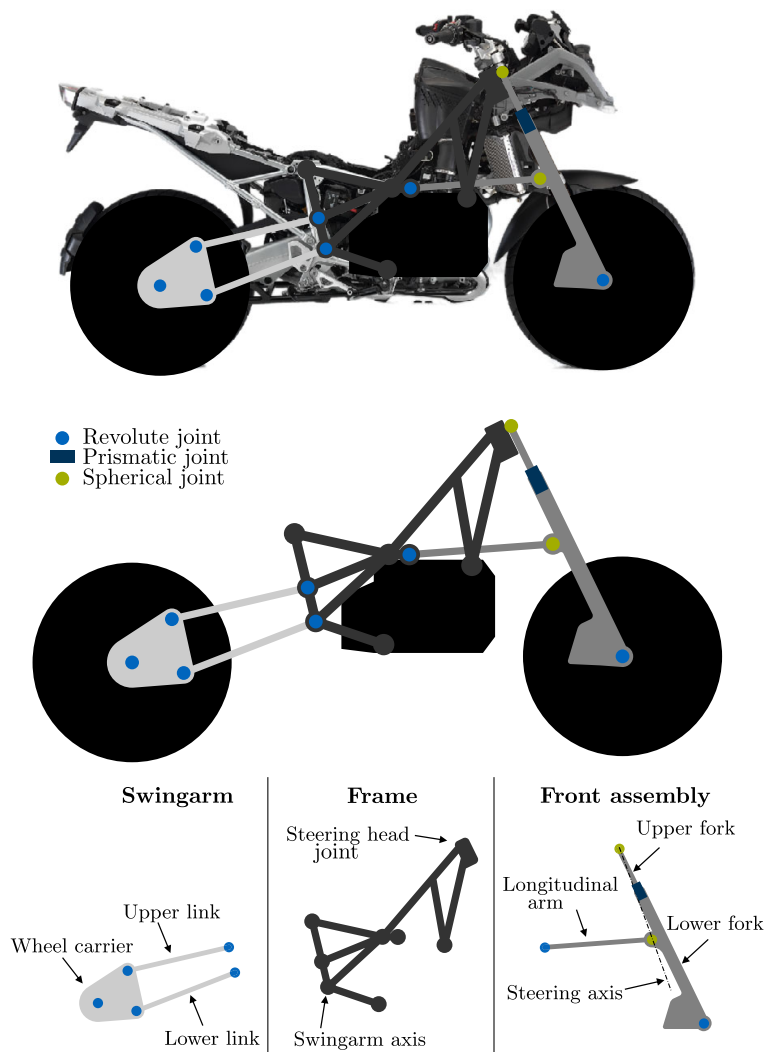
4.1 Motorcycle model

The motorcycle model is based on [11]. The motorcycle weighs 250 kg and is loaded with a rider (88 kg), two side bags and one top bag (40 kg in total). The front suspension is multilink with one longitudinal arm, while the rear suspension is of the four-bar link type swingarm. The Pacejka Magic Formula (MF) is used to model the tire forces [28]. A single contact point is assumed, and the tire thickness is accounted for. The kinematics of the contact point is based on the approach described in [8], where the relative orientation between the wheel carrier and ground is used to determine the reference system of the contact point.

In this work, two different versions of the motorcycle model are presented: one version uses EMBS with flexible bodies and is identical to that in [11]. The structural components modeled as flexible bodies are the frame, connected to a rigid engine, the front assembly, composed of the fork bridge, two stanchions, longitudinal arm and lower fork, and the swingarm, composed of lower link, upper link and wheel carrier. In the present work, this version is compared to a model of the same motorcycle that uses only rigid bodies and the lumped stiffness approach for representing the flexibilities. The parameters for the lumped stiffness models are identified with the method presented in Sect. 4.2. The theory of EMBS for modeling flexible bodies is explained in [11]. More information about the flexible multibody models is provided in the appendix.

With reference to Fig. 1, first, the model without flexibilities is described. It is composed of the following subsystems, bodies, and degrees of freedom (DOFs):

Fig. 1 Schematic representation of the motorcycle and its sub-assemblies. The image of the real motorcycle has been taken with permission from [29]



- *Main frame* of the motorcycle (including engine, fuel tank, and part of the driveline); it is constituted by a single rigid body, with 6 DOFs in 3D space (3 translations and 3 rotations about the inertial axes of the body).
- *Driver*, modeled as an additional rigid body split into two parts (not shown in Fig. 1): lower body fixed with respect to the main frame and upper body with one DOF of relative rotation with respect to the lower body, describing the rider's passive lean motion.
- *Front assembly*, composed of 3 rigid bodies: upper fork, including handlebars, lower fork, including wheel carrier, and longitudinal arm. Kinematically, the front assembly has 2 DOFs of relative motion with respect to the main frame; the first DOF is a rotation about the steering axis; the second one, for a fixed steering angle, is represented by a planar motion of the 3 members of the subsystem, yielding the front suspension travel. This can be inferred from Fig. 1, where the front assembly can be visualized as a spatial mechanism with 3 moving members with respect to the main frame, connected by one revolute joint, one prismatic joint, and two spherical joints (one placed at the steering head, the other one placed at the connection between longitudinal arm and lower steering assembly; the centers of these two spherical joints identify the position of the steering axis).
- *Front wheel*, including all rotating elements with the front wheel, modeled as a single rigid body with single contact point tire, and one DOF of relative motion with respect to the lower front assembly (rotation).

- *Swingarm*, composed of 3 rigid bodies (upper link, lower link, including transmission shaft, and wheel carrier). Kinematically, the swingarm represents a four-bar linkage, with one DOF of relative planar motion with respect to the main frame, describing the rear suspension travel. This can be inferred from Fig. 1, where the swingarm can be seen as a planar four-bar linkage, with 3 moving members with respect to the main frame, connected by 4 revolute joints.
- *Rear wheel*, including all rotating elements with the rear wheel, modeled as a single rigid body with single contact point tire, and one DOF of relative motion with respect to the rear wheel carrier (rotation).

At this stage, the flexibility of the 3 subsystems (main frame, front assembly, and swingarm) is introduced into the model by means of lumped stiffness elements. First, the front assembly and the swingarm are assumed to be “frozen” in a configuration of interest for the analysis. Then, each of the 3 subsystems is split into two rigid bodies connected by a fictitious revolute joint with a spring/damper element. This way, a (small) deformation of a flexible body is approximated by the relative (small) rotation between two rigid bodies about a deformation axis. Clearly, this requires the addition of 3 internal DOFs to the model, one for each flexible subsystem. Regarding the two bodies which compose the frame: one has the steering head joint, and the other provides the attachment point for the swingarm and longitudinal arm of the front assembly. For the front assembly and swingarm, the flexibility of the lumped stiffness model is obtained by introducing a massless body attached to the wheel carrier through the revolute joint associated with the lumped stiffness model. The wheel is then attached with the rotational DOF to the massless body itself. This way, the effect of flexibility on the wheel movement is reproduced.

For simulations, the open-source multibody simulation software MBSim [30] is used. The model order reduction needed for EMBS is carried out in Python with a code based on [31]; see [11] for further details.

4.2 Identification method

In this section, an identification method for lumped stiffness models is proposed aimed at representing with sufficient accuracy the effect of structural flexibility on weave and wobble. The basic procedure to create a lumped stiffness model starting from a single elastic body consists of splitting the body into two rigid bodies connected by a revolute joint. A rotational spring/damper is then associated with that joint. This way, a continuous (small) deformation of the elastic body is approximated by the relative rotation of two rigid bodies about a deformation axis. This approximation procedure needs to identify several parameters: the location and orientation of the revolute joint, the rotational stiffness and damping, and the inertia associated with each of the two bodies.

The adopted identification procedure, similar to that presented in [22–24], is described here referring to the simple case of a beam, as presented in Fig. 2. At one end of the undeformed beam, a reference system $O; x, y, z$ is fixed so that the axis of the beam lays in the plane (x, z) . At the opposite end of the beam, another reference system $O'; x', y', z'$ is fixed so that x' and z' are parallel to x and z , respectively. It is now assumed that the beam is clamped at point O and free at point O' . An external load F_y is applied at point O' in y direction, causing a small displacement, which moves the point from position q_0 to position q . In general, this also produces a small rotation of the reference system fixed at point O' . Therefore, under the effect of the external load, the planes defined by (x, z) and (x', z') are no longer parallel. Their intersection identifies the deformation axis, which can be adopted

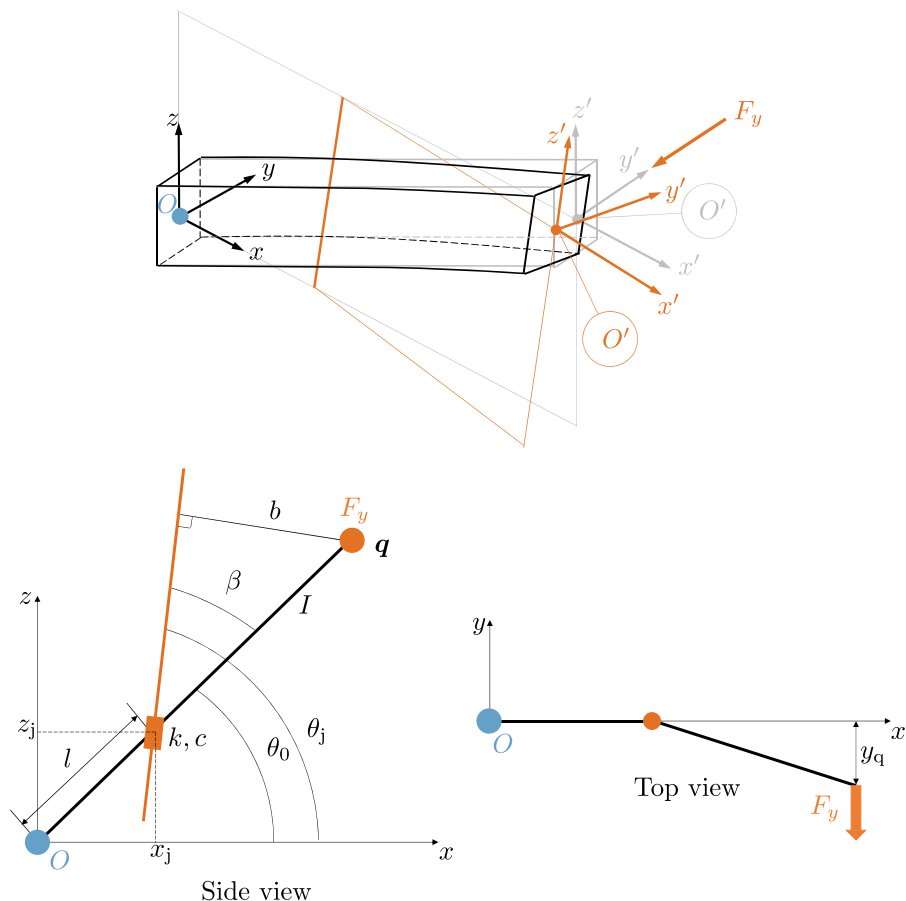


Fig. 2 Deformation axis of a beam cantilevered at the origin O (light blue dot) and having the load F applied to the free end (orange dot). (Color figure online)

for approximating the small deflection of the beam by means of the relative rotation of two rigid bodies.

Three types of tests are used: quasi-static test, harmonic test, and eigenvalue analysis. In the quasi-static test, a force is applied slowly so that the dynamics of the component is not excited. For the harmonic test, the load is applied with a sinusoidal wave oscillation, where the excitation frequency is constant throughout the test. In the eigenvalue analysis, the first bending and torsional eigenmodes and the related eigenvalues are identified. The amplitude of the forces applied to the components has been determined considering the loads that the components will experience during typical driving conditions, where the deformations remain in the linear range.

Based on these concepts, the procedure for identification of the lumped stiffness parameters shown in Fig. 2 can be defined. The explanation is divided into two parts: the identification of the geometric parameters l, β, b and the identification of stiffness k , damping c and vibrating inertia J .

The tests are carried out with simulations where the frame, front assembly, and swingarm are modeled with the same flexible bodies used for the motorcycle model in [11]. The measurements needed for the tests are provided by the simulation software itself.

4.2.1 Identification of l, β, b

The geometric parameters can be calculated either with static or harmonic tests. Define $\mathbf{q} = [x_q, y_q, z_q]$ the position of the free end and \mathbf{R} its orientation matrix with respect to the

fixed inertial frame. With the static test, these values are measured after the quasi-static load has reached its maximum, while, during the harmonic test, the values from peak displacement are used.

The deformed plane is represented by $a_1x + a_2y + a_3z + a_4 = 0$. $\mathbf{n} = [a_1, a_2, a_3]$ is the vector perpendicular to the displaced plane of symmetry. As in Fig. 2, the plane of symmetry of the component is the x-z plane, and the vector is equal to the second column of matrix \mathbf{R} : $\mathbf{n} = \mathbf{R}_y$. Knowing the vectors \mathbf{n} and \mathbf{q} , the coefficient a_4 of the plane equation can be determined:

$$a_4 = -(a_1x_q + a_2y_q + a_3z_q). \quad (1)$$

With the assumption that the plane of symmetry of the component under the test is the x-z plane, the position of the revolute joint can be found, see orange rectangle in Fig. 2. It could lay at any point along the deformation axis in Fig. 2. In this work, the revolute joint is placed at the intersection between the deformation axis and the line joining the origin of the inertial frame and the position $\mathbf{q}_0 = [x_{q_0}, y_{q_0}, z_{q_0}]$ of the loaded end in its unloaded configuration. This line has the equation $z = \frac{z_{q_0}}{x_{q_0}}x$. Substituting $y = 0$ in the equation of the plane gives the equation of the deformation axis:

$$z = -\frac{a_1}{a_3}x - \frac{a_4}{a_3}. \quad (2)$$

The x coordinate x_j of the revolute joint can be calculated by substituting $z = \frac{z_{q_0}}{x_{q_0}}x$ in Equation (2):

$$x_j = -\frac{a_4}{a_1 + a_3 \frac{z_{q_0}}{x_{q_0}}}. \quad (3)$$

The coordinate z_j is then automatically determined:

$$z_j = \frac{z_{q_0}}{x_{q_0}}x_j. \quad (4)$$

With these coordinates, the parameter l can be calculated:

$$l = \cos \left(\text{atan} \left(\frac{z_j}{x_j} \right) - \text{atan} \left(\frac{z_{q_0}}{x_{q_0}} \right) \right) \sqrt{x_j^2 + z_j^2}. \quad (5)$$

The cosine term is needed to determine if the revolute joint is at the positive or negative side of the x axis.

The angle β is calculated as difference between two angles:

$$\beta = \text{atan} \left(-\frac{a_1}{a_3} \right) - \text{atan} \left(\frac{z_{q_0}}{x_{q_0}} \right) = \theta_j - \theta_0. \quad (6)$$

The angle β is wrapped between 0 and π , since the orientation of the revolute joint is insensitive to rotations of π . In fact, a rotational spring/damper element is assigned to the revolute joint, which acts equally in both directions of rotation.

Finally, the calculation of the moment arm b is given as:

$$b = (L - l) \sin \beta, \quad (7)$$

where $L = \sqrt{x_{q_0}^2 + z_{q_0}^2}$ is the distance between loaded end and the origin in the unloaded configuration.

The harmonic test provides one set of parameter l, β, b for every peak. The lumped stiffness model is then parameterized by the mean over these sets. In particular, the excitation is applied until the mean settles within a specified tolerance band.

4.2.2 Identification of k, c, J

The rotational stiffness k can be calculated by dividing the moment of the force F about the deformation axis by the rotation of the free end about the axis itself:

$$k = \frac{F_{st} \cdot b}{\text{asin}\left(\frac{y_{qst}}{b}\right)}, \tag{8}$$

where F_{st} and y_{qst} are the values of force amplitude and related displacement from a static test. b is the moment arm resulting either from the static or harmonic test, depending on the test chosen for identifying the geometric parameters in Sect. 4.2.1.

For the identification of c and J a different approach based on the eigenvalue analysis of each flexible body model is used. After identifying the first bending and torsional eigenmodes and under the assumption that they are sufficiently decoupled, the related eigenvalues are calculated. For underdamped systems, as it is the case for structural components, these can be expressed in the form:

$$\lambda_{1,2} = -\zeta_n \omega_n \pm j \omega_n \sqrt{1 - \zeta_n^2}, \tag{9}$$

where ω_n is the modal natural frequency, and ζ_n is the modal damping ratio. Note that Equation (9) is valid under the assumption of proportional viscous damping, which is acceptable in the case under analysis due to small amounts of structural damping. The imaginary part of Equation (9) provides the damped modal eigenfrequency ω_d . The modal natural frequency ω_n can be obtained from numerical simulation without damping or as the modulus of the eigenvalues $\lambda_{1,2}$ in Equation (9). Knowing ω_n and ω_d , the modal damping ratio ζ_n can be calculated. At this point, the modal inertia J and the damping c result from:

$$J = \frac{k}{\omega_n^2}, \tag{10}$$

$$c = 2\zeta_n J \omega_n. \tag{11}$$

This yields J and c for each of the two eigenmodes. Under the assumption of viscous damping, c can be directly used in the rotational spring damper element associated with the revolute joint.

4.2.3 Stiffness decomposition

For the sensitivity analysis in Sect. 4.3, two separated parameters for the bending and torsional stiffnesses are needed. However, the static test identifies only one stiffness value. The authors of [24] propose a method to split the stiffness identified with a static test between the deformation axes corresponding to the bending and torsion axes. Instead of only one revolute joint, the resulting lumped stiffness model has two revolute joints with rotation axes having the same directions of the bending and torsion axes. This concept is shown in

Fig. 3 Schematic representation of the stiffness decomposition: the stiffness about the static deformation axis is split into two stiffnesses about the bending and torsion axes

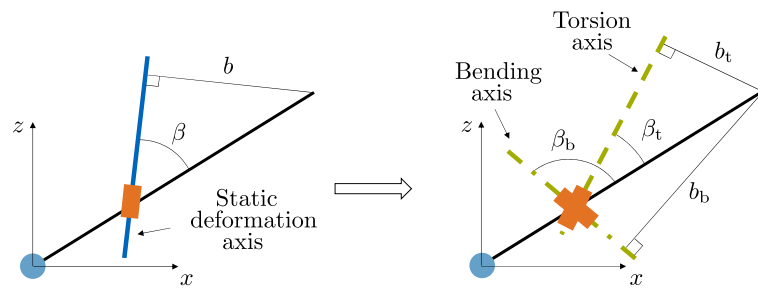


Fig. 3. This way, two stiffness parameters are available, but the overall flexural behavior of the lumped stiffness model is the same as that parameterized with just one revolute joint.

In the following, the procedure described in [24] is briefly summarized. Three tests with the component are needed: static test to identify the stiffness k , orientation β , and arm b ; a harmonic test with the first bending eigenfrequency to identify the orientation β_b and arm b_b ; and a harmonic test with the first torsional eigenfrequency to identify the orientation β_t and arm b_t . The unknowns are the stiffnesses about the bending axis k_b and torsion axis k_t . For the following two equations, two assumptions are made [24]: the displacement of the loaded end due to rotation about the static deformation axis is equal to the sum of the displacements due to rotations about bending and torsion axes, and the rotation about the static deformation axis of the loaded end is equal to the sum of the rotations about the bending and torsion axes. Additionally, as explained in [24], the assumption of small rotations is made. This makes it possible to consider the resultant rotation as the vector sum of components, where the order in which the rotations are performed is irrelevant. The adopted computational procedure is taken from [24]. The two unknowns k_b , k_t can be found by solving the system of equations:

$$\frac{b^2}{k} = \frac{b_b^2}{k_b} + \frac{b_t^2}{k_t}, \quad (12a)$$

$$\tan \beta = \frac{\frac{b_b}{k_b} \sin \beta_b + \frac{b_t}{k_t} \sin \beta_t}{\frac{b_b}{k_b} \cos \beta_b + \frac{b_t}{k_t} \cos \beta_t}. \quad (12b)$$

4.3 Sensitivity analysis

As explained in Sect. 3, the aim of the sensitivity analysis is to investigate the separated influence on weave and wobble of bending and torsional flexibility of each structural component on weave and wobble. The framework to carry out this analysis is provided by [25–27]. Basically, the influence of varying the stiffness parameters (main factors) on the damping of weave and wobble is analyzed. The procedure can be divided into three steps:

1. Definition of a stability index for weave and wobble.
2. Calculation of analysis of variance (ANOVA) to understand if there are interactions between the main factors.
3. If the interactions between the main factors are negligible, a linear correlation coefficient can be used (Pearson correlation coefficient) to show if an increase in the main factors, i.e., the stiffness parameters, leads to an increase or decrease in the stability index.

Starting from a plot of the real part of the eigenvalue of weave and wobble over longitudinal speed, the following two situations shown in Fig. 4 can be distinguished:

- The stability boundary is never crossed in the considered speed range, i.e. the real part of the eigenmode is negative at each speed. In this case, the stability index is defined as

minimum distance between the curve of the real part and the stability boundary:

$$s_1 = \max(\text{Re}(\lambda)). \quad (13)$$

- The stability boundary is crossed at least once, i.e. its real part becomes positive. In this case, the stability index is defined as the ratio between the velocity range where the mode is stable and the whole velocity range considered:

$$s_2 = \frac{\|\mathbf{v}_{\text{stable}}\|}{v_{\text{max}} - v_{\text{min}}}, \quad (14)$$

where $\mathbf{v}_{\text{stable}}$ represents the interval of velocities where the mode is stable, see the thick segments in Fig. 4. In the case shown in Fig. 4, $\|\mathbf{v}_{\text{stable}}\| = (v_1 - v_{\text{min}}) + (v_{\text{max}} - v_2)$, where v_1 and v_2 are the points of the first and second roots, respectively. Depending on the shape of the curve, another calculation may be necessary, but the meaning of the index s_2 does not change. If there is only one root, only one interval for $\|\mathbf{v}_{\text{stable}}\|$ is identified. No more than two crossings are expected when studying weave and wobble as a function of the speed.

With reference to Fig. 4, it can be seen that the stability index s_2 is defined relatively to the whole interval of velocities achievable by the motorcycle. If the motorcycle is unstable in the whole velocity range, then $s_2 = 0$ (minimum stability, given by the fact that one or more eigenvalues have always positive real part in the whole velocity range). If the motorcycle is stable in the whole velocity range, then $s_2 = 1$ (maximum stability, given by the fact that one eigenvalue is at the stability threshold, with zero real part).

Equations (13) and (14) can be combined into a single stability index s :

$$s = \|\min(0, s_1)\| + s_2. \quad (15)$$

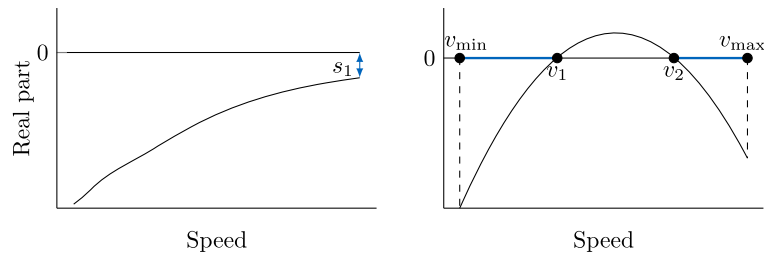
When the real part of the eigenvalue is always negative, $s_2 = 1$ and $s > 1$. If the stability boundary is reached, the first part of Equation (15) is zero, as s_1 is positive, and the index s varies between 0, which means that the eigenmode is unstable in the whole speed range, and 1, which indicates that the curve of the real part touches the stability boundary but never crosses it.

In the present work, the stability index is defined separately for low (40-100 km h⁻¹) and high (100-210 km h⁻¹) speeds. This covers all the relevant speeds up to the maximal speed of the motorcycle considered; speeds lower than 40 km h⁻¹ are not relevant for studying weave and wobble in motorcycles. The distinction of the speed ranges is necessary, particularly for wobble, because parameters, such as the fork bending stiffness, act oppositely at a low and high speed [5–8]. The use of a single index for the whole speed range would fail to capture this distinction, thus falsifying the sensitivity analysis.

Similarly to [25–27], a full factorial design with two levels is chosen for an ANOVA with the stability index as response variable. The nominal values identified with the procedure in 4.2.3 are varied by $\pm 10\%$. There are two stiffness values for each of the three considered structural components; this way, $2^6 = 64$ combinations are tested. After this analysis, it can be recognized if the variability of the six main factors is dominant, or if the interactions between them have a nonnegligible importance. The ANOVA is carried out with the `anovan` function of MATLAB.

Finally, if the interactions between the main factors are negligible, Doria [25] proposes to use the Pearson correlation coefficient to determine the effect of each factor, evaluated at the two levels, on the stability index. Using the same nomenclature as in [25], the Pearson

Fig. 4 Representation of stability indexes. Left: no crossing of the stability boundary, the index in Equation (13) is used. Right: two crossings of the stability boundary, the index in Equation (14) is used



correlation coefficient is ρ_{IF} , where F is the factor (stiffness), and I is the index (weave or wobble stability index), and it is defined as follows:

$$\rho_{IF} = \frac{\sigma_{IF}}{\sigma_I \sigma_F}. \tag{16}$$

σ_I , σ_F , σ_{IF} are, respectively, the variance of the index, the variance of each factor, and the covariance between index and factor:

$$\begin{aligned} \sigma_I^2 &= \frac{1}{n} \sum_{i=1}^n (I_i - \bar{I})^2, \\ \sigma_F^2 &= \frac{1}{n} \sum_{i=1}^n (F_i - \bar{F})^2, \\ \sigma_{IF}^2 &= \frac{1}{n} \sum_{i=1}^n (I_i - \bar{I})(F_i - \bar{F}), \end{aligned} \tag{17}$$

where n is the number of combinations of the factors, 64 in this case.

A value of ρ_{IF} close to 1 or -1 indicates either positive or negative strong correlation of the index I to the factor F [32].

5 Results

This section is divided into three subsections. Section 5.1 shows the results of the identification method presented in Sect. 4.2. In particular, the deformation axes of every structural component identified with static and harmonic tests are visualized. In Sect. 5.2, the accuracy in the simulation of weave and wobble of the lumped stiffness models with identified parameters is evaluated by comparing the results with the flexible multibody motorcycle model. Section 5.3 presents the results of the sensitivity analysis.

5.1 Results of parameter identification

The deciding point when identifying the lumped stiffness parameters is to pick the right load combination. In fact, as presented in [22, 23], static and harmonic loads identify different parameters. Figures 5, 6, and 7 show the deformation axes for every structural component with the static and harmonic test. The x axis represents the longitudinal axis of the motorcycle, and the z axis points upwards. The blue line is the deformation axis identified with the static test. The two green lines are the deformation axes resulting from harmonic tests having the frequency of the first bending and torsional eigenmodes, named bending and torsion axes. Table 1 shows the first torsional and bending eigenfrequencies for each component.

Fig. 5 Visualization of deformation axes of the frame with different loads. The component is fixed at the engine mounts and the load is applied to the steering head joint. (Color figure online)

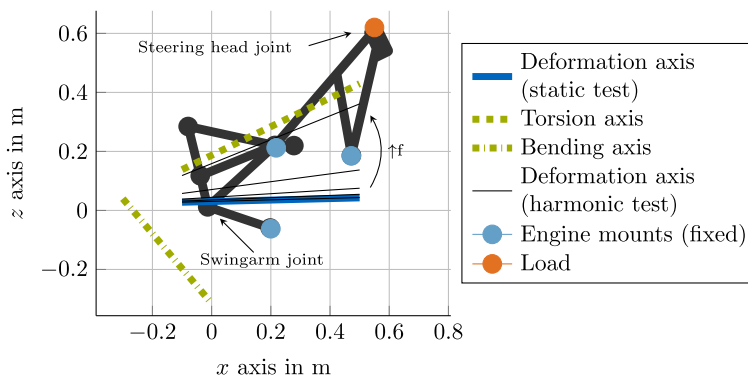


Fig. 6 Visualization of deformation axes of the front assembly with different loads. The component is clamped at the steering head joint and at the revolute joint of the longitudinal arm. The load is applied to the wheel axis. (Color figure online)

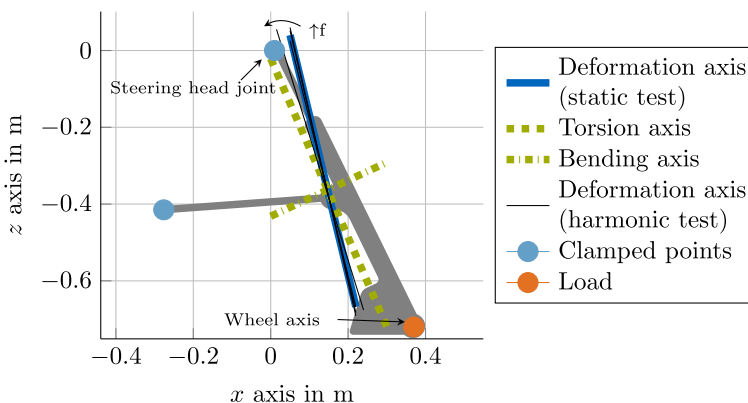


Fig. 7 Visualization of deformation axes of the swingarm with different loads. The component is fixed at the swingarm joint and the load is applied to the wheel axis. (Color figure online)

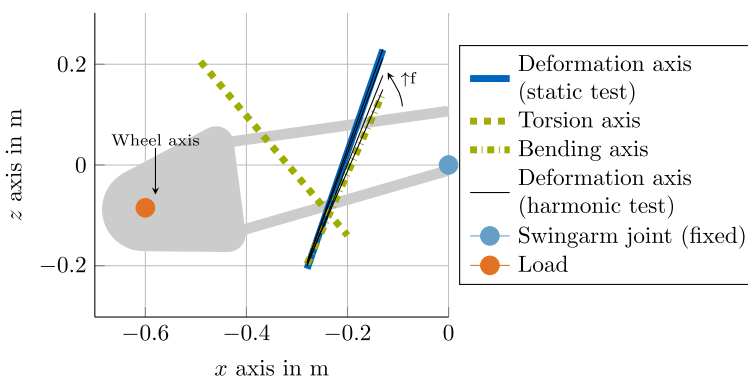


Table 1 First torsional and bending eigenfrequency of frame, front assembly, and swingarm

Component	Eigenfrequency	Mode shape
Frame	74 Hz	Torsion
	93 Hz	Bending
Front assembly	28 Hz	Torsion
	79 Hz	Bending
Swingarm	112 Hz	Bending
	321 Hz	Torsion

The black thin lines show the deformation axes when the excitation frequency of the harmonic test is varied from 1 Hz to a frequency of 5 Hz below the first eigenfrequency of the component. Similarly to Fig. 2, the light blue dots are the points where the component is fixed to the inertial frame, and the orange dots are the points where the load is applied.

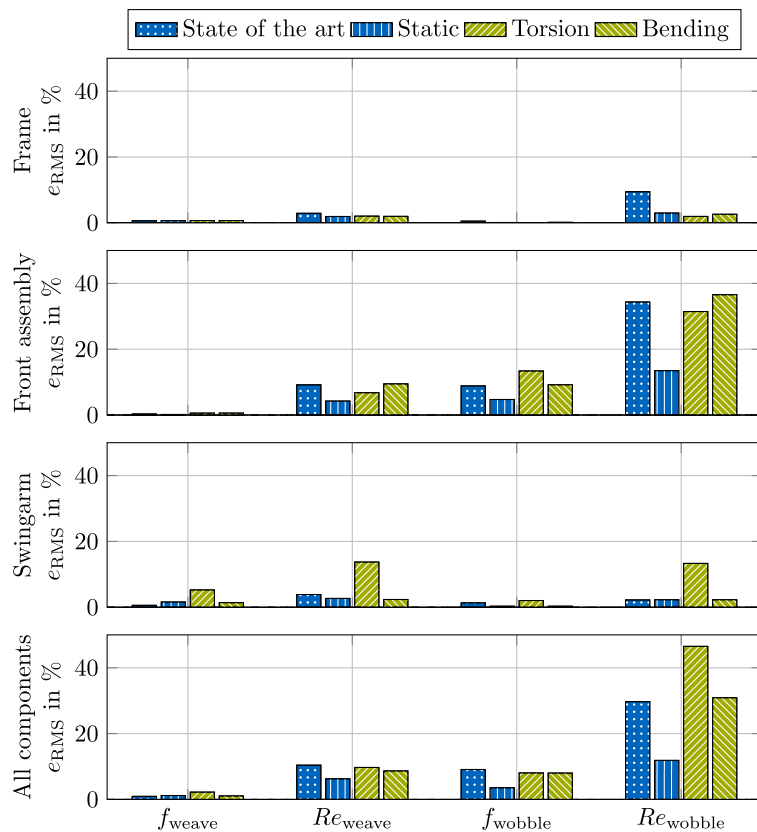
In Fig. 5, the frame is fixed at the engine mounts, and the load is applied to the steering head joint. The choice of fixing the engine mounts allows the consideration of the contribution of the engine to the overall stiffness. In fact, in the motorcycle, the frame is mounted on the engine itself, which is assumed rigid in this paper. The eigenfrequencies in Table 1 are obtained with the tank and saddle mounted on the frame and modeled as rigid bodies with mass and inertia. The torsion axis is nearly parallel to the line joining the swingarm joint and the steering head joint, where the load is applied. The bending axis is nearly perpendicular to the torsion axis and lays behind the swingarm joint, signaling that, when oscillating with the first bending eigenmode, the steering head joint mainly translates along the y axis, i.e. in the direction orthogonal to the symmetry plane of the frame. The static deformation axis is a combination of torsion and bending; this is due to the fact that the frequencies of the first torsion and bending eigenfrequencies are close in value. As expected, by sweeping the frequency of the harmonic excitation, the deformation axis moves from the static deformation axis to the deformation axis of the first eigenmode, i.e., the torsion axis.

The front assembly is clamped at the steering head joint and at the joint between the longitudinal arm and the frame to avoid the movement of the suspension (Fig. 6). The load is applied at the wheel axis. The longitudinal arm of the multilink suspension is also shown. The torsion axis is, as expected, nearly parallel to the fork axis, while the bending axis is almost perpendicular to it. Also, in this case, the static deformation axis is a combination of torsion and bending. However, torsion dominates the deformation of the assembly for a static excitation because the eigenmode with the lowest eigenfrequency is torsional, and the frequency of the first bending eigenmode is significantly higher (Table 1). This is different from conventional forks that generally have lower bending stiffness than torsional stiffness [22]. The high bending stiffness in the present case can be attributed to the presence of the longitudinal arm. The harmonic test with increasing frequency (black lines in Fig. 6) identifies a deformation axis that progressively moves from the static axis to the axis of the eigenmode.

The swingarm, Fig. 7, is fixed at the joint with the frame, and the force is applied to the wheel axis. As mentioned in Sect. 4.1, it is a four-bar link composed of a lower link, upper link, and wheel carrier. Unlike frame and front assembly, the first eigenmode is a bending one, see Table 1. The bending axis is, as expected, almost perpendicular to the main arm and link, and the torsion axis is nearly perpendicular to the bending axis. The static deformation axis is dominated by bending because it is the first eigenmode, and the first torsional eigenmode has a significantly higher eigenfrequency. Also, in this case, when increasing the frequency of the harmonic test, the deformation axis moves from the static axis to the axis of the first eigenmode.

When building the lumped stiffness model of a structural component, the single body must be split into two bodies. Regarding the frame, the inertia of the body to which the handlebar is attached is the one identified through the test in Sect. 4.2.2. The mass of the frame, engine, tank, and saddle is concentrated into the other body to which the swingarm and the longitudinal arm of the front assembly are connected; the inertia of this body is calculated such that the overall inertia of the motorcycle remains the same. For the front assembly and swingarm, the identified inertia is assigned to the massless body used for the lumped stiffness model, see Sect. 4.1. Inertia must then be removed to ensure that the overall inertia remains constant. In the case of the front assembly, this inertia is removed from the lower fork, while for the swingarm, the inertia is removed from the wheel carrier.

Fig. 8 Root mean square error in percentage of lumped stiffness models compared to the flexible multibody models



5.2 Accuracy of identified lumped stiffness models

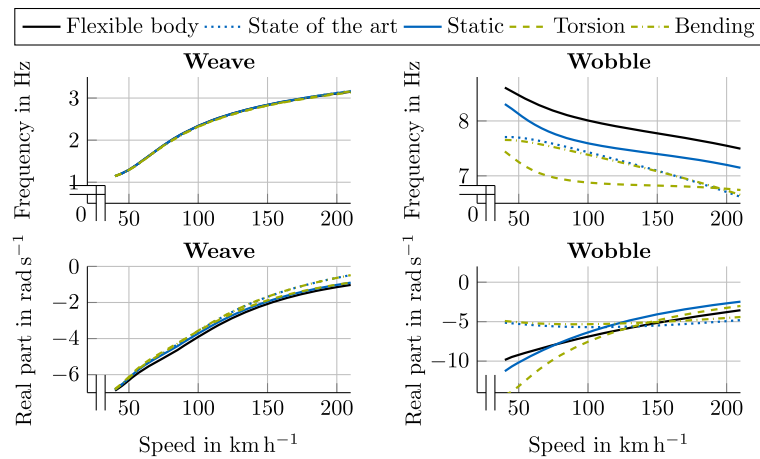
At this point, the accuracy of lumped stiffness models in simulating the influence of flexibilities on weave and wobble is investigated. For that, the models are compared to the flexible multibody motorcycle model presented in [11], which is considered the “ground truth”. In particular, the eigenfrequency f and real part Re of weave and wobble are determined between 40 and 210 km h⁻¹, and the root mean square error in percentage between the lumped stiffness models and the flexible body models is calculated:

$$e_{RMS\%} = \frac{\sqrt{\frac{1}{N} \sum_{i=1}^N (x_{lu} - x_{fl})^2}}{\bar{x}_{fl}} \cdot 100. \quad (18)$$

N is the number of speed values for which weave and wobble are simulated. x_{lu} , x_{fl} are either the frequency or the real part of weave or wobble calculated with the lumped stiffness and flexible body model, respectively. \bar{x}_{fl} is the mean over the speed range of either frequency or real part calculated with the flexible body model.

The results are shown with the bar diagram in Fig. 8. In the first three plots, the frame, front assembly, and swingarm are studied separately: for each case, only the flexibility of that component is included in the motorcycle model, with either lumped stiffness or flexible multibody approach. The last plot represents the case where the flexibility of all structural components is modeled simultaneously. Different lumped stiffness models are shown in Fig. 8. The one marked with “State of the art” uses the common assumptions found in the literature for the orientation of the revolute joints; moreover, the stiffness values are measured with static tests on the flexible multibody model of each structural component. The case marked with “Static” uses the identification procedure of Sect. 4.2 with the quasi-static

Fig. 9 Effect of the flexibility of the front assembly on weave and wobble (only the flexibility of the front assembly is modeled): comparison between flexible body, state-of-the-art lumped stiffness, and lumped stiffness models parameterized with the procedure in Sect. 4.2



application of the load. The bars marked with “Torsion” and “Bending” also use the identification procedure but with harmonic tests at the frequency of the first torsional and bending eigenmodes of the flexible body, respectively. “State of the art” and “Static” lumped stiffness models are obtained with a static test because they approximate the response of the component to static loads; for this reason, they both do not use the identified inertia. In contrast, “Torsion” and “Bending” lumped stiffness models approximate the frequency response of the component at the first torsional and bending eigenfrequencies. For this reason, Equation (10) is applied to the first torsional and bending eigenfrequencies, thus obtaining the modal inertia about the torsional and bending axes, respectively. The distribution of the inertia is done as explained at the end of Sect. 5.1.

Figure 8 does not show the error of lumped stiffness models parameterized with harmonic tests with a frequency below the first eigenfrequency of the flexible component because their results are similar to the lumped stiffness models parameterized either with the static test or harmonic test at the first eigenfrequency. In particular, for frequencies up to 10–20 Hz lower than the first eigenfrequency, the static test and the harmonic test identify very similar parameters (see Figs. 5, 6, and 7), and, therefore, the resulting lumped stiffness models are equivalent. In the rest of this section, the accuracy of the lumped stiffness models of the structural components is analyzed separately.

5.2.1 Frame

The “State of the art” lumped stiffness model of the frame represents the frame torsion with a revolute joint at the steering head joint with a rotation axis perpendicular to the fork axis [5]; the front assembly is then attached to that joint. In the present paper, the related stiffness is measured with a static moment applied to the steering head joint and perpendicular to the fork axis. As the frame of the present motorcycle is very stiff, all lumped stiffness models show low error in almost all cases. However, the “State of the art” model presents a relatively high error in the real part of the wobble eigenvalue, whereas the lumped stiffness models with parameters identified by the procedure in the present work perform significantly better. In particular, it has been verified that the “State of the art” model shows an eigenvalue with smaller real part (in modulus) at high speed than the “ground truth”, which signifies the stiffness is too high, see, e.g., [5–7].

5.2.2 Front assembly

The state-of-the-art approach for modeling the bending flexibility of the front assembly is to put a revolute joint with a rotation axis perpendicular to the fork axis. The related stiffness is

measured with a static lateral force applied to the wheel axis, see [11]. The revolute joint is located at the position of the spherical joint of the longitudinal arm, see [11] for more details on this decision. For the “State of the art” and “Static” lumped stiffness models, it has been verified that it is important that the inertia of the lower fork is activated during the motion of the wheel due to flexibility. For this reason, the inertia of the lower fork is moved to the massless body used for the definition of the lumped stiffness model while ensuring that the position of the center of gravity is not changed. In the “Torsion” and “Bending” lumped stiffness models, instead, the identified modal inertia is assigned to the massless body to correctly represent the frequency response of the component at the first bending and torsion eigenfrequencies. The front assembly is the component where the lumped stiffness models have the highest error, in particular in the real part of wobble. For this reason, it is worth looking in more detail at the evolution of weave and wobble with speed, shown in Fig. 9. The plots clarify that the “Static” lumped stiffness model provides the best approximation of the “ground truth”, i.e., the flexible multibody model. Interestingly, the “State of the art” lumped stiffness model and the “Bending” lumped stiffness model provide very similar results. This is due to the fact that the bending axis is almost perpendicular to the fork axis, see Fig. 6, and the resulting lumped stiffness model is therefore very similar to the “State of the art” model. This configuration, however, does not accurately represents the deformation of the front assembly when simulating weave and wobble.

5.2.3 Swingarm

For the swingarm, there is no general trend in the state-of-the-art. For this reason, the “State of the art” model here represents a possible simplified modeling approach for simulating the swingarm torsion: a revolute joint with a rotation axis parallel to the vehicle x axis (longitudinal axis) is put between the wheel center and the wheel carrier, see for example [33]. The related stiffness derives from a static test where a moment parallel to the vehicle x axis is applied to the wheel axis. The swingarm of the present motorcycle model has high stiffness, and, therefore, the differences between the models are small. The “Static” lumped stiffness model has the lowest error. In contrast, the “Torsion” lumped stiffness model shows a high error.

5.2.4 All components

The same considerations made above apply to the case where the flexibility of all structural components is modeled simultaneously: the largest error is in the real part of the wobble eigenmode, whereby the lumped stiffness models parameterized with the static test only show an error of at most 10%, thus overperforming the other lumped stiffness models.

In summary, the “Static” lumped stiffness models show the smallest error for every structural component and they offer a relevant improvement in accuracy compared to the state-of-the-art. The “Torsion” and “Bending” lumped stiffness models have higher errors than the “Static” lumped stiffness model so that the static test seems the best approach for parameterizing lumped stiffness models having the aim of modeling weave and wobble.

It is worth pointing out that the damping and inertia parameters identified through Equation (10) and (11) have a minor influence on weave and wobble. The main parameters influencing the stability of the two eigenmodes are the stiffness and location of the revolute joint. This is the reason why, for the lumped stiffness model identified with the static test, a very small value of damping is used. It can be calculated by multiplying the identified rotational stiffness by the proportionality constant $\gamma = 0.001$ s, thus obtaining $c = \gamma k$.

Table 2 Nominal values of stiffness about the static deformation axis k and stiffness about the torsion k_t and bending k_b axis after decomposition with the method in Sect. 4.2.3

	k in N m rad^{-1}	k_t in N m rad^{-1}	k_b in N m rad^{-1}
Frame	$1.03 \cdot 10^6$	$3.75 \cdot 10^5$	$3.59 \cdot 10^6$
Front assembly	$1.06 \cdot 10^4$	$5.95 \cdot 10^3$	$1.71 \cdot 10^5$
Swingarm	$1.33 \cdot 10^5$	$1.04 \cdot 10^6$	$1.39 \cdot 10^5$

5.3 Sensitivity analysis

In this section, a sensitivity analysis is carried out to answer the question of which stiffness within each component has the highest impact on the stability of weave and wobble. The stability index defined in Sect. 4.3 is used. Two separated analyses are done for the low speeds ($40\text{--}100 \text{ km h}^{-1}$) and high speeds ($100\text{--}210 \text{ km h}^{-1}$). This allows for the identification of the stiffness parameters that have opposite effects according to the speed range considered.

Once the parameters for the static deformation axis of each structural component are identified in Sect. 5.1, the stiffness about that axis is split along the torsion and bending axes with the procedure in Sect. 4.2.3. Table 2 presents these values for every structural component. The obtained stiffness values about torsion and bending axes are then varied in the range $\pm 10\%$, and the stability indexes for each of the 64 combinations are calculated.

First of all, the ANOVA is carried out to check which percentage of the variability of the stability index is due to main effects and how much depends on interactions between factors. For each stability index, approximately 99% of the variability is due to main factors. Therefore, the evaluation with the Pearson correlation coefficient is possible.

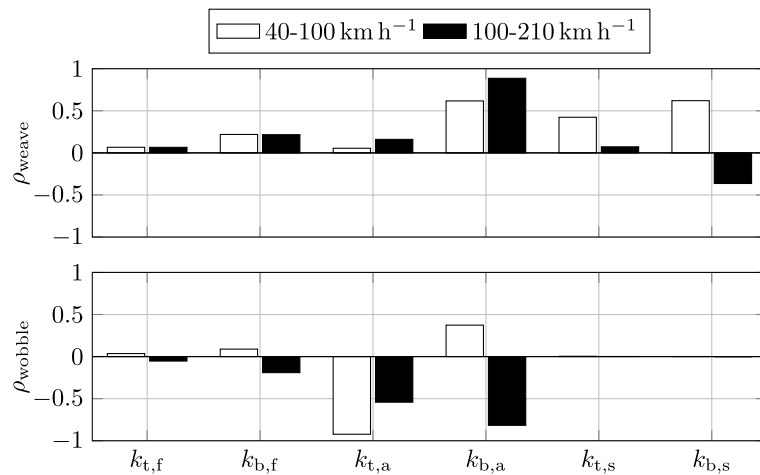
It has been verified that, for the motorcycle considered and for any combination of the lumped stiffness parameters, weave and wobble never cross the stability boundary, so only the stability index in Equation (13) is used.

Fig. 10 shows the Pearson correlation coefficients for every stiffness and distinguishes between weave and wobble. The subscript used must be interpreted as follows: the first letter indicates the type of flexibility (t for torsion and b for bending), and the second letter indicates the structural component (f is the frame, a is the front assembly, and s is the swingarm). A positive correlation coefficient means that an increase in the considered stiffness leads to increased damping of the mode.

The bar plot of wobble makes it clear why this analysis was conducted separately for the low- and high-speed ranges. There are stiffness parameters, such as torsional and bending stiffness of the frame and bending stiffness of the front assembly, that oppositely contribute to the two speed ranges.

At this point, some considerations about a stability-optimized design of structural components can be made. The following is valid for the present structural components and the shown nominal stiffness values; the extension to components with other designs can be a further research topic. High-frame torsional and bending stiffnesses have positive effects on the high-speed weave and low-speed wobble but a slightly negative effect on the high-speed wobble, which overlaps with experimental tests carried out in [34]. The front assembly is the part whose stiffness has the strongest effect on both eigenmodes. Too high torsional stiffness should be avoided because it destabilizes wobble at every speed and has only a small stabilizing effect on weave. Finding the optimal value of bending stiffness is a tricky task: on the one hand, the high bending stiffness of front assembly stabilizes the high-speed weave and the low-speed wobble; on the other hand, it strongly destabilizes the high-speed wobble. This stiffness should be therefore designed considering the characteristics of the whole motorcycle, such as its overall geometry and weight distribution, tire properties and

Fig. 10 Pearson correlation coefficients of weave and wobble for every structural stiffness



the presence of a steering damper. Please note that the torsion axis of the frame and the bending axis of the front assembly have similar orientation, see Fig. 5 and 6. In fact, they produce qualitatively similar results. The smaller sensitivity of the frame torsion is due to two effects: its nominal value is very high, so even with a variation of 10%, the stiffness always remains high; the front assembly bending flexibility directly affects the motion of the front wheel, while the frame torsional flexibility does that indirectly through the motion of the front assembly, which in the present case is also affected by the presence of the longitudinal arm. The swingarm stiffness hardly affects wobble, which is mainly influenced by the parameters of the motorcycle's front. Reducing swingarm bending stiffness brings positive effects to the high-speed weave but negative effects to the low-speed weave. However, weave is never critical at low speed, so an optimized design for the investigated configuration of the swingarm would involve relatively low bending stiffness but high torsional stiffness.

Of course, when reducing the stiffness of structural components with the aim of saving weight, the effects on driving dynamics as a whole and strength requirements must also be taken into account.

6 Conclusions

This paper proposes a method for parameterizing lumped stiffness models of motorcycle structural components. For that, static and harmonic tests are carried out in simulations with the components modeled as flexible bodies.

The main objective is to evaluate whether the lumped stiffness models parameterized with this method are accurate enough to simulate the influence of flexibilities on weave and wobble. The motorcycle model with lumped stiffnesses is therefore compared to the flexible multibody motorcycle model, which is considered “ground truth” because it has the most realistic modeling of flexibilities. The error of lumped stiffness models can be evaluated by simulating the frequency and real part of weave and wobble with these two models. Results show that the most suitable test for parameterizing lumped stiffness models with the aim of simulating weave and wobble is the static test. Moreover, the presented method for parameterization allows a significant improvement in accuracy compared to the state-of-the-art lumped stiffness models, which are generally based on assumptions for the position of the revolute joints used to model the flexibility.

It can be concluded that thanks to the presented method, lumped stiffness models reach enough accuracy to simulate the effect of flexibilities on weave and wobble. For modeling

phenomena with higher frequency, such as comfort tests, lumped stiffness model parameterized with harmonic tests at higher frequency could provide better results. However, there is also the possibility that, in these situations, only flexible multibody models provide sufficient accuracy thanks to their ability to reproduce frequency contents in a broad range.

The second main contribution of this work is the sensitivity analysis of component stiffnesses to point out which stiffness within each component has the highest impact on the stability and to make suggestions for an optimized design of structural components of the motorcycle model considered in this paper. The results stress the big influence of the flexibilities of the front assembly on both weave and wobble. Its torsional stiffness should not be too high to avoid the destabilization of wobble, while its bending stiffness should be optimized considering that a high value is advantageous for the high-speed weave damping and low-speed wobble damping but detrimental for the high-speed wobble damping. Finally, the flexibilities of swingarm only influence weave, and a stability-optimized design could involve relatively low bending stiffness but high torsional stiffness.

These considerations about possible optimal design are valid for the present components with the characteristics of the deformation axes provided. Literature shows that components with alternative constructions present different deformation characteristics, so the extension to other designs for the structural components could be a further research topic. The method presented in this paper is suitable for all types of structural components so that this extension can be easily carried out.

Appendix A

In this appendix, a summary of the information in [11] about the flexible multibody motorcycle model is reported.

As mentioned in Sect. 4.1, the following structural components of the motorcycle are modeled as flexible bodies:

- Frame, which is fixed to a rigid engine.
- Front assembly, which is composed of fork bridge, two stanchions, longitudinal arm, and lower fork.
- Swingarm, which is composed of lower link, upper link, and wheel carrier.

These bodies are initially modeled with FEM. However, they contain up to 10^6 degrees of freedom, so it would be impossible to directly include them in a multibody simulation environment because this would lead to unacceptable computation time. Therefore, model order reduction (MOR) is applied. In [11], the Craig-Bampton method is used, which has the peculiarity of distinguishing between the boundary and internal degrees of freedom. The boundary degrees of freedom serve as an attachment point for other bodies in an assembly or to apply external forces and are preserved by the reduction with the Craig-Bampton method. The internal degrees of freedom are reduced by applying modal truncation. In particular, the first 20 fixed-interface modes have been kept for each body. This way, the frequency content up to 600 Hz is included in the reduced order bodies. Table A.1 shows the degrees of freedom for each flexible body before and after MOR with Craig-Bampton. The degrees of freedom of the reduced order models are expressed as a sum to distinguish the number of boundary degrees of freedom (second number) from the number of selected modes.

For embedding the reduced order models of the structural components in the multibody simulation environment of the motorcycle, the Floating Frame of Reference Formulation is

Table A.1 Degrees of freedom of the flexible bodies before and after the model order reduction

		DOFs FEM	DOFs after MOR
Frame		$3,8 \cdot 10^6$	20+54
Front assembly	Fork bridge	$8,0 \cdot 10^5$	20+9
	Stanchions (each)	$2,1 \cdot 10^5$	20+9
	Lower fork	$1,7 \cdot 10^6$	20+18
	Longitudinal arm	$4,7 \cdot 10^5$	20+12
Swingarm	Lower link	$2,7 \cdot 10^6$	20+15
	Upper link	$4,1 \cdot 10^5$	20+6
	Wheel carrier	$2,1 \cdot 10^6$	20+12

used, which is suitable for describing the deformation of bodies that undergo small linear elastic displacement combined with big nonlinear rigid body motions.

The flexible multibody model of the frame and front assembly has been validated by comparing the stiffness resulting from static tests on the real components. In particular, the frame has been tested by clamping it at the swingarm axis and applying a lateral force at the steering head joint. The stiffness resulting from the flexible body deviates 6.4% from the experimental data. The front assembly is clamped at the steering head joint, and the lateral force is applied to the wheel axis. In this case, the error between experiment and simulation is 0.5%. The validation for the swingarm was not possible because no measurements were available.

Author contributions Francesco Passigato initiated the idea of the paper and contributed significantly to the concept, modeling, and results. Alexander Schramm made significant contributions in the development of methods and in the review phase. Silvio Sorrentino and Alessandro De Felice contributed to the review phase. Achim Gordner contributed to significant discussion of the results. Frank Diermeyer contributed to the whole concept of the paper. Frank Diermeyer gave final approval for publication of this version and is in agreement with all aspects of the work. As a guarantor, he accepts responsibility for the overall integrity of this paper.

Funding Open Access funding enabled and organized by Projekt DEAL. Francesco Passigato is funded by BMW Group (Germany).

Data Availability The model data belong to BMW Group and can therefore not be published.

Declarations

Ethical Approval Not applicable

Competing interests The authors declare no competing interests.

Open Access This article is licensed under a Creative Commons Attribution 4.0 International License, which permits use, sharing, adaptation, distribution and reproduction in any medium or format, as long as you give appropriate credit to the original author(s) and the source, provide a link to the Creative Commons licence, and indicate if changes were made. The images or other third party material in this article are included in the article's Creative Commons licence, unless indicated otherwise in a credit line to the material. If material is not included in the article's Creative Commons licence and your intended use is not permitted by statutory regulation or exceeds the permitted use, you will need to obtain permission directly from the copyright holder. To view a copy of this licence, visit <http://creativecommons.org/licenses/by/4.0/>.

References

1. Cossalter, V., Lot, R., Maggio, F.: The modal analysis of a motorcycle in straight running and on a curve. *Meccanica* **39**, 1–16 (2004)
2. Cossalter, V.: *Motorcycle Dynamics*, 2. english edn. Lulu Press, S.I, Padova, Italy (2006)
3. Sharp, R.S., Limebeer, D.J.N.: A motorcycle model for stability and control analysis. *Multibody Syst. Dyn.* **6**, 123–142 (2001)
4. Sharp, R.S.: The stability and control of motorcycles. *J. Mech. Eng. Sci.* **13**(5), 316–329 (1971)
5. Sharp, R.S., Alstead, C.J.: The influence of structural flexibilities on the straight-running stability of motorcycles. *Veh. Syst. Dyn.* **9**(6), 327–357 (1980). <https://doi.org/10.1080/00423118008968629>
6. Spierings, P.T.J.: The effects of lateral front fork flexibility on the vibrational modes of straight-running single-track vehicles. *Veh. Syst. Dyn.* **10**(1), 21–35 (1981). <https://doi.org/10.1080/00423118108968633>
7. Cossalter, V., Lot, R., Massaro, M.: The influence of frame compliance and rider mobility on the scooter stability. *Veh. Syst. Dyn.* **45**(4), 313–326 (2007). <https://doi.org/10.1080/00423110600976100>
8. Passigato, F., Eisele, A., Wisselmann, D., Gordner, A., Diermeyer, F.: Analysis of the phenomena causing weave and wobble in two-wheelers. *Appl. Sci.* **10**(19), 6826 (2020). <https://doi.org/10.3390/app10196826>
9. Schwertassek, R., Wallrapp, O., Shabana, A.A.: Flexible multibody simulation and choice of shape functions. *Nonlinear Dyn.* **20**(4), 361–380 (1999)
10. Doria, A., Formentini, M.: Identification of the structural modes of high performance bicycles in the perspective of wobble control: parts a and b. In: *Proceedings of the ASME Design Engineering Technical Conference*, vol. 4, pp. 551–560 (2011). www.scopus.com
11. Passigato, F., Gordner, A., Diermeyer, F.: Modeling of the weave and wobble eigenmodes of motorcycles using flexible multibody simulation *International Design Engineering Technical Conferences and Computers and Information in Engineering Conference*, Vol 9: 18th International Conference on Multibody Systems, Nonlinear Dynamics, and Control (MSNDC) (2022). <https://doi.org/10.1115/DETC2022-89945>.
12. Koenen, C., Pacejka, H.B.: The influence of frame elasticity and simple rider body dynamics on free vibrations of motorcycles in curves. *Veh. Syst. Dyn.* **10**(2–3), 70–73 (1981). <https://doi.org/10.1080/00423118108968637>
13. Koenen, C.: *The Dynamic Behaviour of a Motorcycle when Running Straight Ahead and when Cornering*: Delft. Techn. Hogeschool, Proefschrift **1983** (1983)
14. Sharp, R.S.: Stability, control and steering responses of motorcycles. *Veh. Syst. Dyn.* **35**(4–5), 291–318 (2001). <https://doi.org/10.1076/vesd.35.4.291.2042>
15. Sharp, R.S., Evangelou, S., Limebeer, D.J.N.: Advances in the modelling of motorcycle dynamics. *Multibody Syst. Dyn.* **12**(3), 251–283 (2004)
16. Sharp, R.S., Limebeer, D.J.N.: On steering wobble oscillations of motorcycles. *Proc. Inst. Mech. Eng., Part C, J. Mech. Eng. Sci.* **218**(12), 1449–1456 (2004). <https://doi.org/10.1243/0954406042690434>
17. Evangelou, S., Limebeer, D.J.N., Sharp, R.S., Smith, M.C.: Mechanical steering compensators for high-performance motorcycles. *Trans. ASME J. Appl. Mech.* **74**(2), 332–346 (2007)
18. Evangelou, S., Limebeer, D.J.N., Tomas-Rodriguez, M.: Suppression of burst oscillation in racing motorcycle. *J. Appl. Mech.* **80** (2013)
19. Sharp, R.S., Watanabe, Y.: Chatter vibrations of high-performance motorcycles. *Veh. Syst. Dyn.* **51**(3), 393–404 (2013). <https://doi.org/10.1080/00423114.2012.727440>
20. Cossalter, V., Lot, R., Massaro, M.: An advanced multibody code for handling and stability analysis of motorcycles. *Meccanica* **46**(5), 943–958 (2011). <https://doi.org/10.1007/s11012-010-9351-7>
21. Doria, A., Favaron, V., Taraborrelli, L., Roa, S.: Parametric analysis of the stability of a bicycle taking into account geometrical, mass and compliance properties. *Int. J. Veh. Des.* **75**(1–4), 91–123 (2017)
22. Cossalter, V., Doria, A., Massaro, M., Taraborrelli, L.: Experimental and numerical investigation on the motorcycle front frame flexibility and its effect on stability. *Mech. Syst. Signal Process.* **60–61**, 452–471 (2015). <https://doi.org/10.1016/j.ymsp.2015.02.011>
23. Taraborrelli, L., Favaron, V., Doria, A.: The effect of swingarm stiffness on motorcycle stability: experimental measurements and numerical simulations. *Int. J. Veh. Syst. Model. Test.* **12**(3/4), 240 (2017). <https://doi.org/10.1504/IJVSMT.2017.089981>
24. Doria, A., Taraborrelli, L.: The twist axis of frames with particular application to motorcycles. *Proc. Inst. Mech. Eng., Part C, J. Mech. Eng. Sci.* **230**(17), 3026–3039 (2016). <https://doi.org/10.1177/0954406215604862>
25. Doria, A., Roa, S.: On the influence of tyre and structural properties on the stability of bicycles. *Veh. Syst. Dyn.* **56**(6), 947–966 (2018)
26. Doria, A., Roa, S., Muñoz, L.: Stability analysis of bicycles by means of analytical models with increasing complexity. *Mech. Sci.* **10**(1), 229–241 (2019). <https://doi.org/10.5194/ms-10-229-2019>

27. Roa, S., Doria, A., Muñoz, L.: Optimization of the bicycle weave and wobble modes. *ASME* **3** (2018). <https://doi.org/10.1115/DETC2018-86132>
28. Pacejka, H.B.: *Tyre and Vehicle Dynamics*, 2 edn. Elsevier Butterworth-Heinemann, Amsterdam and Heidelberg (2006)
29. BMW Group: the new BMW R 1200 GS. <https://www.press.bmwgroup.com/global/article/detail/T0132324EN/the-new-bmw-r-1200-gs>
30. Schindler, T., Förg, M., Friedrich, M., Schneider, M., Esefeld, B., Huber, R., Zandler, R., Ulbrich, H.: In: *Analysing Dynamical Phenomenons: Introduction to mbsim. The 1st Joint International Conference on Multibody System Dynamics*, 2010 May 25-27, Lappeenranta, Finland (2010)
31. Meyer, C.H., Lerch, C., Maierhofer, J.: AMfe. Chair of Applied Mechanics, Technical University of Munich. <https://github.com/AppliedMechanics/AMfe>
32. Schober, P., Boer, C., Schwarte, L.: Correlation coefficients: appropriate use and interpretation. *Anesth. Analg.* **126**(5), 1763–1768 (May 2018). <https://doi.org/10.1213/ANE.0000000000002864>
33. Dipl.-Ing. Dirk Wisselmann: *Motorrad-Fahrdynamik-Simulation. Modellbildung, Validierung und Anwendung*: PhD Thesis. VDI-Berichte, Dachau (1992)
34. Roe, G.E., Thorpe, T.E.: *The influence of frame structure on the dynamics of motorcycles stability* SAE Technical Papers (1989)

Publisher's Note Springer Nature remains neutral with regard to jurisdictional claims in published maps and institutional affiliations.

4.4 Application Example of the Optimization of Stiffness Distribution

In this section, it is shown how the information provided by the methodology presented in Section 4.3 can be used to reduce the mass of structural components while enhancing the stability of the weave and wobble eigenmodes. A common way to reduce the mass of a component is to use less material, which generally implies a reduction of its stiffness. Obviously, the challenge is to select to which component this stiffness reduction should be applied without impairing the stability of weave and wobble. In fact, as explained in Section 2.2.2 and 2.2.3, when the chassis components have too low of a stiffness, the motorcycle could show high-speed weave stability issues. The methodology presented in Section 4.3 allows the designer to decide which structural component can be considered for the stiffness reduction and, within the structural component itself, whether it is better to reduce the bending or the torsional stiffness.

For Figure 4.10, the same nomenclature of Section 4.3 is used:

- ρ is the Pearson Correlation Coefficient.
- $k_{t,f}$ and $k_{b,f}$ are the torsional and bending stiffness of the frame, respectively.
- $k_{t,a}$ and $k_{b,a}$ are the torsional and bending stiffness of the front assembly, respectively.
- $k_{t,s}$ and $k_{b,s}$ are the torsional and bending stiffness of the swingarm, respectively.

The “baseline” configuration in Figure 4.10 is the same used in Section 4.3 and its correlation coefficients are shown by the first set of bars. Starting from this configuration, three subsequent steps of stiffness reduction are carried out, whose sensitivity analyses are shown with the remaining sets of bars:

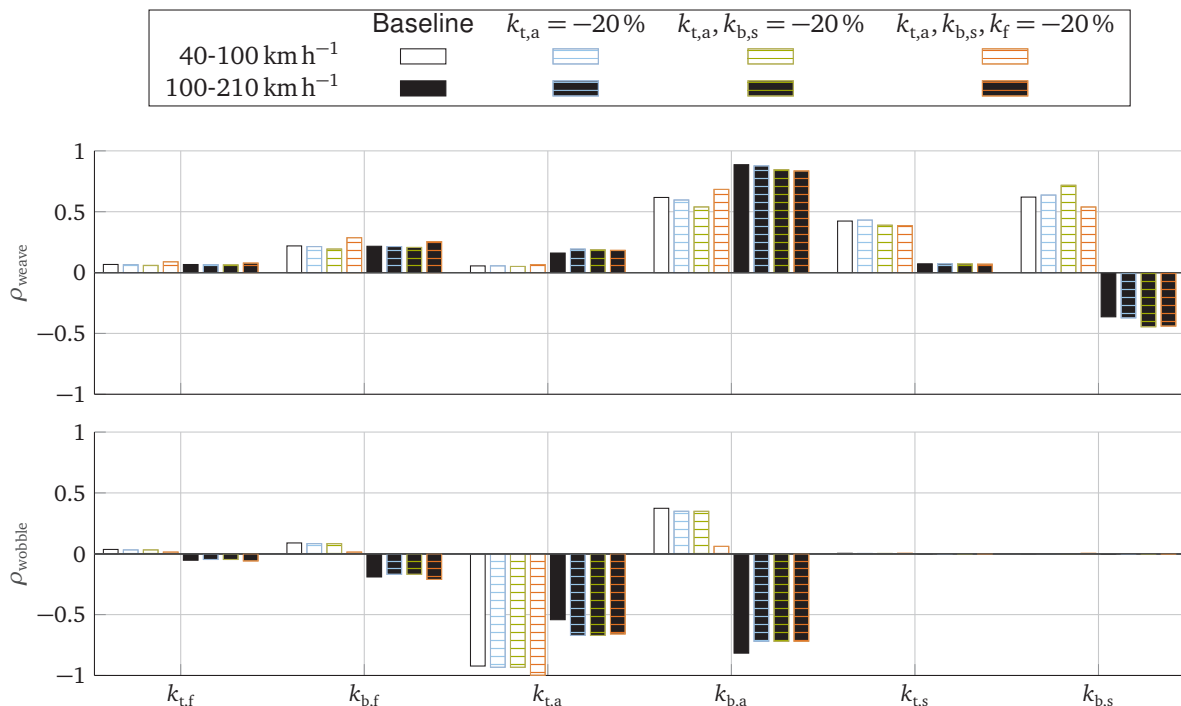


Figure 4.10: Sensitivity analyses of the three subsequent steps of stiffness reduction.

1. The torsional stiffness of the front assembly $k_{t,a}$ is reduced by 20%. $k_{t,a}$ is a good candidate for stiffness reduction because it has negative correlation coefficients at both speed ranges for wobble and only small positive correlation coefficients for weave. This means that a reduction of this stiffness would stabilize the wobble at low and high speeds, while having only a minor destabilizing effect on weave. The correlation coefficients resulting from this new configuration are shown by the bars with light blue lines in Figure 4.10. As expected, compared to the previous configuration, the correlation coefficients of the stiffness $k_{t,a}$ change after its reduction, especially in the high speed range. In particular, the correlation coefficient for wobble becomes more negative, which would suggest to further reduce this stiffness. However, concurrently, the correlation coefficient for weave becomes more positive, which indicates to increase the stiffness. Moreover, the reduction of $k_{t,a}$ has an effect on the correlation coefficients of $k_{b,a}$, in particular that for wobble at high speed, which gets less negative.
2. Starting from the configuration of 1., the bending stiffness of the swingarm $k_{b,s}$ is reduced by 20%. The decision is made considering that this stiffness has negative correlation coefficient on weave at high speeds and no effect on wobble. This indicates that a reduction of this stiffness would stabilize weave in the speed range where it is generally lightly damped (Section 4.1). The positive correlation coefficient for weave at low speeds is less critical because in this speed range weave is highly damped. The correlation coefficients of the new configuration are shown in Figure 4.10 with the green lines. The main change compared to the previous configuration is in the correlation coefficients for weave of $k_{b,s}$. In particular, the coefficients for both speed ranges increase in value.
3. Starting from the configuration of 2., the torsional and bending stiffness of the frame $k_{t,f}, k_{b,f}$ are reduced by 20%. This decision is less obvious than the previous steps. In fact, $k_{t,f}$ and $k_{b,f}$ have positive correlations coefficients for weave and opposite correlation coefficients for wobble in the low and high speed ranges. Therefore, after reducing them, the evolution of the eigenmodes in the whole velocity range must be checked. This is shown in Figure 4.11 and discussed below. The correlation coefficients after reducing the frame stiffnesses are shown in Figure 4.10 with orange lines. The change in the frame stiffnesses influences the correlation coefficients of several other stiffnesses, in particular $k_{t,a}, k_{b,a}$ and $k_{b,s}$. This can be explained considering that the frame is the supporting element for the front assembly and swingarm so that changing its stiffness alters the stiffness ratios between the structural components.

The considerations made above show the versatility of this methodology, which allows at every step of the stiffness reduction to monitor how all sensitivities evolve. This is particularly important to decide which stiffness to reduce in the next step and to make sure that no unexpected effects occur, which could compromise the stability.

After reducing the stiffnesses, it is important to check how the stability of the weave and wobble eigenmodes changes compared to the initial configuration. This is shown in Figure 4.11, where the stability of the motorcycle with the new stiffness configuration is analyzed. The diagrams show how the weave eigenmode remains basically unchanged, while the wobble stability is slightly improved in the whole considered speed range. The increased stability of wobble can be mainly attributed to the reduction in $k_{t,a}$. While the reduction of only $k_{t,a}, k_{t,f}, k_{b,f}$ would be

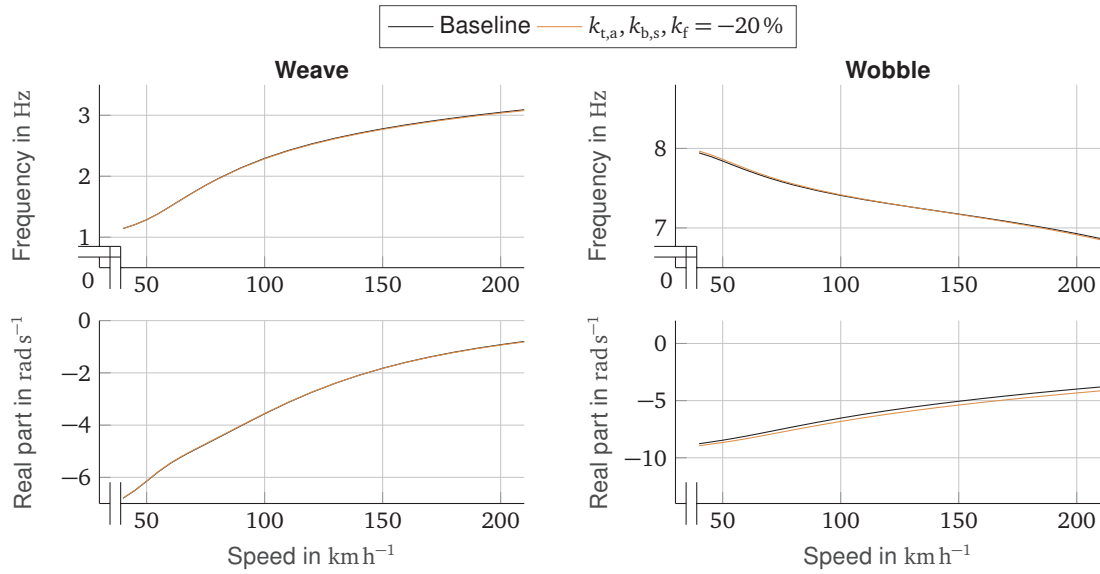


Figure 4.11: Change in the weave and wobble eigenmodes after applying stiffness reduction.

detrimental for the weave stability, a deterioration in weave damping is prevented by reducing at the same time $k_{b,s}$, which, as discussed above, has a positive effect on high-speed weave stability. This result stresses the utility of the proposed methodology: by observing the information provided, it was possible to achieve the competing objectives of reducing the stiffness and thus also the mass of structural components while at the same time improving the motorcycle stability in the whole speed range.

In this first version of the methodology, the designer has still to decide which component to reduce by looking at the correlation coefficients. An algorithm for automatically iterating through all structural components is possible, however, it should be adapted to considered the multiple requirements to the structural design, such as strength, fatigue and durability, which is beyond the scope of the present thesis.

After changing the stiffness distribution of structural components, the effect on several other aspects of motorcycle dynamics should be considered, such as the response when driving over curbs during cornering and the potential changes in the steering feedback. For that, the methodology proposed in Section 4.3 could be extended to consider different performance criteria in addition to the stability of weave and wobble. A maximum of 20% for stiffness reduction has been considered to limit the present study to realistic configurations.

5 A Control System for the Stabilization Weave and Wobble [ITSC 2021]

In Chapter 4, it has been shown how to adapt the chassis stiffnesses to increase the stability of the weave and wobble eigenmodes. As mentioned in the introduction, another possibility to enhance the stability properties of a motorcycle is by using a stabilizing controller. In the present publication, two control strategies for a steering actuator are proposed with the following closed-loop requirements:

- Guaranteeing the stability of the weave and wobble eigenmodes throughout the whole operating range of the motorcycle.
- No interference with the rider's control action.

The steering actuator—which applies a moment directly to the steering system—was chosen as active stabilizing system based on the ideas provided by previous works in the field. The fundamental idea is to extend the functionality of the steering damper, which on the one hand improves the stability of wobble but on the other hand destabilizes weave. For this reason, the damping coefficient of a steering damper must always be chosen considering this trade off [14, 62]. To overcome this limitation, passive [62], semi-active [165] and active [172] systems have been developed. Passive and semi-active systems present some limitations compared to active systems. For active systems, a suitable control strategy must be developed. In [172], the control strategy is based on a linearized model and is therefore limited in its applicability to the whole operating range of the motorcycle. Finally, the controller proposed in [172] is mainly focused on the improvement of the stabilization of wobble.

In this publication, two approaches for the synthesis of the stabilizing controller are proposed: a gain-scheduling proportional controller and an \mathcal{H}_∞ controller. The control signals used are yaw rate $\dot{\psi}$ and steering rate $\dot{\delta}$, because, as shown in Section 4.3, they are representative of weave and wobble, respectively. The controllers are developed using the motorcycle model presented in Section 4.1, whereby some parameters such as the mass distribution have been adapted to represent a motorcycle with weave stability issues at high speed.

The gain-scheduling controller is based on a simple law: $\tau = k_{\dot{\psi}}\dot{\psi} + k_{\dot{\delta}}\dot{\delta}$. $\dot{\psi}$, $\dot{\delta}$ are the yaw rate and steering rate, respectively and $k_{\dot{\psi}}$, $k_{\dot{\delta}}$ are the controller parameters. These parameters are determined with a procedure that leverages the multibody motorcycle model and that provides optimal control parameters for several combinations of speed and roll angle in the relevant operating range.

The \mathcal{H}_∞ controller has the structure shown in Figure 5.1. G is the system model and contains the transfer functions between the modeled disturbances, i.e., lateral force F_y and steering moment τ_d , and the outputs, i.e., yaw rate $\dot{\psi}$ and steering rate $\dot{\delta}$. These transfer functions are obtained with a system identification procedure, where the necessary data are generated with the multibody motorcycle model. Compared to [172], where a linearized motorcycle model is

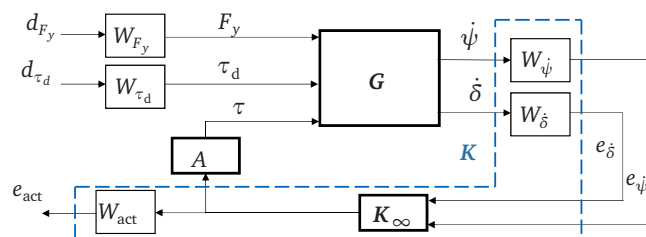


Figure 5.1: Block diagram of the \mathcal{H}_∞ controller [186].

used, the system identification process has the advantage of reducing the number of state space variables yet still correctly modeling the frequency and damping of weave and wobble. This facilitates the controller synthesis and increases the performance of the final controller.

Finally, the weights $W_{\dot{\psi}}$, $W_{\dot{\delta}}$, W_{act} are used to shape the controllers so that the closed-loop requirements mentioned above are satisfied. The novelty compared to the previous works such as [172] is an optimization procedure that automatically calculates the weights, so that the common trial-and-error process is overcome. Moreover, the \mathcal{H}_∞ controller in [172] only takes into account steering torque disturbances and uses only the steering rate as control signal. As mentioned above, in the present publication also lateral force disturbances are modeled and, additionally to the steering rate $\dot{\delta}$, the yaw rate $\dot{\psi}$ is used, which allows better damping of the weave eigenmode.

Results show that both controllers are able to solve the high-speed stability issue of the motorcycle considered. This is demonstrated in Figure 5.2, which shows a time simulation at 180 km h^{-1} , where the motorcycle is excited with either a steering moment impulse or a lateral force impulse to simulate, for example, an excitation coming from the road or from lateral wind. The motorcycle would be unstable, as the oscillation with increasing amplitude shows. Both controllers successfully stabilize the motorcycle, with the \mathcal{H}_∞ controller showing slightly better performance

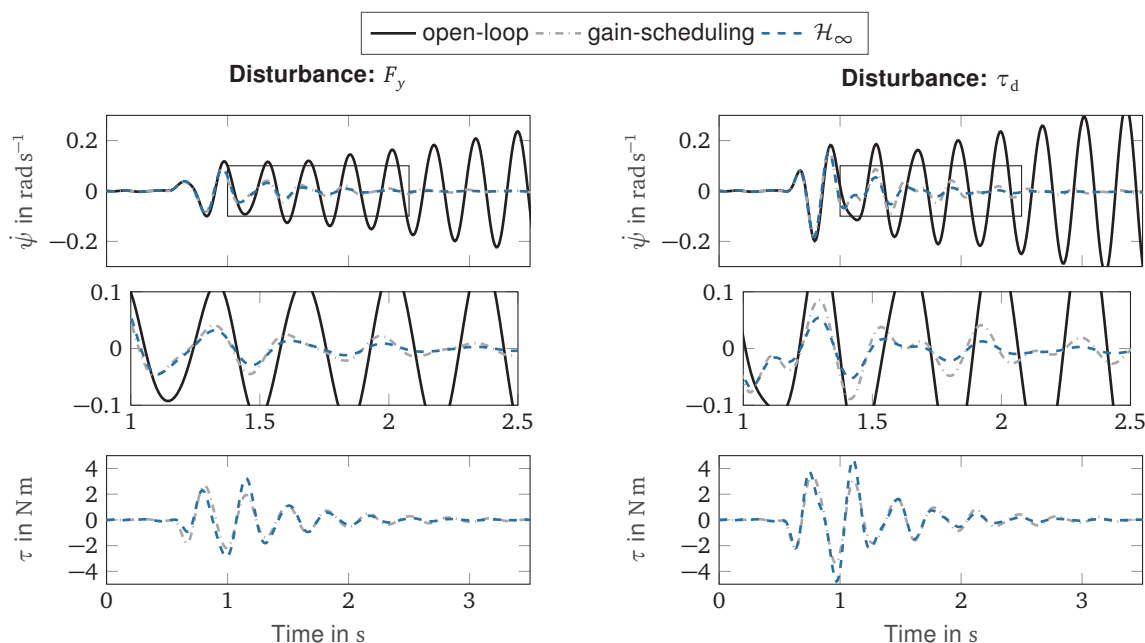


Figure 5.2: Comparison of the controllers' behavior after excitation of the weave mode at 180 km h^{-1} with either steering moment impulse or lateral force impulse. The plots in the middle are a magnification of the respective plots above. The plots below show the steering moment applied by the steering actuator [186].

than the proportional gain-scheduling controller because it damps the oscillation more quickly. Moreover, it has been shown that both controllers do not interfere with normal driving conditions. However, to satisfy this requirement, the proportional gain-scheduling controller requires proper filtering of the yaw rate and steering rate signals with a high pass filter, which filters out the low frequencies deriving from normal maneuvers. In the \mathcal{H}_∞ controller, these filters are not needed because the requirements on the actuation frequencies are specified through the weights.

With the gain-scheduling controller, the values of the controller gains are selected from a look-up table containing the gains for different combinations of speed and roll angle. To make sure that this switching does not cause stability problems of the controller itself, extensive simulation for several working conditions have been carried out, showing that the controller does not causes instabilities in the simulated configurations.

Contributions

F. P. as the first author initiated the idea of the paper and contributed significantly to the concept, modeling, and results. A. W. made significant contributions in the modeling and review phase. A. G. contributed to the review phase. F. D. contributed to the whole concept of the paper. F. D. gave final approval for publication of this version and is in agreement with all aspects of the work. As a guarantor, he accepts responsibility for the overall integrity of this paper.

Copyright notice

©2021 IEEE. Reprinted, with permission, F. Passigato, A. Wischnewski, A. Gordner, F. Diermeyer, "Two Approaches for the Synthesis of a Weave-Wobble-stabilizing Controller in Motorcycles," *2021 IEEE Intelligent Transportation System Conference (ITSC)*, 2021, pp. 3496-3501, doi: 10.1109/ITSC48978.2021.9565019.

Two Approaches for the Synthesis of a Weave-Wobble-stabilizing Controller in Motorcycles

Francesco Passigato¹, Alexander Wischnewski², Achim Gordner³ and Frank Diermeyer¹

Abstract—Weave and wobble are well-known eigenmodes of motorcycles. Depending on the motorcycle parameters, these modes may become unstable, thus impairing safety and maneuverability.

Steering dampers are fitted in modern motorcycles to improve the wobble stability and prevent the kick-back phenomenon. However, they have a detrimental effect on the weave stability, so that the damping coefficient is a trade-off between wobble and weave stability. Even though a similar problem concerning the vertical dynamics of passenger cars is well documented, there are not so many applications which try to optimize this trade-off for motorcycles. In the present work, two control strategies for a steering controller are presented, which help to optimize the trade-off. The first one is a proportional controller, where the controller parameters are optimized for several speeds. The second one is based on \mathcal{H}_∞ controller synthesis coupled with a model identification process. Both controllers are able to increase the stability range of a specific motorcycle model. In particular, the high speed weave stability issue is solved. The \mathcal{H}_∞ controller performs better than the proportional controller and, even though it is synthesized for a single speed, it demonstrates the desired behavior over a wide speed range.

I. INTRODUCTION

Mechanical systems have characteristic eigenmodes. The most important eigenmodes of motorcycles involving the lateral dynamics are capsize, weave and wobble [1]–[3]. Capsize is a non-oscillating mode corresponding to the motorcycle tilting over [3] and is dominated by roll and lateral displacement of the vehicle [4]. Weave and wobble are instead oscillating eigenmodes. Weave involves roll, yaw, steering-head rotation and lateral displacement and has an eigenfrequency in the range 1-4 Hz [3]. Wobble is dominated by the steering head rotation and its eigenfrequency lies in the range 5-10 Hz [2]. For the present work only the weave and wobble are of interest.

The literature includes a number of papers in which the parameter influencing weave and wobble are analyzed [5]–[11]. Modern motorcycles are often fitted with a steering damper whose main function is to improve the wobble mode damping and avoid the kick-back phenomenon. However, it is detrimental for the stability of the weave mode, so that the damping value of this mechanical component is always a trade-off [12], [13].

¹Francesco Passigato (corresponding author) and Frank Diermeyer are with the Chair of Automotive Technology, Faculty of Mechanical Engineering, Technical University of Munich, 85748 Garching (Munich), Germany francesco.passigato@tum.de

²Alexander Wischnewski is with the Chair of Automatic Control, Faculty of Mechanical Engineering, Technical University of Munich, 85748 Garching (Munich), Germany

³Achim Gordner is with the BMW Group, Munich, Germany

This paper presents a solution for solving this problem. Two control strategies for a steering controller are presented, which allow the damping of the weave and wobble modes to be simultaneously increased. The first concept is a proportional controller using yaw and steering rates as control variables. These variables were chosen on the basis of previous literature and because they are representative of weave and wobble, respectively. The main novelty for this controller is coupling with an optimization process which uses a non-linear motorcycle model [10] to determine the optimal controller parameters. The second concept is based on the \mathcal{H}_∞ controller synthesis [14]. In this case, the main contributions are: a data-based system identification process that makes it possible to achieve an efficient model for the controller synthesis. The data are generated with a non-linear motorcycle model [10]. The other contribution is an optimization process to determine the weights for the controller synthesis by specifying concrete closed-loop requirements. This simplifies the controller synthesis because normally the weights are obtained by trial and error.

Both controllers are tested in the time domain with the non-linear motorcycle model presented in [10].

II. STATE OF THE ART

The problem of solving the conflict in determining the damping coefficient for the steering damper has already been tackled in the literature using different approaches. The damping (decay ratio) of the weave and wobble eigenmodes is strongly dependent on the current motorcycle state, in particular on the speed and the roll angle [1], [3], [6], [12]. This poses additional challenges to the control strategy.

De Filippi et al. [15] implement a control strategy for a semi-active steering damper. The basic idea is to transfer the control strategies "Sky Hook" and "Ground Hook", which were originally developed for the vertical dynamic, to the lateral dynamics. In this way, the damping coefficient is adapted to the current state of the motorcycle, thus making it possible to partially solve the trade-off between weave and wobble stability.

Another solution using passive mechanical components is proposed by Evangelou et al. [12]. The classical steering damper is substituted by a so-called mechanical compensator, which includes three components: a spring, a damper and an inerter. With this solution, the authors achieve a second order impedance between the steering rate and the steer torque applied by the compensator. This, combined with a proper optimization of the impedance parameters, improves the damping of the weave mode while maintaining similar

wobble damping when compared to an optimized steering damper.

Based on the idea of using a second order impedance, Evangelou et al. [16] implement a control strategy for a steering actuator using \mathcal{H}_∞ controller synthesis. The controller structure is, however, different from the structure used for the \mathcal{H}_∞ controller in the present paper. Compared to the steering compensator, this solution has two advantages: that the parameters can be easily adjusted and that an extension of the control strategy with an adaptive or parameter-varying version is possible. The results show some improvements with respect to the compensator, in particular thanks to the possibility of including disturbances in the control synthesis.

Massaro et al. [17] develop a rider model for trajectory following. The controller for the lateral dynamics is a PID controller that contains, in addition to the terms for path following, two terms proportional to the yaw and steering rate. The authors state that these terms improve both weave and wobble damping. However, the effect of including these terms in the control strategy is not analyzed.

This paper is organized as follows: Section III presents two methods for the synthesis of a weave-wobble stabilizing controller. Section IV demonstrates advantages and disadvantages of the controllers by use of simulations. The paper concludes in Section V.

III. CONTROLLER SYNTHESIS

This Section presents two control strategies the purpose of which is to improve the weave and wobble damping. They must satisfy two requirements:

- 1) Ensure the stability of the weave and wobble modes.
- 2) No actuation during a normal steering maneuver or steady-state turn.

The following notation is used: F_y is a lateral force disturbance; τ_d the steering torque disturbance; τ is the control torque applied by the steering controller; $\dot{\psi}$ is the yaw rate; $\dot{\delta}$ is the steering rate.

The motorcycle model presented in [10] is used for the controller synthesis. This is a multibody model developed with the software ‘MBSim’ (www.mbsim-env.de). It uses the Pacejka Magic Formula for motorcycle tires [18] and is able to reproduce the chassis stiffnesses with lumped parameters and the passive rider behavior. The model parameters have been artificially adapted to represent a heavily laden motorcycle with a total weight of 390 kg (including motorcycle, rider and luggage) and having high speed weave stability issues: in the simulations, the weave becomes unstable starting from about 160 km h^{-1} . The synthesis process will then tune the controller to compensate for this problem, while also ensuring that the wobble remains well-damped.

A. Proportional controller

The idea of a proportional controller for stabilizing both weave and wobble was presented in [17]. However, the benefits of such a controller were not indicated. The control torque is calculated using the following equation:

$$\tau = k_\psi \dot{\psi} + k_\delta \dot{\delta} \quad (1)$$

where k_ψ, k_δ are the two control parameters that need to be determined. The first term in (1) is proportional to the yaw rate and improves the weave damping. The second term in (1) works analogously to a steering damper and improves the wobble damping [17].

The control parameters can be determined by solving an optimization process. A common procedure is to formulate the optimization process using a model obtained from linearizing a non-linear motorcycle model around a certain working condition [4], [17], [19]. In the present work, the controller defined in (1) is coupled with an optimization that is carried out for different combinations of speeds and roll angles. The optimization is performed using the non-linear motorcycle model. The simulation is carried out with initial speed v_0 and initial roll angle ρ_0 . The weave and wobble are triggered with an impulse lateral force F_y on the motorcycle frame at the steer joint. The force is applied at the beginning of the simulation and then the motorcycle response is simulated for t_{end} seconds. In this simulation, the controller (1) is implemented and the parameters k_ψ, k_δ are defined outside the model. They are changed by an optimization routine in Matlab® which minimizes the cost functional (2). The minimization function used is `fminsearch()`.

$$J_1 = w_\psi \sum_{t=t_1}^{t_{\text{end}}} |\dot{\psi}(t)| + w_\delta \sum_{t=t_1}^{t_{\text{end}}} |\dot{\delta}(t)|. \quad (2)$$

w_ψ, w_δ are scalar weights. The two sums $\sum_{t=t_1}^{t_{\text{end}}}$ represent the mean of the yaw rate and steering rate over the last $t_{\text{end}} - t_1$ seconds of simulation time. The absolute value ensures that the sum is positive and that sample points with opposite sign (as it happens in an oscillation around 0) do not delete with each other. The optimization therefore tunes the parameters k_ψ, k_δ so that the resulting controller compensates the excitation caused by F_y . This corresponds to damping out the weave oscillation, represented by $\dot{\psi}$, and the wobble oscillation, represented by $\dot{\delta}$. During a steady-state turn we have $\dot{\psi} \neq 0$. Therefore, for minimizing the cost functional (2), the motorcycle should be brought to the straight running position, which is not the aim of the controller. To avoid this, a high pass filter is applied to the signal $\dot{\psi}$. This filters out the constant component of $\dot{\psi}$ during a steady-state turn and only leaves the component related to the weave oscillation. The high pass filter is also advantageous for the final application of the controller. In fact, it also ensures that the controller does not interfere with low-frequency control actions of the rider, for example during a steering maneuver.

Let $v_{\text{opt}} \in \mathbb{R}^{n_v}, \rho_{\text{opt}} \in \mathbb{R}^{n_\rho}$ be the vectors of the speed and roll angles for which k_ψ, k_δ are to be optimized. The optimization problem is:

$$\min_{k_\psi, k_\delta} J_1(t_1, t_{\text{end}}, v_{0,i}, \rho_{0,j}). \quad (3)$$

It provides the optimal values of k_ψ, k_δ for every combination $[v_{0,i}, \rho_{0,j}]$ with $i = 1 \dots n_v, j = 1 \dots n_\rho$.

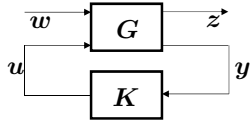


Fig. 1: Block diagram of a general \mathcal{H}_∞ controller.

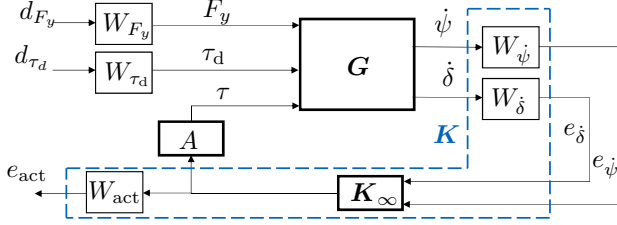


Fig. 2: Block diagram of the current \mathcal{H}_∞ controller.

B. \mathcal{H}_∞ controller

The block diagram of a general \mathcal{H}_∞ controller is shown in Fig. 1, where G is the system to be controlled and K is the controller. The underlying feature of a \mathcal{H}_∞ controller is its capability to minimize the effect of disturbance inputs w on the model outputs z . This is equivalent to solving the following optimization problem [20]:

$$\min_{K(s)} \|G_w(s)\|_\infty, \quad (4)$$

i.e. the resulting controller minimizes the maximum singular value of the transfer function between the disturbances w and the outputs z . This ensures that the system response remains bounded, i.e. it is stable with a certain stability margin (robust stability) [14].

For the synthesis of an \mathcal{H}_∞ controller, a linear model G of the motorcycle is needed in the form of a transfer function or of a state space formulation [14], [20]. It is possible to export the state space model directly from the multibody environment. However, for the motorcycle model used in this paper, this would lead to a state space model with 36 state variables, which makes the controller synthesis difficult. Another possibility is to use a model identification technique, as described in [21]. The System Identification Toolbox from Matlab® allows this process to be carried out easily. The model identification is done in the following steps:

- Define the vectors w, z, y, u needed for the controller synthesis.
- Generate an input-output sequence using the non-linear motorcycle model. A harmonic excitation is generated for each input at different frequencies in the desired frequency range, with the other inputs equal to 0.
- The System Identification Toolbox uses the input-output sequence to produce the model G .

As stated in the introduction to Section III, the motorcycle model under consideration is critical at high speed because of the instability of the weave mode. The model identification is therefore carried out at 150 km h^{-1} , when the weave is near to the stability bound. Harmonic excitation is used in

the range 0.1 - 5 Hz ($0.6 - 31.4 \text{ rad s}^{-1}$), where both weave and wobble are present.

The structure of the controller used in this paper is shown in Fig. 2. The disturbances considered are the lateral force F_y applied on the motorcycle frame and the steering torque. Two inputs for the steering torque are present. This is necessary because it is considered as both a disturbance τ_d and a control action τ . F_y models a side wind disturbance while τ_d represents a general disturbance acting on the steering assembly (for example road undulations which cause steer moments). The model contains six transfer functions: $\frac{\psi(s)}{F_y(s)}, \frac{\dot{\delta}(s)}{F_y(s)}, \frac{\psi(s)}{\tau_d(s)}, \frac{\dot{\delta}(s)}{\tau_d(s)}, \frac{\psi(s)}{\tau(s)}, \frac{\dot{\delta}(s)}{\tau(s)}$, the last four are pairwise equivalent. Fig. 3 shows the comparison of the transfer function $\frac{\psi(s)}{\tau_d(s)}$ between the model obtained using the System Identification Toolbox ("si") and the model directly exported from the multibody environment ("exp"). There is good accordance both for the magnitude and phase in the frequency range of interest, i.e. where weave and wobble are present. This is also valid for the other transfer functions.

The identified model G has 5 state space variables. Therefore, the system identification process is used as a sort of model order reduction, where the model order is reduced from 36 (linearized state space model exported from the multibody model) to 5, which still represents the important information for the controller synthesis, as shown in Fig. 3. This significantly reduces the computing time for the \mathcal{H}_∞ controller synthesis. It has been also verified that the controller synthesized using the identified model has much better performance than the one synthesized with the linearized model.

The chosen model outputs are the yaw rate $\dot{\psi}$ and the steering rate $\dot{\delta}$ as they are representative of the weave and wobble modes, respectively.

A is the model of a possible steering actuator controlled by the controller K using signal u . It represents the delay of the actuator and is defined as a first order low pass filter with time constant equal to 0.03 s; $A = \frac{1}{(0.03 \cdot 2\pi)s + 1}$.

The \mathcal{H}_∞ controller can be synthesized by specifying weights W that ensure the desired closed loop behavior [14], [16], [20]. In the present work, the weights have the following meanings:

- W_{F_y}, W_{τ_d} are constant normalization factors because the inputs have different magnitudes.
- W_{act} ensures that the controller does not act at low frequencies, so that the controller does not interfere with low-frequency control actions of the rider.
- $W_{\dot{\psi}}, W_{\dot{\delta}}$ ensure the stability of the weave and wobble modes.

The controller will minimize the effect of the disturbances d_{F_y}, d_{τ_d} on the outputs $e_{\dot{\psi}}, e_{\dot{\delta}}$ by sending a signal u to the actuator A which, in the proposed example, applies a steering torque τ to the model G . After solving the optimization problem in (4), a controller K is obtained that includes the weights W in the controller K_∞ (see Figure 2), i.e. the final controller includes and satisfies the closed-loop requirements specified with the weights. The

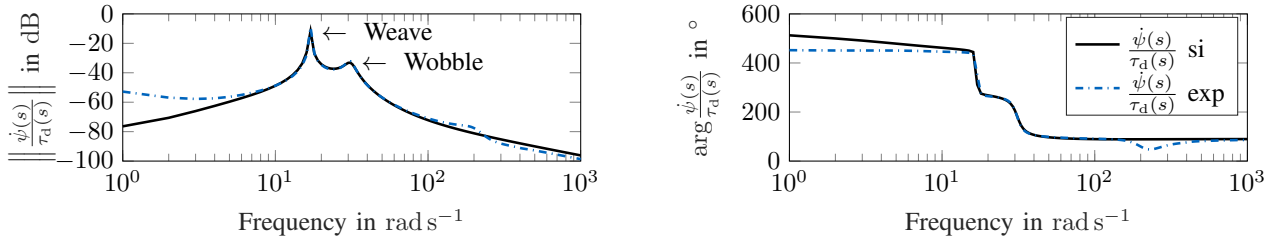


Fig. 3: Comparison between the model obtained with system identification (si) and the exported state space model (exp).

synthesis procedure in this paper uses the Matlab® function `hinfsyn()`. An example with structure similar to Fig. 2 is present in the documentation.

The specification of the transfer functions $W_{\dot{\psi}}$, $W_{\dot{\delta}}$, W_{act} is not a trivial task and is often carried out by trial and error [16]. In the present paper, this task is solved with an optimization that again uses the Matlab® function `fminsearch()`. The weights $W_{\dot{\psi}}$, $W_{\dot{\delta}}$, W_{act} have a general second order transfer function:

$$W = \frac{a_2 s^2 + a_1 s + a_0}{b_2 s^2 + b_1 s + b_0}. \quad (5)$$

The parameters for each weight are provided by the optimization process, which therefore involves $6 \cdot 3 = 18$ parameters. The cost function is:

$$J_2 = \left| \min(0, (\|\mathbf{G}(\omega_{\text{we}})\| - \|\mathbf{G}_{\text{cl}}(\omega_{\text{we}})\|) - \Delta_{\text{we}}) \right| + \left| \min(0, (\|\mathbf{G}(\omega_{\text{wo}})\| - \|\mathbf{G}_{\text{cl}}(\omega_{\text{wo}})\|) - \Delta_{\text{wo}}) \right| + \left| \|\mathbf{G}(\omega < \omega_{\text{low}})\| - \|\mathbf{G}_{\text{cl}}(\omega < \omega_{\text{low}})\| \right| + \left| \|\mathbf{G}(\omega > \omega_{\text{high}})\| - \|\mathbf{G}_{\text{cl}}(\omega > \omega_{\text{high}})\| \right|, \quad (6)$$

Where \mathbf{G}_{cl} is the closed-loop transfer function where the weights are included, $\omega_{\text{we}}, \omega_{\text{wo}}$ are the weave and wobble eigenfrequencies, $\Delta_{\text{we}}, \Delta_{\text{wo}}$ are scalars, ω_{low} is the highest frequency below the critical frequency range and ω_{high} is the lowest frequency above the critical frequency range. (6) is created by considering the following closed-loop requirements: The peaks of the transfer functions of \mathbf{G} (see Fig. 3), corresponding to the weave and wobble eigenmodes, should be attenuated at least by a certain amount. The transfer functions of the closed loop system should not deviate from the original transfer functions of \mathbf{G} outside the critical frequency range. These closed-loop requirements could not be directly implemented in the \mathcal{H}_{∞} controller synthesis, but rather by trial and error tuning of the weights.

IV. RESULTS

We start this section with a frequency-domain-analysis of the performances of the \mathcal{H}_{∞} controller. The same analysis is not possible for the proportional controller because it works with the non-linear model so that the related transfer function is not directly available.

Fig. 4 shows a comparison between the transfer function $\frac{\dot{\psi}(s)}{\tau_d(s)}$ of the open-loop and closed-loop models. The following considerations are also valid for the other transfer functions. The closed-loop requirements formulated in Subsection

III-B are met: the peak relative to the weave eigenmode is reduced by about 30 dB, while the wobble is only marginally mitigated because it is not critical at the speed where model identification is carried out. Moreover, the controller does not change the open-loop transfer functions outside the critical frequency range.

Fig. 5 shows the magnitude of the transfer functions of the weights $W_{\dot{\psi}}, W_{\dot{\delta}}, W_{\text{act}}$ and of the transfer functions of the controller. The weights derive from the optimization problem described in Subsection III-B. The controller \mathbf{K} is composed of two transfer functions: $\frac{u(s)}{\dot{\psi}(s)}, \frac{u(s)}{\dot{\delta}(s)}$. The considerations presented above can also be drawn from Fig. 5: the magnitude of the controller's transfer functions is low outside of the weave-wobble frequency range and, for this reason, it does not interfere with "normal" riding conditions. The transfer function $\frac{u(s)}{\dot{\delta}(s)}$ is similar to that obtained by Evangelou et al. [16], which also had the objective of increasing weave and wobble damping using, however, a different controller structure.

The time domain offers similar interpretations. In this case, a comparison of the performances of the two controllers is possible. Both controllers are applied to the non-linear motorcycle model presented in [10] and briefly described in Section III. Two simulations are carried out.

The first one has the aim of demonstrating that the controllers do not intervene during a "normal" steering maneuver. A cosine steer moment τ_d with period 1.5 s and amplitude 20 N m is applied. The speed used for this simulation is 120 km h⁻¹. Fig. 6 shows the behavior of the open-loop system, the proportional controller and the \mathcal{H}_{∞} controller. The roll angle ρ is observed because it is the most representative state variable to judge whether the controller influences a steering maneuver. The two controllers perform similarly. However, the \mathcal{H}_{∞} controller performs better than the proportional controller: the maximum deviation from the open-loop system is about 0.4° for the proportional controller and 0.2° for the \mathcal{H}_{∞} controller. Moreover, the \mathcal{H}_{∞} controller does not require the high pass filter applied to $\dot{\psi}$ (as for the proportional controller), because the appropriate filters are already specified in the controller synthesis with to the weighting factors $W_{\dot{\psi}}, W_{\dot{\delta}}, W_{\text{act}}$.

The second simulation is to compare the capability of the two controllers in damping an unstable weave oscillation. We recall that for the motorcycle considered in the present work, the weave mode is most critical. The simulation is

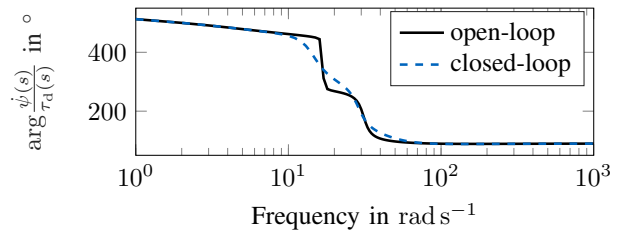
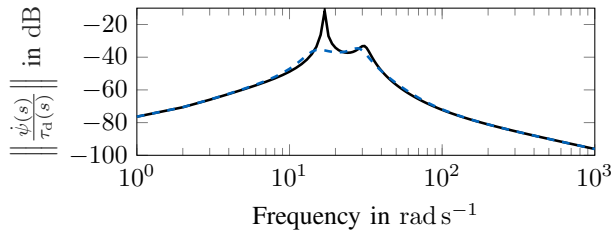


Fig. 4: Transfer functions of the open-loop and closed-loop systems.

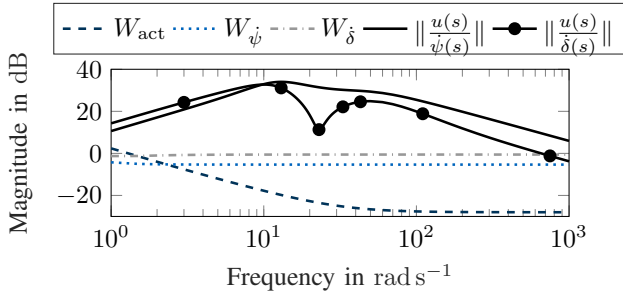


Fig. 5: Transfer functions of \mathcal{H}_∞ controller and weights.

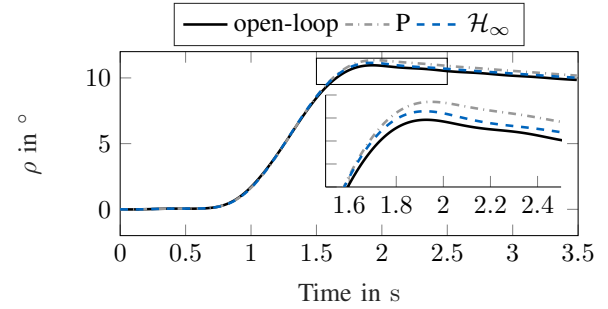


Fig. 6: Comparison of the controllers' behavior during a low frequency steering maneuver at 120 km h⁻¹.

carried out at 180 km h⁻¹ and two disturbances are used: F_y impulse of 0.2 s with amplitude 120 N; τ_d impulse of 0.2 s with amplitude 20 N m. The upper figures in Fig. 7 show the yaw rate, which is representative of the weave eigenmode, for the two impulse disturbances. The original model would be unstable. Both the controllers are able to stabilize the motorcycle. However, the \mathcal{H}_∞ controller performs slightly better because it damps out the oscillation more quickly (see the middle plots in Fig. 7). The difference between the controllers is bigger when the disturbance τ_d is used. The reason is that only F_y is used for the synthesis of the proportional controller, while both disturbances are considered in the synthesis of the \mathcal{H}_∞ controller. The moment applied by the steering actuator (lower figures in Fig. 7) to compensate for the weave instability assumes similar values (max 4 N m). At 180 km h⁻¹, both controllers are able to deal with τ_d impulse disturbances up to 100 N m and F_y impulse disturbances up to 1600 N. However, this would require actuator torques rapidly varying from 50 N m to -50 N m. The feasibility of such a torque input should be verified on a real actuator. Also in this limit conditions, the \mathcal{H}_∞ controller stabilizes the motorcycle more quickly.

V. CONCLUSIONS

Two control systems have been presented with which the stability range of a specific motorcycle model can be increased. The first one is a proportional controller in which the control parameters are optimized for different speeds and roll angles; the optimization is carried out using a non-linear motorcycle model. The second one is an \mathcal{H}_∞ controller. The novelty for this second controller is that the controller synthesis is carried out using a model obtained with a data-based model identification, where the data are produced with

the non-linear motorcycle model. In this way, the model for the controller synthesis includes only the relevant dynamics for the control strategy, i.e. it correctly reproduces the weave and wobble modes.

The controllers' performances have been tested on the non-linear motorcycle model: the controllers behave similarly. However, the \mathcal{H}_∞ controller performs better than the proportional controller: it damps the weave oscillation more quickly and it has less influence on the low frequency steering maneuver in the speed range considered (120-180 km h⁻¹).

The proportional controller does not require a linearization of the original model. However, its parameters are very sensitive to the boundary conditions used for the simulations in the optimization algorithm, such as the intensity of F_y and the simulation time t_{end} . For this reason, the resulting optimal parameters are always a local optimum. By contrast, the synthesis of the \mathcal{H}_∞ controller offers a more robust environment and can be extended to include other disturbances.

The \mathcal{H}_∞ controller was developed to compensate for high speed weave. For this reason the model used for the controller synthesis was obtained by model identification at 150 km h⁻¹. The results showed that the controller behaves as desired over a wide speed range (120-180 km h⁻¹). At low speed (below 80 km h⁻¹), however, this model is no longer valid because of the nonlinearities in motorcycle dynamics. For this reason, the controller does not behave correctly in this lower speed range. One possibility to avoid this problem is to use two (or three) controllers synthesized using models identified at different speeds. The number of speeds to be considered will probably be smaller than that needed in the optimization of the proportional controller parameters

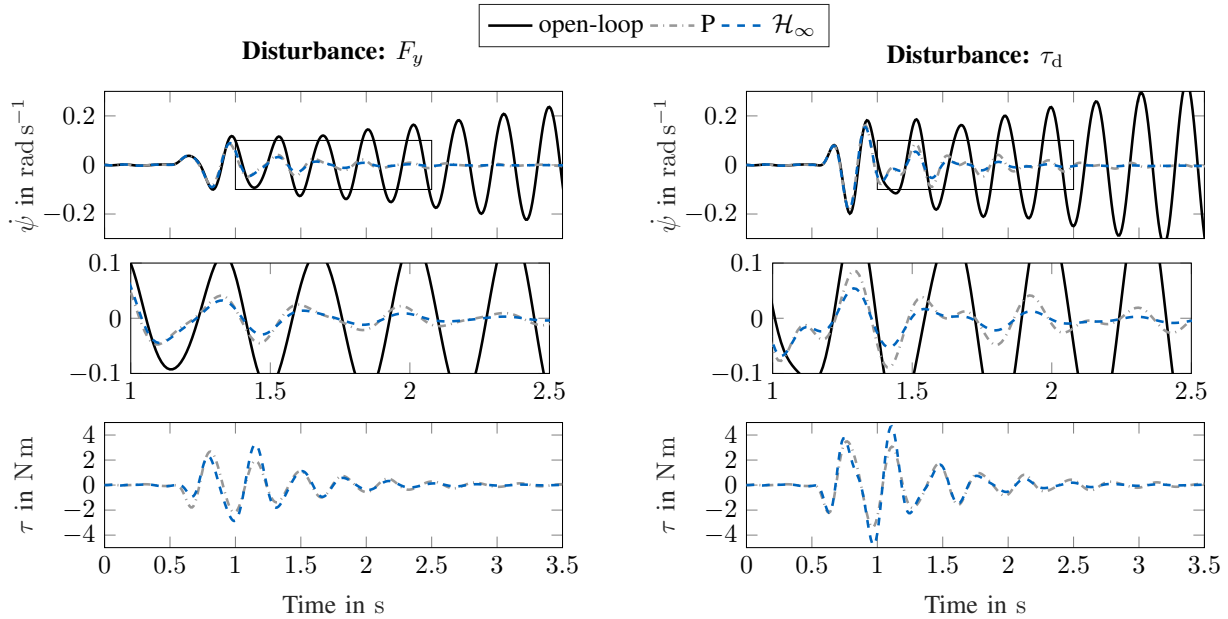


Fig. 7: Comparison of the controllers' behavior after excitation of the weave mode at 180 km h^{-1} with $F_y = 120 \text{ N}$ (left) and $\tau_d = 20 \text{ N m}$ (right) as impulse disturbances (impulse period: 0.2 s). The plots in the middle are a magnification of the respective plots above. The plots below show the steer moment applied by the steering actuator.

because the \mathcal{H}_∞ controller demonstrated superior robustness.

CONTRIBUTIONS

F. P. initiated the idea of the paper and contributed significantly to the concept, modeling, and results. A. W. made significant contributions in the modeling and review phase. A. G. contributed to the review phase. F. D. contributed to the whole concept of the paper. F. D. gave final approval for publication of this version and is in agreement with all aspects of the work. As a guarantor, he accepts responsibility for the overall integrity of this paper.

ACKNOWLEDGMENT

We would like to thank Dr. Dirk Wisselmann and Prof. Martin Förg (University of Landshut) for help in the modeling phase. Thanks also to Thomas Herrmann (Chair of Automotive Technology, Technical University of Munich) for valuable suggestions during the writing phase.

REFERENCES

- [1] R. S. Sharp, "The stability and control of motorcycles," *Journal Mechanical Engineering Science*, vol. 13, no. 5, pp. 316–329, 1971.
- [2] —, "Stability, control and steering responses of motorcycles," *Vehicle System Dynamics*, vol. 35, no. 4-5, pp. 291–318, 2001.
- [3] V. Cossalter, *Motorcycle dynamics*, 2nd ed. S.I.: [Lulu press], 2006.
- [4] M. Massaro, "A nonlinear virtual rider for motorcycles," *Vehicle System Dynamics*, vol. 49, no. 9, pp. 1477–1496, 2011.
- [5] V. Cossalter, R. Lot, and M. Massaro, "The influence of frame compliance and rider mobility on the scooter stability," *Vehicle System Dynamics*, vol. 45, no. 4, pp. 313–326, 2007.
- [6] P. T. J. Splerings, "The effects of lateral front fork flexibility on the vibrational modes of straight-running single-track vehicles," *Vehicle System Dynamics*, vol. 10, no. 1, pp. 21–35, 1981.
- [7] V. Cossalter, A. Doria, R. Lot, and M. Massaro, "The effect of rider's passive steering impedance on motorcycle stability: identification and analysis," *Meccanica*, vol. 46, no. 2, pp. 279–292, 2011.
- [8] C. Koenen and H. B. Pacejka, "The influence of frame elasticity and simple rider body dynamics on free vibrations of motorcycles in curves," *Vehicle System Dynamics*, vol. 10, no. 2-3, pp. 70–73, 1981.
- [9] V. Cossalter, A. Doria, and L. Mitolo, "Inertial and modal properties of racing motorcycles," *SAE Technical Papers*, 2002.
- [10] F. Passigato, A. Eisele, D. Wisselmann, A. Gordner, and F. Diermeyer, "Analysis of the phenomena causing weave and wobble in two-wheelers," *Applied Sciences*, vol. 10, no. 19, p. 6826, 2020.
- [11] A. Doria and S. Roa, "On the influence of tyre and structural properties on the stability of bicycles," *Vehicle System Dynamics*, vol. 56, no. 6, pp. 947–966, 2018.
- [12] S. A. Evangelou, D. J. N. Limebeer, R. S. Sharp, and M. C. Smith, "Mechanical steering compensators for high-performance motorcycles," *Journal of Applied Mechanics, Transactions ASME*, vol. 74, no. 2, pp. 332–346, 2007.
- [13] D. J. N. Limebeer, R. S. Sharp, and S. A. Evangelou, "Motorcycle steering oscillations due to road profiling," *ASME*, vol. 69, pp. 724–739, 2002.
- [14] D. McFarlane and K. Glover, "A loop shaping design procedure using \mathcal{H}_∞ synthesis," *IEEE Transactions on Automatic Control*, vol. 37, no. 6, pp. 759–769, 1992.
- [15] P. de Filippi, M. Tanelli, M. Corno, S. M. Savaresi, and L. Fabbri, "Semi-active steering damper control in two-wheeled vehicles," *IEEE Transactions on Control Systems Technology*, vol. 19, no. 5, pp. 1003–1020, 2011.
- [16] S. A. Evangelou, D. J. N. Limebeer, R. S. Sharp, and M. C. Smith, "An \mathcal{H}_∞ loop-shaping approach to steering control for high-performance motorcycle," *Lecture Notes in Control and Information Sciences*, vol. 329, pp. 257–275, 2006.
- [17] M. Massaro and R. Lot, "Application of laplace transform techniques to non-linear control optimization," *Proc of the multibody dynamics 2007. Milano, Italy, June 25–28, 2007*, 2007.
- [18] H. B. Pacejka and I. Besselink, *Tire and vehicle dynamics*, 3rd ed. Oxford: Butterworth - Heinemann, 2012.
- [19] R. S. Sharp, "Optimal linear time-invariant preview steering control for motorcycles," *Vehicle System Dynamics*, vol. 44, no. sup1, pp. 329–340, 2006.
- [20] J. Lunze, *Regelungstechnik 2: Mehrgrößensysteme, Digitale Regelung*, 10th ed. Springer-Verlag, 2020.
- [21] Y. Kamata and H. Nishimura, "System identification and attitude control of motorcycle by computer-aided dynamics analysis," *SAE of Japan*, vol. 24, pp. 411–416, 2003.

6 Conclusions

In this chapter, the main results are summarized and ideas for further developments of the presented methods are formulated.

6.1 Summary

In this thesis, the problem of increasing the stability of the weave and wobble eigenmodes in motorcycles has been considered. The proposed solution leverages two main aspects: the search for an optimal distribution of structural stiffness that enhances the stability properties of the motorcycle and the development of a stabilizing controller for a steering actuator. The first approach is suitable for application in the design phase of motorcycles. The second solution allows the enhancement of the stability during operation, i.e., in real driving conditions.

In Section 4.2, a flexible multibody model has been proposed, which allows the reproduction with high accuracy of the effect of structural flexibilities on the stability of the weave and wobble eigenmodes. Results showed that the front assembly has the highest impact, whereby a stiff front assembly enhances the high-speed stability of weave and the low-speed stability of wobble, while it deteriorates the high-speed stability of wobble. Moreover, based on the motorcycle considered in the present thesis, it can be argued that the frames of modern motorcycles tend to be extremely stiff. This trend is certainly motivated by the attempt to increase the high-speed stability of weave; however, modern frames sometimes reach stiffness values that are not necessary under the perspective of weave and wobble stability. In fact, as discussed in Section 2.2.2, a too stiff frame could even cause high speed wobble instabilities (kick-back). Moreover, a reduction of the stiffness implies less material usage, which leads to mass reduction and savings in production costs. This highlights that even modern motorcycles have potential for improving the design of their structural components.

Based on this consideration, in Section 4.3 a methodology has been proposed to optimize the distribution of structural stiffness with the aim of improving the stability of the weave and wobble eigenmodes. The method provides information about the sensitivity on the stability of weave and wobble of the bending and torsional stiffness of the main structural components of a motorcycle, i.e., frame, front assembly and swingarm. This information can be used by the designer to improve the design of these structural components. The method is based on a lumped stiffness motorcycle model, which allows to study each stiffness separately. Since the accuracy of lumped stiffness models strongly depends on their parameterization, a procedure has been proposed to build a lumped stiffness motorcycle model, where the influence of flexibilities on weave and wobble is modeled with an accuracy similar to that of a flexible multibody model.

In Section 4.4, an example application of the methodology is proposed: using the information presented by the methodology, the stiffness of the structural components has been reduced by

20% in three subsequent steps. Results show that, for the motorcycle considered, this stiffness reduction leaves weave unaltered while it improves the stability of wobble. Moreover, the stiffness reduction is associated with a mass reduction, which, as mentioned above, enhances the longitudinal and lateral dynamics.

In Chapter 5, two controllers for a steering actuator have been proposed, which have the aim of increasing the stability of the weave and wobble eigenmodes. The gain-scheduling proportional controller can be easily tuned to produce an appropriate control action in the whole operating range of the motorcycles. The H_∞ controller presents higher robustness and gives the possibility to account for model uncertainties. Both controllers are able to successfully stabilize an unstable motorcycle. Moreover, it has been proven that they do not interfere during normal maneuvering, such as cornering.

For the design of new motorcycles, the proposed methodology can be combined to design lightweight motorcycles with relatively low stiffness—whereby the reduced mass would bring advantages on fuel efficiency and low speed maneuverability. A motorcycle with low stiffness would likely result in stability issues, especially for the high-speed weave. However, these could be solved with the proposed control system, thus obtaining a lightweight motorcycle with the desired stability properties. Of course, a chassis with low stiffness could present problems on other aspects of the riding experience, which have to be evaluated separately. Moreover, since without the stabilizing action of the controller the motorcycle could be unstable, a proper certification for the control-actuation system would be necessary for such a system to be industrialized.

6.2 Outlook

Study of the Effect of Structural Flexibility on Weave and Wobble

The studies proposed in Section 4.3 and Section 4.4 are carried out with a single motorcycle model, which is based on the stiffness data of a real motorcycle. However, it could happen that, using other stiffness data as basis, the results of the study change. An example is shown in Figure 6.1, where the initial configuration of the stiffnesses used in Section 4.3 is varied by reducing the bending stiffness of the front assembly by 50%. With this variation, the intent is to reach a value for the bending stiffness which is similar to that of conventional telescopic forks. In fact, the motorcycle used in Section 4.3 has a Telelever front suspension, which has a significantly higher bending stiffness than conventional telescopic forks. Compared to the standard configuration, which produces the sensitivity analysis in Figure 4.9, the sensitivity of the bending stiffness of the front assembly increases significantly, while the sensitivity of its torsional stiffness is reduced. The sensitivity of the other stiffnesses remains almost unchanged. This experiment indicates that, when carrying out a design optimization, the initial configuration to which the optimization has to be applied must be considered carefully and a generalization of the conclusions is not always possible. However, the proposed methodology gives the possibility to easily adapt the initial condition, thus facilitating the study of stiffness configurations relative to different motorcycles.

In Section 4.2, two of the most common methods for MOR have been used, i.e., Craig-Bampton and modal truncation. Further research could involve testing different methods for MOR and the development of methods for automatic MOR of second-order systems. For that, already existing methods could be adopted [117, 128, 143, 145]. Alternatively, the method presented by

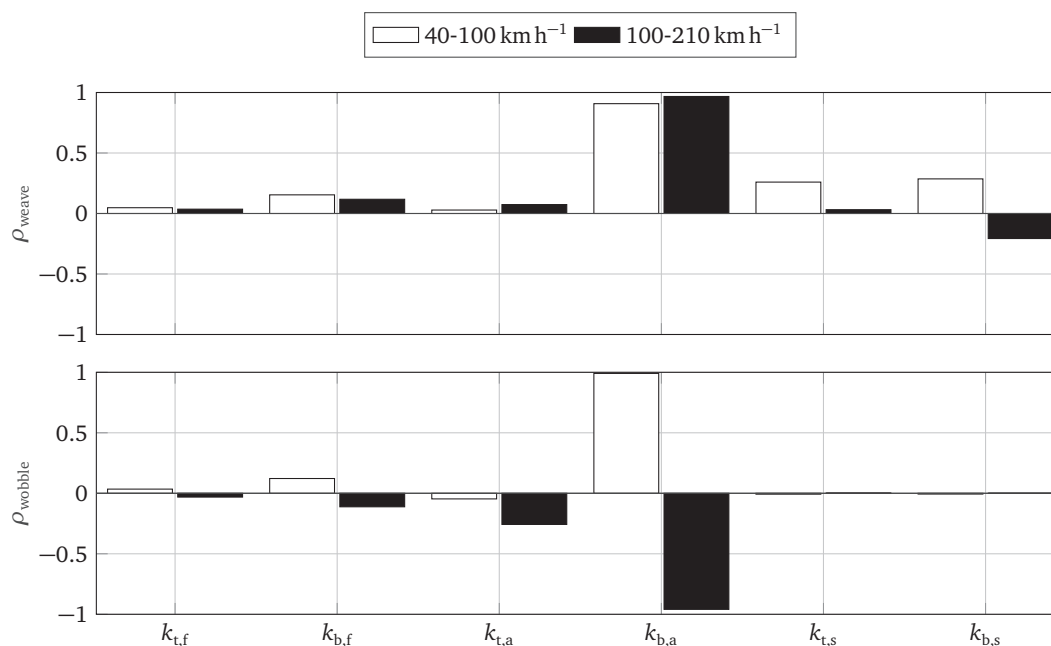


Figure 6.1: Sensitivity of the structural stiffnesses on the stability of weave and wobble. For the calculation, the same procedure proposed in Section 4.3 is adopted. However, the initial configuration of the stiffnesses is varied by reducing the bending stiffness of the front assembly $k_{b,a}$ by 50%.

Druskin et al. [146, 147] for first order system could be extended to second order systems. The application of alternative methods for MOR could increase the accuracy of the flexible multibody motorcycle model or, concurrently, allow to reduce the size of the flexible multibody model while providing the same accuracy.

An interesting evolution of the motorcycle model could be the adoption of the rigid ring model for the calculation of the tire forces [21, p. 587]. This approach is generally adapted for simulating high frequency phenomena, i.e., with frequency well above that of the weave and wobble eigenmodes. However, a study comparing the rigid ring model and the classical Pacejka Magic Formula in the computation of weave and wobble could be an objective of future work.

Finally, in this thesis, the studies of the effect of structural flexibilities on weave and wobble have been carried out in straight running. As explained in Section 2.2.1, in cornering these eigenmodes change because of the coupling between in-plane and out-of-plane dynamics. Therefore, it would be interesting to understand if the conclusions about the influence of structural flexibilities on weave and wobble in straight running can be generalized to steady-state cornering. Preliminary studies in a student thesis [187] show that this influence remains qualitatively the same, thus supporting that the considerations proposed in the present thesis can be extended to steady-state cornering.

Controller for a Steering Actuator

In this thesis, the stabilizing controller has not been tested on a real motorcycle. Therefore, it would be interesting in further research to understand how the sensor noise would impact the controller accuracy. Under this perspective, the \mathcal{H}_∞ controller has the advantage that it can be designed to be tolerant to sensor noise.

Possible extensions of the controller structures proposed in Chapter 5 could involve increasing their accuracy.

A first aspect to be considered is the actuator's dynamic. In Chapter 5, it is modeled as a first order delay. However, real actuators can also present a dead time, meaning that the actuator needs a certain amount of time to even start responding to the control signal. The introduction of this effect in the controller design could improve its performance.

Another challenge consists in developing a controller that is able to deal with different longitudinal speeds and roll angles of the motorcycle, which influence the motorcycle response to external input. This challenge is tackled by the proposed gain-scheduling controller with a look-up table that contains a combination of controller parameters for several working point in the whole operating range of the motorcycle. The \mathcal{H}_∞ controller partially solves this challenge thanks to the robustness of its structure, which can be designed to be tolerant to model uncertainties. However, a possibility to increase the controller accuracy would be to synthesize the controller leveraging the theory of Linear Parameter Varying (LPV) control [188], whereby the nonlinear motorcycle model would be approximated by a linear model with varying parameters, where the varied parameters are speed and roll angle. LPV control offers the advantage that the linear control theory can be applied, but the resulting controller would still be able to handle parameter variations.

Another possibility to increase the controller accuracy would be adapting the controller parameters to changes of the motorcycle properties. The controllers proposed in Chapter 5 rely on fixed parameters identified with a specific motorcycle model. Imagining a situation where the controllers are applied to a real motorcycle, it could happen that, during driving, some motorcycle parameters deviate from those contained in the motorcycle model. This could happen, for example, if the tire coefficients change because of temperature changes or if the motorcycle is fitted with bags. An adaptive controller would be able to compensate for these effects and therefore further increase the controller performance. This could be achieved, for example, using a motorcycle model running on the internal hardware of the motorcycle where some of the parameters are adapted on-line. This model could then be used to synthesize a new controller. For ensuring fast adaptation, an efficient model is needed. In this case, the lumped stiffness motorcycle model proposed in Section 4.3 could be a candidate because it presents a speedup of about 3200x compared to the flexible multibody model.

Finally, it is possible to develop a controller that employs the steering actuator for realizing other dynamic functions, such as supporting the rider to reduce the steering effort or a safety function able to recognize a slip situation and to act on the steering to prevent a fall.

List of Figures

Figure 2.1:	Root locus plot of the eigenvalues of a motorcycle.....	8
Figure 2.2:	Sprung and unsprung masses	8
Figure 2.3:	Representation of the weave and wobble oscillations	9
Figure 2.4:	Example of a cradle frame from the BMW R80/R100	11
Figure 2.5:	Frame of the BMW K100.....	12
Figure 2.6:	Exemplary frames from modern motorcycles	12
Figure 2.7:	Types of telescopic forks	13
Figure 2.8:	BMW Telelever system	14
Figure 2.9:	BMW Duolever system	15
Figure 2.10:	BMW Paralever system.....	15
Figure 2.11:	Lumped stiffness approach for modeling the bending of a beam	20
Figure 2.12:	Representation of the motion of a flexible body with the FFRF.....	22
Figure 2.13:	Steps for including a flexible body in an MBS environment.....	23
Figure 2.14:	Block diagram of a typical \mathcal{H}_∞ controller structure.....	31
Figure 4.1:	Weave eigenfrequency and real part as a function of speed	40
Figure 4.2:	Compass plots of the weave eigenvector at different speeds	40
Figure 4.3:	Wobble eigenfrequency and real part as a function of speed	41
Figure 4.4:	Lumped stiffness model of the front fork (front view)	41
Figure 4.5:	Effect of the flexibility of the structural components on weave and wobble	70
Figure 4.6:	Comparison flexible multibody model vs lumped stiffness model.....	71
Figure 4.7:	Pipeline for building a high accuracy lumped stiffness motorcycle model..	83
Figure 4.8:	Error of lumped stiffness models with respect to the flexible multibody model	84
Figure 4.9:	Correlation coefficients of weave and wobble for the structural stiffnesses	86
Figure 4.10:	Sensitivity analyses of the three subsequent steps of stiffness reduction ..	110
Figure 4.11:	Weave and wobble eigenmodes after applying stiffness reduction.....	112
Figure 5.1:	Block diagram of the \mathcal{H}_∞ controller.....	114
Figure 5.2:	Controllers' behavior after excitation of the weave mode.....	114
Figure 6.1:	Sensitivity of structural stiffnesses on the stability of weave and wobble ...	125

List of Tables

Table 2.1:	Most relevant eigenmodes and external-induced oscillations of motorcycles. f is the abbreviation for eigenfrequency and d for damping.	10
Table 3.1:	Pros and cons of lumped stiffness and flexible multibody approach considering the requirements for the development of a methodology for stiffness-optimization.	37

Bibliography

- [1] M. Hamer, „Brimstone and bicycles,“ *New Scientist*, vol. 2428, pp. 48–49, 2005.
- [2] P. Le Roux and P. N. Blezard, „From the Motorised Bike to the Two-Wheeled Car,“ *VDI-Berichte*, no. 875, pp. 1–19, 1991.
- [3] M. Kuehn, „Analyse des Motorradunfallgeschehens,“ *Unfallforschung der Versicherer*, 2008.
- [4] J. Stoffregen, *Motorradtechnik: Grundlagen und Konzepte von Motor, Antrieb und Fahrwerk*, (SpringerLink Bücher), 9., vollständig überarbeitete und ergänzte Auflage, Wiesbaden, Springer Vieweg, 2018, ISBN: 9783658074463. DOI: 10.1007/978-3-658-07446-3.
- [5] Motorrad. „KTM 790 Duke, BMW F 900 R und Triumph Street Triple R: Die Mittelklasse hat sich verändert. 100 PS, mindestens 750 cm³ Hubraum und 200 km/h sind hier nichts Ungewöhnliches. Wir testen drei Naked Bikes dieser beliebten Klasse.“ 2023. [Online]. Available: <https://www.motorradonline.de/naked-bike/mittelklasse-naked-bikes-im-vergleichstest-ktm-790-duke-bmw-f-900-r-und-triumph-street-triple-r/> [visited on 02/01/2023].
- [6] MotorCycles Data. „Global Electric Motorcycles Industry Exceeds 10 Million Annual Sales,“ 2023. [Online]. Available: <https://www.motorcyclesdata.com/2023/01/12/electric-motorcycles-market/> [visited on 02/01/2023].
- [7] T. R. Kane, „The Effect of Frame Flexibility on High Speed Weave of Motorcycles,“ *SAE Technical Papers*, 1978.
- [8] D. H. Weir and J. W. Zeller, „Experimental investigation of the transient behaviour of motorcycles,“ *SAE 790266*, pp. 962–978, 1979.
- [9] G. E. Roe and T. E. Thorpe, „The Influence of Frame Structure on the Dynamics of Motorcycles Stability,“ *SAE Technical Papers*, vol. 98, no. 6, pp. 1319–1330, 1989.
- [10] V. Cossalter and J. Sadauckas, „Elaboration and quantitative assessment of manoeuvrability for motorcycle lane change,“ *Vehicle System Dynamics*, vol. 44, no. 12, pp. 903–920, 2006, DOI: 10.1080/00423110600742072.
- [11] A. L. Schwab, J. P. Meijaard and J. Kooijman, „Lateral dynamics of a bicycle with a passive rider model: stability and controllability,“ *Vehicle System Dynamics*, vol. 50, no. 8, pp. 1209–1224, 2012, DOI: 10.1080/00423114.2011.610898.
- [12] C. Koenen, „The dynamic behaviour of a motorcycle when running straight ahead and when cornering,“ PhD Thesis, Mechanical, Maritime and Materials Engineering, TUDelft, 1983.
- [13] H. Burg and A. Moser, *Handbuch Verkehrsunfallrekonstruktion: Unfallaufnahme, Fahrdynamik, Simulation*, (SpringerLink Bücher), Wiesbaden, Springer Vieweg, 2017, ISBN: 9783658161439. DOI: 10.1007/978-3-658-16143-9.

- [14] D. J. N. Limebeer, R. S. Sharp and S. Evangelou, „Motorcycle Steering Oscillations due to Road Profiling,“ *Journal of Applied Mechanics*, vol. 69, no. 6, pp. 724–739, 2002, DOI: 10.1115/1.1507768.
- [15] A. Doria, M. Formentini and M. Tognazzo, „Experimental and numerical analysis of rider motion in weave conditions,“ *Vehicle System Dynamics*, vol. 50, no. 8, pp. 1247–1260, 2012, DOI: 10.1080/00423114.2011.621542.
- [16] C. Juden, „Headsets and Steering, Questions and Answers,“ *Cycle Magazine*, pp. 1997–2006, 2003.
- [17] S. A. Evangelou, D. J. N. Limebeer and M. Tomas-Rodriguez, „Suppression of Burst Oscillations in Racing Motorcycles,“ *Journal of Applied Mechanics*, vol. 80, no. 1, 2013, DOI: 10.1115/1.4006491.
- [18] V. Cossalter, *Motorcycle dynamics*, 2. English ed., S.I., [Lulu press], 2006, ISBN: 9781430308614.
- [19] R. S. Sharp, „Stability, Control and Steering Responses of Motorcycles,“ *Vehicle System Dynamics*, vol. 35, no. 4-5, pp. 291–318, 2001, DOI: 10.1076/vesd.35.4.291.2042.
- [20] M. Tanelli, M. Corno, De Filippi, Pierpaolo, S. Rossi, S. M. Savaresi and L. Fabbri, „Control-oriented steering dynamics analysis in sport motorcycles: modeling, identification and experiments,“ *IFAC Proceedings Volumes*, vol. 43, no. 10, pp. 468–473, 2009, DOI: 10.3182/20090706-3-FR-2004.00077.
- [21] H. B. Pacejka and I. Besselink, *Tire and vehicle dynamics*, 3. ed., Oxford, Butterworth - Heinemann, 2012, ISBN: 978-0-08-097016-5.
- [22] V. Cossalter, A. Doria, M. Formentini and M. Peretto, „Experimental and numerical analysis of the influence of tyres’ properties on the straight running stability of a sport-touring motorcycle,“ *Vehicle System Dynamics*, vol. 50, no. 3, pp. 357–375, 2012, DOI: 10.1080/00423114.2011.587520.
- [23] V. Cossalter, R. Lot and M. Massaro, „The influence of frame compliance and rider mobility on the scooter stability,“ *Vehicle System Dynamics*, vol. 45, no. 4, pp. 313–326, 2007, DOI: 10.1080/00423110600976100.
- [24] Bikereifen24. „Reifenfreigabe Motorrad – Zulassung, Eintragung, Gesetze,“ 2023. [Online]. Available: <https://bikereifen24.de/motorradreifen-zulassung/> [visited on 02/16/2023].
- [25] ADAC. „Motorradreifen: Freigaben und Unbedenklichkeitserklärungen,“ 2023. [Online]. Available: <https://www.adac.de/-/media/pdf/motorrad/reifenfreigaben-motorraeder.pdf> [visited on 02/01/2023].
- [26] M. P. Bendsøe and O. Sigmund, *Topology optimization: Theory, methods, and applications*, (Engineering online library), 2. ed., corrected printing, Berlin and Heidelberg, Springer, 2004, ISBN: 364207698X.
- [27] T. Foale, *Motorcycle handling and chassis design: The art and science*, 2. printing, S.I., 2003, ISBN: 8493328618.
- [28] R. S. Sharp and C. J. Alstead, „The Influence of Structural Flexibilities on the Straight-running Stability of Motorcycles,“ *Vehicle System Dynamics*, vol. 9, no. 6, pp. 327–357, 1980, DOI: 10.1080/00423118008968629.
- [29] K. Lake, R. Thomas and O. Williams, „The influence of compliant chassis components on motorcycle dynamics: an historical overview and the potential future impact of carbon fibre,“ *Vehicle System Dynamics*, vol. 50, no. 7, pp. 1043–1052, 2012, DOI: 10.1080/00423114.2011.647824.

- [30] Honda. „Honda Moto Riding Assist,“ 2023. [Online]. Available: <https://www.honda.de/motorcycles/experience-honda/news-and-events/2017-01-27-honda-moto-riding-assist.html> [visited on 02/02/2023].
- [31] Yamaha Motor Company. „EPS Steering Support System for Motorcycles,“ 2023. [Online]. Available: <https://www.yamaha-motor.com.au/discover/news-and-events/news/motorcycle/2022/march/yamaha-motor-develops-eps-steering-support-system-for-motorcycles> [visited on 02/01/2023].
- [32] L. Meirovitch, *Elements of vibration analysis*, New York, USA, Mc Grow Hill, 1975.
- [33] A. M. Lyapunov, „The general problem of the stability of motion,“ *International Journal of Control*, vol. 55, no. 3, pp. 531–534, 1992, DOI: 10.1080/00207179208934253.
- [34] T. L. Schmitz and K. S. Smith, *Mechanical Vibrations: Modeling and Measurement*, (Springer eBook Collection), 2nd ed. 2021, Cham, Springer International Publishing and Imprint Springer, 2021, ISBN: 9783030523442. DOI: 10.1007/978-3-030-52344-2.
- [35] P. L. Gatti, *Advanced mechanical vibrations: Physics, mathematics and applications*, First edition, Boca Raton, London, and New York, CRC PRESS Taylor & Franzis Group, 2021, ISBN: 9781351008594. DOI: 10.1201/9781351008600.
- [36] G. Szeidl and L. P. Kiss, *Mechanical Vibrations: An Introduction*, (Springer eBook Collection), 1st ed. 2020, Cham, Springer International Publishing and Imprint Springer, 2020, ISBN: 9783030450748. DOI: 10.1007/978-3-030-45074-8.
- [37] J. Adamy, *Nichtlineare Systeme und Regelungen*, 3., bearb. u. erw. Aufl. 2018, Berlin, Heidelberg, Springer Berlin Heidelberg, 2018, ISBN: 9783662556856.
- [38] R. S. Sharp, S. Evangelou and D. J. N. Limebeer, „Advances in the Modelling of Motorcycle Dynamics,“ *Multibody System Dynamics*, vol. 12, no. 3, pp. 251–283, 2004, DOI: 10.1023/B:MUBO.0000049195.60868.a2.
- [39] V. Cossalter, R. Lot and F. Maggio, „A Multibody Code for Motorcycle Handling and Stability Analysis with Validation and Examples of Application,“ in *SAE Technical Paper Series*, 2003, DOI: 10.4271/2003-32-0035.
- [40] V. Cossalter, R. Lot and F. Maggio, „The Modal Analysis of a Motorcycle in Straight Running and on a Curve,“ *Meccanica*, vol. 39, pp. 1–16, 2004, DOI: 10.1023/A:1026269926222.
- [41] P. T. J. Spierings, „The Effects of Lateral Front Fork Flexibility on the Vibrational Modes of Straight-Running Single-Track Vehicles,“ *Vehicle System Dynamics*, vol. 10, no. 1, pp. 21–35, 1981, DOI: 10.1080/00423118108968633.
- [42] D. J. N. Limebeer, R. S. Sharp and S. Evangelou, „The stability of motorcycles under acceleration and braking,“ *Proceedings of the Institution of Mechanical Engineers, Part C: Journal of Mechanical Engineering Science*, vol. 215, no. 9, pp. 1095–1109, 2001, DOI: 10.1177/095440620121500910.
- [43] D. J. N. Limebeer and A. Sharma, „Burst Oscillations in the Accelerating Bicycle,“ *Journal of Applied Mechanics*, vol. 77, no. 6, 2010, DOI: 10.1115/1.4000909.
- [44] E. de Vries and H. B. Pacejka, „Motorcycle Tyre Measurements and Models,“ *Vehicle System Dynamics*, vol. 29, no. sup1, pp. 280–298, 1998, DOI: 10.1080/00423119808969565.
- [45] D. J. N. Limebeer and R. S. Sharp, „Bicycles, motorcycles, and models,“ *IEEE Control Systems Magazine*, vol. 26, no. 5, pp. 34–61, 2006, DOI: 10.1109/MCS.2006.1700044.

- [46] V. Cossalter, R. Lot and F. Maggio, „The Influence of Tire Properties on the Stability of a Motorcycle in Straight Running and Curves,“ in *SAE Technical Paper Series*, 2002, DOI: 10.4271/2002-01-1572.
- [47] R. S. Sharp, „The Influence of the Suspension System on Motorcycle Weave-mode Oscillations,“ *Vehicle System Dynamics*, vol. 5, no. 3, pp. 147–154, 1976, DOI: 10.1080/00423117608968410.
- [48] R. S. Sharp and C. G. Giles, „Motorcycle Front Wheel Patter in Heavy Braking,“ *Vehicle System Dynamics*, vol. 12, no. 1-3, pp. 159–160, 1983, DOI: 10.1080/00423118308968746.
- [49] D. Wisselmann, *Motorrad-Fahrdynamik-Simulation: Modellbildung, Validierung und Anwendung*, (Fortschrittberichte VDI Reihe 12, Verkehrstechnik, Fahrzeugtechnik). vol. 176, Als Ms. gedr, Düsseldorf, VDI-Verl., 1992, ISBN: 3181476129.
- [50] R. S. Sharp and D. J. N. Limebeer, „On steering wobble oscillations of motorcycles,“ *Proceedings of the Institution of Mechanical Engineers, Part C: Journal of Mechanical Engineering Science*, vol. 218, no. 12, pp. 1449–1456, 2004, DOI: 10.1243/0954406042690434.
- [51] R. S. Sharp and Y. Watanabe, „Chatter vibrations of high-performance motorcycles,“ *Vehicle System Dynamics*, vol. 51, no. 3, pp. 393–404, 2013, DOI: 10.1080/00423114.2012.727440.
- [52] V. Cossalter, R. Lot and M. Massaro, „An advanced multibody code for handling and stability analysis of motorcycles,“ *Meccanica*, vol. 46, no. 5, pp. 943–958, 2011, DOI: 10.1007/s11012-010-9351-7.
- [53] G. Catania, L. Leonelli and N. Mancinelli, „A Multibody Motorcycle Model for the Analysis and Prediction of Chatter Vibrations,“ in *Proceedings of the ASME International Mechanical Engineering Congress and Exposition - 2013: Presented at ASME 2013 International Mechanical Engineering Congress and Exposition; November 15 - 21, 2013, San Diego, California, USA*, San Diego, California, USA, 2014, ISBN: 978-0-7918-5642-0. DOI: 10.1115/IMECE2013-62903.
- [54] A. Schramm, L. Leonelli and S. Sorrentino, „Driveline Stability in Racing Motorcycles: Analysis of a Three Degrees of Freedom Minimal Model,“ *Journal of Applied and Computational Mechanics*, vol. 9, no. 2, pp. 404–418, 2023, DOI: 10.22055/jacm.2022.41157.3709.
- [55] M. Boccione, F. Cheli, M. Pezzola and R. Viganò, „Static and Dynamic Properties of a Motorcycle Frame: Experimental and Numerical Approach,“ *WIT Transactions on Modelling and Simulation*, vol. 41, 2005, DOI: 10.2495/CMEM050501.
- [56] G. E. Roe and T. E. Thorpe, „A solution of the low-speed wheel flutter instability in motorcycles,“ *Journal Mechanical Engineering Science*, vol. 18, no. 2, pp. 57–65, 1976, DOI: 10.1243/JMES_JOUR_1976_018_012_02.
- [57] M. Raines, „Application of the Finite Element Method to Motorcycle Frame Design,“ *VDI-Berichte*, no. 875, pp. 43–51, 1991.
- [58] 3D CAD BROWSER. „,“ 2023. [Online]. Available: www.3dcadbrowser.com [visited on 02/01/2023].
- [59] P. Schilling, *Das grosse Buch vom Motorrad*, München, Südwest-Verlag, 1977, ISBN: 9783517006017.

- [60] BMW Group. „The new BMW R 1200 GS,“ 2023. [Online]. Available: <https://www.press.bmwgroup.com/global/article/detail/T0132324EN/the-new-bmw-r-1200-gs> [visited on 02/01/2023].
- [61] BMW Group. „BMW K 1200 S Vorderradführung Duolever,“ 2023. [Online]. Available: <https://www.press.bmwgroup.com/deutschland/photo/detail/P90098277> [visited on 02/01/2023].
- [62] S. Evangelou, D. J. N. Limebeer, R. S. Sharp and M. C. Smith, „Mechanical steering compensators for high-performance motorcycles,“ *Journal of Applied Mechanics*, vol. 74, no. 2, pp. 332–346, 2007, DOI: 10.1115/1.2198547.
- [63] S. Evangelou, D. J. N. Limebeer, R. S. Sharp and C. S. Malcolm, „Control of Motorcycle Steering Instabilities,“ *IEEE Control Systems Magazine*, vol. 26, no. 5, pp. 78–88, 2006, DOI: 10.1109/MCS.2006.1700046.
- [64] V. Cossalter, A. Doria and L. Mitolo, „Inertial and Modal Properties of Racing Motorcycles,“ *SAE Technical Papers*, vol. 111, no. 6, pp. 2461–2468, 2002.
- [65] R. S. Sharp and D. J. N. Limebeer, „A Motorcycle Model for Stability and Control Analysis,“ *Multibody System Dynamics*, vol. 6, pp. 123–142, 2001, DOI: 10.1023/A:1017508214101.
- [66] A. Doria and L. Taraborrelli, „The twist axis of frames with particular application to motorcycles,“ *Proceedings of the Institution of Mechanical Engineers, Part C: Journal of Mechanical Engineering Science*, vol. 230, no. 17, pp. 3026–3039, 2016, DOI: 10.1177/0954406215604862.
- [67] M. Raines and T. E. Thorpe, „The Relationship between Twist Axis and Effective Torsional Stiffness of a Motorcycle Frame,“ *Proceedings of the Institution of Mechanical Engineers, Part D: Transport Engineering*, vol. 200, no. 1, pp. 69–73, 1986, DOI: 10.1243/PIME_PROC_1986_200_165_02.
- [68] A. Doria, V. Favaron, L. Taraborrelli and S. Roa, „Parametric analysis of the stability of a bicycle taking into account geometrical, mass and compliance properties,“ *International Journal of Vehicle Design*, vol. 75, no. 1-4, pp. 91–123, 2017, DOI: 10.1504/IJVD.2017.090908.
- [69] A. Doria and S. Roa, „On the influence of tyre and structural properties on the stability of bicycles,“ *Vehicle System Dynamics*, vol. 56, no. 6, pp. 947–966, 2018, DOI: 10.1080/00423114.2017.1403032.
- [70] A. Doria, S. Roa and L. Muñoz, „Stability analysis of bicycles by means of analytical models with increasing complexity,“ *Mechanical Sciences*, vol. 10, no. 1, pp. 229–241, 2019, DOI: 10.5194/ms-10-229-2019.
- [71] M. K. Verma, R. A. Scott and L. Segel, „Effect of Frame Compliance on the Lateral Dynamics of Motorcycles,“ *Vehicle System Dynamics*, vol. 9, no. 4, pp. 181–206, 1980, DOI: 10.1080/00423118008968622.
- [72] A. Doria and M. Formentini, „Identification of the Structural Modes of High Performance Bicycles in the Perspective of Wobble Control,“ in *Proceedings of the ASME International Design Engineering Technical Conferences and Computers and Information in Engineering Conference - 2011: Presented at ASME 2011 International Design Engineering Technical Conferences and Computers and Information in Engineering Conference, August 28 - 31, 2011, Washington, D.C, Washington, DC, USA, 2012*, pp. 551–560, ISBN: 978-0-7918-5481-5. DOI: 10.1115/DETC2011-47030.

- [73] V. Cossalter, A. Doria, M. Massaro and L. Taraborrelli, „Experimental and numerical investigation on the motorcycle front frame flexibility and its effect on stability,“ *Mechanical Systems and Signal Processing*, vol. 60-61, pp. 452–471, 2015, DOI: 10.1016/j.ymssp.2015.02.011.
- [74] L. Taraborrelli, V. Favaron and A. Doria, „The effect of swingarm stiffness on motorcycle stability: experimental measurements and numerical simulations,“ *International Journal of Vehicle Systems Modelling and Testing*, vol. 12, no. 3/4, p. 240, 2017, DOI: 10.1504/IJVSMT.2017.089981.
- [75] D. J. N. Limebeer and M. Massaro, *Dynamics and optimal control of road vehicles*, Oxford, Oxford University press, 2018, ISBN: 9780198825722.
- [76] G. Ferretti, B. Scaglioni and A. Rossi, „Multibody Model of a Motorbike with a Flexible Swingarm,“ in *Proceedings of the 10th International Modelica Conference*, Lund, Sweden, 2014, DOI: 10.3384/ecp14096273.
- [77] F. J. W. Whipple, „The Stability of the Motion of a Bicycle,“ *Quarterly Journal of Pure and Applied Mathematics*, vol. 30, no. 120, pp. 312–348, 1899.
- [78] E. Carvallo, *Théorie Du Mouvement Du Monocycle et de La Bicyclette*, Paris, France, Gauthier-Villars, 1901.
- [79] R. S. Sharp, „The stability and control of motorcycles,“ *Journal Mechanical Engineering Science*, vol. 13, no. 5, pp. 316–329, 1971, DOI: 10.1243/JMES_JOUR_1971_013_051_02.
- [80] D. Schramm and M. Hiller, *Vehicle Dynamics: Modeling and Simulation*, Softcover reprint of the original 2nd edition 2018, Berlin, Springer Berlin and Springer, 2018, ISBN: 9783662571989.
- [81] R. Schwertassek, O. Wallrapp and A. A. Shabana, „Flexible Multibody Simulation and Choice of Shape Functions,“ *Nonlinear Dynamics*, vol. 20, pp. 361–380, 1999, DOI: 10.1023/A:1008314826838.
- [82] H. R. Schwarz and N. Köckler, *Numerische Mathematik*, (Studium), 7., überarb. Aufl., Wiesbaden, Vieweg + Teubner, 2009, ISBN: 9783834806833.
- [83] R. S. Sharp, „The Application of Multi-Body Computer Codes to Road Vehicle Dynamics Modelling Problems,“ *Proceedings of the Institution of Mechanical Engineers, Part D: Journal of Automobile Engineering*, vol. 208, no. 1, pp. 55–61, 1994, DOI: 10.1243/PIME_PROC_1994_208_158_02.
- [84] Hexagon. „Adams,“ 2023. [Online]. Available: <https://hexagon.com/en/products/product-groups/computer-aided-engineering-software/adams> [visited on 02/01/2023].
- [85] Dassault Systemes. „Simpack,“ 2023. [Online]. Available: <https://www.3ds.com/products-services/simulia/products/simpack/> [visited on 02/01/2023].
- [86] Mechanical Simulation. „Bikesim,“ 2023. [Online]. Available: <https://www.carsim.com/products/bikesim/index.php> [visited on 02/01/2023].
- [87] MathWorks. „Simscape,“ 2023. [Online]. Available: <https://www.mathworks.com/products/simscape.html> [visited on 02/01/2023].
- [88] D. A. Levinson and T. R. Kane, „AUTOLEV — A New Approach to Multibody Dynamics,“ in *Multibody Systems Handbook*, W. Schiehlen, ed. Berlin, Heidelberg: Springer Berlin Heidelberg, 1990, pp. 81–102, ISBN: 978-3-642-50997-1. DOI: 10.1007/978-3-642-50995-7_7.

- [89] SMC International Training. „autoSIM-200,“ 2023. [Online]. Available: https://static.smc.eu/binaries/content/assets/smc_ee/trainingsystems/autosim-200_en.pdf [visited on 02/01/2023].
- [90] zbMATH. „Mesa Verde,“ 2023. [Online]. Available: <https://zbmath.org/software/21815> [visited on 02/01/2023].
- [91] University of Stuttgart. „Neweul-M2,“ 2023. [Online]. Available: <https://www.itm.uni-stuttgart.de/en/software/neweul-m/> [visited on 02/01/2023].
- [92] T. Schindler, M. Förg, M. Friedrich, M. Schneider, B. Esefeld, R. Huber, R. Zandler and H. Ulbrich, „Analysing Dynamical Phenomenons: Introduction to MBSim,“ in *The 1st Joint International Conference on Multibody System Dynamics*, Lappeenranta, Finland, 2010.
- [93] M. Gani, R. Sharp and D. Limebeer, „Multi-body simulation software in the study of two-wheeled road vehicles,“ in *Proceedings of the 35th IEEE Conference on Decision and Control: December 11 - 13, 1996, Portopia Hotel and International Convention Center, Kobe, Japan*, Kobe, Japan, 1996, 2804–2805 vol.3, ISBN: 0-7803-3590-2. DOI: 10.1109/CDC.1996.573540.
- [94] R. S. Sharp, S. Evangelou and D. J. N. Limebeer, „Multibody Aspects of Motorcycle Modelling with Special Reference to Autosim,“ in *Advances in computational multibody systems: Revised and enlarged versions of selected communications presented at the ECCOMAS Thematic Conference in Multibody Dynamics 2003 that took place in Lisbon* (Computational Methods in Applied Sciences). vol. 2, J. A. C. Ambrósio, ed. Dordrecht: Springer, 2005, pp. 45–68, ISBN: 1-4020-3392-3. DOI: 10.1007/1-4020-3393-1_3.
- [95] V. Cossalter, A. Doria, R. Lot and M. Massaro, „The effect of rider’s passive steering impedance on motorcycle stability: identification and analysis,“ *Meccanica*, vol. 46, no. 2, pp. 279–292, 2011, DOI: 10.1007/s11012-010-9304-1.
- [96] V. E. Bulsink, A. Doria, D. van de Belt and B. Koopman, „The effect of tyre and rider properties on the stability of a bicycle,“ *Advances in Mechanical Engineering*, vol. 7, no. 12, 2015, DOI: 10.1177/1687814015622596.
- [97] A. Doria and M. Tognazzo, „The influence of the dynamic response of the rider’s body on the open-loop stability of a bicycle,“ *Proceedings of the Institution of Mechanical Engineers, Part C: Journal of Mechanical Engineering Science*, vol. 228, no. 17, pp. 3116–3132, 2014, DOI: 10.1177/0954406214527073.
- [98] G. Sequenzia, S. M. Oliveri, G. Fatuzzo and M. Calì, „An advanced multibody model for evaluating rider’s influence on motorcycle dynamics,“ *Proceedings of the Institution of Mechanical Engineers, Part K: Journal of Multi-body Dynamics*, vol. 229, no. 2, pp. 193–207, 2015, DOI: 10.1177/1464419314557686.
- [99] S. Zhu, S. Murakami and H. Nishimura, „Motion Analysis of A Motorcycle Taking Account of Rider’s Effects,“ in *Proceedings, Bicycle and Motorcycle Dynamics 2010. Symposium on the Dynamics and Control of Single Track Vehicles*, Delft, The Netherlands, 2010.
- [100] M. Plöchl, J. Edelmann, B. Angrosch and C. Ott, „On the wobble mode of a bicycle,“ *Vehicle System Dynamics*, vol. 50, no. 3, pp. 415–429, 2012, DOI: 10.1080/00423114.2011.594164.
- [101] R. Barbagallo, G. Sequenzia, S. M. Oliveri and A. Cammarata, „Dynamics of a high-performance motorcycle by an advanced multibody/control co-simulation,“ *Proceedings of the Institution of Mechanical Engineers, Part K: Journal of Multi-body Dynamics*, vol. 230, no. 2, pp. 207–221, 2016, DOI: 10.1177/1464419315602825.

- [102] R. Lot, „A Motorcycle Tire Model for Dynamic Simulations: Theoretical and Experimental Aspects,“ *Meccanica*, vol. 39, no. 3, pp. 207–220, 2004, DOI: 10.1023/B:MECC.0000022842.12077.5c.
- [103] L. Leonelli and N. Mancinelli, „A multibody motorcycle model with rigid-ring tyres: formulation and validation,“ *Vehicle System Dynamics*, vol. 53, no. 6, pp. 775–797, 2015, DOI: 10.1080/00423114.2015.1014820.
- [104] A. Doria, L. Taraborrelli and M. Urbani, „A Modal Approach for the Study of the Transient Behavior of Motorcycle and Scooter Tires,“ in *Proceedings of the ASME International Design Engineering Technical Conferences and Computers and Information in Engineering Conference - 2014: Presented at ASME 2014 International Design Engineering Technical Conferences and Computers and Information in Engineering Conference; August 17 - 20, 2014, Buffalo, New York, USA*, Buffalo, New York, USA, 2014, ISBN: 978-0-7918-4634-6. DOI: 10.1115/DETC2014-34023.
- [105] A. L. Schwab, J. P. Meijaard and J. M. Papadopoulos, „Benchmark results on the linearized equations of motion of an uncontrolled bicycle,“ *Journal of Mechanical Science and Technology*, vol. 19, no. Suppl 1, pp. 292–304, 2005, DOI: 10.1007/bf02916147.
- [106] J. Kooijman and A. L. Schwab, „A review on bicycle and motorcycle rider control with a perspective on handling qualities,“ *Vehicle System Dynamics*, vol. 51, no. 11, pp. 1722–1764, 2013, DOI: 10.1080/00423114.2013.824990.
- [107] A. A. Popov, S. Rowell and J. P. Meijaard, „A review on motorcycle and rider modelling for steering control,“ *Vehicle System Dynamics*, vol. 48, no. 6, pp. 775–792, 2010, DOI: 10.1080/00423110903033393.
- [108] B. Lohmann, T. Bechtold, P. Eberhard, J. Fehr, D. J. Rixen, M. C. Varona, Christopher Lerch, Yuan, C. D., E. B. Rudnyi, B. Fröhlich, P. Holzwarth, D. Grunert, C. H. Meyer and J. B. Rutzmoser, „Model order reduction in mechanical engineering,“ in *Model Order Reduction, Volume 3: Applications* pp. 33–74, DOI: 10.1515/9783110499001-002.
- [109] C. G. Giles and R. S. Sharp, „Static and Dynamic Stiffness and Deflection Mode Measurements on a Motorcycle, with particular Reference to Steering Behaviour,“ in *I Mech E Conference Publications (Institution of Mechanical Engineers)*, 1983, pp. 185–192.
- [110] S. Kulkarni and A. A. Shabana, „Spatial ANCF/CRBF beam elements,“ *Acta Mechanica*, vol. 230, no. 3, pp. 929–952, 2019, DOI: 10.1007/s00707-018-2294-0.
- [111] J. R. Canavin and P. W. Likins, „Floating Reference Frames for Flexible Spacecraft,“ *Journal of Spacecraft and Rockets*, vol. 14, no. 12, pp. 724–732, 1977, DOI: 10.2514/3.57256.
- [112] C. Nowakowski, J. Fehr, M. Fischer and P. Eberhard, „Model Order Reduction in Elastic Multibody Systems using the Floating Frame of Reference Formulation,“ *IFAC Proceedings Volumes*, vol. 45, no. 2, pp. 40–48, 2012, DOI: 10.3182/20120215-3-AT-3016.00007.
- [113] P. Holzwarth and P. Eberhard, „SVD-based improvements for component mode synthesis in elastic multibody systems,“ *European Journal of Mechanics - A/Solids*, vol. 49, pp. 408–418, 2015, DOI: 10.1016/j.euromechsol.2014.08.009.
- [114] M. Lehner and P. Eberhard, „A two-step approach for model reduction in flexible multibody dynamics,“ *Multibody System Dynamics*, vol. 17, no. 2-3, pp. 157–176, 2007, DOI: 10.1007/s11044-007-9039-5.

- [115] P. Holzwarth, „Modellordnungsreduktion für substrukturierte mechanische Systeme,“ Dissertation, Shaker Verlag GmbH, 2017.
- [116] J. J. O’Shea, P. Jayakumar, D. Mechergui, A. A. Shabana and L. Wang, „Reference Conditions and Substructuring Techniques in Flexible Multibody System Dynamics,“ *Journal of Computational and Nonlinear Dynamics*, vol. 13, no. 4, 2018, DOI: 10.1115/1.4039059.
- [117] J. Fehr, *Automated and error controlled model reduction in elastic multibody systems*, (Schriften aus dem Institut für Technische und Numerische Mechanik der Universität Stuttgart). vol. Bd. 21, Aachen, Shaker, 2011, ISBN: 9783844005509.
- [118] R. Schwertassek and O. Wallrapp, *Dynamik flexibler Mehrkörpersysteme: Methoden der Mechanik zum rechnergestützten Entwurf und zur Analyse mechatronischer Systeme ; mit 25 Tabellen*, (Grundlagen und Fortschritte der Ingenieurwissenschaften), Braunschweig and Wiesbaden, Vieweg, 1999, ISBN: 3528066296.
- [119] J. Fehr and P. Eberhard, „Simulation process of flexible multibody systems with non-modal model order reduction techniques,“ *Multibody System Dynamics*, vol. 25, no. 3, pp. 313–334, 2011, DOI: 10.1007/s11044-010-9238-3.
- [120] A. Cammarata and C. M. Pappalardo, „On the use of component mode synthesis methods for the model reduction of flexible multibody systems within the floating frame of reference formulation,“ *Mechanical Systems and Signal Processing*, vol. 142, 2020, DOI: 10.1016/j.ymsp.2020.106745.
- [121] A. A. Shabana and G. Wang, „Durability analysis and implementation of the floating frame of reference formulation,“ *Proceedings of the Institution of Mechanical Engineers, Part K: Journal of Multi-body Dynamics*, vol. 232, no. 3, pp. 295–313, 2018, DOI: 10.1177/1464419317731707.
- [122] A. Zwölfer and J. Gerstmayr, „The nodal-based floating frame of reference formulation with modal reduction,“ *Acta Mechanica*, vol. 232, no. 3, pp. 835–851, 2021, DOI: 10.1007/s00707-020-02886-2.
- [123] T. Ruiner, J. Fehr, B. Haasdonk and P. Eberhard, „A-posteriori error estimation for second order mechanical systems,“ *Acta Mechanica Sinica*, vol. 28, no. 3, pp. 854–862, 2012, DOI: 10.1007/s10409-012-0114-7.
- [124] B. Besselink, U. Tabak, A. Lutowska, N. van de Wouw, H. Nijmeijer, D. J. Rixen, M. E. Hochstenbach and W. Schilders, „A comparison of model reduction techniques from structural dynamics, numerical mathematics and systems and control,“ *Journal of Sound and Vibration*, vol. 332, no. 19, pp. 4403–4422, 2013, DOI: 10.1016/j.jsv.2013.03.025.
- [125] J. W. Strutt, *The Theory of Sound: With an Historical Introduction by Robert B. Lindsay*, (Dover Books on Physics and Mathematical Physics). vol. 2, 2. ed., repr, New York, Dover, 1945.
- [126] R. J. Guyan, „Reduction of stiffness and mass matrices,“ *AIAA Journal*, vol. 3, no. 2, p. 380, 1965, DOI: 10.2514/3.2874.
- [127] R. Craig and M. Bampton, „Coupling of substructures for dynamic analyses,“ *AIAA Journal*, vol. 6, no. 7, pp. 1313–1319, 1968, DOI: 10.2514/3.4741.
- [128] J. Fehr and P. Eberhard, „Error-controlled model reduction in flexible multibody dynamics,“ *Journal of Computational and Nonlinear Dynamics*, vol. 5, no. 3, 2010, DOI: 10.1115/1.4001372.

- [129] B. C. Moore, „Principal Component Analysis in Linear Systems: Controllability, Observability, and Model Reduction,“ *IEEE Transactions on Automatic Control*, vol. 26, no. 1, pp. 17–32, 1981, DOI: 10.1109/TAC.1981.1102568.
- [130] S. Gugercin and A. C. Antoulas, „A Survey of Model Reduction by Balanced Truncation and Some New Results,“ *International Journal of Control*, vol. 77, no. 8, pp. 748–766, 2004, DOI: 10.1080/00207170410001713448.
- [131] Z. Bai, „Krylov subspace techniques for reduced-order modeling of large-scale dynamical systems,“ *Applied Numerical Mathematics*, vol. 43, no. 1-2, pp. 9–44, 2002, DOI: 10.1016/S0168-9274(02)00116-2.
- [132] E. Grimme, „Krylov Projection Methods for Model Order Reduction,“ PhD Thesis, University of Illinois at Urbana-Champaign, 1997.
- [133] S. B. Salimbahrami and B. Lohmann, „Order reduction of large scale second-order systems using Krylov subspace methods,“ *Linear Algebra and its Applications*, vol. 415, no. 2-3, pp. 385–405, 2006, DOI: 10.1016/j.laa.2004.12.013.
- [134] T.-J. Su and R. R. Craig, „Model reduction and control of flexible structures using Krylov vectors,“ *Journal of Guidance, Control, and Dynamics*, vol. 14, no. 2, pp. 260–267, 1991, DOI: 10.2514/3.20636.
- [135] S. Gugercin, A. C. Antoulas and C. Beattie, „H2 Model Reduction for Large-Scale Linear Dynamical Systems,“ *SIAM Journal on Matrix Analysis and Applications*, vol. 30, no. 2, pp. 609–638, 2008, DOI: 10.1137/060666123.
- [136] Z. Bai and Y. Su, „Dimension Reduction of Large-Scale Second-Order Dynamical Systems via a Second-Order Arnoldi Method,“ *SIAM Journal on Scientific Computing*, vol. 26, no. 5, pp. 1692–1709, 2005, DOI: 10.1137/040605552.
- [137] D. C. Sorensen and A. C. Antoulas, „On Model Reduction of Structured Systems,“ in *Dimension reduction of large-scale systems: Proceedings of a workshop held in Oberwolfach, Germany, October 19 - 25, 2003 ; with 29 tables* (Lecture Notes in Computational Science and Engineering). vol. 45, P. Benner, ed. Berlin: Springer, 2005, pp. 117–130, ISBN: 3-540-24545-6. DOI: 10.1007/3-540-27909-1_4.
- [138] S. B. Salimbahrami, „Structure Preserving Order Reduction of Large Scale Second Order Models,“ Dissertation, Technische Universität München, München, 2005.
- [139] C.-C. Chu, H.-C. Tsai and M.-H. Lai, „Structure preserving model-order reductions of MIMO second-order systems using Arnoldi methods,“ *Mathematical and Computer Modelling*, vol. 51, no. 7-8, pp. 956–973, 2010, DOI: 10.1016/j.mcm.2009.08.028.
- [140] Y. Chahlaoui, D. Lemonnier, A. Vandendorpe and P. van Dooren, „Second-order balanced truncation,“ *Linear Algebra and its Applications*, vol. 415, no. 2-3, pp. 373–384, 2006, DOI: 10.1016/j.laa.2004.03.032.
- [141] T. Reis and T. Stykel, „Balanced truncation model reduction of second-order systems,“ *Mathematical and Computer Modelling of Dynamical Systems*, vol. 14, no. 5, pp. 391–406, 2008, DOI: 10.1080/13873950701844170.
- [142] P. Benner, P. Kürschner and J. Saak, „An improved numerical method for balanced truncation for symmetric second-order systems,“ *Mathematical and Computer Modelling of Dynamical Systems*, vol. 19, no. 6, pp. 593–615, 2013, DOI: 10.1080/13873954.2013.794363.

- [143] J. Fehr, M. Fischer, B. Haasdonk and P. Eberhard, „Greedy-based approximation of frequency-weighted Gramian matrices for model reduction in multibody dynamics,“ *ZAMM - Journal of Applied Mathematics and Mechanics / Zeitschrift für Angewandte Mathematik und Mechanik*, vol. 93, no. 8, pp. 501–519, 2013, DOI: 10.1002/zamm.201200014.
- [144] D. Enns, „Model reduction with balanced realizations: An error bound and a frequency weighted generalization,“ in *The 23rd IEEE Conference on Decision and Control*, Las Vegas, Nevada, USA, 1984, pp. 127–132, DOI: 10.1109/CDC.1984.272286.
- [145] S. Wyatt, „Issues in Interpolatory Model Reduction: Inexact Solvers, Second-order Systems and DAEs,“ Dissertation, Virginia Polytechnic Institute and State University, Blacksburg, Virginia, 2012.
- [146] V. Druskin and V. Simoncini, „Adaptive rational Krylov subspaces for large-scale dynamical systems,“ *Systems & Control Letters*, vol. 60, no. 8, pp. 546–560, 2011, DOI: 10.1016/j.sysconle.2011.04.013.
- [147] V. Druskin, V. Simoncini and M. Zaslavsky, „Adaptive tangential interpolation in rational Krylov subspaces for mimo dynamical systems,“ *SIAM Journal on Matrix Analysis and Applications*, vol. 35, no. 2, pp. 476–498, 2014, DOI: 10.1137/120898784.
- [148] R. Craig and E. Blades, „Substructure System Identification: Reduced-order Models,“ *WIT Transactions on The Built Environment*, vol. 22, 1996, DOI: 10.2495/DCSS960231.
- [149] D. de Klerk, D. J. Rixen and S. N. Voormeeren, „General Framework for Dynamic Substructuring: History, Review and Classification of Techniques,“ *AIAA Journal*, vol. 46, no. 5, pp. 1169–1181, 2008, DOI: 10.2514/1.33274.
- [150] D. J. Rixen, *Structural Dynamics: Lecture Notes, unpublished manuscript*, 2017.
- [151] R. H. MacNeal, „A hybrid method of component mode synthesis,“ *Computers & Structures*, vol. 1, no. 4, pp. 581–601, 1971, DOI: 10.1016/0045-7949(71)90031-9.
- [152] S. Rubin, „Improved Component-Mode Representation for Structural Dynamic Analysis,“ *AIAA Journal*, vol. 13, no. 8, pp. 995–1006, 1975, DOI: 10.2514/3.60497.
- [153] D. J. Rixen, „A dual Craig–Bampton method for dynamic substructuring,“ *Journal of Computational and Applied Mathematics*, vol. 168, no. 1-2, pp. 383–391, 2004, DOI: 10.1016/j.cam.2003.12.014.
- [154] B.-S. Liao, Z. Bai and W. Gao, „The important modes of subsystems: A moment-matching approach,“ *International Journal for Numerical Methods in Engineering*, vol. 70, no. 13, pp. 1581–1597, 2007, DOI: 10.1002/nme.1940.
- [155] D. C. Kammer and M. J. Triller, „Selection of component modes for Craig-Bampton substructure representations,“ *Journal of Vibration and Acoustics*, vol. 118, no. 2, 1996, DOI: 10.1115/1.2889657.
- [156] S. Ricci, M. Troncossi and A. Rivola, „Modal Selection Through Effective Interface Mass With Application to Flexible Multibody Cranktrain Dynamics,“ *Journal of Computational and Nonlinear Dynamics*, vol. 9, no. 1, 2014, DOI: 10.1115/1.4025280.
- [157] D. Givoli, P. E. Barbone and I. Patlashenko, „Which are the important modes of a subsystem?,“ *International Journal for Numerical Methods in Engineering*, vol. 59, no. 12, pp. 1657–1678, 2004, DOI: 10.1002/nme.935.
- [158] J.-G. Kim and P.-S. Lee, „An enhanced Craig-Bampton method,“ *International Journal for Numerical Methods in Engineering*, vol. 103, no. 2, pp. 79–93, 2015, DOI: 10.1002/nme.4880.

- [159] D. Krattiger, L. Wu, M. Zacharczuk, M. Buck, R. J. Kuether, M. S. Allen, P. Tiso and M. R. W. Brake, „Interface Reduction for Hurty Craig-Bampton Substructured Models Review and Improvements,” *Mechanical Systems and Signal Processing*, vol. 114, pp. 579–603, 2019, DOI: 10.1016/j.ymssp.2018.05.031.
- [160] P. Koutsovasilis and M. Beiteltschmidt, „Comparison of model reduction techniques for large mechanical systems,” *Multibody System Dynamics*, vol. 20, no. 2, pp. 111–128, 2008, DOI: 10.1007/s11044-008-9116-4.
- [161] R. J. Allemang, „The modal assurance criterion - Twenty years of use and abuse,” *Sound and Vibration*, vol. 37, no. 8, pp. 14–21, 2003.
- [162] M. C. Varona, A. Castagnotto, T. Wolf, R. Eid, M. Pak and T. Moser, *Modeling and Reduction of Complex Systems: Lecture notes, unpublished manuscript*, 2020.
- [163] S. Evangelou, „Control of motorcycles by variable geometry rear suspension,” *2010 IEEE International Conference on Control Applications*, pp. 148–154, 2010, DOI: 10.1109/CCA.2010.5611082.
- [164] Y. Watanabe and M. W. Sayers, „The Effect of a New Stability Control on the Simulated Cornering Behavior of Motorcycles,” *Bicycle and Motorcycle Dynamics*, vol. 2016.
- [165] De Filippi, Pierpaolo, M. Tanelli, M. Corno, S. M. Savaresi and L. Fabbri, „Semi-Active Steering Damper Control in Two-Wheeled Vehicles,” *IEEE Transactions on Control Systems Technology*, vol. 19, no. 5, pp. 1003–1020, 2011, DOI: 10.1109/TCST.2010.2070068.
- [166] S. Piantini, A. Giorgetti, N. Baldanzini, C. Monti and M. Pierini, „Design of a Motorcycle Steering Damper for a Safer Ride,” *Machines*, vol. 8, no. 2, p. 24, 2020, DOI: 10.3390/machines8020024.
- [167] G. Schiffer, H. Gerrit and J. Priese, „Motorcycle Provided with a Steering Damper: US Patent,” Patent 20070176392, August 02, 2007.
- [168] T. Wakabayashi and K. Sakai, „Development of electronically controlled hydraulic rotary steering damper for motorcycles,” *International Motorcycle Conference, 5th, 2004, Essen, Germany*, vol. 11, pp. 490–509, 2004.
- [169] Honda. „The Steering Damper Comes of Age,” 2023. [Online]. Available: <https://hondanews.com/en-US/powersports/releases/release-84a452fa6f90fd25a70dd9004c34c457-the-steering-damper-comes-of-age> [visited on 02/01/2023].
- [170] De Filippi, Pierpaolo and S. M. Savaresi, „A Mixed Frequency/Time-Domain Method to Evaluate the Performance of Semi-Active Steering Damper Control Strategies During Challenging Maneuvers,” in *Proceedings of the ASME Dynamic Systems and Control Conference and Bath/ASME Symposium on Fluid Power and Motion Control - 2011: Presented at ASME Dynamic Systems and Control Conference and Bath/ASME Symposium on Fluid Power and Motion Control, October 31 - November 2, 2011, Arlington, Virginia, USA, Arlington, Virginia, USA, 2012*, pp. 815–822, ISBN: 978-0-7918-5476-1. DOI: 10.1115/DSCC2011-5913.
- [171] M. C. Smith, „Synthesis of mechanical networks: the inerter,” *IEEE Transactions on Automatic Control*, vol. 47, no. 10, pp. 1648–1662, 2002, DOI: 10.1109/TAC.2002.803532.
- [172] S. Evangelou, D. J. N. Limebeer, R. S. Sharp and M. C. Smith, „An H_∞ loop-shaping approach to steering control for high-performance motorcycle,” *Lecture Notes in Control and Information Sciences*, vol. 329, pp. 257–275, 2006, DOI: 10.1007/11664550_14.

- [173] D. McFarlane and K. Glover, „A Loop Shaping Design Procedure Using H_∞ Synthesis,“ *IEEE Transactions on Automatic Control*, vol. 37, no. 6, pp. 759–769, 1992, DOI: 10.1109/9.256330.
- [174] J. R. Leigh, *Control theory: A guided tour*, (IET control engineering series). vol. 72, 3rd ed (Online-Ausg.), London, Institution of Engineering and Technology, 2012, ISBN: 9781849192286.
- [175] J. Lunze, *Regelungstechnik 2: Mehrgrößensysteme, Digitale Regelung*, 10th ed. 2020, Springer-Verlag, 2020, ISBN: 9783662607602. DOI: 10.1007/978-3-662-60760-2.
- [176] R. Toscano and P. Lyonnet, „Robust PID controller tuning based on the heuristic Kalman algorithm,“ *Automatica*, vol. 45, no. 9, pp. 2099–2106, 2009, DOI: 10.1016/j.automatica.2009.05.007.
- [177] S. Mammar, S. Espie and C. Honvo, „Motorcycle modelling and roll motion stabilization by rider leaning and steering torque,“ in *2005 IEEE International Conference on Control Applications*, Toronto, Ont, 2005, pp. 1421–1426, ISBN: 0-7803-9354-6. DOI: 10.1109/CCA.2005.1507331.
- [178] Y. Kamata and H. Nishimura, „System identification and attitude control of motorcycle by computer-aided dynamics analysis,“ *JSAE Review*, vol. 24, no. 4, pp. 411–416, 2003, DOI: 10.1016/S0389-4304(03)00071-7.
- [179] K. Glover, J. Sefton and D. C. McFarlane, „A tutorial on loop shaping using H-infinity robust stabilisation,“ *Transactions of the Institute of Measurement & Control*, vol. 14, no. 3, pp. 157–168, 1992, DOI: 10.1177/014233129201400306.
- [180] K. Glover and D. McFarlane, „Robust stabilization of normalized coprime factor plant descriptions with H-infinity-bounded uncertainty,“ *IEEE Transactions on Automatic Control*, vol. 34, no. 8, pp. 821–830, 1989, DOI: 10.1109/9.29424.
- [181] F. Klinger, J. Nusime, J. Edelmann and M. Plöchl, „Wobble of a racing bicycle with a rider hands on and hands off the handlebar,“ *Vehicle System Dynamics*, vol. 52, no. sup1, pp. 51–68, 2014, DOI: 10.1080/00423114.2013.877592.
- [182] F. Passigato, A. Eisele, D. Wisselmann, A. Gordner and F. Diermeyer, „Analysis of the Phenomena Causing Weave and Wobble in Two-Wheelers,“ *Applied Sciences*, vol. 10, no. 19, p. 6826, 2020, DOI: 10.3390/app10196826.
- [183] F. Passigato. „Motorcycle Model,“ 2023. [Online]. Available: https://github.com/TUMFTM/motorcycle_model [visited on 02/01/2023].
- [184] F. Passigato, A. Gordner and F. Diermeyer, „Modeling of the Weave and Wobble Eigenmodes of Motorcycles Using Flexible Multibody Simulation,“ in *Proceedings of the ASME 2022 International Design Engineering Technical Conferences and Computers and Information in Engineering Conference. Volume 9: 18th International Conference on Multibody Systems, Nonlinear Dynamics, and Control (MSNDC)*, 2022, DOI: 10.1115/DETC2022-89945.
- [185] F. Passigato, A. Schramm, F. Diermeyer, S. Sorrentino, A. Gordner and A. de Felice, „Identification of Lumped Stiffness Parameters for a Motorcycle Model in Investigating Weave and Wobble,“ *Multibody System Dynamics*, 2023, DOI: 10.1007/s11044-023-09899-4.

- [186] F. Passigato, A. Wischnewski, A. Gordner and F. Diermeyer, „Two Approaches for the Synthesis of a Weave-Wobble-stabilizing Controller in Motorcycles,“ in *2021 IEEE International Intelligent Transportation Systems Conference (ITSC)*, 2021, pp. 3496–3501, DOI: 10.1109/ITSC48978.2021.9565019.
- [187] D. Esser, „Analyse des Einflusses von Fahrwerkssteifigkeit auf den Weave und Wobble Eigenmoden von Motorrädern in der Schräglage,“ Semester Thesis, Institute of Automotive Technology, Technical University of Munich, Munich, Germany, 2023.
- [188] C. Briat, *Linear Parameter-Varying and Time-Delay Systems: Analysis, Observation, Filtering Control*, (Advances in Delays and Dynamics). vol. 3, 1. Aufl., s.l., Springer-Verlag, 2014, ISBN: 978-3-662-44049-0. DOI: 10.1007/978-3-662-44050-6.

Prior Publications

During the development of this dissertation, publications and student theses were written in which partial aspects of this work were presented.

Journals; Scopus/Web of Science listed (peer-reviewed)

- [182] F. Passigato, A. Eisele, D. Wisselmann, A. Gordner and F. Diermeyer, „Analysis of the Phenomena Causing Weave and Wobble in Two-Wheelers,“ *Applied Sciences*, vol. 10, no. 19, p. 6826, 2020, DOI: 10.3390/app10196826.
- [185] F. Passigato, A. Schramm, F. Diermeyer, S. Sorrentino, A. Gordner and A. de Felice, „Identification of Lumped Stiffness Parameters for a Motorcycle Model in Investigating Weave and Wobble,“ *Multibody System Dynamics*, 2023, DOI: 10.1007/s11044-023-09899-4.

Conferences, Periodicals; Scopus/Web of Science listed (peer-reviewed)

- [184] F. Passigato, A. Gordner and F. Diermeyer, „Modeling of the Weave and Wobble Eigenmodes of Motorcycles Using Flexible Multibody Simulation,“ in *Proceedings of the ASME 2022 International Design Engineering Technical Conferences and Computers and Information in Engineering Conference. Volume 9: 18th International Conference on Multibody Systems, Nonlinear Dynamics, and Control (MSNDC)*, 2022, DOI: 10.1115/DETC2022-89945.
- [186] F. Passigato, A. Wischnewski, A. Gordner and F. Diermeyer, „Two Approaches for the Synthesis of a Weave-Wobble-stabilizing Controller in Motorcycles,“ in *2021 IEEE International Intelligent Transportation Systems Conference (ITSC)*, 2021, pp. 3496–3501, DOI: 10.1109/ITSC48978.2021.9565019.

Patents

F. Passigato, M. Flossmann, A. Wahl and L. K. Stolle, „Verfahren zur Reibwerterkennung am Vorderrad eines Zweirades mittels Lenkmomentsensorik: Patent application pending,“ Patent,

Non-thesis-relevant publications; Scopus/Web of Science listed (peer-reviewed)

T. Herrmann, F. Passigato, J. Betz and M. Lienkamp, „Minimum Race-Time Planning-Strategy for an Autonomous Electric Racecar,“ in *2020 IEEE 23rd International Conference on Intelligent Transportation Systems (ITSC)*, Rhodes, Greece, 2020, pp. 1–6, ISBN: 978-1-7281-4149-7. DOI: 10.1109/ITSC45102.2020.9294681.

Thesis-relevant open-source software

[183] F. Passigato. „Motorcycle Model,“ 2023. [Online]. Available: https://github.com/TUMFTM/motorcycle_model [visited on 02/01/2023].

Supervised Students' Theses

The following student theses were written within the framework of the dissertation under the supervision of the author in terms of content, technical and scientific support as well as under relevant guidance of the author. In the following, the bachelor, semester and master theses relevant and related to this dissertation are listed. Many thanks to the authors of these theses for their extensive support within the framework of this research project.

- [187] D. Esser, „Analyse des Einflusses von Fahrwerkssteifigkeit auf den Weave und Wobble Eigenmoden von Motorrädern in der Schräglage,“ Semester Thesis, Institute of Automotive Technology, Technical University of Munich, Munich, Germany, 2023.
- V. Boskovic, „Alternative Methoden für die Entwicklung eines Regler zur Trajektorienverfolgung in der fahrdynamischen Simulation von Motorrädern,“ Semester Thesis, Institute of Automotive Technology, Technical University of Munich, Munich, Germany, 2023.
- M. Caspary, „Sensitivitätsanalyse eines MKS Motorradmodells,“ Semester Thesis, Institute of Automotive Technology, Technical University of Munich, Munich, Germany, 2021.
- Y. Gao, „Untersuchung von nichtlinearen stabilisierenden Regelungskonzepten für Motorräder,“ Semester Thesis, Institute of Automotive Technology, Technical University of Munich, Munich, Germany, 2021.
- M. Härtl, „Entwicklung eines Regelungskonzepts für die Verbesserung der Motorradstabilität,“ Master's Thesis, Institute of Automotive Technology, Technical University of Munich, Munich, Germany, 2020.
- P. Kardos, „Parametrische Modellidentifikation für ein Motorradmodell,“ Master's Thesis, Institute of Automotive Technology, Technical University of Munich, Munich, Germany, 2023.
- G. Oswald, „Umsetzung eines Systems für die Gleichgewichtsstabilisierung von Einspurfahrzeugen,“ Master's Thesis, Institute of Automotive Technology, Technical University of Munich, Munich, Germany, 2020.
- C. Ploß, „Erstellung von Fahrscenarien für die Untersuchung der Motorradfahrdynamik,“ Semester Thesis, Institute of Automotive Technology, Technical University of Munich, Munich, Germany, 2022.
- L. Scheller, „Using a GPU for Matrix-Vector Multiplication,“ IDP, Institute of Automotive Technology, Technical University of Munich, Munich, Germany, 2022.
- H. Xu, „Verbesserung eines Reglers für Trajektorienverfolgung in der fahrdynamischen Simulation eines Motorrades,“ Semester Thesis, Institute of Automotive Technology, Technical University of Munich, Munich, Germany, 2022.